Testing alternative theories of Quantum Mechanics with Optomechanics, and effective modes for Gaussian linear Optomechanics

Thesis by
Bassam Helou

In Partial Fulfillment of the Requirements for the
Degree of
Doctor of Philosophy

CALIFORNIA INSTITUTE OF TECHNOLOGY
Pasadena, California

2019
Defended 12/11/2018

Bassam Helou
ORCID: 0000-0003-2760-7622

ACKNOWLEDGEMENTS

My time at Caltech wasn't just an academic journey. I would like to first thank the people who made a lasting impact on my self. Haixing Miao was a great mentor, and his outlook on life continues to inspire me. William H. Hurt welcomed me to his family, re-ignited a love of reading, and shared his worldview with me. Robert Wills cultivated a love of the outdoors. Karthik Seetharam cultivated a love of working out. Zhewei Chen cultivated a love of climbing and other outdoor adventures. Locatelli Rao gave me some tools and understanding of physical therapy. Lee Coleman introduced me to mindfulness meditation.

I am also thankful for friends who have me kept me sane over the years: Anandh Swaminathan, Stephan Zheng, Rose Yu, Li Zhiquin, Tejas Deshpande, Zachary Mark, Linhan Shen, Eric Wolff, Min-feng Tu, Nicole Yunger-Halpern, Pavan Bilgi, Evan Miyazano, Ivan Papusha, Jenia Mozgunov, Howard Hui, Daniel Naftalovich, Stephen Perry, Krzysztof Chalupka, Xiaoyu Shi, Becky Schwantes, Jacklyn Phu, Corwin Shiu, Tung Wongwaitayakornkul, Mark Harfouche, Rebecca Herrera, Luis Goncalves, Vipul Singhal, Tobias Bischoff, Chris Rollins, Julius Su, Reed Scharff, Elena Murchikova and Tal Einav. I'd also like to thank the Alpine club for organizing many amazing trips. I'd also like to thank 'the drunkest table' for staying in touch and organizing many events. Specifically, I'd like to thank Tony Liao, Utkarth Gaur, Mike Wang, Andrew Ng, Velora Chan, the two Jon Ngs, Jimmy Lu, Hecheng Wang, Roshny Francis, Adrienne Wang and Patricia Ko.

I am thankful for many stimulating discussions with other researchers that made me feel like I was part of a community. I would like to thank Maaneli Derakhshani, Antoine Tilloy, Huan Yang, Yiqiu Ma, P. C. E. Stamp, Dan Carney, Belinda Pang and Xiang Li.

I'd like to thank my family for their unwavering support: Hikmat Helou, Mohamad Helou, Akram Helou, Randa Helou, Rym Helou, Randa Kabbara, Malek Kabbara, Khaled Helou, my grandfather Akram Helou and Houda Helou. I'd like to also thank extended family for their support: Amer Mikkewi, Mo Mikkewi, Kareem Mikkewi, Jihad Mikkewi, Vivian Cunanan, Wilfredo Cunanan, Bernadette Glen, Douglas Murray, Alex Murray, Molly Purnell, Kelley Purnell and Mark Purnell.

I'd like to thank the ISP office, JoAnn Boyd, Jennifer Blankenship, Alfrida King and Christy Jenstad for their kindness and amazing administrative support.

I'd like to thank CTLO and the Caltech library staff for being supportive of my ideas.

I'd also like to thank Kerry Vahala for allowing me to experiment with TA ideas.

Finally, I'd like to thank Yanbei Chen for his patience, support and the freedom he gave me. His boundless creativity and curiosity is inspirational. I am a much better researcher and problem solver because of him!

ABSTRACT

Optomechanics has made great strides in theory and experiments over the past decade, which culminated in the first direct detection of gravitational waves in 2015 by LIGO. This thesis explores how optomechanics can be used to test fundamental physics other than the theory of general relativity. Our emphasis will be on falsifiable theories (ultimately, only experiments can decide whether a theory is correct) that address two outstanding issues in quantum mechanics: the measurement problem, and reconciling quantum mechanics with the theory of general relativity. In particular, we show that the space experiment LISA pathfinder places aggressive bounds on two objective collapse models, which are non-linear stochastic modifications of the Schroedinger equation that can resolve the measurement problem. Moreover, we show that state-of-the-art torsion pendulum experiments can test the Schroedinger-Newton theory, which is the non-relativistic limit of a non-linear theory combining quantum mechanics with a fundamentally classical spacetime.

Along the way, we propose how to resolve two major difficulties with determining the predictions of non-linear quantum mechanics in an actual experiment. First, we cannot use the density matrix formalism in non-linear quantum mechanics and so we have to suggest and justify a particular ensemble for the thermal bath. Separating out quantum and classical fluctuations helped us propose a reasonable ensemble. Second, most researchers believe that deterministic non-linear quantum mechanics must violate the no-signaling condition. We show this isn't necessarily the case because different interpretations of quantum mechanics make different predictions in non-linear quantum mechanics. We propose an interpretation, the causal-conditional prescription, that doesn't violate causality by noticing that once we fix an initial state, the evolution of a system under many non-linear theories is equivalent to evolution under a linear Hamiltonian with feedback. The mapping allows us to leverage the tools of quantum control, and it tells us that if the non-linear parameters of a non-linear Hamiltonian respond causally (*i.e.* with an appropriate delay) to measurement results, then the theory can be made causal.

We also contribute to the theory of quantum optomechanics. We introduce two new bases that one can view environment modes with. In linear optomechanics a system interacts with an infinite number of bath modes. We show that the interaction can be reduced to one with finite degrees of freedom. Moreover, at any particular time, the system is correlated with only a finite number of bath modes. We show that if we make the assumption that we can measure any commuting environment modes, then this basis allows us to understand the one-shot quantum Cramer-Rao bound in a simple way, and allows us to sweep large parameter regimes and so find promising optomechanics topologies for quantum state preparation tasks that we can then analyze without the assumption of being able to measure any observable of the environment. We also use this basis to show that when we are interested in the conditional dynamics of a test mass, we can only adiabatically eliminate

a lossy cavity when we measure the optomechanical system at a slow enough rate. Finally, we develop an analytic filter for obtaining the state of a generic optomechanical system that interacts linearly with its environment and is driven by Gaussian states, and where the outgoing light is measured with a non-linear photon-counting measurement. We hope that our work will help researchers explore optomechanics topologies that make use of photon counters.

PUBLISHED CONTENT AND CONTRIBUTIONS

B. Helou, J. Luo, H. Yeh, C. Shao, B. J. J. Slagmolen, D. E. McClelland, and Y. Chen (2017). "Measurable signatures of quantum mechanics in a classical spacetime". In: PRD **96**, 044008. DOI: 10.1103/PhysRevD.96.044008.
BH participated in the conception of the project, co-wrote the manuscript, co-carried the calculations, carried out the simulations and co-analyzed the results.

B. Helou, B J. J. Slagmolen, D. E. McClelland, and Y. Chen (2017). "LISA pathfinder appreciably constrains collapse models". In: PRD **95**, 084054. DOI: 10.1103/PhysRevD.95.084054.
BH participated in the conception of the project, co-wrote the manuscript, co-carried the calculations, carried out the simulations and co-analyzed the results.

B. Helou, and Y. Chen (2017). "Different interpretations of quantum mechanics make different predictions in non-linear quantum mechanics, and some do not violate the no-signaling condition". In: arXiv:1709.06639.
BH conceived of the project, co-developed the results, and wrote the manuscript

TABLE OF CONTENTS

LIST OF ILLUSTRATIONS

Number *Page*

LIST OF TABLES

Chapter 1

INTRODUCTION

1.1 Overview

By directly detecting gravitational waves, LIGO validated the use of optomechanics for testing fundamental physics. The discovery also spurred research in how gravitational wave astronomy can test whether the theory of general relativity will break down in the strong gravity regime. Concurrently, researchers have been looking at whether optomechanics can be used to test alternative theories of Quantum Mechanics (QM). The search for alternatives of QM is fueled by two issues: the measurement problem, and reconciling QM with the theory of general relativity.

The measurement problem describes a fundamental conceptual difficulty with QM. The Schroedinger equation deterministically predicts the dynamics of a particle's wavefunction. However, if we wish to probe the particle's state with a measurement device' (a concept in QM with no concrete definition), we no longer use deterministic linear evolution equations. Instead, we have to switch to a non-deterministic non-linear formalism. The non-determinism is conceptually unsatisfying, but isn't the main issue. Since the Schroedinger's equation can predict the dynamics of any collection of particles, it should be able to predict the dynamics of the measurement device. However, that doesn't seem to be the case.

The measurement problem can also be understood in a different way. Quantum mechanics has been spectacularly successful at predicting the behavior of microscopic particles, such as electrons and atoms, but the macroscopic world doesn't exhibit any of the weirdness of quantum mechanics. Nothing around us seems to be in a superposition of different states, and no large object is entangled with any other large object. We'd like to understand why the macroscopic world is so well described by classical mechanics.

Theoretical solutions to these issues exist. String theory and loop quantum gravity promote gravity to the quantum realm. However, the signatures of quantum gravity are extremely weak and cannot be detected with current state-of-the-art technology. As a result, these theories are outside this thesis' scope. We are only concerned with theories that are falsifiable in the near future. The Everett interpretation of QM, Stochastic mechanics [13], and Bohmian Mechanics all resolve the measurement problem. With the possible exception of Stochastic Mechanics, they make the exact

same predictions as standard QM, and so are not falsifiable and are outside this thesis' scope. Ultimately, only experiments can decide whether a theory is correct.

Other solutions exist, but they are not as popular because they suffer from some conceptual issues and their formalism isn't as appealing (Occam's razor would choose other solutions over them). Nonetheless, researchers have recently demonstrated that these theories are falsifiable with current optomechanics technology. This thesis builds upon their work. We show how current optomechanics experiments place bounds on some of the parameters of some of these theories. We also discuss how low-frequency optomechanics experiments can test the idea that gravity is fundamentally classical. Moreover, we show that fundamentally classical gravity doesn't necessarily violate causality.

Along the way, we make contributions to the fundamental theory of optomechanics. We introduce two new bases that one can view environment modes with. The first basis reduces the interaction between a linear optomechanical system (with a finite number of internal modes) and an environment with an infinite number of internal modes to an interaction with finite degrees of freedom. The second basis simplifies the correlation structure between an optomechanical system and its environment at any particular time: the system is only correlated with a finite number of effective environment modes. This simplified entanglement structure allowed us to derive the one-shot quantum Cramer-Rao bound in a simple way. We also use this structure to explain why adiabatically eliminating a lossy cavity can grossly underestimate the conditional variances of a strongly-monitored cavity-optomechanical setup. When such a setup is strongly driven, a small amount of information becomes trapped in the cavity's state, and a large amount of information about the test mass escapes to the environment. We can recover the latter information by measuring the outgoing light, thereby reducing our uncertainty about the test mass' state. However, eventually we become limited by the information that is locked in the cavity and which we cannot recover. Finally, an important goal of optomechanics is to prepare a test mass in a state with a negative Wigner function (which is an indisputable sign of quantum behavior). A promising proposal, which has been partially realized in experiments, is to use a photon counter and an appropriately detuned laser. Photon counting is a non-linear measurement scheme, which greatly complicates the theory as it is no longer linear. We developed an analytic filter to obtain the conditional state of such a system. We hope that our work will help researchers explore optomechanics topologies that make use of photon counters.

The rest of this chapter briefly reviews objective collapse models, and the theory

that gravity is fundamentally classical. This chapter also provides short summaries of my projects. The subsequent chapters contain my works on these projects.

1.2 Introduction to collapse models

This section briefly reviews objective collapse models. We refer the interested reader to Refs. [5, 4, 16] for an exhaustive review.

Objective collapse models modify Schroedinger's equation to solve the measurement problem. Such a modification has to satisfy five constraints. First, it has to be non-linear, because measurements seem to break the linearity of quantum mechanics. Second, the modification is stochastic because non-linear modifications of quantum mechanics violate the no-signaling condition [35]. Although we show this isn't always the case (see Chapter 4), making collapse models stochastic greatly simplifies them. Otherwise, one would have to determine how a deterministic theory could agree with Born's rule. Third, the predictions of collapse models have to match Born's rule. There is evidence, but no definitive proof, that collapse models agree with Born's rule for any measurement topology [6, 5]. Fourth, the predictions have to match existing experimental data. This means that the modifications to Schroedinger's equation should negligibly affect the behavior of microscopic particles, while strongly affecting the dynamics of macroscopic bodies to the extent that they'd behave classically. Fifth, the theory has to be causal.

One could argue that spontaneous collapse models should also be consistent with relativistic quantum field theories. Relativistic extensions of collapse models is an ongoing research project. It is a difficult endeavor because the Bell test experiments imply that the wavefunction collapses instantaneously (or at least faster than the speed of light).

Objective collapse models seem daunting to learn because there are so many of them. As in Refs. [40, 38, 14], we will present a unified view of most collapse models, and then specialize to two of the most popular models: the Continuous Spontaneous Localization (CSL) model, and the Diosi-Penrose (DP) model.

Ironically, even though objective collapse models were proposed to resolve the measurement problem, they can be stated in terms of the formalism of continuous measurements in standard quantum mechanics. In fact, continuous and Markovian modifications that satisfy the constraints we've indicated above have to correspond to the continuous measurement of a particular operator [3, 15]. For CSL and DP,

that particular operator is a smeared version of the mass density operator:

$$\hat{\Phi}(\boldsymbol{x}) = \sum_j m_j \hat{\Phi}_j(\boldsymbol{x}), \tag{1.1}$$

$$\hat{\Phi}_j(\boldsymbol{x}) = \int d^3\boldsymbol{y}\, g(\boldsymbol{y}-\boldsymbol{x})\, \psi_j^\dagger(\boldsymbol{y})\, \psi(\boldsymbol{y}), \tag{1.2}$$

where g is the smearing function, j labels different matter fields, and $\psi_j^\dagger(\boldsymbol{y})$ creates a particle from the jth matter field at location $\boldsymbol{y}$. It is no surprise that CSL and DP pick the mass density operator at different locations to be the degree of freedom that is monitored, because collapse models need to prevent superpositions of massive bodies over large distances. In the non-relativistic limit, $\hat{\Phi}(\boldsymbol{x})$ in first quantized form is (assuming just one type of particle)

$$\hat{\Phi}(\boldsymbol{x}) \xrightarrow[quantization]{first} m \int d^3\boldsymbol{y}\, g(\boldsymbol{y}-\boldsymbol{x})\, |\boldsymbol{y}\rangle \langle \boldsymbol{y}|. \tag{1.3}$$

$\hat{\Phi}(\boldsymbol{x})$ will be monitored everywhere, resulting in the master equation ($\hbar = 1$)

$$\begin{aligned} d\hat{\rho}(t) = & -i\left[\hat{H}, \hat{\rho}(t)\right] dt - \frac{1}{8}\int d^3\boldsymbol{x} d^3\boldsymbol{y} \Gamma(\boldsymbol{x},\boldsymbol{y}) \left[\hat{\Phi}(\boldsymbol{x}), \left[\hat{\Phi}(\boldsymbol{y}), \hat{\rho}(t)\right]\right] dt \\ & + \frac{1}{2}\int d^3\boldsymbol{x} d^3\boldsymbol{y} \Gamma(\boldsymbol{x},\boldsymbol{y}) \mathcal{H}\left[\hat{\Phi}(\boldsymbol{x})\right](\hat{\rho}(t))\, dW(\boldsymbol{y},t), \end{aligned} \tag{1.4}$$

where $\hat{H}$ is the total Hamiltonian for the system, and the superoperator $\mathcal{H}$ is

$$\mathcal{H}\left[\hat{\Phi}(\boldsymbol{x})\right](\hat{\rho}) = \left\{\hat{\Phi}(\boldsymbol{x}), \hat{\rho}\right\} - 2\mathrm{Tr}\left(\hat{\Phi}(\boldsymbol{x})\,\hat{\rho}\right)\hat{\rho}. \tag{1.5}$$

$dW(\boldsymbol{y},t)$ is a Brownian motion process and its correlation function is

$$\mathbb{E}\left(dW(\boldsymbol{y},t)\, dW(\boldsymbol{x},t')\right) = \Gamma^{-1}(\boldsymbol{x},\boldsymbol{y})\, \delta(t-t')\, dt^2. \tag{1.6}$$

It is important to note that Eq. (1.4) is just a way to present and interpret collapse models, which are phenomenological and were created to address the measurement problem. Collapse models were not derived from first principles and they have no ontologies associated with them. Nonetheless, Eq. (1.4) makes a substantial claim: such an evolution equation describes all measurements (even non-position measurements, such as measurements of spin). Only one evolution equation is enough to describe all quantum phenomena and we no longer have to interrupt unitary evolution with projection operators.

For CSL and DP, g is a Gaussian (it's width is traditionally denoted as r_{CSL} for CSL, and a 'regularization parameter' for DP). CSL simply chooses uncorrelated measurement results:

$$\Gamma_{CSL}(\boldsymbol{x}, \boldsymbol{y}) = \gamma \delta(\boldsymbol{x} - \boldsymbol{y}), \tag{1.7}$$

while DP chooses

$$\Gamma_{DP}(\boldsymbol{x}, \boldsymbol{y}) = \frac{\gamma}{|\boldsymbol{x} - \boldsymbol{y}|}. \tag{1.8}$$

For the DP model, γ has the same dimensions as the gravitational constant G. This isn't surprising because DP is motivated (by heuristic arguments) to gravity introducing noise in the Schroedinger equation because the time derivative in this equation is ambiguous when spacetime is in a superposition state.

In Eq. (1.4), we don't have access to the measurement record and so we have to take the expectation value of $d\hat{\rho}$ with respect to the stochastic variables dW. The last term in Eq. (1.4) averages to 0, and we are left with the predictions of standard quantum mechanics (the first term), and decoherence (the second term) which will be the signature of objective collapse models. In optomechanics, the decoherence results in an additional white noise force on the test mass' center of mass motion (see supplemental material of [24]).

Various experiments have placed upper bounds on CSL and DP's parameters. For example, we showed that the space experiment LISA pathfinder places the best bounds on CSL and DP at low frequencies. Theorists have also placed rough lower bounds by imposing that the CSL and DP models have to be strong enough to match the fast rate at which measurement devices collapse a wavefunction. The upper and lower bounds are still separated by orders of magnitude. It might be a while before we can decisively rule out collapse models.

Finally, we end with some hope. Although collapse models are justifiably ad-hoc and non-elegant extensions of quantum mechanics, a recent experiment has found evidence for a non-thermal force of unknown origin [41]. The experiment doesn't offer conclusive evidence for collapse models, but warrants further investigation. The European Commission has recently awarded a €4.4 million grant for an experiment that monitors the position of small micrometer-scale levitated glass spheres at an unprecedented accuracy.

1.3 Alternatives to quantum gravity

Theorists have faced enormous difficulties in quantizing the theory of general relativity (GR). Part of the difficulty is that quantum theory and GR treat time and space

(*i.e.* spacetime) differently. In quantum mechanics, spacetime is an absolute background but is a dynamical object in GR. Nonetheless, researchers have succeeded in constructing elegant theories that quantize gravity. There is no experimental evidence for any of these theories, nor do we expect that in the near future any laboratory experiment will detect any of the very weak signatures of these theories. Because of this, some researchers have moved away from quantum gravity, and are looking at other models that reconcile quantum mechanics with gravity.

1.3.1 Overview of alternative models of quantum gravity, and outlook

The simplest alternative model first appeared nearly half a century ago by Møller and Rosenfeld [22, 32]. Specifically, they proposed that spacetime is sourced by the quantum expectation value of the stress energy tensor:

$$G_{\mu\nu} = 8\pi \left\langle \Phi | \hat{T}_{\mu\nu} | \Phi \right\rangle , \tag{1.9}$$

with $G = c = 1$, and where $G_{\mu\nu}$ is the Einstein tensor of a (3+1)-dimensional classical spacetime. $\hat{T}_{\mu\nu}$ is the operator representing the energy-stress tensor, and $|\Phi\rangle$ is the wave function of all (quantum) matter and fields that evolve within this classical spacetime. The non-relativistic limit of Eq. (1.9) is easy to understand. The probability density of a particle gravitates. For example, a single non-relativistic particle's wavefunction, $\chi(\vec{r})$, evolves as

$$i\hbar\partial_t \chi(\vec{r}, t) = \left[-\frac{\hbar^2}{2m}\nabla^2 + V(\vec{r}) + U(t, \vec{r}) \right] \chi(\vec{r}, t) , \tag{1.10}$$

where $V(\vec{r})$ is the non-gravitational potential energy at $\vec{r}$ and $U(t, \vec{r})$ is the Newtonian self-gravitational potential and is sourced by $\chi(\vec{r})$:

$$\nabla^2 U(t, x) = 4\pi G m \left| \chi(t, x) \right|^2 . \tag{1.11}$$

Recently other models have appeared that don't allow spacetime to be in an arbitrary superposition of states. This author is aware of two promising models: one is the Correlated WordLines (CWL) theory, and the other is Tilloy's *et al.* innovative use of collapse models to source gravity [40, 39]. Similar to collapse models, Tilloy's *et al.*'s models are phenomonological but we can interpret the math in terms of known linear quantum mechanics processes. The collapse model's math maps to an agent monitoring a certain degree of freedom (like the a smoothed out mass density) everywhere in space. Gravity then emerges as feedback: the agent uses

the collected measurement results to apply a feedback force everywhere in space and that is equal to the gravitational force. Compared to the Schroedinger-Newton theory, Tilloy's *et al.*'s proposals have one appealing feature: they have a clear ontology: the wavefunction isn't a probability density and a mass density at the same time.

CWL modifies the path integral by having the different paths gravitate [36]. Its structure is complicated because CWL takes quantum field theory and adds graviton propagators between different Feynman-Keldysh diagrams . Moreover, Stamp *et al.* are still working on understanding CWL's structure, and making sure it is issue-free. CWL's exact formulation has been revised lately to ensure that CWL passes quantum field theory consistency tests [2].

The author believes that understanding and contrasting the predictions of these different models will greatly benefit the alternative quantum gravity community. Since each prevents spacetime from being in arbitrary superposition, we believe their predictions won't be substantially different. Moreover, they would give us a road map to design a class of experiments that could test the idea that gravity is approximately classical. Although, each of the above models is likely to be refuted, they direct us to what the signatures of an approximately classical spacetime might look like. If such a concept is true, this class of experiments could find evidence for it.

Another important research direction is to remedy the conceptual issues that these models suffer from. As it did for us, such an endeavor could generate new ideas and variations of the models above. Eventually, we also hope that addressing the conceptual issues of these models would generate more widespread acceptance of alternatives of quantum gravity to the broader physics research community.

1.3.2 Contributions to fundamental semi-classical gravity

This thesis focuses on the experimental signatures of fundamental semi-classical gravity. Yang *et al.* determined the dynamics of an optomechanical system under the Schroedinger Newton equation [44]. Specifically, they showed that if an object has its center of mass' displacement fluctuations much smaller than fluctuations of the internal motions of its constituent atoms, then its center of mass, with quantum state $|\psi\rangle$, observes

$$i\hbar\frac{d\,|\psi\rangle}{dt} = \left[\hat{H}_{NG} + \frac{1}{2}M\omega_{SN}^2\left(\hat{x} - \langle\psi|\hat{x}|\psi\rangle\right)^2\right]|\psi\rangle \tag{1.12}$$

where M is the mass of the object, $\hat{H}_{NG}$ is the non-gravitational part of the Hamiltonian, $\hat{x}$ is the center of mass position operator, and ω_{NS} is a frequency scale that is determined by the matter distribution of the object. For materials with single atoms sitting close to lattice sites, we have

$$\omega_{SN} \equiv \sqrt{\frac{Gm}{6\sqrt{\pi}\Delta x_{zp}^3}} \tag{1.13}$$

where m is the mass of the atom, and Δx_{zp} is the standard deviation of the crystal's constituent atoms' displacement from their equilibrium position along each spatial direction due to quantum fluctuations. A pedagogical explanation of the derivation of Eq. (1.12) can be found in Ref. [18].

Eq. (1.12) isn't enough to predict the result of an experiment because it doesn't take into account thermal noise or measurements. Adding thermal noise is well-understood in linear optomechanics. We use the Langevin formalism to add a fluctuating force to the Heisenberg equations of motion. We determine the strength of the fluctuating force from the state of the bath, which is a mixed state of the form $\exp\left(-\hat{H}_{th}/k_B T\right)$ where $\hat{H}_{th}$ and T are the Hamiltonian and temperature of the thermal bath, respectively. However, Eq. (1.12) is non-linear, and in Non-Linear Quantum Mechanics (NLQM), there is no Heisenberg picture, and we cannot use density matrices. At first, we addressed these issues within the context of Eq. (1.12). We showed that for the Hamiltonian in Eq. (1.12), we can define an effective Heisenberg picture that depends on the initial or final state of the system. Moreover, we argued (but did not prove) that the thermal bath's state is composed of a mixture of coherent states, whose quantum fluctuations is just vacuum and whose classical fluctuations are related to the amplitude of the coherent states. Quantum fluctuations introduce noise through expectation values over quantum states, whereas classical fluctuations introduce noise through an ensemble average over a classical distribution of the classical thermal force's distribution.

In linear QM, Born's rule tells us how to calculate the probability of an experiment obtaining a particular measurement result. However, we discovered that in NLQM, Born's rule becomes ambiguous. We show this with a simple example. In linear QM, the probability that an initial state $|i\rangle$ evolves under some unitary operator $\hat{U}$ and is then measured to be $|m\rangle$ is

$$p_{i\to m} = \left|\langle m|\hat{U}|i\rangle\right|^2 . \tag{1.14}$$

We can write $p_{i\to m}$ in many equivalent ways. For example,

$$p_{m\to i} = \left|\left\langle i\middle|\hat{U}^\dagger\middle|m\right\rangle\right|^2 = p_{i\to m}. \tag{1.15}$$

The issue is that $p_{i\to m}$ and $p_{m\to i}$ become, in general, different in NLQM:

$$p^{NLQM}_{i\to m} = |\langle m\,|\,\mathcal{U}i\rangle|^2, \tag{1.16}$$

$$p^{NLQM}_{m\to i} = \left|\left\langle i\,\middle|\,\mathcal{U}^\dagger m\right\rangle\right|^2, \tag{1.17}$$

where $|\mathcal{U}i\rangle$ is the evolved $|i\rangle$ and $\left|\mathcal{U}^\dagger m\right\rangle$ is the backwards evolved $|m\rangle$, under a non-linear Hamiltonian. In Chapter 3, we didn't explore the issue any further, and used $p^{NLQM}_{i\to m}$ and $p^{NLQM}_{m\to i}$ as inspirations for two prescriptions that assign probabilities to measurements in NLQM. We termed the first, which is inspired by $p^{NLQM}_{i\to m}$ as pre-selection, and we termed the second, which is inspired by $p^{NLQM}_{m\to i}$ as post-selection. Pre-selection imposes the initial state of an experiment as the initial condition for the non-linear evolution, whereas post-selection imposes the measured states as conditions on the state of the system-environment at the final time of the experiment. These prescriptions allowed us to explore the range of possible signatures of fundamental semi-classical gravity, and the constraints on experiments that would detect them. We concluded that both prescriptions predict a deviation from quantum mechanics at the frequency $\sqrt{\omega^2_{cm} + \omega^2_{SN}}$ where ω_{cm} is the resonant frequency of the mechanical resonator. If $\omega_{cm} \ll \omega_{SN}$, pre-selection predicts a peak that is easily detectable with current low-frequency torsion pendulum experiments. Note that ω_{SN} can be significantly boosted by constructing the mechanical resonantor with the appropriate material. ω_{SN} is at most about 0.49 for Osmium and is 0.36 for the more common Tungsten metal. On the other hand, post-selection predicts a dip that is harder to detect. In addition to $\omega_{cm} \ll \omega_{SN}$, the input laser power has to be fine tuned, the test mass' quality factor has to be very high (around 10^7), and the temperature has to be very low (around 1K). Even then, experimentalists have to wait on the order of a month to rule out or verify the Schroedinger-Newton theory with the post-selection prescription.

After this work, we endeavored to better understand measurements in NLQM. In Chapter 4, we showed that the ambiguity of Born's rule in NLQM can be stated differently: different interpretations of quantum mechanics make different predictions in NLQM. We also showed that this ambiguity can be thought of as a degree of freedom to ensure that NLQM meets the no-signaling condition. We showed that out of the well-known interpretations of quantum mechanics, the Everett

interpretation (which the pre-selection prescription is equivalent to) doesn't violate causality. However, for fundamental semi-classical gravity, it's been ruled out decades ago [25] and more recently by LISA pathfinder. We also showed that we can craft a new prescription that doesn't violate the no-signaling condition. Whenever a measurement occurs at some spacetime location (x, t), only non-linearities in the future light cone of (x, t) get updated to incorporate the result of this measurement. We termed this prescription the causal-conditional prescription

In Chapter 5, we approach measurements in NLQM from a different perspective. We show that once we fix the initial state of a system, evolution under a non-linear Hamiltonian is equivalent to evolution under a linear Hamiltonian with feedback. Specifically, we consider non-linear Hamiltonians of the form

$$i\hbar\partial_t \left|\psi\left(t\right)\right\rangle = \hat{H}_{NLQM} \left|\psi\left(t\right)\right\rangle \tag{1.18}$$

where the non-linear Hamiltonian is

$$\hat{H}_{NLQM} = \hat{H}_L + \sum_i \beta_i \phi\left(x_i, t, \psi\left(t\right)\right) \hat{V}_i. \tag{1.19}$$

$\hat{H}_L$ is the linear part of $\hat{H}$, and doesn't depend on the wavefunction. The second term represents a classical field that couples to our quantum system through $\hat{V}_i$ at positions x_i. The classical field follows its own equation of motion:

$$\mathcal{L}\phi\left(x, t\right) = S\left(x, t, \psi\left(t\right)\right) \tag{1.20}$$

where $\mathcal{L}$ is a differential operator and $S\left(x, t, \psi\left(t\right)\right)$ is a source term that, in general, depends on $\psi\left(t\right)$. The β_i are constants. Note that the sum $\sum_i$ could in general contain an integral.

The equivalence between NLQM and quantum feedback is powerful for two reasons. First, it allows us to leverage the tools and concepts developed for quantum feedback. Second, it allows us to determine how measurements can be added to NLQM in a causal way. Feedback is causal only when the feedback force depends on measurement results collected in the past light cone of where the feedback is applied. Therefore, NLQM is causal only when the classical field $\phi\left(x, t\right)$ depends on measurement results collected in the past light cone of (x, t).

With a causal prescription for adding measurements to NLQM, and a mapping that allows us to leverage the tools of quantum feedback, we calculated the signature of the Schroedinger-Newton theory with the causal-conditional prescription. The

last outstanding issue of the Schroedinger-Newton theory is ensuring that it doesn't violate the Bianchi identity. We hope it will be resolved some day.

1.4 Overview of contributions to the theory of optomechanics

1.4.1 Advances in optomechanics

Over the past decade, our understanding of quantum state preparation, verification and control in the field of optomechanics has improved substantially [11, 21, 23]. Concurrently, optomechanics technology has seen many breakthroughs. Researchers have cooled test masses to their quantum mechanical ground state cooling [10]. They have also observed the asymmetry between the spectra of transmitted red-detuned and blue-detuned light's amplitude fluctuations when a test mass, or the collective motion of atoms, are near their ground state [33, 37, 27, 8]. Researchers now also have much better control over their experiment. In Refs. [29, 42, 17], experimentalists substantially cool their test masses through feedback control.

There have been other breakthroughs in optomechanics. In Ref. [30], Purdy *et al.* have detected signatures of the fluctuating radiation pressure force on the test mass in the outgoing light's fluctuations. Moreover, the center of mass motion of test masses has been squeezed below the Heisenberg uncertainty level [43, 28, 20]. Optomechanics has also been used to generate squeezed light [31, 34, 9]. By driving optomechanics setups in a special way, and by using photon counters instead of homodyne detection, experimentalists have measured individual quanta of phonons in mechanical resonators [19, 12].

1.4.2 Contributions to the theory of unmonitored linear optomechanics

In optomechanics, a system is driven by a continuum of light. As a result, the system has interacted and is correlated with an infinity of modes. This can be conceptually daunting, and could complicate calculations. Traditionally, researchers have worked in the Fourier domain where, at steady state, degrees of freedom at different frequencies are independent. The Fourier basis is the preferred basis to work in if one is interested in evaluating the sensitivity of an optomechanical system to a signal over a certain bandwidth. The Fourier basis has also been successfully used to analyze quantum state preparation and verification in optomechanics. However, the Fourier basis has two main drawbacks. First, we are limited to steady state dynamics which can be problematic in pulsed optomechanics, where the system's initial state isn't necessarily forgotten. Second, an optomechanical system is correlated with, and interacts with, a continuum of environment modes in the Fourier basis. This makes it difficult to solve certain optimization problems, such as optimally picking the

quadratures of the outgoing light to measure in order to maximize the entanglement between two degrees of freedom of the system (*e.g.* a cavity's field and a test mass' center of mass motion).

We developed two bases that separately simplify either the dynamics or the entanglement structure of a system with its environment. If a researcher is solely interested in either the dynamics, or the entanglement structure, then using these new bases mean that the researcher only has to consider m effective environment modes, where m is the number of degrees of freedom of the optomechanical system. However, there is a caveat. These bases have to be applied to the entirety of the environment, which is composed of different fields (such as thermal and optical bosonic fields). This means that the bases have limited practical applicability, because experimentalists can only measure optical environment modes. Nonetheless, the bases can provide analytic insights to problems that seem intractable if we limit ourselves to only measuring optical modes.

The first basis, which we discuss in detail in Chapter 6, simplifies the system's dynamics. At any particular time τ, the optomechanical interaction can be considered as a scattering process, during which Heisenberg operators of the incoming environmental modes, plus the system modes at the initial time of the experiment, are transformed the Heisenberg operators of the outgoing environmental modes, plus the system modes at time τ.

We'll assume that the system has n degrees of freedom, whose ladder operators we denote in vector form by

$$\boldsymbol{b} = \begin{pmatrix} \hat{b}_1 & \hat{b}_2 & \dots & \hat{b}_n \end{pmatrix}^T. \tag{1.21}$$

Denote the incoming environment modes' ladder operators by

$$\boldsymbol{a}_{in} = \begin{pmatrix} \hat{a}_1 & \hat{a}_2 & \dots & \hat{a}_N \end{pmatrix}, \tag{1.22}$$

where for ease of presentation we've assumed that environment is composed of a single bosonic field, and we've discretized time from the initial time of the experiment till time τ into N time steps. Denote the time evolved counterparts of $\boldsymbol{a}_{in}$ by $\boldsymbol{a}_{out}$. In linear optimechanics, the scattering process can be written in matrix form:

$$\boldsymbol{w} = M\boldsymbol{v}. \tag{1.23}$$

where

$$\boldsymbol{w} \equiv \begin{pmatrix} \boldsymbol{a}_{out} \\ \boldsymbol{a}_{out}^{\dagger} \\ \boldsymbol{b}(\tau) \\ \boldsymbol{b}^{\dagger}(\tau) \end{pmatrix}, \quad \boldsymbol{v} \equiv \begin{pmatrix} \boldsymbol{a}_{in} \\ \boldsymbol{a}_{in}^{\dagger} \\ \boldsymbol{b}(0) \\ \boldsymbol{b}^{\dagger}(0) \end{pmatrix}. \tag{1.24}$$

By using that $\boldsymbol{w}$ satisfies the same commutation relations as $\boldsymbol{v}$, we can show that M must satisfy constraints that make it possible to define new effective incoming environment modes $\boldsymbol{A}_{in}$, and their time-evolved counterpart $\boldsymbol{A}_{out}$, that simplify the scattering process' structure into two separable parts. $\boldsymbol{b}(0)$ and n modes in $\boldsymbol{A}_{in}$ scatter into $\boldsymbol{b}(\tau)$ and n modes in $\boldsymbol{A}_{out}$. The remainder of the $N-n$ modes in $\boldsymbol{A}_{in}$ scatter into the remainder of the $N-n$ modes in $\boldsymbol{A}_{out}$, as is shown in Fig. 1.1.

The second basis, which we discuss in detail in Chapter 7, simplifies the system's entanglement structure with its environment at any particular time τ. Before we present this basis, we will introduce some basic notation. The system's modes occupy a Gaussian Wigner function with a covariance matrix we denote by V_{sys}. Similarly, the environment modes occupy a Gaussian Wigner function with a covariance matrix we denote by V_{env}. Moreover, denote the eigenoperators associated the symplectic eigenvalues of V_{sys} by $\boldsymbol{s}$, and the eigenoperators associated with the symplectic eigenvalues of V_{env} by $\boldsymbol{e}$. For example, to obtain $\boldsymbol{s}$, we symplectically diagonalize V_{sys}, which means we find a symplectic matrix S that satisfies

$$SV_{sys}S^{T} = \Lambda \tag{1.25}$$

where Λ is a block diagonal matrix of the form

$$\oplus_{i=1}^{n} \begin{pmatrix} \nu_i & 0 \\ 0 & \nu_i \end{pmatrix} \tag{1.26}$$

and we've assumed again that the system has n degrees of freedom. The existence of S is guaranteed by the Williamson theorem. $\boldsymbol{s}$ is

$$S\boldsymbol{x}(\tau) \tag{1.27}$$

where $\boldsymbol{x}(\tau)$ is a vector of $2n$ operators in the Heisenberg picture. Each operator corresponds to a quadrature of a degree of freedom of the system (for example, if the system has one degree of freedom, the center of mass motion of a test mass, then $\boldsymbol{x}(\tau) = \begin{pmatrix} \hat{x}(\tau) & \hat{p}(\tau) \end{pmatrix}^{T}$).

The phase-space Schmidt decomposition theorem tells us that in the new basis $\boldsymbol{e}$, all

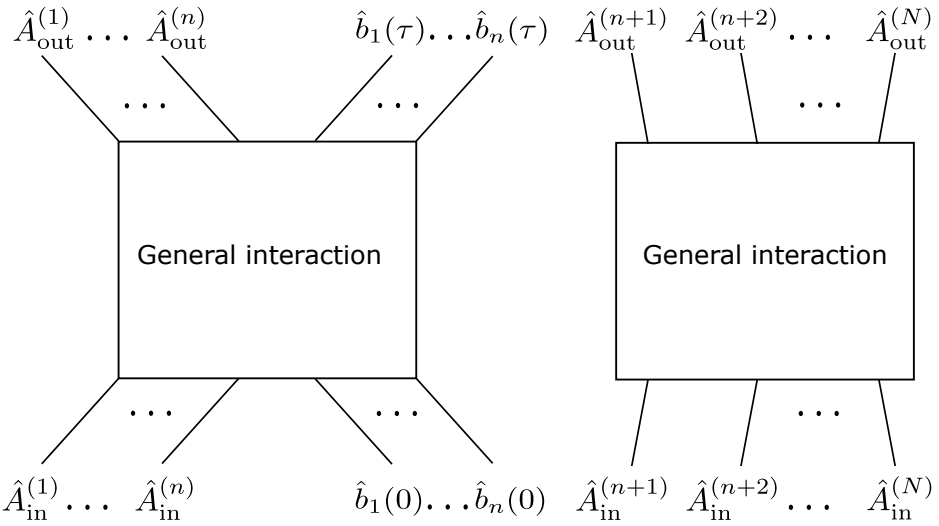

Figure 1.1: An optomechanical system with n degrees of freedom interacts with n effective input modes, $\hat{A}^{(1)}_{in}$ through $\hat{A}^{(n)}_{in}$, which evolve into n effective output modes, $\hat{A}^{(1)}_{out}$ through $\hat{A}^{(n)}_{out}$. The operators $\hat{b}_1$ through $\hat{b}_n$ represent system degrees of freedom. The remainder of the effective environment modes scatter into themselves and nothing else.

modes, except n, are in vacuum [7, 1]. Each of these n modes is correlated with only one mode of $\boldsymbol{s}$ and with nothing else. With this simplified entanglement structure, we showed that we can understand the one-shot quantum Cramer-Rao bound in a simple way, and seemingly intractable problems, like maximizing the entanglement between a test mass and a cavity, become open to large-scale numerical analysis. However, we have to make the assumption that we can measure any commuting environment modes. Although this assumption is unrealistic, it allows to efficiently sweep a large parameter regime, and so find promising optomechanics topologies that we'd then analyze more carefully.

1.4.3 Contributions to conditional optomechanics

We cannot directly extract information from an optomechanical system. We need a probe (usually a driving laser) to interact with the system. We then measure the outgoing probe's degrees of freedom. Processing the measurement results would give us information about the state of the system, and on any external forces that act on the system. Moreover, we can use the probe to steer the system towards quantum states of interest. The system doesn't just partially imprint its state on the probe. The interaction between the system and the probe is reciprocal, so the probe, with its own state and fluctuations, partially imprints itself on the system. Moreover,

the interaction entangles the system to the probe, so that when we measure the probe, the system's state changes through wavefunction collapse. In this section, we are interested in the conditional dynamics of the system, which are its dynamics conditioned on the measurement results of the probe.

The conditional dynamics are simplest when we linearly measure only commuting observables of the probe (for light, this means a homodyne or heterodyne measurement scheme), when the probe's state is Gaussian and when the probe drives the system strongly enough that the interaction between them can be linearized. In such a case, Helge *et al.* have shown that the optomechanical system can be mapped to a classical dynamical system [23], opening up classical estimation and control theory tools (which this author has enthusiastically used) to the quantum optomechanics researcher. The mapping allows us to obtain analytic insights into the system's conditional dynamics, and poses an interesting question: is a linear Gaussian quantum optomechanical system effectively classical? A system is indisputably quantum when its Wigner function is negative over some region, but the mapping tells us that a linear Gaussian optomechanical system has a Gaussian and so positive Wigner function. Nonetheless, such systems could be genuinely quantum because Gaussian Wigner functions can exhibit entanglement, a distinctly quantum property, and more importantly, a macroscopic test mass can have a Gaussian Wigner function that is highly delocalized in space. Classical macroscopic objects are never at multiple locations at the same time! On the other hand, in classical control theory, the fundamental object whose dynamics we track is a probability distribution (*i.e.* our uncertainty) over a system's degrees of freedom. As a result, this mapping is a stark example of a century old question in quantum mechanics: does the wavefunction represent anything real or is it a subjective quantity containing our knowledge about the world?

In Chapter 8, we show that studying the conditional dynamics of a cavity-optomechanical system requires more care than studying the unconditional dynamics. When a cavity is sufficiently lossy, it can be adiabatically eliminated from the dynamics. However, if the system is measured fast enough, then such an approximation fails. We used the phase-space Schmidt decomposition theorem to gain analytic insights on why this occurs. As we drive an optomechanical system stronger and stronger, the system's fluctuations become increasingly dominated by the fluctuations of the optical bath (*i.e.* the system becomes increasingly slaved by the optical bath). This is the ideal case for quantum state preparation, as when we measure the outgoing light, we eliminate our uncertainty about the optical bath's state, and so we project the system into a highly pure state. However, in a cavity-optomechanical system, there are

two degrees of freedom: the cavity field and the test mass' center of mass motion. Measuring the optical bath gives us information on their *joint* state. Entanglement between them can limit us from extracting a lot information about either of them. Adiabatic elimination fails when we become limited by the entanglement between the cavity and the test mass. We've extracted so much information about the test mass that we become limited by the information about the test mass that is locked in the cavity.

In Chapter 9, we develop an analytic filter for calculating the state of an optomechanical system that is driven by Gaussian states and interacts linearly, conditioned on the measurement results of a photon counter. This work was motivated by Galland *et al.*'s proposal to use photon counters and appropriately detuned light to prepare test masses in a Fock state [26]. The formalism they used to show that the test mass is in a Fock state is only applicable to simple setups. We hope that our filter will help researchers explore a range of optomechanics topologies that make use of photon counters.

Bibliography

[1] Gerardo Adesso. *Entanglement of Gaussian states*. PhD thesis, Salerno U., 2007.

[2] A. O. Barvinsky, D. Carney, and P. C. E. Stamp. Structure of correlated worldline theories of quantum gravity. *Phys. Rev. D*, 98:084052, Oct 2018.

[3] Angelo Bassi, Detlef Dürr, and Günter Hinrichs. Uniqueness of the equation for quantum state vector collapse. *Phys. Rev. Lett.*, 111:210401, Nov 2013.

[4] Angelo Bassi and GianCarlo Ghirardi. Dynamical reduction models. *Physics Reports*, 379(5):257 – 426, 2003.

[5] Angelo Bassi, Kinjalk Lochan, Seema Satin, Tejinder P. Singh, and Hendrik Ulbricht. Models of wave-function collapse, underlying theories, and experimental tests. *Rev. Mod. Phys.*, 85:471–527, Apr 2013.

[6] Angelo Bassi and Davide G M Salvetti. The quantum theory of measurement within dynamical reduction models. *Journal of Physics A: Mathematical and Theoretical*, 40(32):9859, 2007.

[7] Alonso Botero and Benni Reznik. Modewise entanglement of gaussian states. *Phys. Rev. A*, 67:052311, May 2003.

[8] Nathan Brahms, Thierry Botter, Sydney Schreppler, Daniel W. C. Brooks, and Dan M. Stamper-Kurn. Optical detection of the quantization of collective atomic motion. *Phys. Rev. Lett.*, 108:133601, Mar 2012.

[9] Daniel W. C. Brooks, Thierry Botter, Sydney Schreppler, Thomas P. Purdy, Nathan Brahms, and Dan M. Stamper-Kurn. Non-classical light generated by quantum-noise-driven cavity optomechanics. *Nature*, 488(7412):476–480, Aug 2012.

[10] J. Chan, T. P. M. Alegre, A. H. Safavi-Naeini, J. T. Hill, A. Krause, S. Gröblacher, M. Aspelmeyer, and O. Painter. Laser cooling of a nanomechanical oscillator into its quantum ground state. *Nature*, 478:89–92, October 2011.

[11] Yanbei Chen. Macroscopic quantum mechanics: theory and experimental concepts of optomechanics. *Journal of Physics B: Atomic, Molecular and Optical Physics*, 46(10):104001, 2013.

[12] Justin D. Cohen, Sean M. Meenehan, Gregory S. MacCabe, Simon Groblacher, Amir H. Safavi-Naeini, Francesco Marsili, Matthew D. Shaw, and Oskar Painter. Phonon counting and intensity interferometry of a nanomechanical resonator. *Nature*, 520(7548):522–525, Apr 2015. Letter.

[13] M. Derakhshani. Stochastic Mechanics Without Ad Hoc Quantization: Theory And Applications To Semiclassical Gravity. *ArXiv e-prints*, March 2018.

[14] L. Diósi. How to teach and think about spontaneous wave function collapse theories: not like before. *ArXiv e-prints*, October 2017.

[15] Lajos Diósi. Comment on "uniqueness of the equation for quantum state vector collapse". *Phys. Rev. Lett.*, 112:108901, Mar 2014.

[16] Giancarlo Ghirardi. Collapse theories. In Edward N. Zalta, editor, *The Stanford Encyclopedia of Philosophy*. Metaphysics Research Lab, Stanford University, fall 2018 edition, 2018.

[17] Jan Gieseler, Bradley Deutsch, Romain Quidant, and Lukas Novotny. Subkelvin parametric feedback cooling of a laser-trapped nanoparticle. *Phys. Rev. Lett.*, 109:103603, Sep 2012.

[18] Domenico Giulini and André Großardt. Centre-of-mass motion in multiparticle schrödinger–newton dynamics. *New Journal of Physics*, 16(7):075005, 2014.

[19] Sungkun Hong, Ralf Riedinger, Igor Marinković, Andreas Wallucks, Sebastian G. Hofer, Richard A. Norte, Markus Aspelmeyer, and Simon Gröblacher. Hanbury brown and twiss interferometry of single phonons from an optomechanical resonator. *Science*, 2017.

[20] F. Lecocq, J. B. Clark, R. W. Simmonds, J. Aumentado, and J. D. Teufel. Quantum nondemolition measurement of a nonclassical state of a massive object. *Phys. Rev. X*, 5:041037, Dec 2015.

[21] Haixing Miao, Stefan Danilishin, Helge Müller-Ebhardt, Henning Rehbein, Kentaro Somiya, and Yanbei Chen. Probing macroscopic quantum states with a sub-heisenberg accuracy. *Phys. Rev. A*, 81:012114, Jan 2010.

[22] C. Moller. *Les Theories Relativistes de la Gravitation*. CNRS, Paris, 1962.

[23] Helge Müller-Ebhardt, Henning Rehbein, Chao Li, Yasushi Mino, Kentaro Somiya, Roman Schnabel, Karsten Danzmann, and Yanbei Chen. Quantum-state preparation and macroscopic entanglement in gravitational-wave detectors. *Phys. Rev. A*, 80:043802, Oct 2009.

[24] Stefan Nimmrichter, Klaus Hornberger, and Klemens Hammerer. Optomechanical sensing of spontaneous wave-function collapse. *Phys. Rev. Lett.*, 113:020405, Jul 2014.

[25] Don N. Page and C. D. Geilker. Indirect evidence for quantum gravity. *Phys. Rev. Lett.*, 47:979–982, Oct 1981.

[26] Don N. Page and C. D. Geilker. Indirect evidence for quantum gravity. *Phys. Rev. Lett.*, 47:979–982, Oct 1981.

[27] R. W. Peterson, T. P. Purdy, N. S. Kampel, R. W. Andrews, P.-L. Yu, K. W. Lehnert, and C. A. Regal. Laser cooling of a micromechanical membrane to the quantum backaction limit. *Phys. Rev. Lett.*, 116:063601, Feb 2016.

[28] J.-M. Pirkkalainen, E. Damskägg, M. Brandt, F. Massel, and M. A. Sillanpää. Squeezing of quantum noise of motion in a micromechanical resonator. *Phys. Rev. Lett.*, 115:243601, Dec 2015.

[29] M. Poggio, C. L. Degen, H. J. Mamin, and D. Rugar. Feedback cooling of a cantilever's fundamental mode below 5 mk. *Phys. Rev. Lett.*, 99:017201, Jul 2007.

[30] T. P. Purdy, R. W. Peterson, and C. A. Regal. Observation of radiation pressure shot noise on a macroscopic object. *Science*, 339(6121):801–804, 2013.

[31] T. P. Purdy, P.-L. Yu, R. W. Peterson, N. S. Kampel, and C. A. Regal. Strong optomechanical squeezing of light. *Phys. Rev. X*, 3:031012, Sep 2013.

[32] L. Rosenfeld. On quantization of fields. *Nuclear Physics*, 40(0):353 – 356, 1963.

[33] Amir H. Safavi-Naeini, Jasper Chan, Jeff T. Hill, Thiago P. Mayer Alegre, Alex Krause, and Oskar Painter. Observation of quantum motion of a nanomechanical resonator. *Phys. Rev. Lett.*, 108:033602, Jan 2012.

[34] Amir H. Safavi-Naeini, Simon Groblacher, Jeff T. Hill, Jasper Chan, Markus Aspelmeyer, and Oskar Painter. Squeezed light from a silicon micromechanical resonator. *Nature*, 500(7461):185–189, Aug 2013. Letter.

[35] Christoph Simon, Vladimír Bužek, and Nicolas Gisin. No-signaling condition and quantum dynamics. *Phys. Rev. Lett.*, 87:170405, Oct 2001.

[36] P. C. E. Stamp. Rationale for a correlated worldline theory of quantum gravity. *New Journal of Physics*, 17(6):065017, June 2015.

[37] J. D. Teufel, T. Donner, D. Li, J. W. Harlow, M. S. Allman, K. Cicak, A. J. Sirois, J. D. Whittaker, K. W. Lehnert, and R. W. Simmonds. Sideband cooling of micromechanical motion to the quantum ground state. *Nature*, 475:359–363, July 2011.

[38] Antoine Tilloy. *Mesure continue en mécanique quantique : quelques résultats et applications*. PhD thesis, 2016. Thèse de doctorat dirigée par Bernard, Denis Physique Paris Sciences et Lettres 2016.

[39] Antoine Tilloy. Ghirardi-rimini-weber model with massive flashes. *Phys. Rev. D*, 97:021502, Jan 2018.

[40] Antoine Tilloy and Lajos Diósi. Sourcing semiclassical gravity from spontaneously localized quantum matter. *Phys. Rev. D*, 93:024026, Jan 2016.

[41] A. Vinante, R. Mezzena, P. Falferi, M. Carlesso, and A. Bassi. Improved noninterferometric test of collapse models using ultracold cantilevers. *Phys. Rev. Lett.*, 119:110401, Sep 2017.

[42] D. J. Wilson, V. Sudhir, N. Piro, R. Schilling, A. Ghadimi, and T. J. Kippenberg. Measurement-based control of a mechanical oscillator at its thermal decoherence rate. *Nature*, 524:325–329, August 2015.

[43] E. E. Wollman, C. U. Lei, A. J. Weinstein, J. Suh, A. Kronwald, F. Marquardt, A. A. Clerk, and K. C. Schwab. Quantum squeezing of motion in a mechanical resonator. *Science*, 349(6251):952–955, 2015.

[44] Huan Yang, Haixing Miao, Da-Shin Lee, Bassam Helou, and Yanbei Chen. Macroscopic quantum mechanics in a classical spacetime. *Phys. Rev. Lett.*, 110:170401, Apr 2013.

Chapter 2

LISA PATHFINDER APPRECIABLY CONSTRAINS COLLAPSE MODELS

B. Helou, B J. J. Slagmolen, D. E. McClelland, and Y. Chen, 2017, PRD **95**, 084054

Abstract

Spontaneous collapse models are phenomological theories formulated to address major difficulties in macroscopic quantum mechanics. We place significant bounds on the parameters of the leading collapse models, the Continuous Spontaneous Localization (CSL) model and the Diosi-Penrose (DP) model, by using LISA Pathfinder's measurement, at a record accuracy, of the relative acceleration noise between two free-falling macroscopic test masses. In particular, we bound the CSL collapse rate to be at most $(2.96 \pm 0.12)\times 10^{-8}$ s^{-1}. This competitive bound explores a new frequency regime, 0.7 mHz to 20 mHz, and overlaps with the lower bound $10^{-8\pm2}$ s^{-1} proposed by Adler in order for the CSL collapse noise to be substantial enough to explain the phenomenology of quantum measurement. Moreover, we bound the regularization cut-off scale used in the DP model to prevent divergences to be at least 40.1 ± 0.5 fm, which is larger than the size of any nucleus. Thus, we rule out the DP model if the cut-off is the size of a fundamental particle.

2.1 Introduction

Spontaneous collapse models are modifications of quantum mechanics which have been proposed to explain why macroscopic objects behave classically, and to address the measurement problem. The most widely studied collapse models are the Continuous Spontaneous Localization (CSL) and the Diosi-Penrose (DP) models.

The CSL model is parametrized by two scales: λ_{CSL}, which sets the strength of the collapse noise, and r_{CSL}, which sets the correlation length of the noise. For a nucleon in a spatial superposition of two locations separated by a distance much greater than r_{CSL}, λ_{CSL} is the average localization rate [1]. The quantity r_{CSL} has usually been phenomenologically taken to be 100 nm [6], and we will follow this convention.

The DP model adds stochastic fluctuations to the gravitational field, and is mathematically equivalent to the gravitational field being continuously measured [11, 10, 6]. The latter statement leaves the DP model with no free parameters, but a regulariza-

tion parameter, σ_{DP}, is usually introduced to prevent divergences for point masses.

Nimmrichter et al., in [18], show that the effect of these models on an optomechanical setup, where the center of mass position of a macroscopic object is probed, can be summarized by an additional white noise force, $F(t)$, acting on the system, and with a correlation function of

$$\langle F(t) F(t') \rangle = D_C \delta(t - t') . \tag{2.1}$$

For CSL, D_C is given by

$$D_{CSL} = \lambda_{CSL} \left(\frac{\hbar}{r_{CSL}} \right)^2 \alpha \tag{2.2}$$

with α a geometric factor [18]. LISA pathfinder has quasi-cubic test masses, which we will approximate as perfect cubes. For a cube with length $b \gg r_{CSL}$,

$$\alpha \approx \frac{8\pi\rho^2 r_{CSL}^4 b^2}{m_0^2} \tag{2.3}$$

where ρ is the material density, and m_0 the mass of a nucleon. For the DP model, D_C is given by

$$D_{DP} \approx \frac{G\hbar}{6\sqrt{\pi}} \left(\frac{a}{\sigma_{DP}} \right)^3 M\rho \tag{2.4}$$

with M the test mass' mass, and a the lattice constant of the material composing the test mass [18].

An optomechanics experiment would need to have very low force noise to significantly constrain collapse models. LISA pathfinder measures the relative acceleration noise between two free-falling test masses at a record accuracy of $\sqrt{S_a} = 5.2 \pm 0.1$ fm s$^{-2}/\sqrt{Hz}$ for frequencies between 0.7 mHz and 20 mHz [4], and so is a promising platform to test collapse models. We will use S_a, and relevant details on the LISA pathfinder test mass which we present in table 2.1, to provide an upper bound on λ_{CSL} and a lower bound on σ_{DP}.

We note that S_a has steadily decreased by about a factor of 1.5 since the start of science operations in LISA pathfinder [4], and has continued to significantly decrease since the results were published in June 2016 [22]. For the remainder of this article, we will use the conservative value of 5.2 fm s$^{-2}/\sqrt{Hz}$ for $\sqrt{S_a}$, but we

Table 2.1: LISA pathfinder test mass parameters (Ref. [3]). We estimated ρ and a with weighted averages of the densities and lattice constants, respectively, of the materials in the alloy that the test masses are made out of. The composition of this alloy is 73% Au and 27% Pt.

Quantity	Description	Value
M	Mass	1.928 kg
ρ	Density	19881 kg/m^3
a	Lattice constant	4.0 Å
b	Side length	46 mm

will also present bounds obtained from a postulated sensitivity level of

$$\sqrt{S_a^{pos}} = 3.5 \text{ fm s}^{-2}/\sqrt{Hz},$$

which is about 1.5 times smaller than $\sqrt{S_a}$.

2.2 Constraining the collapse models

We can bound the parameters of collapse models by measuring the force noise of a test mass in an experiment, and attributing unknown noise to the stochastic force $F(t)$.

In LISA pathfinder, Brownian thermal noise provides the dominant contribution to the differential acceleration noise at frequencies between 1 mHz and 20 mHz. However, the value of this contribution is not precisely known. As a result, we follow a simple and uncontroversial analysis which attributes all acceleration noise to the collapse models' stochastic forces:

$$S_a = 2S_F/M^2, \tag{2.5}$$

where $S_F = 2D_C$ is the single sided spectrum of the collapse force. The factor of 2 in Eq. (2.5) follows from the collapse noise on each test mass adding up, because the spontaneous collapse force acts independently on each of the two test masses, which are separated by about 38 cm, a distance much larger than r_{CSL} and σ_{DP}. Therefore, we can place an upper bound on D_C of

$$D_C \leq D_C^{max} = M^2 S_a/4. \tag{2.6}$$

Using Eq. (2.2), we can then bound λ_{CSL} to

$$\lambda_{CSL} \leq \lambda_{CSL}^{max}, \tag{2.7}$$

with

$$\lambda_{CSL}^{max} = \frac{m_0^2}{32\pi\hbar^2 r_{CSL}^2}\left(\frac{M}{\rho}\right)^2 \frac{1}{b^2} S_a \tag{2.8}$$

$$= 2.96 \times 10^{-8}\ \mathrm{s}^{-1}, \tag{2.9}$$

where we have substituted in the values shown in table 2.1 for ρ, M and b. If we use S_a^{pos} instead of S_a, then we reduce λ_{CSL}^{max} to $1.34 \times 10^{-8}\ \mathrm{s}^{-1}$.

In addition, using Eq. (2.4), we can bound σ_{DP} to

$$\sigma_{DP} \geq \sigma_{DP}^{min}, \tag{2.10}$$

with

$$\sigma_{DP}^{min} = \left(\frac{2\hbar G}{3\sqrt{\pi}}\frac{\rho}{m}\frac{1}{S_a}\right)^{1/3} a = 40.1\ \mathrm{fm}, \tag{2.11}$$

where we have substituted in the values shown in table 2.1 for ρ, M and a. If we use S_a^{pos} instead of S_a, then we increase σ_{DP}^{min} to 52.2 fm.

2.3 Discussion

LISA pathfinder provides a competitive bound on λ_{CSL}. λ_{CSL}^{max} is three orders of magnitude lower than the bound $10^{-5}\ \mathrm{s}^{-1}$, which Feldmann and Tumulka [13] calculated from Gerlich et al.'s matter wave inteferometry experiment of organic compounds up to 430 atoms large [15]. Another matter wave interferometry experiment from the same group [12] places a bound of $5 \times 10^{-6}\ \mathrm{s}^{-1}$, as calculated in [20].

Moreover, λ_{CSL}^{max} is comparable to bounds on λ_{CSL} obtained from measuring spontaneous heating from the collapse noise. Bilardello et al. place a bound of $5\times10^{-8}\ \mathrm{s}^{-1}$ [7], by analyzing the heating rate of a cloud of Rb atoms cooled down to picokelvins [17]. Note that Bilardello et al.'s bound depends on the temperature of the CSL noise field, and on the reference frame with respect to which the CSL noise field is at rest with [7]. The standard formulation of CSL has the collapse noise field at a temperature of infinity, but the theory could be modified to include different temperatures. The incorporation of dissipation within CSL is based on the dissipative CSL (dCSL) theory proposed by Smirne and Bassi [19].

Other competitive upper bounds have been obtained from cosmological data, the

lowest of which, 10^{-9} s^{-1}, is from the heating of the intergalactic medium [1]. However, this bound is also sensitive to the temperature of the collapse noise field [19]. Moreover, our interest in this article is for controlled experiments.

In addition to providing an aggressive upper bound, LISA pathfinder explores the low frequency regime of 0.7 mHz to 20 mHz. In Fig. 2.1, we compare λ_{CSL}^{max} to bounds obtained from experiments operating in different frequency regimes. If S_a^{pos} is used instead of S_a, then LISA pathfinder provides the smallest upper bound of all experiments operating below a THz scale.

LIGO's measurement of the differential displacement noise between two test masses in the frequency regime 10 Hz to 10 kHz places upper bounds of at most about 10^{-5} s^{-1}. In [21], an upper bound of about 2×10^{-8} s^{-1} is obtained by analyzing the excess heating of a nanocantilever's fundamental mode at about 3.1 kHz. A record upper bound of 10^{-11} s^{-1} is placed in [14, 9] by examining the spontaneous x-ray emission rate from Ge. This bound could be greatly reduced if the collapse noise is non-white at the very high frequency of 10^{18} s^{-1} [6].

Furthermore, the bound λ_{CSL}^{max} appreciably constrains the CSL model because it overlaps with some of the proposed lower bounds on λ_{CSL}. Adler investigates the measurement process of latent image formation in photography and places a lower bound of $\lambda_{CSL} \simeq 2.2\times10^{-8\pm2}$ s^{-1} [1]. Moreover, Bassi et al. place a lower bound of $\lambda_{CSL} \simeq 10^{-10\pm2}$ s^{-1} by investigating the measurement-like process of human vision of six photons in a superposition state [5]. Note that a lower bound of about 10^{-17} s^{-1}, proposed by Ghirardi, Pearle and Rimini [16], is also sometimes considered. Its justification comes from the requirement that an apparatus composed of about 10^{15} nucleons settle to a definite outcome in about 10^{-7} s or less [2].

LISA pathfinder also provides a competitive bound on σ_{DP}. The nanocantilever experiment [21] places a lower bound on σ_{DP} of about 1.5 fm, which is much lower than σ_{DP}^{min}. More importantly, the calculated value for σ_{DP}^{min} of 40.1 ± 0.5 fm is larger than the size of any nucleus. Consequently, σ_{DP}^{min} rules out the DP model if the regularization scale σ_{DP} is chosen to be the size of a fundamental particle such as a nucleon.

2.4 Acknowledgments

We acknowledge support from the NSF grants PHY-1404569 and PHY-1506453, from the Australian Research Council grants FT130100329 and DP160100760, and from the Institute for Quantum Information and Matter, a Physics Frontier Center.

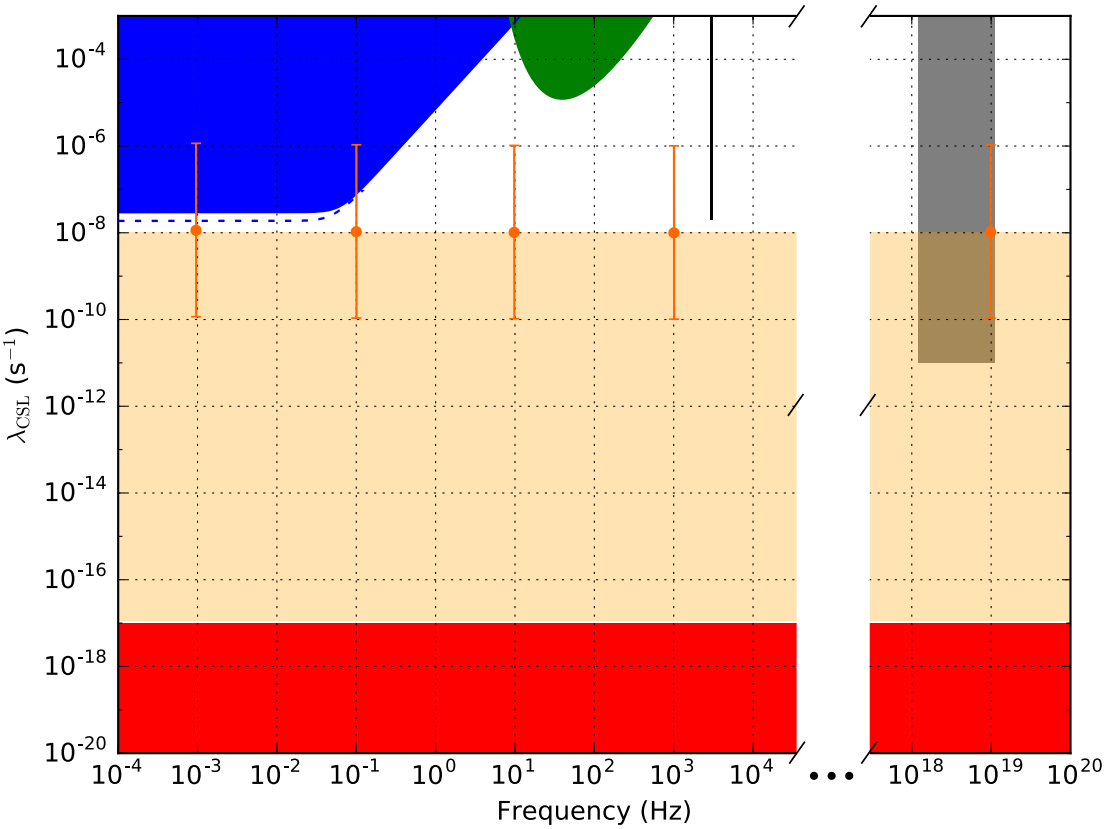

Figure 2.1: Upper and lower bounds on the CSL collapse rate λ_{CSL} obtained from laboratory experiments operating at different frequencies. Blue, green, black and gray regions: exclusion regions obtained from LISA pathfinder, LIGO, a millikelvin-cooled nanocantilever [21] and spontaneous emission from Ge [14, 9], respectively. Our calculation of the bounds obtained from LIGO follow that of [8]. The dashed blue line is the upper bound limit obtained from the LISA pathfinder results if S_a^{pos} were used instead of S_a. The red and orange domains are regions in which the collapse rate is too slow to explain the lack of macroscopic superpositions and measurements, respectively. The red region is below the lower bound of 10^{-17} s^{-1} proposed by Ghirardi, Pearle and Rimini [16]. The orange region's boundary is the Adler lower bound $10^{-8\pm2}$ s^{-1}, below which latent image formation on a photographic emulsion consisting of silver halide suspended in gelatine wouldn't occur fast enough [1]. The orange error bars reflect the uncertainty in this lower bound.

Bibliography

[1] Stephen L Adler. Lower and upper bounds on csl parameters from latent image formation and igm heating. *J. Phys. A*, 40(12):2935, 2007.

[2] Stephen L. Adler and Angelo Bassi. Is quantum theory exact? *Science*, 325(5938):275–276, 2009.

[3] F Antonucci et al. Lisa pathfinder: mission and status. *Classical and Quant. Gravity*, 28(9):094001, 2011.

[4] M. Armano et al. Sub-femto-*g* free fall for space-based gravitational wave observatories: Lisa pathfinder results. *Phys. Rev. Lett.*, 116:231101, Jun 2016.

[5] A. Bassi, D.-A. Deckert, and L. Ferialdi. Breaking quantum linearity: Constraints from human perception and cosmological implications. *EPL (Europhysics Letters)*, 92(5):50006, 2010.

[6] Angelo Bassi, Kinjalk Lochan, Seema Satin, Tejinder P. Singh, and Hendrik Ulbricht. Models of wave-function collapse, underlying theories, and experimental tests. *Rev. Mod. Phys.*, 85:471–527, Apr 2013.

[7] M. Bilardello, S. Donadi, A. Vinante, and A. Bassi. Bounds on collapse models from cold-atom experiments. *ArXiv e-prints*, May 2016.

[8] M. Carlesso, A. Bassi, P. Falferi, and A. Vinante. Experimental bounds on collapse models from gravitational wave detectors. *ArXiv e-prints*, June 2016.

[9] C. Curceanu, B. C. Hiesmayr, and K. Piscicchia. X-rays help to unfuzzy the concept of measurement. *ArXiv e-prints*, February 2015.

[10] L. Diósi. Models for universal reduction of macroscopic quantum fluctuations. *Phys. Rev. A*, 40:1165–1174, Aug 1989.

[11] L. Diósi. A universal master equation for the gravitational violation of quantum mechanics. *Physics Letters A*, 120(8):377 – 381, 1987.

[12] Sandra Eibenberger, Stefan Gerlich, Markus Arndt, Marcel Mayor, and Jens Tuxen. Matter-wave interference of particles selected from a molecular library with masses exceeding 10 000 amu. *Phys. Chem. Chem. Phys.*, 15:14696–14700, 2013.

[13] William Feldmann and Roderich Tumulka. Parameter diagrams of the grw and csl theories of wavefunction collapse. *J. Phys. A*, 45(6):065304, 2012.

[14] Qijia Fu. Spontaneous radiation of free electrons in a nonrelativistic collapse model. *Phys. Rev. A*, 56:1806–1811, Sep 1997.

[15] Stefan Gerlich, Sandra Eibenberger, Mathias Tomandl, Stefan Nimmrichter, Klaus Hornberger, Paul J. Fagan, Jens Tüxen, Marcel Mayor, and Markus Arndt. Quantum interference of large organic molecules. *Nature Communications*, 2:263, 4 2011.

[16] Gian Carlo Ghirardi, Philip Pearle, and Alberto Rimini. Markov processes in hilbert space and continuous spontaneous localization of systems of identical particles. *Phys. Rev. A*, 42:78–89, Jul 1990.

[17] Tim Kovachy, Jason M. Hogan, Alex Sugarbaker, Susannah M. Dickerson, Christine A. Donnelly, Chris Overstreet, and Mark A. Kasevich. Matter wave lensing to picokelvin temperatures. *Phys. Rev. Lett.*, 114:143004, Apr 2015.

[18] Stefan Nimmrichter, Klaus Hornberger, and Klemens Hammerer. Optomechanical sensing of spontaneous wave-function collapse. *Phys. Rev. Lett.*, 113:020405, Jul 2014.

[19] Andrea Smirne and Angelo Bassi. Dissipative continuous spontaneous localization (CSL) model. *Sci Reports*, 5:12518, 2015.

[20] M. Toroš and A. Bassi. Bounds on Collapse Models from Matter-Wave Interferometry. *ArXiv e-prints*, January 2016.

[21] A. Vinante, M. Bahrami, A. Bassi, O. Usenko, G. Wijts, and T. H. Oosterkamp. Upper bounds on spontaneous wave-function collapse models using millikelvin-cooled nanocantilevers. *Phys. Rev. Lett.*, 116:090402, Mar 2016.

[22] W. J. Weber. Private Communication.

Chapter 3

MEASURABLE SIGNATURES OF QUANTUM MECHANICS IN A CLASSICAL SPACETIME

B. Helou, J. Luo, H. Yeh, C. Shao, B. J. J. Slagmolen, D. E. McClelland, and Y. Chen, 2017, PRD **96**, 044008

Abstract

We propose an optomechanics experiment that can search for signatures of a fundamentally classical theory of gravity and in particular of the many-body Schroedinger-Newton (SN) equation, which governs the evolution of a crystal under a self-gravitational field. The SN equation predicts that the dynamics of a macroscopic mechanical oscillator's center of mass wavefunction differ from the predictions of standard quantum mechanics [29]. This difference is largest for low-frequency oscillators, and for materials, such as Tungsten or Osmium, with small quantum fluctuations of the constituent atoms around their lattice equilibrium sites. Light probes the motion of these oscillators and is eventually measured in order to extract valuable information on the pendulum's dynamics. Due to the non-linearity contained in the SN equation, we analyze the fluctuations of measurement results differently than standard quantum mechanics. We revisit how to model a thermal bath, and the wavefunction collapse postulate, resulting in two prescriptions for analyzing the quantum measurement of the light. We demonstrate that both predict features, in the outgoing light's phase fluctuations' spectrum, which are separate from classical thermal fluctuations and quantum shot noise, and which can be clearly resolved with state of the art technology.

3.1 Introduction

Advancements in quantum optomechanics has allowed the preparation, manipulation and characterization of the quantum states of macroscopic objects [1, 16, 6]. Experimentalists now have the technological capability to test whether gravity could modify quantum mechanics. One option is to consider whether gravity can lead to decoherence, as conjectured by Diosi and Penrose [21, 8, 7], where the gravitational field around a quantum mechanical system can be modeled as being continuously monitored. A related proposal is the Continuous Spontaneous Localization (CSL) model, which postulates that a different mass-density sourced field is being continuously monitored [4]. In both cases, gravity could be considered as having a

"classical component", in the sense that transferring quantum information through gravity could be impeded, or even forbidden [14]. Another option, proposed by P.C.E. Stamp, adds gravitational correlations between quantum trajectories [26].

In this paper, we consider a different, and more dramatic modification, where the gravitational interaction is kept classical. Specifically, the space-time geometry is sourced by the quantum expectation value of the stress energy tensor [24, 17, 5]:

$$G_{\mu\nu} = 8\pi \left\langle \Phi | \hat{T}_{\mu\nu} | \Phi \right\rangle, \tag{3.1}$$

with $G = c = 1$, and where $G_{\mu\nu}$ is the Einstein tensor of a (3+1)-dimensional classical spacetime. $\hat{T}_{\mu\nu}$ is the operator representing the energy-stress tensor, and $|\Phi\rangle$ is the wave function of all (quantum) matter and fields that evolve within this classical spacetime. Such a theory arises either when researchers considered gravity to be *fundamentally classical*, or when they ignored quantum fluctuations in the stress energy tensor, $T_{\mu\nu}$, in order to approximately solve problems involving quantum gravity. The latter case is referred to as *semiclassical gravity* [13], in anticipation that this *approximation* will break down if the stress-energy tensor exhibits substantial quantum fluctuations. In this article, we propose an optomechanics experiment that would test Eq. (3.1). Other experiments have been proposed [12, 9], but they do not address the difficulties discussed below.

Classical gravity, as described by Eq. (3.1), suffers from a dramatic conceptual drawback rooted in the statistical interpretation of wavefunctions. In order for the Bianchi identity to hold on the left-hand side of Eq. (3.1), the right-hand side must be divergence free, but that would be violated if we reduced the quantum state. In light of this argument, one can go back to an interpretation of quantum mechanics where the wavefunction does not reduce. At this moment, the predominant interpretation of quantum mechanics that does not have wave-function reduction is the relative-state, or "many-world" interpretation, in which all possible measurement outcomes, including macroscopically distinguishable ones, exist in the wavefunction of the universe. Taking an expectation over that wavefunction leads to a serious violation of common sense, as was demonstrated by Page and Geilker [19].

Another major difficulty is *superluminal* communication, which follows from the nonlinearities implied by Eq. (3.1) (refer to section §3.2 for explicit examples of non-linear Schroedinger equations). Superluminal communication is a *general* symptom of wavefunction collapse in nonlinear quantum mechanics [1]. Entangled and iden-

[1] We note that the issue of superluminal communication could be resolved by adding a stochastic

tically prepared states, distributed to two spatially separated parties A and B, and then followed by projections at B and a period of nonlinear evolution at A, can be used to transfer signals superluminally [22, 3, 10, 25].

In this paper, we do not solve the above conceptual obstacles. Instead, we highlight an *even more serious issue* of nonlinear quantum mechanics: its dependence on the formulation of quantum mechanics. Motivated by the *time-symmetric formulation* of quantum mechanics [23], we show that there are multiple prescriptions of assigning the probability of a measurement outcome, that are equivalent in standard quantum mechanics, but become distinct in nonlinear quantum mechanics. It is our hope that at least one such formulation will not lead to superluminal signaling. We defer the search for such a formulation to future work, and in this paper, we simply choose two prescriptions, and show that they give different experimental signatures in torsional pendulum experiments. These signatures hopefully scope out the type of behavior classical gravity would lead to if a non superluminal-signaling theory indeed exists.

This paper is organized as follows. In section 3.2, we review the non-relativistic limit of Eq. (3.1), called the *Schroedinger-Newton theory*, as applied to optomechanical setups, and without including quantum measurements. We determine that the signature of the Schroedinger-Newton theory in the free dynamics of the test mass is largest for low frequency oscillators such as torsion pendulums, and for materials, such as Tungsten and Osmium, with atoms tightly bound around their respective lattice sites. In section 3.3, we remind the reader that in nonlinear quantum mechanics the density matrix formalism cannot be used to describe thermal fluctuations. As a result, we propose a particular ensemble of pure states to describe the thermal bath's state. In section 3.4, we discuss two strategies, which we term pre-selection and post-selection, for assigning a statistical interpretation to the wavefunction in the Schroedinger-Newton theory. In section 3.5, we obtain the signatures of the pre- and post-selection prescriptions in torsional pendulum experiments. In section 3.6, we show that it is feasible to measure these signatures in state of the art experiments. Finally, we summarize our main conclusions in section 3.7.

3.2 Free dynamics of an optomechanical setup under the Schroedinger-Newton theory

In this section, we discuss the Schroedinger-Newton theory applied to optomechanical setups without quantum measurement. We first review the signature of the theory

extension to the theory of classical gravity, as was proposed by Nimmrichter [18]. However, although the theory removes the nonlinearity at the ensemble level, it also eliminates the signature of the nonlinearity in the noise spectrum.

in the free dynamics of an oscillator, and discuss associated design considerations. We then develop an effective Heisenberg picture, which we refer to as a *state dependent Heisenberg picture*, where only operators evolve in time. However, unlike the Heisenberg picture, the equations of motion depend on the boundary quantum state of the system that is being analyzed. Finally we present the equations of motion of our proposed optomechanical setup.

3.2.1 The center-of-mass Schroedinger-Newton equation

The Schrödinger-Newton theory follows from taking the non-relativistic limit of Eq. (3.1). The expectation value in this equation gives rise to a nonlinearity. In particular, a single non-relativistic particle's wavefunction, $\chi(\vec{r})$, evolves as

$$i\hbar\partial_t\chi(\vec{r},t) = \left[-\frac{\hbar^2}{2m}\nabla^2 + V(\vec{r}) + U(t,\vec{r})\right]\chi(\vec{r},t), \tag{3.2}$$

where $V(\vec{r})$ is the non-gravitational potential energy at $\vec{r}$ and $U(t,\vec{r})$ is the Newtonian self-gravitational potential and is sourced by $\chi(\vec{r})$:

$$\nabla^2 U(t,x) = 4\pi G m\,|\chi(t,x)|^2\,. \tag{3.3}$$

A many-body system's center of mass Hamiltonian also admits a simple description, which was analyzed in [29]. If an object has its center of mass' displacement fluctuations much smaller than fluctuations of the internal motions of its constituent atoms, then its center of mass, with quantum state $|\psi\rangle$, observes

$$i\hbar\frac{d\,|\psi\rangle}{dt} = \left[\hat{H}_{NG} + \frac{1}{2}M\omega_{SN}^2\left(\hat{x} - \langle\psi|\hat{x}|\psi\rangle\right)^2\right]|\psi\rangle \tag{3.4}$$

where M is the mass of the object, $\hat{H}_{NG}$ is the non-gravitational part of the Hamiltonian, $\hat{x}$ is the center of mass position operator, and ω_{SN} is a frequency scale that is determined by the matter distribution of the object. For materials with single atoms sitting close to lattice sites, we have

$$\omega_{SN} \equiv \sqrt{\frac{Gm}{6\sqrt{\pi}\Delta x_{zp}^3}} \tag{3.5}$$

where m is the mass of the atom, and Δx_{zp} is the standard deviation of the crystal's constituent atoms' displacement from their equilibrium position along each spatial direction due to quantum fluctuations.

Note that the presented formula for ω_{SN} is larger than the expression for ω_{SN} presented in [29] by a factor of $\sqrt{2}$. As explained in [11], the many body non-linear gravitational interaction term presented in Eq. (3) of [29] should not contain a factor of 1/2, which is usually introduced to prevent overcounting. The SN interaction term between one particle and another is not symmetric under exchange of both of them. For example, consider two (1-dimensional) identical particles of mass m. The interaction term describing the gravitational attraction of the first particle, with position operator $\hat{x}_1$, to the second is given by

$$-Gm^2 \int dx_1\, dx_2 \frac{|\psi(x_1, x_2)|^2}{|\hat{x}_1 - x_2|},$$

which is not symmetric under the exchange of the indices 1 and 2. Moreover, in Appendix 3.8, we show that the expectation value of the total Hamiltonian is not conserved. Instead,

$$E = \left\langle \hat{H}_{NG} + \hat{V}_{SN}/2 \right\rangle \tag{3.6}$$

is conserved, where $\hat{V}_{SN}$ is the SN gravitational potential term. As a result, we take E, which contains the factor of 1/2 present in expressions of the classical many-body gravitational energy, to be the average energy.

If the test mass is in an external harmonic potential, Eq. (3.4) becomes

$$\begin{aligned} i\hbar \frac{d|\psi\rangle}{dt} = &\left[\frac{\hat{p}^2}{2M} + \frac{1}{2} M\omega_{\mathrm{cm}}^2 \hat{x}^2 \right. \\ &\left. + \frac{1}{2} M\omega_{SN}^2 \left(\hat{x} - \langle\psi|\hat{x}|\psi\rangle\right)^2 \right] |\psi\rangle \end{aligned} \tag{3.7}$$

where $\hat{p}$ is the center of mass momentum operator, and $\omega_{\mathrm{cm}} is the resonant frequency of the crystal's motio$

Eq. (3.7) predicts distinct dynamics from linear quantum mechanics. Assuming a Gaussian initial state, Yang *et al.* show that the signature of Eq. (3.7) appears in the rotation frequency

$$\omega_q \equiv \sqrt{\omega_{cm}^2 + \omega_{SN}^2} \tag{3.8}$$

of the mechanical oscillator's quantum uncertainty ellipse in phase space. We illustrate this behavior in Fig. 3.1.

As a consequence, the dynamics implied by the nonlinearity in Eq. (3.4) are most distinct from the predictions of standard quantum mechanics when $\omega_q - \omega_{\mathrm{cm}}$ is as large as possible. This is achieved by having a pendulum with as small of an oscillation eigenfrequency as possible, and made with a material with as high of a

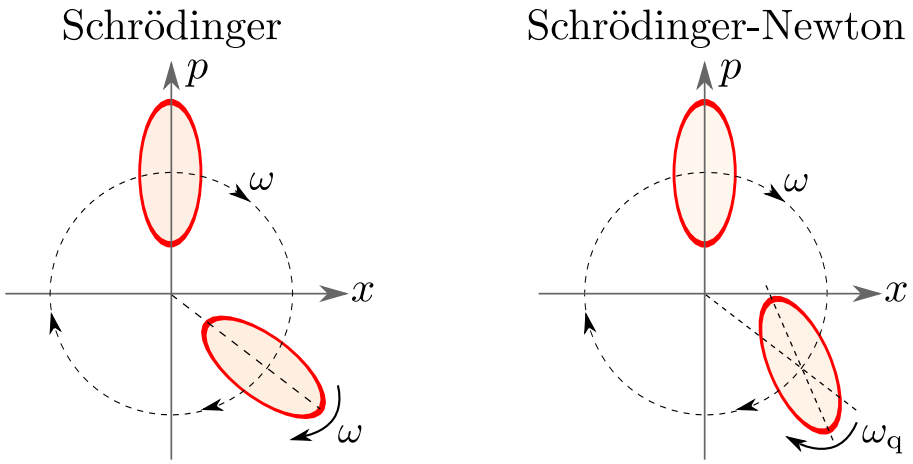

Figure 3.1: Left Panel: according to standard quantum mechanics, both the vector $(\langle\hat{x}\rangle, \langle\hat{p}\rangle)$ and the uncertainty ellipse of a Gaussian state for the center of mass of a macroscopic object rotate clockwise in phase space, at the same frequency $\omega = \omega_{CM}$. Right panel: according to Eq.(3.7), $(\langle x\rangle, \langle p\rangle)$ still rotates at $\omega_{\rm cm}$, but the uncertainty ellipse rotates at $\omega_q \equiv \sqrt{\omega_{\rm cm}{}^2 + \omega_{SN}^2} > \omega_{\rm cm}$. (Figure taken from [29]).

ω_{SN} as possible. The former condition leads us to propose the use of low-frequency torsional pendulums. To meet the latter condition, we notice that ω_{SN} depends significantly on Δx_{zp}, which can be inferred from the Debye-Waller factor,

$$B = u^2/8\pi^2 \tag{3.9}$$

where u is the rms displacement of an atom from its equilibrium position [20]. Specifically, thermal and intrinsic fluctuations contribute to u, *i.e.* $u \gtrsim \sqrt{\Delta x_{zp}^2 + \Delta x_{th}^2}$ with Δx_{th} representing the uncertainty in the internal motion of atoms due to thermal fluctuations.

In Table 3.1, we present experimental data on some materials' Debye-Waller factor, and conclude that the pendulum should ideally be made with Tungsten (W), with $\omega_{SN}^{W} = 2\pi \times 4.04\, mHz$, or Osmium (the densest naturally occurring element) with a theoretically predicted ω_{SN}^{Os} of $2\pi \times 5.49\, mHz$. Other materials such as Platinum or Niobium, with $\omega_{SN}^{Pt} = 2\pi \times 3.2\, mHz$ and $\omega_{SN}^{Nb} = 2\pi \times 1.56\, mHz$ respectively, could be suitable candidates.

3.2.2 State-dependent Heisenberg picture for nonlinear quantum mechanics

In this section, we develop an effective Heisenberg picture for non-linear Hamiltonians similar to the Hamiltonian given by Eq.(3.7). We abandon the Schroedinger picture because the dynamics of a Gaussian optomechanical system are usually

Element	ρ (10^3 kg/m^3)	B^2 (^{2})	ω_{SN} (10^{-2} s^{-1})
Silicon (Si)	2.33	0.1915	4.95
Iron (Fe) (BCC)	7.87	0.12	9.90
Germanium (Ge)	5.32	0.1341	10.39
Niobium (Nb)	8.57	0.1082	13.86
Platinum (Pt)	21.45	0.0677	28.43
Tungsten (W)	19.25	0.0478	35.92
Osmium* (Os)	22.59	0.0323	48.79

Table 3.1: Characteristic Schroedinger-Newton angular frequency ω_{SN} for several elemental crystals. Density is approximated by values at room temperature, and the Debye-Waller factor B (at 1 K) is provided by Ref. [20]. *: Note that Osmium's Debye-Waller factor is solely obtained from theoretical calculations.

examined in the Heisenberg picture where the similarity to classical equations of motion is most apparent.

We are interested in non-linear Schroedinger equations of the form

$$i\hbar\frac{d|\psi\rangle}{dt} = \hat{H}(\zeta(t))|\psi\rangle\,, \tag{3.10}$$

$$\zeta(t) = \langle\psi(t)|\hat{Z}|\psi(t)\rangle, \tag{3.11}$$

where the Hamiltonian $\hat{H}$ is a linear operator that depends on a parameter ζ, which in turn depends on the quantum state that is being evolved. Note that the Schroedinger operator $\hat{Z}$ can depend explicitly on time, ζ can have multiple components, and the Hilbert space and canonical commutation relations are unaffected by the nonlinearities.

3.2.2.1 State-dependent Heisenberg Picture

We now present the effective Heisenberg Picture. Let us identify the Heisenberg and Schroedinger pictures at the initial time $t = t_0$,

$$|\psi_H\rangle = |\psi(t_0)\rangle, \quad \hat{x}_H(t_0) = \hat{x}_S(t_0), \quad \hat{p}_H(t_0) = \hat{p}_S(t_0), \tag{3.12}$$

where $|\psi_H\rangle$ is the quantum state $|\psi\rangle$ in the Heisenberg picture, and we have used the subscripts S and H to explicitly indicate whether an operator is in the Schroedinger or Heisenberg picture, respectively. As we evolve in time in the Heisenberg Picture,

we fix $|\psi_S(t_0)\rangle$, but evolve $\hat{x}_H(t)$ according to

$$\frac{d}{dt}\hat{x}_H(t) = \frac{i}{\hbar}\left[\hat{H}_H(\zeta(t)), \hat{x}_H(t)\right] + \frac{\partial}{\partial t}\hat{x}_H(t), \tag{3.13}$$

$$\zeta(t) = \langle\psi_H|\hat{Z}_H(t)|\psi_H\rangle. \tag{3.14}$$

A similar equation holds for $\hat{p}_H(t)$. We shall refer to such equations as state-dependent Heisenberg equations of motion. Moreover, the Heisenberg picture of an arbitrary operator in the Schroedinger picture

$$\hat{O}_S = f\left(\hat{x}_S, \hat{p}_S, t\right), \tag{3.15}$$

including the Hamiltonian $\hat{H}(\zeta(t))$, can be obtained from $\hat{x}_H(t)$ and $\hat{p}_H(t)$ by:

$$\hat{O}_H\left(t\right) = f\left(\hat{x}_H\left(t\right), \hat{p}_H\left(t\right), t\right). \tag{3.16}$$

3.2.2.2 Proof of the State-Dependent Heisenberg Picture

The state-dependent Heisenberg picture is equivalent to the Schroedinger picture, if at any given time

$$\langle\psi_H|\hat{O}_H(t)|\psi_H\rangle = \langle\psi_S(t)|\hat{O}_S(t)|\psi_S(t)\rangle. \tag{3.17}$$

Before we present the proof, we motivate the existence of a Heisenberg picture with a simple argument. If we (momentarily) assume that the nonlinearity $\zeta\left(t\right)$ is known and solved for, then the non-linear Hamiltonian $\hat{H}\left(\zeta\left(t\right)\right)$ is mathematically equivalent to a linear Hamiltonian,

$$\hat{H}^L\left(\zeta\left(t\right)\right) = \hat{H}\left(\zeta\left(t\right)\right), \tag{3.18}$$

with a classical time-dependent drive $\zeta\left(t\right)$. Since there exists a Heisenberg picture associated with $\hat{H}^L\left(\zeta\left(t\right)\right)$, there exists one for the nonlinear Hamiltonian $\hat{H}\left(\zeta\left(t\right)\right)$.

We now remove the assumption that $\zeta\left(t\right)$ is known and consider linear Hamiltonians, $\hat{H}^L\left(\rho\left(t\right)\right)$, driven by general time-dependent classical drives $\lambda\left(t\right)$. To each $\hat{H}^L\left(\lambda\left(t\right)\right)$ is associated a different unitary operator $\hat{U}_\lambda\left(t\right)$ and so a different Heisenberg picture

$$\hat{O}_H\left(\lambda, t\right) = \hat{U}_\lambda^\dagger\left(t\right)\hat{O}_S\hat{U}_\lambda\left(t\right). \tag{3.19}$$

Next, we choose $\lambda(t)$ in such a way that

$$\langle\psi_H|\hat{O}_H(\lambda, t)|\psi_H\rangle = \langle\psi_S(t)|\hat{O}_S(t)|\psi_S(t)\rangle. \tag{3.20}$$

is met. For the desired effective Heisenberg picture to be self-consistent, $\lambda(t)$ must be obtained by solving

$$\lambda(t) = \left\langle \psi_H | \hat{Z}_H(\lambda, t) | \psi_H \right\rangle, \tag{3.21}$$

which, in general, is a non-linear equation in λ. We will explicitly prove that this choice of $\lambda(t)$ satisfies Eq. (3.20). Note that we will present the proof in the case that the boundary wavefunction is forward time evolved. The proof for backwards time evolution is similar.

We begin the proof by showing that λ and ζ are equal at $t = t_0$,

$$\lambda(t_0) = \left\langle \psi_S(t_0) | \hat{Z}_S | \psi_S(t_0) \right\rangle = \zeta(t_0)$$

because the Schrodinger and state-dependent Heisenberg pictures are, as indicated by Eq. (3.12), identified at the initial time $t = t_0$.

λ and ζ can deviate at later times if the increments $\partial_t \lambda$ and $\partial_t \zeta$ are different. We use the nonlinear Schroedinger equation to obtain the latter increment:

$$\partial_t \zeta(t) = \partial_t \left\langle \psi_S(t) | \hat{Z}_S | \psi_S(t) \right\rangle \tag{3.22}$$

$$= \frac{i}{\hbar} \left\langle \psi_S(r) \right| \left[\hat{H}(\zeta(t)), \hat{Z}_S \right] \left| \psi_S(t) \right\rangle. \tag{3.23}$$

Note that the equation of motion for $\zeta(t)$ is particularly simple to solve in the case of the quadratic Hamiltonian given by Eq. (3.4), because the non-linear part of $\hat{H}(\zeta(t))$ commutes with $\hat{x}$.

On the other hand, by Eq. (3.21),

$$\partial_t \lambda(t) = \frac{i}{\hbar} \left\langle \psi_H \right| \left[\hat{H}_H^L(\lambda(t)), \hat{Z}_H(\lambda, t) \right] \left| \psi_H \right\rangle$$

Making use of Eq. (3.19), and of

$$\hat{H}^L(\lambda(t)) = \hat{U}_\lambda(t) \hat{H}_H^L(\lambda(t)) \hat{U}_\lambda^\dagger(t), \tag{3.24}$$

we obtain

$$\partial_t \lambda(t) = \frac{i}{\hbar} \left\langle \hat{U}_\lambda(t) \psi_H \right| \left[\hat{H}^L(\lambda(t)), \hat{Z}_S \right] \left| \hat{U}_\lambda(t) \psi_H \right\rangle.$$

Furthermore, $\left|\hat{U}_\lambda(t)\,\psi_H\right\rangle$ evolves under

$$i\hbar\frac{d\left|\hat{U}_\lambda(t)\,\psi_H\right\rangle}{dt} = \hat{H}(\lambda(r))\left|\hat{U}_\lambda(t)\,\psi_H\right\rangle \tag{3.25}$$

Notice the similarity with Eq. (3.10).

We have established that the differential equations governing the time evolution of λ and $\left|\hat{U}_\lambda(t)\,\psi_H\right\rangle$, are of the same form as those governing the time evolution of $\zeta(t)$ and $|\psi_S(t)\rangle$. In addition, these equations have the same initial conditions. Therefore, $\lambda(t) = \zeta(t)$ for all times t. Eq. (3.20) then easily follows because we've established that $\hat{H}(\zeta(t))$ and

$$\hat{H}^L\left(\left\langle\psi_H|\hat{Z}_H(\lambda,t)\,|\psi_H\right\rangle\right)$$

are mathematically equivalent for all times t.

3.2.3 Optomechanics without measurements

We propose to use laser light, enhanced by a Fabry-Perot cavity, to monitor the motion of the test mass of a torsional pendulum, as shown in Fig. 3.2. We assume the light to be resonant with the cavity, and that the cavity has a much larger linewidth than ω_q, the frequency of motion we are interested in.

We will add the non-linear Schroedinger-Newton term from Eq. (3.7) to the usual optomechanics Hamiltonian, obtaining

$$\hat{H} \;=\; \hat{H}_{OM} + \frac{1}{2}M\omega_{SN}^2(\hat{x} - \langle\psi|\hat{x}|\psi\rangle)^2, \tag{3.26}$$

where $\hat{H}_{OM}$ is the standard optomechanics Hamiltonian for our system [6]. We have ignored corrections due to light's gravity because we are operating in the Newtonian regime, where mass dominates the generation of the gravitational field. $\hat{H}$ generates the following linearized state dependent Heisenberg equations (with the dynamics of the cavity field adiabatically eliminated, and the "H" subscript omitted):

$$\partial_t\hat{x} = \frac{\hat{p}}{M} \tag{3.27}$$

$$\partial_t\hat{p} = -M\omega_{\rm cm}^2\hat{x} - M\omega_{SN}^2(\hat{x} - \langle\psi|\hat{x}|\psi\rangle) + \alpha\hat{a}_1 \tag{3.28}$$

$$\hat{b}_1 = \hat{a}_1 \tag{3.29}$$

$$\hat{b}_2 = \hat{a}_2 + \frac{\alpha}{\hbar}\hat{x}, \tag{3.30}$$

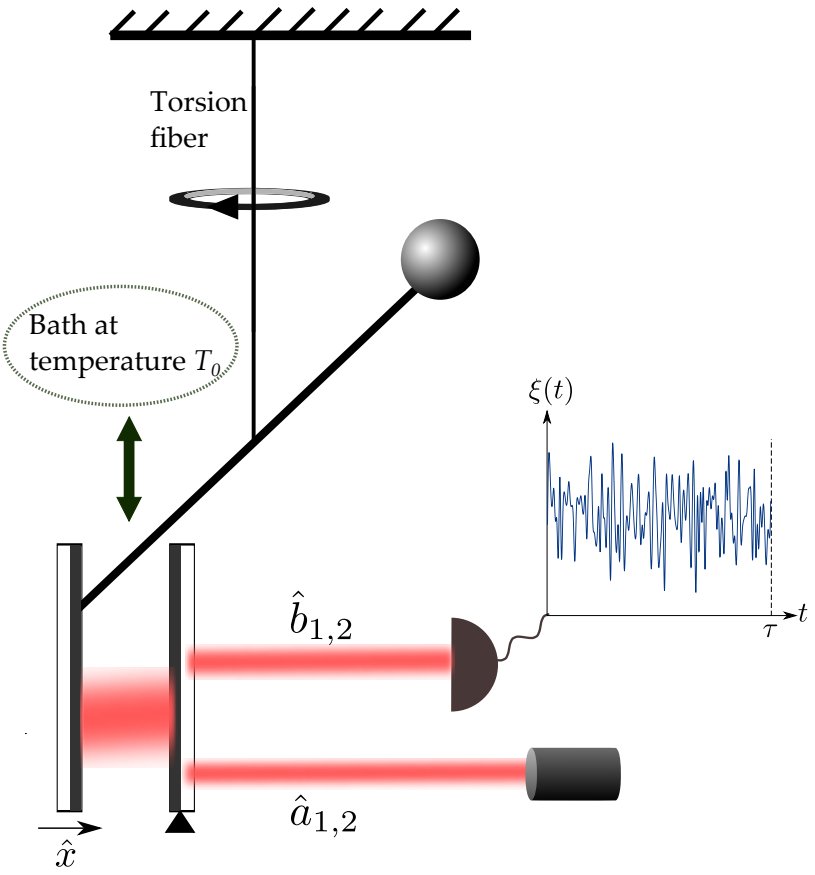

Figure 3.2: The proposed low-frequency optomechanical experiment.

where $\hat{a}_{1,2}$ are the perturbed incoming quadrature fields around a large steady state, and similarly $\hat{b}_{1,2}$ are the perturbed outgoing field quadratures (refer to section 2 of [6] for details). The quantity α characterizes the optomechanical coupling, and depends on the pumping power I_{in} and the input-mirror power transmissivity T of the Fabry-Perot cavity:

$$\alpha^2 = \frac{8I_{in}}{T}\frac{\hbar\omega_c}{c^2}\frac{1}{T}. \tag{3.31}$$

Note that we have a linear system under nonlinear quantum mechanics because the Heisenberg equations are linear in the center of mass displacement and momentum operators, and in the optical field quadratures, including their expectation value on the system's quantum state.

3.3 Nonlinear quantum optomechanics with classical noise

To study realistic optomechanical systems, we must incorporate thermal fluctuations. In linear quantum mechanics, we usually do so by describing the state of the bath with a density operator. However, it is known that the density matrix formalism

cannot be used in non-linear quantum mechanics [3].

Our dynamical system is linear and is driven with light in a Gaussian state, so all system states are eventually Gaussian. Moreover, our system admits a state-dependent Heisenberg picture. Consequently, we can describe fluctuations with distribution functions of linear observables which are completely characterized by their first and second moments. In nonlinear quantum mechanics, the challenge will be to distinguish between quantum uncertainty and the probability distribution of classical forces. The conversion of quantum uncertainty to probability distributions of measurement outcomes is a subtle issue in nonlinear quantum mechanics, and will be postponed until the next section.

Once we have chosen a model for the bath, we will have to revisit the constraint, required for Eq. (3.7) to hold, that the center of mass displacement fluctuations are much smaller than Δx_{zp}. Thermal fluctuations increase the uncertainty in the center of mass motion to the point that in realistic experiments, the total displacement of the test mass will be much larger than Δx_{zp}. Nonetheless, after separating classical and quantum uncertainties, we will show that Eq. (3.7) remains valid, as long as the quantum (and not total) uncertainty of the test mass is much smaller than Δx_{zp}.

Finally, we ignore the gravitational interactions in the thermal bath, as they are expected to be negligible.

3.3.1 Abandoning the density matrix formalism in nonlinear quantum mechanics

In standard quantum mechanics, we use the density matrix formalism when a system is entangled with another system and/or when we lack information about a system's state. The density matrix completely describes a system's quantum state. If two different ensembles of pure states, say $\{|\psi_i\rangle\}$ and $\{|\phi_i\rangle\}$ with corresponding probability distributions p_{ψ_i} and p_{ϕ_i}, have the same density matrix

$$\sum_i p_{\psi_i} |\psi_i\rangle \langle\psi_i| = \sum_i p_{\phi_i} |\phi_i\rangle \langle\phi_i|, \tag{3.32}$$

then they cannot be distinguished by measurements. Furthermore, when either ensemble is time-evolved, they will keep having the same density matrix. However, this statement is no longer true in non-linear quantum mechanics because the superposition principle is no longer valid.

Let us give an example of how our nonlinear Schroedinger equation, given by Eq. (3.7), implies the breakdown of the density matrix formalism. Suppose Alice

and Bob share a collection of entangled states, $|\Phi\rangle$, between Bob's test mass' center of mass degree of freedom and Alice's spin 1/2 particle, with $|\Phi\rangle$ given by

$$\begin{aligned} |\Phi\rangle &= \frac{1}{\sqrt{2}}\left(|\uparrow\rangle\,|\psi_x\rangle + |\downarrow\rangle\,|\psi_{-x}\rangle\right) \\ &= \frac{1}{\sqrt{2}}\left(|\rightarrow\rangle\,|+\rangle + |\leftarrow\rangle\,|-\rangle\right) \end{aligned}$$

where

$$|\rightarrow\rangle \equiv \frac{|\uparrow\rangle + |\downarrow\rangle}{\sqrt{2}} \tag{3.33}$$

$$|\leftarrow\rangle \equiv \frac{|\uparrow\rangle - |\downarrow\rangle}{\sqrt{2}}, \tag{3.34}$$

and $|\psi_{\pm x}\rangle$ are localized states around x and $-x$:

$$|\psi_{\pm x}\rangle = \frac{1}{\sqrt{\sigma\sqrt{\pi}}}\int \exp\left(-\frac{(y \mp x)^2}{2\sigma^2}\right)|y\rangle\, dy. \tag{3.35}$$

We choose $\sigma \ll x$ so that $\langle\psi_x|\psi_{-x}\rangle \approx 0$. Moreover,

$$|\pm\rangle \equiv \frac{1}{\sqrt{2}}\left(|\psi_x\rangle \pm |\psi_{-x}\rangle\right). \tag{3.36}$$

Next, suppose that Alice measures her spins along the $\{|\uparrow\rangle, |\downarrow\rangle\}$ basis, then Bob will be left with the following mixture of states:

$$\chi = \begin{cases} |\psi_x\rangle & \text{with probability 1/2} \\ |\psi_{-x}\rangle & \text{with probability 1/2.} \end{cases} \tag{3.37}$$

On the other hand, if Alice measured her spins along $\{|\rightarrow\rangle, |\leftarrow\rangle\}$ basis, then Bob will be left with the mixture

$$\kappa = \begin{cases} |+\rangle & \text{with probability 1/2} \\ |-\rangle & \text{with probability 1/2.} \end{cases} \tag{3.38}$$

In standard quantum mechanics, both mixtures would be described with the density

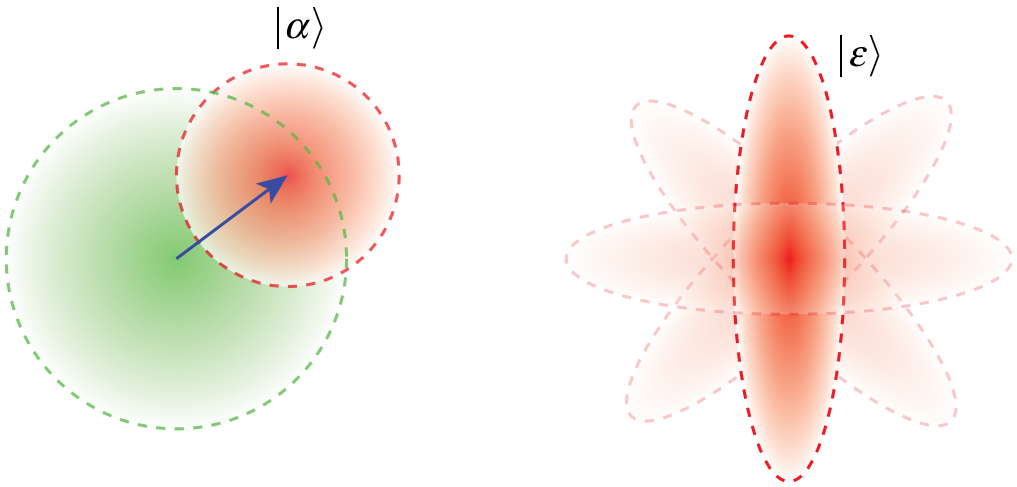

Figure 3.3: Two ways of forming the same Gaussian density matrix. In the left panel, we have an ensemble of coherent states parameterized by a complex amplitude α, which is Gaussian distributed. The red circle depicts the noise ellipse, in phase space, of one such state. The green ellipse depicts the total noise ellipse of the density matrix. In the right panel, we have an ensemble of squeezed states with amplitudes ε, which achieves the same density matrix with a fixed squeeze amplitude and a uniform distribution of squeeze angles.

matrix

$$\rho = \frac{1}{2}|\psi_x\rangle\langle\psi_x| + \frac{1}{2}|\psi_{-x}\rangle\langle\psi_{-x}| \tag{3.39}$$

$$= \frac{1}{2}|+\rangle\langle+| + \frac{1}{2}|-\rangle\langle-|\,. \tag{3.40}$$

However, under the Schroedinger-Newton theory, it is wrong to use ρ because under time evolution both mixtures will evolve differently. Indeed, under time evolution driven by Eq. (3.7) (which has a nonlinearity of $\langle\hat{x}\rangle$) over an infinitesimal period dt, χ and κ no longer remain equivalent because $\langle\pm|\hat{x}|\pm\rangle = 0$, and so κ is unaffected by the nonlinearity.

For this reason, we will have to fall back to providing probability distributions for the bath's quantum state. For a Gaussian state, there are many ways of doing so, as is for example shown in Fig. 3.3. Since this distribution likely has a large classical component (as we argue for in the next section), we will approach the issue of thermal fluctuations by separating out contributions to thermal noise from classical and quantum uncertainty.

3.3.2 Quantum versus classical uncertainty

3.3.2.1 Standard Quantum Statistical Mechanics

Let us consider a damped harmonic oscillator in standard quantum mechanics, which satisfies an equation of motion of

$$M(\ddot{\hat{x}} + \gamma_m \dot{\hat{x}} - \omega_{\rm cm}^2) = \hat{F}_{th}(t), \tag{3.41}$$

where γ_m is the oscillator's damping rate and $\hat{F}_{th}(t)$ a fluctuating thermal force. We have assumed viscous damping. Other forms of damping, such as structural damping, where the retarding friction force is proportional to displacement instead of velocity [28], would reduce the classical thermal noise (which will be precisely defined later in this section) at ω_q, making the experiment easier to perform.

At a temperature $T_0 \gg \hbar\omega_{\rm cm}/k_B$, which accurately describes our proposed setup with a test resonant frequency under a Hz, the thermal force mainly consists of classical fluctuations. We obtain $\hat{F}_{th}(t)$'s spectrum from the fluctuation-dissipation theorem,

$$S_{\hat{F}_{th},\hat{F}_{th}}(\Omega) = 2\hbar \left[\frac{1}{e^{\frac{\hbar\Omega}{k_B T_0}} - 1} + \frac{1}{2} \right] \frac{\mathrm{Im}[G_c(\Omega)]}{|G_c(\Omega)|^2}, \tag{3.42}$$

where $G_c(\Omega)$ is the response function of $\hat{x}$ to the driving force $\hat{F}_{th}(t)$,

$$G_c(\Omega) = \frac{1}{M\left(\omega_{\rm cm}^2 - \Omega(\Omega + i\gamma_m)\right)}, \tag{3.43}$$

and $S_{\hat{F}_{th},\hat{F}_{th}}(\Omega)$ is defined by

$$\langle \hat{F}_{th}(\Omega)\, \hat{F}_{th}^{\dagger}(\Omega') \rangle_{sym} = S_{\hat{F}_{th},\hat{F}_{th}}(\Omega) 2\pi\delta(\Omega - \Omega') \tag{3.44}$$

with

$$\langle \hat{A}\hat{B} \rangle_{sym} \equiv \frac{\langle \hat{A}\hat{B} + \hat{B}\hat{A} \rangle}{2}. \tag{3.45}$$

Note that we have chosen a "double-sided convention" for calculating spectra.

The fact that the motion of the test mass is damped due to its interaction with the heat bath also requires that the thermal force has a (usually small but nevertheless conceptually crucial) quantum component,

$$\left[\hat{F}_{th}(t), \hat{F}_{th}(t') \right] \neq 0, \tag{3.46}$$

which compensates for the decay of the oscillator's canonical commutation relations

due to adding damping in its equations of motion (refer to section 5.5 of [2] for details). Note that the second term in the bracket in Eq. (3.42) provides the zero-point fluctuations of the oscillator as $T \to 0$.

3.3.2.2 Quantum Uncertainty

Let the bath be in some quantum state $|\Phi_B\rangle$ over which we will take expectation values. The thermal force operator acting on the system can then be conveniently decomposed into

$$\hat{F}_{th}(t) = f_{cl}(t) + \hat{f}_{zp}(t) \tag{3.47}$$

where we define

$$f_{cl}(t) = \langle \hat{F}_{th}(t) \rangle, \quad \hat{f}_{zp}(t) = \hat{F}_{th}(t) - \langle \hat{F}_{th}(t) \rangle. \tag{3.48}$$

We use the subscripts "cl" and "zp" because $f_{cl}(t)$ is a complex number, while $\hat{f}_{zp}(t)$ will be later chosen to drive the "zero-point" quantum fluctuation of the mass.

For any operator $\hat{A}$, we shall refer to $\langle \hat{A} \rangle$ as the quantum expectation value and

$$V[\hat{A}] \equiv \langle \hat{A}^2 \rangle - \langle \hat{A} \rangle^2 \tag{3.49}$$

as its quantum uncertainty. We also define the quantum covariance by

$$\mathrm{Cov}[\hat{A}, \hat{B}] = \langle \hat{A}\hat{B} \rangle_{sym} - \langle \hat{A} \rangle \langle \hat{B} \rangle. \tag{3.50}$$

Suppose $|\Phi_B\rangle$ is a Gaussian quantum state, an assumption satisfied by harmonic heat-baths under general conditions [27], then $|\Phi_B\rangle$ is completely quantified by the following moments: the means

$$\langle f_{cl}(t) \rangle = f_{cl}(t), \quad \langle \hat{f}_{zp}(t) \rangle = 0, \tag{3.51}$$

the covariances that include $f_{cl}(t)$

$$\mathrm{Cov}\left[f_{cl}(t), f_{cl}(t')\right] = \mathrm{Cov}\left[f_{cl}(t), \hat{f}_{zp}(t')\right] = 0, \tag{3.52}$$

and those that don't

$$\begin{aligned} \mathrm{Cov}\left[\hat{F}_{th}(t), \hat{F}_{th}(t')\right] &= \mathrm{Cov}\left[\hat{f}_{zp}(t), \hat{f}_{zp}(t')\right] \\ &= \langle \hat{f}_{zp}(t)\, \hat{f}_{zp}(t') \rangle_{sym} \neq 0. \end{aligned}$$

3.3.2.3 Classical Uncertainty

The state $|\Phi_B\rangle$ is drawn from an ensemble with a probability distribution $p(|\Phi_B\rangle)$. For each member of the ensemble, we will have a different quantum expectation $f_{cl}\,(t)$, and a different two-time quantum covariance for $\hat{f}_{zp}\,(t)$. We shall call the variations in these quantities classical fluctuations, because they are due to our lack of knowledge about a system's wavefunction.

The total covariance of the thermal force, using our terminology, is given by:

$$\begin{aligned}&\overline{\left\langle \frac{\hat{F}_{th}(t)\hat{F}_{th}(t') + \hat{F}_{th}(t')\hat{F}_{th}(t)}{2} \right\rangle} \\ =&\overline{\langle \hat{f}_{zp}(t)\hat{f}_{zp}(t')\rangle_{sym}} + \overline{f_{cl}(t)f_{cl}(t')}\,,\end{aligned} \tag{3.53}$$

where $\overline{\langle \quad \rangle}$ denotes taking an ensemble average over different realizations of the thermal bath. Eq. (3.53) is the total thermal noise we obtain, and in standard quantum mechanics there is no way to separately measure quantum and classical uncertainties.

3.3.2.4 Proposed model

We shall assume that $\hat{f}_{zp}$'s two-time quantum covariance, $\langle \hat{f}_{zp}(t)\hat{f}_{zp}(t')\rangle_{sym}$, provides the zero-point fluctuations in the position of the test mass, and that its ensemble average is zero (*i.e.* the uncertainty in $\hat{f}_{zp}\,(t)$ comes solely from quantum mechanics). This results in $\hat{f}_{zp}\,(t)$ having a total spectrum of:

$$S^{qu}_{f_{zp},f_{zp}}\,(\Omega) = \hbar \frac{\mathrm{Im}[G_c(\Omega)]}{|G_c(\Omega)|^2} = \hbar\Omega M\gamma_m\,. \tag{3.54}$$

Moreover, we shall assume that f_{cl}'s two-time ensemble covariance, $\overline{f_{cl}(t)f_{cl}(t')}$, provides the fluctuations predicted by classical statistical mechanics. This results in f_{cl} having a total spectrum of

$$S_{f_{cl}}(\Omega) = \frac{2\hbar}{e^{\frac{\hbar\Omega}{k_B T_0}} - 1} \frac{\mathrm{Im}[G_c(\Omega)]}{|G_c(\Omega)|^2} \approx 2k_B T M\gamma_m\,. \tag{3.55}$$

3.3.3 Validity of the quadratic SN equation

In general, the center of mass wavefunction $|\psi\rangle$ follows the SN equation

$$i\hbar\frac{d|\psi\rangle}{dt} = \left[\hat{H}_{NG} + \hat{V}\right]|\psi\rangle, \tag{3.56}$$

where the gravitational potential $\hat{V}$ can be approximately calculated by taking an expectation value of Eq. (8) in [29] with respect to the internal degrees of freedom's wavefunction:

$$\hat{V} = \int \mathcal{E}(\hat{x} - z) \left|\langle \psi | z \rangle\right|^2 dz \tag{3.57}$$

with $\mathcal{E}$ the "self energy" between a shifted version of the object and itself at the original position. We calculate $\mathcal{E}$ to be

$$\begin{aligned} \mathcal{E}(x) &= GMm\left(\frac{1}{\Delta x_{zp}} - \frac{1}{x}\text{erf}\left(\frac{x}{2\Delta x_{zp}}\right)\right) \\ &= \frac{GMm}{\sqrt{\pi}\Delta x_{zp}}\left(\sqrt{\pi} - 1 + \frac{x^2}{12\Delta x_{zp}^2} - \frac{x^4}{160\Delta x_{zp}^4} + ...\right). \end{aligned}$$

As a result, $\hat{V}$ is in general difficult to evaluate because it depends on an infinite number of expectation values. When the center of mass spread

$$\Delta x_{cm} \equiv \sqrt{\left\langle (\hat{x}(t) - \langle \hat{x}(t) \rangle)^2 \right\rangle} \tag{3.58}$$

is much less than Δx_{zp}, $\mathcal{E}$ can be approximated to quadratic order in x, leading to the simple quadratic Hamiltonian presented in Eq. (3.4) [29]. In this section, we show that classical thermal noise does not affect the condition $\Delta x_{cm} \ll \Delta x_{zp}$.

We include classical thermal noise in our analysis through the following interaction term:

$$\hat{V}_{cl}(t) \equiv -f_{cl}(t)\,\hat{x}. \tag{3.59}$$

We will show that Δx_{cm} does not depend on $f_{cl}(t)$, even when we use the full expression for $\hat{V}$.

We first momentarily ignore $\hat{V}$, and show that under the non-gravitational Hamiltonian, $\hat{H}_{NG}$, Δx_{cm} is unaffected by $f_{cl}(t)$. Since $\hat{H}_{NG}$ is quadratic, then the time-evolved position operator under $\hat{H}_{NG}$, $\hat{x}^{(0)}$, is of linear form

$$\begin{aligned} \hat{x}^{(0)}(t) &= \sum_i \left(c_i(t)\,\hat{q}_i + d_i(t)\,\hat{k}_i\right) + \int G_c(t-z)\,f_{cl}(z)\,dz \\ &\quad + \int r(t,z)\,\hat{a}_1(z)\,dz + \int s(t,z)\,\hat{a}_2(z)\,dz, \end{aligned} \tag{3.60}$$

where $\hat{q}_i$ and $\hat{k}_i$ are canonically conjugate operators of discrete degrees of freedom such as the center of mass mode of the test mass, $G_c(t)$ is the inverse Fourier transform of the response function defined by Eq. (3.43), and $r(t)$ and $s(t)$ are

c-number functions. As a result, the variance of $\hat{x}^{(0)}$ is unaffected by $f_{cl}(t)$.

The full time-evolved position operator (in the state-dependent Heisenberg picture introduced in section II.B), can be expressed in terms of $\hat{x}^{(0)}$ in the following way:

$$\hat{x}_H(t) = \hat{U}_I^\dagger(t)\,\hat{x}^{(0)}(t)\,\hat{U}_I(t), \tag{3.61}$$

where $\hat{U}_I$ is the (state-dependent) interaction picture time-evolution operator associated with

$$\hat{V}_I(t) = \hat{U}_{NG}^\dagger(t)\hat{V}(t)\hat{U}_{NG}(t). \tag{3.62}$$

Specifically, $\hat{U}_I$ is defined by

$$\hat{U} = \hat{U}_{NG}\hat{U}_I, \tag{3.63}$$

where $\hat{U}_{NG}$ is the time-evolution operator associated with $\hat{H}_{NG}$. We will show that $\hat{V}_I$ and $\hat{U}_I$ are independent of $f_{cl}(t)$.

We begin the proof, of $\hat{V}_I$ independent of $f_{cl}(t)$, by conveniently rewriting $|\langle\psi|z\rangle|^2$ in Eq. (3.57) as the expectation value of an operator. We do so by writing the projection $|z\rangle\langle z|$ as a delta function:

$$\hat{V} = \int \mathcal{E}(\hat{x}-z)\,\langle\delta(\hat{x}-z)\rangle\,dz, \tag{3.64}$$

which we then express in the Fourier domain

$$\begin{aligned}\delta(\hat{x}-z) &= \int dx\delta(x-z)\,|x\rangle\langle x| \\ &\propto \int dx\int dk e^{-ik(x-z)}\,|x\rangle\langle x| \propto \int dk e^{-ik(\hat{x}-z)}.\end{aligned}$$

We then substitute this expression into $\hat{V}$, transform $\mathcal{E}$ into the Fourier domain, and obtain

$$\hat{V} \propto \int \mathcal{F}(l)\,e^{-il(\hat{x}-z)}\left\langle e^{-ik(\hat{x}-z)}\right\rangle dk\,dl\,dz, \tag{3.65}$$

where $\mathcal{F}$ is the Fourier transform of $\mathcal{E}$. Finally, we perform the integral over z, obtaining

$$\hat{V} \propto \int \mathcal{F}(k)\,e^{-ik\hat{x}}\left\langle e^{ik\hat{x}}\right\rangle dk. \tag{3.66}$$

In the interaction picture,

$$\begin{aligned}\hat{V}_I(t) &\propto \int \mathcal{F}(k)\, e^{-ik\hat{x}^{(0)}(t)} \left\langle \Psi_0 | e^{ik\hat{x}_H(t)} | \Psi_0 \right\rangle dk \\ &\propto \int \mathcal{F}(k)\, e^{-ik\hat{x}^{(0)}(t)} \times \\ &\quad \left\langle \Psi_0 \middle| \hat{U}_I^\dagger(t) e^{ik\hat{x}^{(0)}(t)} \hat{U}_I(t) \middle| \Psi_0 \right\rangle dk, \end{aligned} \tag{3.67}$$

where $|\Psi_0\rangle$ is the initial wavefunction of the entire system. Notice that the linear dependence of $\hat{x}^{(0)}$ on $f_{cl}(t)$ cancels out in Eq. (3.67). However, $\hat{V}_I$ could still depend on $f_{cl}(t)$ through $\hat{U}_I$. We will show that this is not the case.

The operator

$$\hat{V}_I(0) = \hat{V} \tag{3.68}$$

and the ket

$$\hat{U}_I(0)\,|\Psi_0\rangle = |\Psi_0\rangle \tag{3.69}$$

do not depend on $f_{cl}(t)$ at the initial time $t = 0$. At later times, $f_{cl}(t)$ can only appear through the increments $d\hat{V}_I/dt$ or $d\hat{U}_I\,|\Psi_0\rangle\,/dt$. The latter is given by

$$i\hbar \frac{d}{dt} \hat{U}_I\,|\Psi_0\rangle = \hat{V}_I \hat{U}_I\,|\Psi_0\rangle\,, \tag{3.70}$$

while

$$\begin{aligned} i\hbar \frac{d\hat{V}_I(t)}{dt} &= \int dk \mathcal{F}(k) \Bigg(\left[e^{-ik\hat{x}^{(0)}}, \hat{H}_{NG} \right] \times \\ &\quad \hat{U}_I^\dagger \left\langle e^{ik\hat{x}^{(0)}} \right\rangle_0 \hat{U}_I + e^{-ik\hat{x}^{(0)}} \times \\ &\quad \left\langle \hat{U}_I^\dagger \left[e^{ik\hat{x}^{(0)}}, \hat{H}_{NG} + \hat{V}_I \right] \hat{U}_I \right\rangle_0 \Bigg), \end{aligned} \tag{3.71}$$

where the expectation values $\langle \quad \rangle_0$ are taken over $|\Psi_0\rangle$. In both terms in the sum, the dependence of $\hat{x}^{(0)}$ on $f_{cl}(t)$ cancels out, and so $f_{cl}(t)$ does not explicitly appear in the system of differential equations (3.70) and (3.71). $f_{cl}(t)$ does not also appear in the initial conditions (3.69) and (3.71). Consequently, both $\hat{V}_I$ and $\hat{U}_I$ are independent of $f_{cl}(t)$.

We then use Eq. (3.61) to establish that the center of mass position operator is independent of $f_{cl}(t)$. As a result, the exact expression for Δx_{cm} is also independent of $f_{cl}(t)$. If $\Delta x_{cm} \ll \Delta x_{zp}$ holds in the absence of classical thermal noise, it also holds in the presence of it. We will have to check this assumption in order for the

linear Heisenberg equation to hold. Otherwise, if Δx_{cm} becomes larger than Δx_{zp}, the effect of $\hat{V}$ becomes weaker, because $\hat{V}$ becomes shallower than the quadratic potential

$$\frac{1}{2}M\omega_{SN}^2\left(\hat{x}-\langle\hat{x}\rangle\right)^2.$$

3.3.4 Heisenberg equations of motion with thermal noise included

The dynamics of our proposed model for an open optomechanical system are summarized by the following state-dependent Heisenberg equations:

$$\frac{d\hat{x}}{dt} = \frac{\hat{p}}{M} \tag{3.72}$$

$$\frac{d\hat{p}}{dt} = -M\omega_{\rm cm}^2\hat{x} - \gamma_m\hat{p} - M\omega_{SN}^2(\hat{x}-\langle\hat{x}\rangle) + \alpha\hat{a}_1 + f_{cl} + \hat{f}_{zp} \tag{3.73}$$

$$\hat{b}_1 = \hat{a}_1 \tag{3.74}$$

$$\hat{b}_2 = \hat{a}_2 + \frac{\alpha}{\hbar}\hat{x}, \tag{3.75}$$

where the spectra of $\hat{f}_{zp}(\omega)$ and $f_{cl}(\omega)$ are given by Eqs. (3.54) and (3.55), respectively.

We solve Eqs. (3.72)–(3.75) by working in the frequency domain, and obtain at each frequency ω,

$$\hat{b}_2(\omega) = \hat{A}(\omega) + \frac{\alpha G_c(\omega)}{\hbar} f_{cl}(\omega) + \left\langle\hat{B}(\omega)\right\rangle. \tag{3.76}$$

We separately discuss the three terms. The operator $\hat{A}(\omega)$ is the linear quantum contribution to $\hat{b}_2$:

$$\hat{A}(\omega) \equiv \hat{a}_2(\omega) + \frac{\alpha G_q(\omega)}{\hbar}\left[\alpha\hat{a}_1 + \hat{f}_{zp}(\omega)\right], \tag{3.77}$$

where $\hat{a}_2(\omega)$ represents shot noise,

$$G_q(\omega) \equiv \frac{1}{M\left(\omega_q^2 - \omega^2 - i\omega\gamma_m\right)} \tag{3.78}$$

is the quantum response function of the damped torsional pendulum's center of mass position, $\hat{x}(\omega)$, to the thermal force, and $\alpha\hat{a}_1$ and $\hat{f}_{zp}$ are the quantum radiation-pressure force and the quantum piece of the thermal force acting on the test mass, respectively.

The second term in Eq. (3.76) represents classical thermal noise, with $G_c(\omega)$ defined in Eq. (3.43). Note that the classical and quantum resonant frequencies in $G_c(\omega)$ and $G_q(\omega)$, respectively, differ from each other.

The third term in Eq. (3.76), $\langle \hat{B}(\omega) \rangle$, represents the non-linear contribution to $\hat{b}_2(\omega)$

$$\hat{B}(\omega) \equiv \frac{\alpha \Delta G(\omega)}{\hbar} \left[\alpha \hat{a}_1(\omega) + \hat{f}_{zp}(\omega) \right], \tag{3.79}$$

where we defined

$$\Delta G(\omega) \equiv G_c(\omega) - G_q(\omega). \tag{3.80}$$

In the next section, we discuss the subtle issue of how to convert the wavefunction average $\langle \ldots \rangle$ to the statistics of measurement outcomes.

3.4 Measurements in nonlinear quantum optomechanics

With the assumption of classical gravity, we will have to revisit the wavefunction collapse postulate, because a sudden projective measurement of the outgoing optical field induces a change in the quantum state of any of its entangled partners, including possibly the macroscopic pendulum's state. As a result, we might obtain an unphysical change in the Einstein tensor which violates the Bianchi identity. Moreover, since the Schroedinger-Newton equation is nonlinear, we will show that we have to address an additional conceptual challenge: there is no unique way of extending Born's rule to nonlinear quantum mechanics.

In this section, we propose two phenomenological prescriptions, which we term preselection and post-selection, for determining the statistics of an experiment within the framework of classical gravity.

3.4.1 Revisiting Born's rule in linear quantum mechanics

We will use the wavefunction collapse postulate as a guide. The postulate is mathematically well defined, but can be interpreted in two equivalent ways, which become inequivalent in nonlinear quantum mechanics.

The first interpretation is widely used, and describes a quantum measurement experiment in the following way: a preparation device initializes a system's quantum state to $|i\rangle$, which evolves for some period of time under a unitary operator, $\hat{U}$, to

$$|i\rangle \rightarrow \hat{U}|i\rangle. \tag{3.81}$$

The system then interacts with a measurement device, which collapses the system's

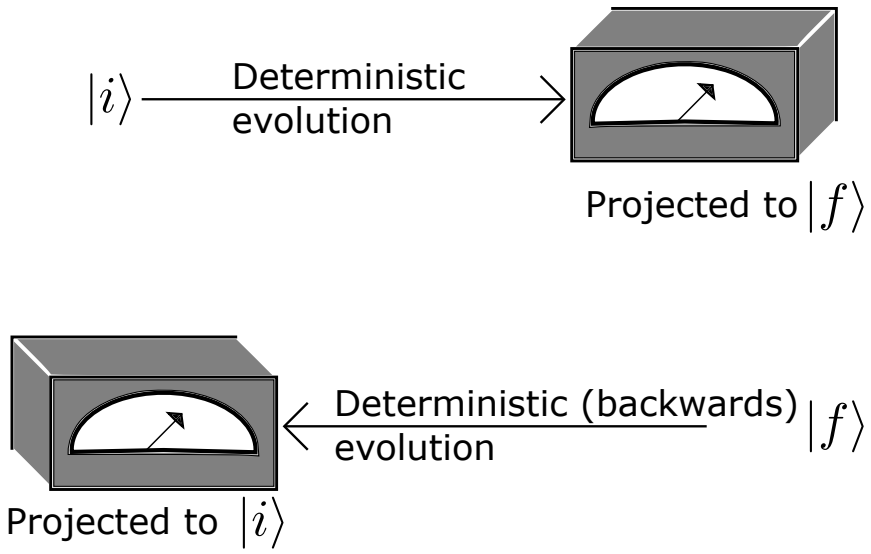

Figure 3.4: The two prescriptions, pre-selection (top) and post-selection (bottom), that can be used to calculate measurement probabilities. Both prescriptions are equivalent in linear quantum mechanics, but become different under non-linear quantum mechanics.

state into an eigenstate, $|f\rangle$, of the observable associated with that device. The probability of the collapse onto $|f\rangle$ is

$$p_{i\to f} \equiv |\langle f|\hat{U}|i\rangle|^2. \tag{3.82}$$

We will refer to this expression of Born's rule as *pre-selection*.

Second, the unitarity of quantum mechanics allows us to rewrite Eq. (3.82) to

$$p_{i\to f} = |\langle i|\hat{U}^\dagger|f\rangle|^2 \equiv p_{i\leftarrow f}. \tag{3.83}$$

Interpreting this expression from right to left, as we did for Eq. (3.82), we can form an alternate, although unfamiliar, narrative: $|f\rangle$ evolves backwards in time to $\hat{U}^\dagger|f\rangle$, and is then projected by the preparation device to the state $|i\rangle$, as is illustrated in Fig. 3.4. We will refer to the formulation of Born's rule based on $p_{i\leftarrow f}$ as *post-selection*.

3.4.2 Pre-selection and post-selection in non-linear quantum mechanics

In non-linear quantum mechanics, the Hamiltonian, and so the time evolution operator, depends on the quantum state of the system. As a result, the pre-selection

version of Born's rule, Eq. (3.82), has to be revised to

$$p_{i\to f} = \left|\langle f|\hat{U}_{|i\rangle}|i\rangle\right|^2 \tag{3.84}$$

where $\hat{U}_{|i\rangle}$ is the (non-linear) time evolution operator which evolves $|i\rangle$ forward in time to $\hat{U}_{|i\rangle}\,|i\rangle$.

Furthermore, the post-selection version of Born's rule, Eq. (3.83), is modified to

$$p_{i\leftarrow f} \propto \left|\langle i|\hat{U}^{\dagger}_{|f\rangle}|f\rangle\right|^2, \tag{3.85}$$

where $\hat{U}^{\dagger}_{|f\rangle}$ is the (non-linear) time evolution operator which evolves $|f\rangle$ backwards in time to $\hat{U}^{\dagger}_{|f\rangle}\,|f\rangle$. The evolution can still be interpreted as running backwards in time, because the non-linear Hamiltonians we are working with, such as in Eq. (3.7), are Hermitian. Moreover, the proportionality sign follows from

$$\sum_f \left|\langle i|\hat{U}^{\dagger}_{|f\rangle}|f\rangle\right|^2$$

being not, in general, normalized to unity.

Notice that $p_{i\to f}$ and $p_{i\leftarrow f}$ are in general different. Consequently, in non-linear quantum mechanics, we can no longer equate the pre-selection and post-selection prescriptions, and we will have to consider both separately.

3.4.3 Pre-selection and post-selection in non-linear quantum optomechanics

In our proposed optomechanical setup, the state $|i\rangle$ is a separable state consisting of the initial state of the test object, and a coherent state of the incoming optical field, which has been displaced to vacuum, $|0\rangle_{in}$ by the transformation $\hat{a}_{1,2} \to \delta\hat{a}_{1,2} + \langle\hat{a}_{1,2}\rangle$. In the pre-selection measurement prescription, as we reach steady state, the test-mass' initial state becomes irrelevant, and the system's state is fully determined by the incoming optical state.

The set of possible states $|f\rangle$ are eigenstates of the field quadrature $b_2(t)$, which can be labeled by a time series

$$|\xi\rangle_{out} \equiv |\{\xi(t) : -\infty < t < +\infty\}\rangle_{out}. \tag{3.86}$$

Similarly to what we discussed for pre-selection, as we reach steady state, the test-mass' initial state becomes irrelevant. This statement can easily be demonstrated if $p_{i\leftarrow f}$ is recast in a form, cf. Eq. (3.90), where the test mass' state is forward-time

evolved and so is driven by light, and undergoes thermal dissipation.

Since $|\xi\rangle_{out}$ labels a collection of Gaussian quantum states, the distribution of the measurement results $\xi(t)$ will be that of a Gaussian random process, characterized by the first and second moments. In standard quantum mechanics, they are given by the mean $\langle \hat{b}_2(t)\rangle$ and the correlation function

$$\langle \hat{b}_2(t)\hat{b}_2(t')\rangle_{sym} - \langle \hat{b}_2(t)\rangle\langle \hat{b}_2(t')\rangle.$$

In nonlinear quantum mechanics, the situation is subtle because $\left\langle \hat{b}_2(t)\right\rangle$ could depend on the measurement results $\xi(t)$.

To determine the expression for the second moment, we will explicitly calculate $p_{i\to f}$ and $p_{i\leftarrow f}$. Since our proposed setup eventually reaches a steady state, we can simplify our analysis by working in the Fourier domain, where fluctuations at different frequencies are independent. Note that we first ignore the classical force $f_{cl}(t)$. We will incorporate it back into our analysis at the end of this section.

The probability of measuring ξ in the pre-selection measurement prescription,

$$p_{i\to f} = p_{0\to\xi} = |_{out}\langle\xi|\hat{U}_{|0\rangle_{in}}|0\rangle_{in}|^2 \tag{3.87}$$

is characterized by the spectrum of the Heisenberg Operator of $\hat{b}_2$ in the following way:

$$p_{0\to\xi} \propto \exp\left[-\frac{1}{2}\int \frac{d\Omega}{2\pi}\frac{|\xi(\Omega) - \langle \hat{b}_2(\Omega)\rangle_0|^2}{S_{A,A}}\right], \tag{3.88}$$

where $\langle b_2(\Omega)\rangle_0$ is the quantum expectation value of the Heisenberg operator $\hat{b}_2(\omega)$, calculated using the state-dependent Heisenberg equations associated with an initial boundary condition of $|0\rangle_{in}$, and $S_{A,A}$ is the spectral density of the linear part of $\hat{b}_2(\Omega)$, $\hat{A}$, evaluated over vacuum:

$$2\pi S_{A,A}(\omega)\delta\left(\omega-\omega'\right) \equiv \left\langle 0\middle|\hat{A}(\omega)\,\hat{A}^{\dagger}\left(\omega'\right)\middle|0\right\rangle_{sym}.$$

Note that the derivation of Eq. (3.88) is presented in Appendix 3.9. In the same Appendix, we also show that in the limit of $\omega_{SN}\to 0$, $p_{0\to\xi}$ recovers the predictions of standard quantum mechanics.

In post-section, the probability of obtaining a particular measurement record is given by

$$p_{i\leftarrow f} = p_{0\leftarrow\xi} = \left|\langle 0|\hat{U}^{\dagger}_{|\xi\rangle_{out}}|\xi\rangle_{out}\right|^2, \tag{3.89}$$

which can be written as

$$p_{0\leftarrow\xi} = \left|{}_{out}\langle\xi|\hat{U}_{|\xi\rangle_{out}}|0\rangle\right|^2 \tag{3.90}$$

where $\hat{U}_{|\xi\rangle_{out}}$ is the time-evolution operator specified by the end-state $|\xi\rangle_{out}$. In Appendix 3.9, we show that $p_{0\leftarrow\xi}$ is given by

$$p_{0\leftarrow\xi} \propto \exp\left[-\frac{1}{2}\int \frac{d\Omega}{2\pi}\frac{|\xi(\Omega) - \langle\hat{b}_2(\Omega)\rangle_\xi|^2}{S_{A,A}}\right], \tag{3.91}$$

where $\langle\hat{b}_2(\Omega)\rangle_\xi$ is the quantum expectation value of $\hat{b}_2(\Omega)$'s Heisenberg operator, obtained with the state-dependent Heisenberg equations associated with the final state $|\xi\rangle$, but evaluated on the incoming vacuum state $|0\rangle$ for $\hat{a}_{1,2}$.

Note that because $\langle b_2(\Omega)\rangle_\xi$ depends on ξ, the probability density given by Eq. (3.91) is modified. We extract the inverse of the new coefficient of $|\xi^2(\Omega)|$ as the new spectrum. We will follow this procedure in section §3.5 C. The normalization of $p_{0\leftarrow\xi}$ is taken care of by the Gaussian function.

Finally, we incorporate classical noise by taking an ensemble average over different realizations of the classical thermal force, $f_{cl}(\omega)$. For instance, the total probability for measuring ξ in pre-selection is

$$\overline{p_{0\leftarrow\xi}} = \int \mathcal{D}x\; p\left(f_{cl}(\omega) = x(\omega)\right) \times p_{0\leftarrow\xi(x(\omega))}, \tag{3.92}$$

where $p\left(f_{cl}(\omega) = x(\omega)\right)$ is the probability that f_{cl} at frequency ω is equal to $x(\omega)$, and $\xi(x(\omega))$ is the measured eigenvalue of the observable $\hat{b}_2$ given that the classical thermal force is given by x. The above integral can be written as a convolution and so is mathematically equivalent to the addition of Gaussian random variables. Thus, assuming independent classical and quantum uncertainties, the total noise spectrum is given by adding the thermal noise spectrum to the quantum uncertainty spectrum calculated by ignoring thermal noise.

3.5 Signatures of classical gravity

With a model of the bath and the pre- and post-selection prescriptions at hand, we proceed to determine how the predictions of the Schroedinger Newton theory for the spectrum of phase fluctuations of the outgoing light differ from those of standard quantum mechanics. We expect the signatures to be around ω_q, the frequency where the Schroedinger Newton dynamics appear at, as was discussed in section §3.2 and in [29].

3.5.1 Baseline: standard quantum mechanics

We calculate the spectrum of phase fluctuations predicted by standard quantum mechanics, $S^{(QM)}_{b_2,b_2}(\omega)$, by setting ω_{SN} to 0 in Eq. (3.76). Making use of

$$S_{a_1,a_1} = S_{a_2,a_2} = 1/2 \qquad S_{a_1,a_2} = 0 \tag{3.93}$$

for vacuum fluctuations of $\hat{a}_1$ and $\hat{a}_2$, we obtain

$$S^{(QM)}_{b_2,b_2}(\omega) = \frac{1}{2} + \frac{\alpha^4}{2\hbar^2}\left|G_c(\omega)\right|^2 + \frac{\alpha^2}{\hbar^2} S^{cl}_{x,x}(\omega), \tag{3.94}$$

where the first and second terms on the RHS represent shot noise and quantum radiation pressure noise respectively, and

$$S^{cl}_{x,x}(\omega) = 2k_B T_0 \frac{\mathrm{Im}\left(G_c(\omega)\right)}{\omega}, \tag{3.95}$$

is the noise spectrum of the center of mass position, $\hat{x}(\omega)$, due to the classical thermal force, $f_{cl}(\omega)$.

We are interested in comparing standard quantum mechanics to the SN theory, which has signatures around ω_q. Therefore, we would need to evaluate $S^{(QM)}_{b_2,b_2}(\omega)$ around ω_q. The first two terms in Eq. (3.94) can be easily evaluated at $\omega = \omega_q$, and in the limit of $\omega_{\mathrm{cm}} \ll \omega_{SN}$,

$$\frac{\alpha^2}{\hbar^2} S^{cl}_{x,x}\left(\omega \approx \omega_q\right) \;=\; \beta\Gamma^2 \tag{3.96}$$

where we have defined two dimensionless quantities,

$$\beta \equiv \frac{\alpha^2}{M\hbar\gamma_m\omega_q}, \qquad \Gamma^2 \;\equiv\; 2\frac{k_B T_0}{\hbar\omega_q}\frac{\gamma_m^2\omega_q^2}{\gamma_m^2\omega_q^2 + \omega_{SN}^4}. \tag{3.97}$$

β characterizes the measurement strength (as α^2 is proportional to the input power), and Γ characterizes the strength of thermal fluctuations. If $Q \gg 1$, we can simplify Γ^2 to

$$\Gamma^2 \approx \frac{2k_B T_0}{\hbar\omega_{SN}^3}\gamma_m^2. \tag{3.98}$$

3.5.2 Signature of preselection

In pre-selection, we evaluate the nonlinearity in Eq. (3.76), $\left\langle \hat{B}(\omega) \right\rangle$, over the incoming field's vacuum state, $|0\rangle_{in}$:

$$ {}_{in}\left\langle 0 \middle| \hat{B}(\omega) \middle| 0 \right\rangle_{in} = 0. $$

Consequently, we can directly use Eq. (3.88) to establish that under the pre-selection measurement prescription, the noise spectrum of $\hat{b}_2$ is $S_{A,A}$. Taking an ensemble average over the classical force f_{cl} adds classical noise to the total spectrum:

$$ S^{(pre)}_{b_2,b_2}(\omega) = S_{A,A}(\omega) + \frac{\alpha^2}{\hbar^2} S^{cl}_{x,x}(\omega). \tag{3.99} $$

Making use of Eq. (3.93), we obtain

$$ S_{A,A}(\omega) = \frac{1}{2} + S_{RQ}(\omega) \tag{3.100} $$

$$ S_{RQ}(\omega) \equiv \frac{\alpha^4}{2\hbar^2} \left| G_q(\omega) \right|^2 + \frac{\alpha^2 \left| G_q(\omega) \right|^2}{\hbar^2} S^{qu}_{f_{zp},f_{zp}}(\omega). \tag{3.101} $$

The first term in $S_{A,A}$, 1/2, is the shot noise background level, and $S_{RQ}(\omega)$ is the noise from quantum radiation pressure forces and quantum thermal forces. Moreover, $S^{qu}_{f_{zp},f_{zp}}(\omega)$, given by Eq. (3.54), is the noise spectrum from vacuum fluctuations of the quantum thermal force $\hat{f}_{zp}(\omega)$.

Around ω_q, in the narrowband limit $\gamma_m \ll \omega_q$, the quantum back action noise dominates and so

$$ S^{(pre)}_{b_2,b_2}(\omega) \approx \left(\frac{1}{2} + \beta\Gamma^2 \right) \times \left[1 + \frac{\beta(\beta+2)}{2\left(1/2 + \beta\Gamma^2\right)} \frac{1}{1 + \dfrac{(\omega - \omega_q)^2}{4\gamma_m^2}} \right]. $$

As a result, the signature of classical gravity under the pre-selection prescription

can be summarized as a Lorentzian

$$S(\omega) \propto 1 + \frac{h_{pre}}{1 + 4\dfrac{(\omega - \omega_q)^2}{\Delta_{pre}^2}} \tag{3.102}$$

with a height and a full width at half maximum (FWHM) given by

$$h_{pre} = \frac{\beta(\beta+2)}{2\left(1/2 + \beta\Gamma^2\right)}, \quad \Delta_{pre} = \gamma_m, \tag{3.103}$$

respectively. We plot the pre-selection spectrum around ω_q in Fig. 3.5.

Limits on the measurement strength

Our results are valid only if the Schroedinger Newton potential can be approximated as a quadratic potential, which is necessary for linearizing the state-dependent Heisenberg equations, as we described in Sec. 3.3.3.

Specifically, we must ensure that the spread of the center of mass wavefunction excluding contributions from classical noise is significantly less than Δx_{zp}, which is on the order of $10^{-11} - 10^{-12}$ m for most materials (as can be determined from the discussion in section 3.2.1 and Ref. [20]). We calculate Δx_{cm} at steady state to be

$$\begin{aligned} \langle \hat{x}^2 \rangle - \langle \hat{x} \rangle^2 &= \alpha^2 \int_{-\infty}^{+\infty} \left| G_q^2(\omega) \right| \left[\frac{1}{2} + \frac{S_{f_{zp}}(\omega)}{\alpha^2} \right] \frac{d\omega}{2\pi} \\ &\approx \frac{\beta+2}{2} \frac{\hbar}{2M\omega_q}, \end{aligned} \tag{3.104}$$

where the expectation value is carried over vacuum of the input field, $|0\rangle_{in}$.

3.5.3 Signature of post-selection

In post-selection, we evaluate the nonlinearity in Eq. (3.76), $\left\langle \hat{B}(\omega) \right\rangle$, over the collection of eigenstates measured by the detector, $|\xi\rangle_{out}$. To determine

$$\left\langle \hat{B}(\omega) \right\rangle_{\xi} \equiv {}_{out}\left\langle \xi \middle| \hat{B}(\omega) \middle| \xi \right\rangle_{out}, \tag{3.105}$$

we will make use of the fact that $|\xi\rangle_{out}$ is also an eigenstate of $\hat{A}(\omega)$ with an eigenvalue we call

$$\eta(\omega) = \xi(\omega) - \left\langle \hat{B}(\omega) \right\rangle_{\xi}. \tag{3.106}$$

The equality follows from Eq. (3.76) with classical thermal noise ignored, which we will incorporate at the end of the calculation. Notice that if we express $\left\langle \hat{B}(\omega) \right\rangle_{\xi}$ in terms of $\eta\left(\omega\right)$, we can also express it in terms of $\xi\left(\omega\right)$.

Our strategy will be to project $\hat{B}\left(t\right)$ onto the space spanned by the operators $\hat{A}\left(z\right)$ for all times z:

$$\hat{B}\left(t\right) = \int_{-\infty}^{T} K\left(t-z\right)\hat{A}\left(z\right)dz + \hat{R}\left(t\right), \tag{3.107}$$

where $\hat{R}\left(t\right)$ is the error operator in the projection. As a result,

$$\left\langle \hat{B}\left(t\right)\right\rangle_{\xi} = \int_{-\infty}^{T} K\left(t-z\right)\eta\left(z\right)dz + \left\langle \hat{R}\left(t\right)\right\rangle_{\xi}, \tag{3.108}$$

where we made use of the definition of $\eta(t)$. In Appendix 3.10, we show that if we choose $K(t)$ in such a way that $\hat{R}(t)$ and $\hat{A}(z)$ are uncorrelated for all times t and z,

$${}_{in}\left\langle 0\right|\hat{R}\left(t\right)\hat{A}\left(z\right)\left|0\right\rangle_{in} + {}_{in}\left\langle 0\right|\hat{A}\left(z\right)\hat{R}\left(t\right)\left|0\right\rangle_{in} = 0 \tag{3.109}$$

then $\left\langle \hat{R}\left(t\right)\right\rangle_{\xi} = 0$.

In the long measurement time limit, $T \gg 1$, we make use of Eq. (3.107) to express $\hat{R}(t)$ in terms of $\hat{B}(t)$ and $\hat{A}(z)$ and then Fourier transform Eq. (3.109) to solve for $K(\omega)$. We obtain

$$K\left(\omega\right) = \frac{S_{B,A}\left(\omega\right)}{S_{A,A}\left(\omega\right)}. \tag{3.110}$$

Making use of Eq. (3.106), we express $\left\langle \hat{B}\left(\omega\right)\right\rangle_{\xi}$ in terms of $\xi(\omega)$,

$$\left\langle \hat{b}_2\left(\omega\right)\right\rangle_{\xi} = \left\langle \hat{B}\left(\omega\right)\right\rangle_{\xi} = \frac{\xi\left(\omega\right)}{1+K\left(\omega\right)}, \tag{3.111}$$

which we then substitute into Eq. (3.91) to establish that post-selection's spectrum (without classical thermal noise) is given by

$$\left|1+K\left(\omega\right)\right|^2 S_{A,A}\left(\omega\right).$$

We finally add the contribution of classical thermal noise to $\hat{b}_2$'s spectrum, and obtain

$$S^{(post)}_{b_2,b_2}\left(\omega\right) = \left|1+K\left(\omega\right)\right|^2 S_{A,A}\left(\omega\right) + \frac{\alpha^2}{\hbar^2} S^{cl}_{x,x}\left(\omega\right). \tag{3.112}$$

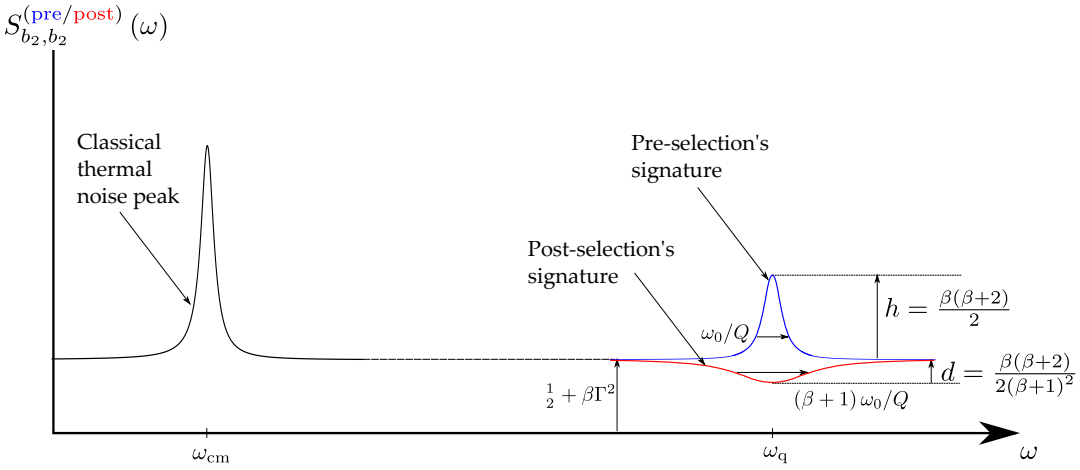

Figure 3.5: A depiction of the predicted signatures of semi-classical gravity. The pre-selection measurement prescription's signature is a narrow and tall Lorentzian peak, while the post-selection measurement prescription's signature is a shallow but wide Lorentzian dip. Both prescriptions predict a Lorentzian peak of thermal noise at ω_{cm}. Note that the figure is not to scale and throughout this article, we follow the convention of 2-sided spectra.

Around ω_q, we apply a narrowband approximation on $\left|G_q(\omega)\right|^2$, and obtain

$$S^{(post)}_{b_2,b_2}\left(\omega \approx \omega_q\right) \approx \left(\frac{1}{2}+\beta\Gamma^2\right)\left(1+D(\omega)\right), \tag{3.113}$$

where

$$D(\omega) \equiv -\frac{\beta(\beta+2)\gamma_m^2}{2\left(1/2+\beta\Gamma^2\right)\left((\beta+1)^2\gamma_m^2+4\left(\omega-\omega_q\right)^2\right)}$$

is a Lorentzian. By comparing $S^{(post)}_{b_2,b_2}(\omega)$ with $S^{(QM)}_{b_2,b_2}(\omega)$, given by Eq. (3.94), we conclude that $1+D(\omega)$ is the signature of post-selection. We summarize it in the following way:

$$1+D(\omega) = 1-\frac{d_{post}}{1+4\dfrac{(\omega-\omega_q)^2}{\Delta^2_{post}}} \tag{3.114}$$

with the depth of the dip, and its FWHM given by

$$d_{post} = \frac{\beta(\beta+2)}{2\left(1/2+\beta\Gamma^2\right)(\beta+1)^2}, \quad \Delta_{post} = (\beta+1)\gamma_m, \tag{3.115}$$

respectively. A summary of the post-selection spectrum around ω_q is depicted in Fig. 3.5.

3.6 Feasibility analysis

In this section, we determine the feasibility of testing the Schroedinger-Newton theory with state of the art optomechanics setups. We will evaluate how long a particular setup would need to run for before it can differentiate between the flat noise background predicted by standard quantum mechanics around ω_q:

$$S^{(QM)}_{b_2,b_2}\left(\omega \approx \omega_q\right) = 1/2 + \beta\Gamma^2, \tag{3.116}$$

and the signatures of the pre- and post- measurement prescriptions,

$$\begin{aligned} S^{(pre)}_{b_2,b_2}\left(\omega \approx \omega_q\right) &\approx \left(\frac{1}{2} + \beta\Gamma^2\right)\left(1 + \frac{h_{pre}}{1 + 4\dfrac{(\omega-\omega_q)^2}{\Delta^2_{pre}}}\right) \\ S^{(post)}_{b_2,b_2}\left(\omega \approx \omega_q\right) &\approx \left(\frac{1}{2} + \beta\Gamma^2\right)\left(1 - \frac{d_{post}}{1 + 4\dfrac{(\omega-\omega_q)^2}{\Delta^2_{post}}}\right), \end{aligned}$$

with h_{pre} and Δ_{pre} defined by Eq. (3.103), and d_{post} and Δ_{post} defined by Eq. (3.115).

Note that our analysis holds when the classical thermal noise peak is well resolved from the SN signatures at ω_q. Specifically, we require that $\omega_q - \omega_{\rm cm}$ be much larger than γ_m. For torsion pendulums, this is not a difficult constraint, as ω_{SN} is on the order of 0.1 s^{-1} for many materials, as is shown in Table 3.1.

3.6.1 Likelihood ratio test

We will perform our statistical analysis with the likelihood ratio test. Specifically, we will construct an estimator, Y, which expresses how likely the data collected during an experiment for a period τ is explained by standard quantum mechanics or the Schroedinger-Newton theory.

The estimator Y is given by the logarithm of the ratio of the likelihood functions associated with each theory:

$$Y = \ln \frac{p\left(\mathcal{D}|\mathrm{QM}\right)}{p\left(\mathcal{D}|\mathrm{SN}\right)}$$

where $p(\mathcal{D}|\text{QM})$ is the likelihood for measuring the data

$$\mathcal{D} = \{\xi(t) : 0 < t < \tau\}$$

conditioned on standard quantum mechanics being correct, and $p(\mathcal{D}|\text{SN})$ is the probability of measuring the data conditioned on the Schroedinger-Newton theory, under the pre-selection or post-selection measurement prescription, being true. Note that we will compare the predictions of standard quantum mechanics with the Schroedinger Newton theory under each prescription separately. All likelihood probabilities are normal distributions characterized by correlation functions which are inverse Fourier transforms of the spectra presented at the beginning of this section.

We can form a decision criterion based on Y. If Y exceeds a given threshold, y_{th}, we conclude that gravity is not fundamentally classical. If Y is below the negative of that threshold, we conclude that the data can be explained with the Schroedinger Newton theory. Otherwise, no decision is made.

With this strategy, we can numerically estimate how long the experiment would need to last for before a decision can be confidently made. We call this period τ_{min} and define it to be the shortest measurement time such that there exists a threshold y_{th} which produces probabilities of making an incorrect decision, and of not making a decision that are both below a desired confidence level p.

3.6.2 Numerical simulations and results

We determined in the last section that the signatures of pre-selection and post-selection are both Lorentzians. By appropriately processing the measurement data, $\xi(t)$, the task of ruling out or validating the Schroedinger Newton theory can be reduced to determining whether fluctuations of data collected over a certain period of time is consistent with a flat or a Lorentzian spectrum centered around 0 frequency:

$$S_{h(d)}(\omega) = 1 + \frac{h(-d)}{1 + 4\omega^2/\gamma^2} \quad \text{or} \quad S(\omega) = 1, \tag{3.117}$$

where γ is the full width at half maximum, $S_{h(d)}$ corresponds to a Lorentzian peak (dip) with height h (depth d) on top of white noise.

The data can be processed by filtering out irrelevant features except for the signatures

of post- and pre-selection around ω_q, and then shifting the spectrum:

$$\tilde{\xi}(t) \equiv e^{-i\omega_q t} \int_{\omega_q-\sigma}^{\omega_q+\sigma} \xi(\Omega)\, e^{i\Omega t} d\Omega, \tag{3.118}$$

where $\xi(\Omega)$ is the Fourier transform of $\xi(t)$, and σ has to be larger than the signatures' width but smaller than the separation between the classical thermal noise feature at $\omega_{\rm cm}$ and the signatures at ω_q. Two independent real quadratures can then be constructed out of linear combinations of $\tilde{\xi}(t)$:

$$\tilde{\xi}_c(t) \equiv \frac{\tilde{\xi}(t) + \tilde{\xi}^*(t)}{2}, \qquad \tilde{\xi}_s(t) \equiv \frac{\tilde{\xi}(t) - \tilde{\xi}^*(t)}{2i}. \tag{3.119}$$

We will carry out an analysis of the measurement time with $\tilde{\xi}_c(t)$ in mind.

We numerically generated data whose fluctuations are described by white noise, or lorentzians of different heights and depths. For example, in Fig. 3.6, we show the distribution of Y for two sets of 10^5 simulations of $\tilde{\xi}_c(t)$ over a period of $200/\gamma$ (with γ set to 1). In one set, $\tilde{\xi}_c(t)$ is chosen to have a spectrum of S_d with $d = 0.62$, and in the second set, $\tilde{\xi}_c(t)$ has a spectrum of 1. The resultant distribution for both sets is a generalized chi-squared distribution which seems approximately Gaussian. Fig. 3.6 is also an example of our likelihood ratio test: if the collected measurement data's estimator satisfies $Y < -y_{th}$, for $y_{th} = 2$, we decide that its noise power spectrum is S_d, if $Y > y_{th}$, white noise and if $-y_{th} \leq Y \leq y_{th}$, no decision is made. In table 3.2, we show the associated probabilities of these different outcomes. Note that the choice of y_{th} is important, and would drastically vary the probabilities in this table.

We then determined the shortest measurement time, τ_{min}, needed to distinguish between a lotentzian spectrum and white noise, such that the probability of making a wrong decision and of not making a decision are both below a confidence level, p, of 10%. Our analysis is shown in Fig. 3.7. Since $\tilde{\xi}_c(t)$ and $\tilde{\xi}_s(t)$ are independent, we halved τ_{min}, as an identical analysis to the one performed on $\tilde{\xi}_c(t)$ can also be conducted on $\tilde{\xi}_s(t)$.

As shown in Fig. 3.7(a), numerical simulations of the minimum measurement time needed to decide between white noise and a spectrum of the form S_h, are well fitted by

$$\tau_{min}(h) \approx \frac{27}{h^{0.73}} \times \frac{1}{\gamma/2}, \tag{3.120}$$

where $1/(\gamma/2)$ is the Lorentzian signature's associated coherence time. The fit

	$\mathbb{P}$ (correct)	$\mathbb{P}$ (wrong)	$\mathbb{P}$ (indecision)
Data has S_d spectrum	78.7%	1.1%	20.2%
Data has $S = 1$ spectrum	80.2%	2.1%	17.7%

Table 3.2: The probabilities of the different outcomes of the likelihood ratio test on a particular measurement data stream with an estimator following either of the two distributions shown in Fig. 3.6. The three possible outcomes are (1) deciding that the data has a spectrum of S_d, (2) deciding that it has a white noise spectrum ($S = 1$) or (3) making no decisions at all. $\mathbb{P}$ (correct) stands for the probability of deciding (1) or (2) correctly, $\mathbb{P}$ (wrong) is the probability of making the wrong decision on what spectrum explains the data, and $\mathbb{P}$ (indecision) is the probability of outcome 3. Note that a different table would have been generated if a different threshold, y_{th}, had been chosen in Fig. 3.6.

breaks down for heights less than about 10. However, as we show in the next section, current experiments can easily access the regime of large peak heights.

In Fig. 3.7(b), we show that numerical simulations of the minimum measurement time needed to decide between white noise and a spectrum of the form S_d, are well fitted by

$$\tau_{min}(d) \approx \left(\frac{18.3}{d^2} - \frac{10.7}{d}\right) \times \frac{1}{\gamma/2}. \tag{3.121}$$

This fit is accurate, except when d is close to 1. In the next section, we show that this parameter regime is of no interest to us.

Moreover, we ran simulations for higher confidence levels p (in %). We show our numerical results for pre-selection in Fig. 3.8. For h between 1000 and 4000, a decrease in p from 10% to 1% results in a 4.5-5.5 fold increase in τ_{min}. Our results for post-selection are presented in Fig. 3.9. For $d = 0.62$ (which, as we show in the next section, is the normalized depth level at which most low thermal noise experiments will operate at), then τ_{min} as a function of p is well summarized by

$$\tau_{min}(d = 0.62, p) \approx \left(2.94 - 7.38 \times \text{erfc}^{-1}\left(\frac{p}{100}\right)\right)^2 \times \frac{1}{\gamma/2}.$$

We can also fit $\tau_{min}(d, p)$ at other values of d by a function of this form.

In the following sections, we present scaling laws for the minimum measurement time, τ_{min}, given a confidence level of 10%, in terms of the parameters of an optomechanics experiment, and with the measurement strength β optimized over, for both the pre-selection and post-selection measurement prescriptions.

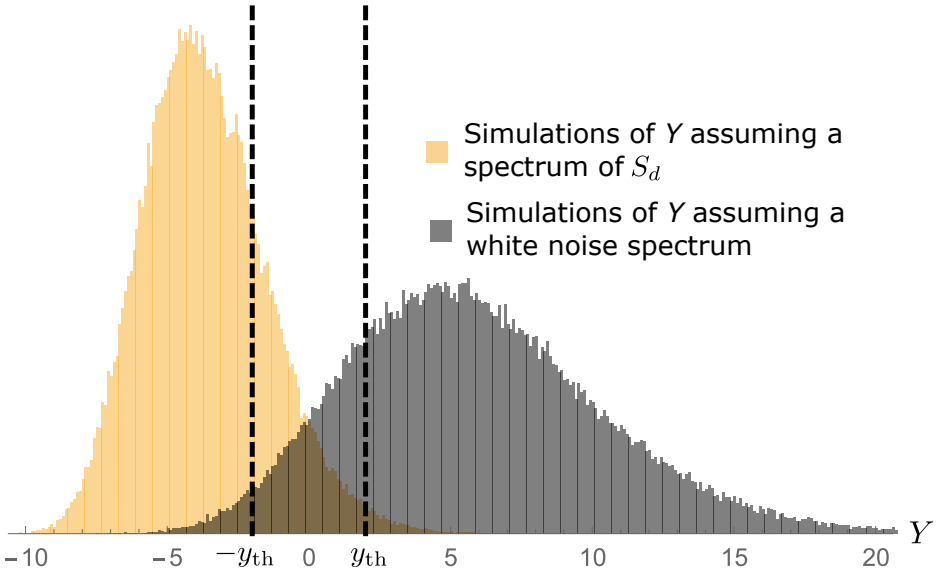

Figure 3.6: A histogram showing the distribution of two sets of 10^5 realizations of $\tilde{\xi}_c(t)$ over a period of $200/\gamma$ (with γ set to 1), and a time discretization of $dt = 0.14/\gamma$. In one set, $\tilde{\xi}_c(t)$ is chosen to have a spectrum of S_d with $d = 0.62$, and in the second set, $\tilde{\xi}_c(t)$ has a spectrum of 1. y_{th}, which is chosen to be 2 in this example, allows us to construct a decision criterion: if the collected measurement data's estimator satisfies $Y < -y_{th}$, we decide that its noise power spectrum is S_d, if $Y > y_{th}$, white noise and if $-y_{th} \leq Y \leq y_{th}$, no decision is made.

3.6.3 Time required to resolve pre-selection's signature

The normalized pre-selection signature's height, h_{pre} given by Eq. (3.103), is a monotonically increasing function of β. Consequently, the larger β is, the easier it would be to distinguish pre-selection from standard quantum mechanics. Using Eq. (3.103) and the fit given in Fig. 3.7a of $13.5/h^{0.73}$ (in units of the Lorentzian signature's coherence time), τ_{min} in the limit of large β scales as approximately

$$\tau_{min} \approx \frac{27}{\gamma_m}\left(\frac{2\Gamma^2}{\beta}\right)^{0.73}. \tag{3.122}$$

It seems that arbitrarily increasing the measurement strength would yield arbitrarily small measurement times. However, as explained in subsection 3.5.2, our results hold for $\Delta x_{cm} \ll \Delta x_{zp}$, which places a limit on β of

$$\beta \ll \frac{2\Delta x_{zp}^2}{\hbar/(2M\omega_q)},$$

where we made use of the expression for Δx_{cm} given by Eq. (3.104).

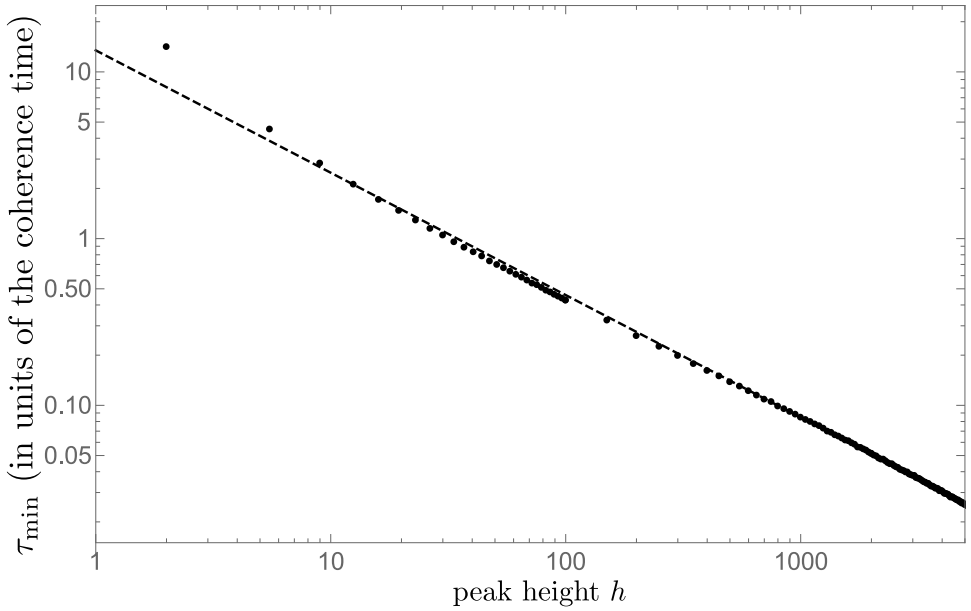

(a) Time required to distinguish a flat spectrum from a Lorentzian peak. The dashed line is a fit of $13.5/h^{0.73}$.

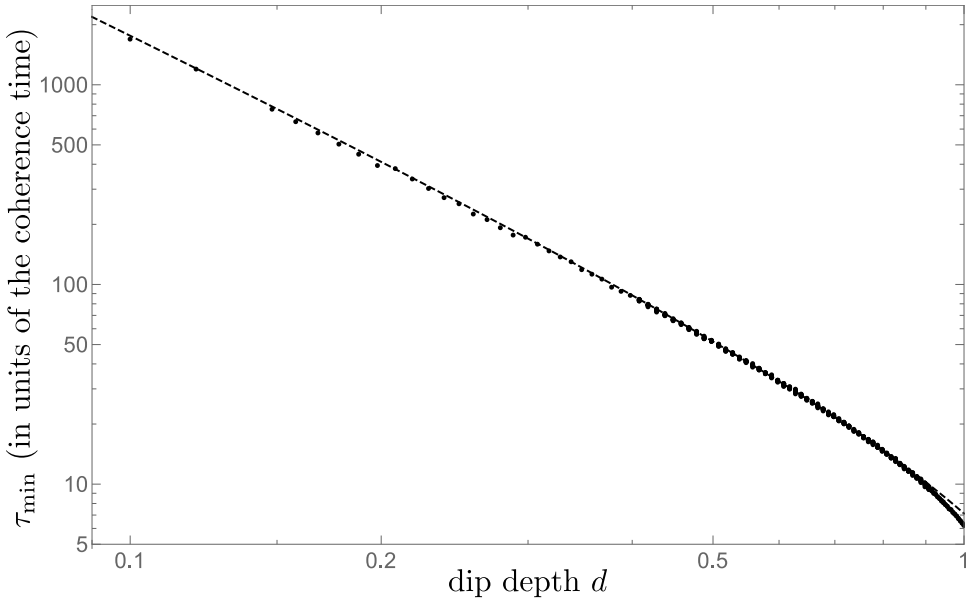

(b) Time required to distinguish a flat spectrum from a Lorentzian dip. The dashed line is a fit of $18.3/d^2 - 10.7/d$.

Figure 3.7: Simulation results showing the minimum measurement time, τ_{min}, required to distinguish between a Lorentzian spectrum and a flat background in such a way that the probabilities of indecision and of making an error are both below 10%. Plot (a) shows results for a Lorentzian peak, while plot (b) is for a Lorentzian dip. The coherence time is given by the inverse of the half width at half maximum of the Lorentzian. Note that both plots are log-log plots.

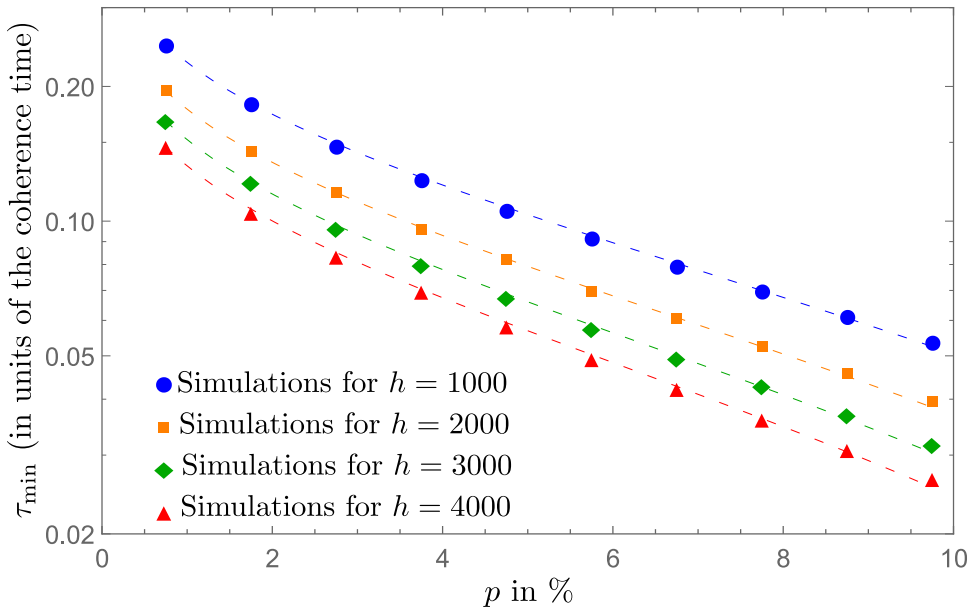

Figure 3.8: Simulation results showing the minimum measurement time, τ_{min}, required to distinguish between the Schroedinger-Newton theory with the pre-selection measurement prescription (which has the signature of a Lorentzian with depth h) and standard quantum mechanics in such a way that the probabilities of indecision and of making an error are both below $p\%$. The coherence time is given by the inverse of the half width at half maximum of the Lorentzian. Note that the y-axis is on a log scale. Moreover, the dashed lines are *only* to guide the eye (and are fits of the form $a\ \ln(p) + b$).

Placing the limit on β at $1/10$ the quoted value above, for $h \gtrsim 10$, τ_{min} scales with the experimental parameters in the following way:

$$\tau_{min} \sim 1.6 \text{ hours} \times \left(\frac{T_0}{300\ K}\right)^{0.73} \times \left(\frac{\omega_{\rm cm}}{2\pi \times 10\ mHz}\right)^{0.47} \times \left(\frac{184\ amu}{m}\right)^{0.49} \times \left(\frac{200\ g}{M}\right)^{0.73} \times \left(\frac{10^4}{Q}\right)^{0.47} \times \left(\frac{0.359\ s^{-1}}{\omega_{SN}}\right)^{1.96} \tag{3.123}$$

where m is the mass of a constituent atom of the test mass, and we have assumed that the test mass is made out of Tungsten.

Using the expressions for the measurement strength and for α^2, given by Eq. (3.97) and Eq. (5.44), respectively, we determine that the input optical power needed to reach the above quoted value of τ_{min} is

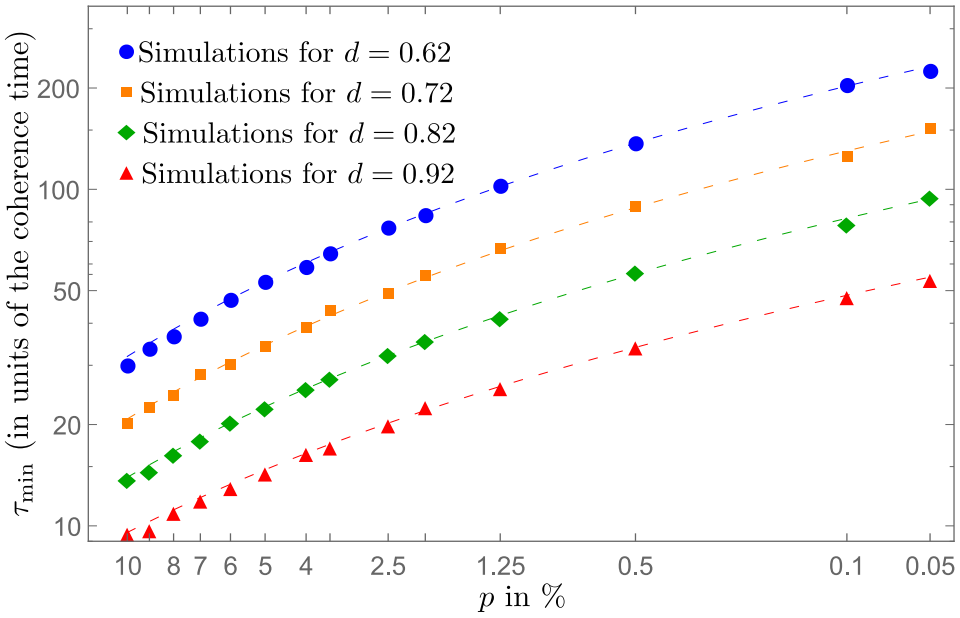

Figure 3.9: Simulation results showing the minimum measurement time, τ_{min}, required to distinguish between the Schroedinger-Newton theory with the post-selection measurement prescription (which has the signature of a Lorentzian with depth d) and standard quantum mechanics in such a way that the probabilities of indecision and of making an error are both below p%. The coherence time is given by the inverse of the half width at half maximum of the Lorentzian. Note that the x-axis is scaled by the inverse of the complimentary error function, $erfc^{-1}$, and the y-axis is on a log scale. Moreover, the dashed lines are to guide the eye and are fits of the form $\left(a - b \times erfc^{-1}\left(p/100\right)\right)^2$.

$$I_{in} \approx 432 \text{ mW} \times \left(\frac{10^4}{Q}\right) \times \left(\frac{m}{184\ amu}\right)^{2/3} \times \left(\frac{M}{200\ g}\right)^2 \times \left(\frac{\omega_{\text{cm}}}{2\pi \times 10\ mHz}\right) \times \left(\frac{\omega_{SN}}{0.359\ s^{-1}}\right)^{2/3} \times \left(\frac{2\pi \times 0.2\ THz}{\omega_c}\right) \times \left(\frac{T}{10^{-2}}\right)^2. \tag{3.124}$$

We are allowed to make use of the fit presented in Fig. 3.7(a), of $\tau_{min} = 27/h^{0.73}$ (in units of the coherence time), which holds only for $h \gtrsim 10$, because the pre-selection signature's normalized peak height can be easily made to satisfy this constraint.

Indeed, for the parameters given above

$$h \approx 8235 \times \left(\frac{Q}{10^4}\right)^2 \times \left(\frac{m}{184\ amu}\right)^{2/3} \times \left(\frac{M}{200\ g}\right) \times \left(\frac{2\pi \times 10\ mHz}{\omega_{\rm cm}}\right)^2 \times \left(\frac{\omega_{SN}}{0.359\ s^{-1}}\right)^{8/3} \times \left(\frac{300\ K}{T_0}\right).$$

3.6.4 Time required to resolve post-selection's signature

As indicated by Eq. (3.115), the depth and width of post-selection's signature are determined by 3 parameters: β, Γ^2 and γ_m. For a given Γ^2, we can determine the optimal measurement strength β that would minimize τ_{min}. We numerically carried out this analysis, and we show our results in Fig. 3.10. For Γ^2 less than about 0.1, the optimal choice of the measurement strength seems to follow a simple relationship:

$$\beta_{opt} \approx \frac{0.31}{\Gamma^2},$$

with a corresponding measurement time, τ_{min}, of about $200\Gamma^2/\gamma_m$. Note that this is a soft minimum, as large deviations from β_{opt} still yield near optimal values of τ_{min}. Specifically, measurement strengths roughly between $0.1/\Gamma^2$ and $0.7/\Gamma^2$ achieve measurement times below $225\Gamma^2/\gamma_m$.

Moreover, in the parameter regime of $\Gamma^2 < 0.1$, the normalized post-selection dip depth at β_{opt} is 0.62, which falls well in the region where the fit presented in Fig. 3.7(b), of $\tau_{min} = 18.3/d^2 - 10.7/d$ (in units of the coherence time), is accurate.

In the limit of $\omega_{SN} \gg \omega_{\rm cm}$, the optimal measurement time scales as

$$\tau_{min} \sim 13 \text{ days} \times \left(\frac{10^7}{Q}\right) \times \left(\frac{T_0}{1\ K}\right) \times \left(\frac{0.488\ s^{-1}}{\omega_{SN}}\right)^3 \times \left(\frac{\omega_{\rm cm}}{2\pi \times 4\ mhz}\right), \tag{3.125}$$

where we assumed that the mechanical oscillator is made out of Osmium. Moreover, the input optical power needed to reach the above quoted value of τ_{min} is

$$I_{in} \approx 4.8 \text{ nW} \times \left(\frac{Q}{10^7}\right) \times \left(\frac{1\ K}{T_0}\right)^2 \times \left(\frac{M}{200\ g}\right)^2 \times \left(\frac{2\pi \times 4\ mHz}{\omega_{\rm cm}}\right) \times \left(\frac{\omega_{SN}}{0.488\ s^{-1}}\right)^4 \times \left(\frac{2\pi \times 0.2\ THz}{\omega_c}\right) \times \left(\frac{T}{10^{-2}}\right)^2. \tag{3.126}$$

Finally, we note that the experiment does not need to remain stable, or to operate, for the entire duration of τ_{min}. Since the coherence time of the post-selection signature,

$$\frac{1}{(\beta_{opt}+1)\gamma_m},$$

is much less than τ_{min} (in the example above, the coherence time is 5 hours), the experiment can be repeatedly run over a single coherence time. Alternatively, numerous experiments can be run in parallel.

3.7 Conclusions

We proposed optomechanics experiments that would look for signatures of classical gravity. This theory appreciably modifies the free unmonitored dynamics of the test mass when the following two criteria are met. First, the choice of material for the test mass is crucial. We recommend crystals with tightly bound heavy atoms around their lattice sites. Tungsten and Osmium crystals meet this criterion. Second, we recommend that the resonant frequency of the test mass be as small as possible. Torsion pendulums meet this requirement.

When adding thermal noise and measurements to our analysis, we encountered two conceptual difficulties. Both appear because the Schroedinger-Newton equation is non-linear. The first difficulty is the breakdown of the density matrix formalism. As a consequence, we had to propose a specific ensemble of pure states to describe the quantum state of the thermal bath.

The second difficulty is generalizing Born's rule to nonlinear quantum mechanics. In section §3.4, we provided two prescriptions for calculating probabilities in the Schroedinger-Newton theory. The first prescription, which we term pre-selection, takes the probability of obtaining a particular measurement result to be the modulus squared of the overlap between the forward-evolved initial state, which we choose as a boundary state for the non-linear time evolution operator, and the eigenstate corresponding to that measurement result. The second prescription, which we term post-selection, takes the probability of obtaining a particular measurement result to be the modulus squared of the overlap between the backwards-evolved measured eigenstate, which we choose as a boundary state for the non-linear evolution operator, and the initial state. Note that the predictions of both pre-selection and post-selection are consistent with that of linear quantum mechanics in the limit that the Schroedinger-Newton nonlinearity vanishes (*i.e.* $\omega_{SN} \to 0$).

We then proceeded to obtain the signatures of classical gravity predicted by both

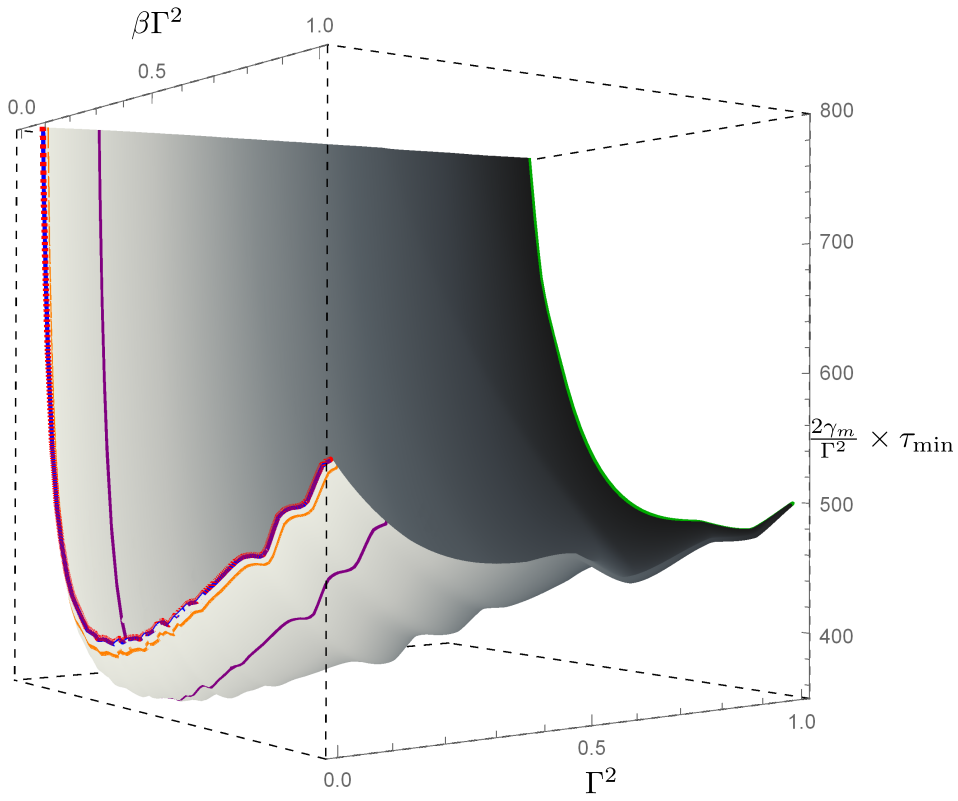

(a) τ_{min} for different values of Γ^2, β and γ_m

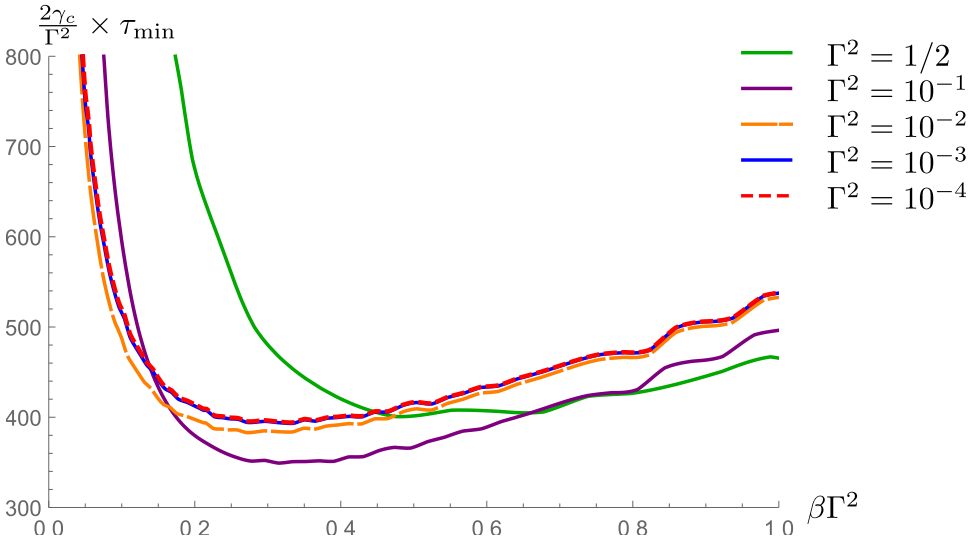

(b) τ_{min} for fixed values of Γ^2

Figure 3.10: Minimum measurement time required to distinguish between the Schroedinger-Newton theory with the post-selection measurement prescription and standard quantum mechanics in such a way that the probabilities of indecision and of making an error are both below 10%. Note that we interpolated the data given in Fig. 3.7 to create this figure.

these prescriptions in the spectrum of phase fluctuations of the outgoing light. Both signatures are Lorentzians centered around the frequency ω_q. The pre-selection prescription predicts a peak, while post-selection predicts a dip. We summarize these features in figure 3.5, which is valid when the resonant frequency of the mechanical oscillator, $\omega_{\rm cm}$, is much smaller than ω_{SN}.

Finally, in the limit of the classical thermal noise peak being well separated from the SN signatures, we numerically simulated the experiment's expected measurement results and determined that pre-selection is easily testable with current optomechanics technology. However, testing post-selection will be much more challenging, although is feasible with state-of-the-art experimental parameters. In particular, we require cryogenic temperatures and a high Q low frequency torsion pendulum made out of a material with a high ω_{SN}. Eq. (3.125) contains the scaling of the minimum measurement time required to confidently test post-selection with these experimental parameters.

Acknowledgments

We thank K. Thorne, J. Preskill, P.C.E. Stamp, H. Miao, Y. Ma, C. Savage, and H. Yang for discussions. Research of Y.C. and H.L. are supported by NSF grants PHY-1404569 and PHY-1506453, as well as the Institute for Quantum Information and Matter, a Physics Frontier Center.

3.8 Appendix: Conservation of energy in the SN theory

Consider the SN equation for a collection of N particles of mass m:

$$\hat{V}_{SN} = -Gm^2 \sum_{ij=1}^{N} \int dx_j \frac{p_j\left(x_j\right)}{\left|\hat{x}_i - x_j\right|} \tag{3.127}$$

where $p_j\left(x_j\right)$ is the probability distribution for the jth particle to be at location x_j:

$$p_j\left(x_j\right) = \int \left(\prod_{i=1}^{N} dy_i\right) \delta\left(y_j - x_j\right) \left|\Psi\left(y_1, y_2, ..., y_N\right)\right|^2 . \tag{3.128}$$

Ψ is the many-body wavefunction for these N particles.

Let us investigate conservation of energy within the SN theory. In standard quantum mechanics, the energy operator is given by the Hamiltonian. Our non-linear Hamiltonian is

$$\hat{H} = \sum_{i=1}^{N} \frac{\hat{P}_i^2}{2m} + \hat{V}_{NG}\left(\hat{x}_1, ..., \hat{x}_N\right) + \hat{V}_{SN}, \tag{3.129}$$

where $\hat{V}_{NG}\left(\hat{x}_1, ..., \hat{x}_N\right)$ encodes the non-gravitational potential energy. Under the non-linear SN theory, $\hat{H}$ is not conserved because of $\hat{V}_{SN}$'s dependence on the wavefunction:

$$\frac{d\hat{H}}{dt} = \frac{\partial \hat{H}}{\partial t} = \partial_t \hat{V}_{SN} \neq 0 \tag{3.130}$$

Is there a quantity that is conserved? Consider

$$\hat{E} = \sum_{i=1}^{N} \frac{\hat{P}_i^2}{2m} + \hat{V}_{NG}\left(\hat{x}_1, ..., \hat{x}_N\right) + \beta \hat{V}_{SN}, \tag{3.131}$$

where β is to be determined such that $d\left\langle \hat{E} \right\rangle / dt = 0$. We will show that $\beta = 1/2$ meets this condition.

We begin the proof with the Heisenberg equation of motion for $\hat{E}$. By expressing $\hat{E}$ as $\hat{H} - (1-\beta)\hat{V}_{SN}$, we obtain

$$\begin{aligned} \frac{d\hat{E}}{dt} &= \frac{i}{\hbar}\left[\hat{H}, \hat{E}\right] + \frac{\partial \hat{E}}{\partial t} \\ &= \frac{i(1-\beta)Gm^2}{2\hbar m} \sum_i \sum_{jk} \int dx_k \left[\hat{P}_i^2, \frac{p_k\left(x_k\right)}{\left|\hat{x}_j - x_k\right|}\right] - \beta Gm^2 \sum_{ij=1}^{N} \int dx_j \frac{\dot{p}_j\left(x_j\right)}{\left|\hat{x}_i - x_j\right|}. \end{aligned} \tag{3.132}$$

Taking the expectation value of both sides, and evaluating the commutator in the

first term, we obtain

$$\begin{aligned}\frac{d\left\langle \hat{E}\right\rangle }{dt} &= \frac{-\left(1-\beta\right)Gm}{2}\sum_{ik}\int dx_{k}\left\langle \hat{P}_{i}\frac{p_{k}\left(x_{k}\right)}{\left|\hat{x}_{i}-x_{k}\right|^{2}}+\frac{p_{k}\left(x_{k}\right)}{\left|\hat{x}_{i}-x_{k}\right|^{2}}\hat{P}_{i}\right\rangle \\ &\quad -\beta Gm^{2}\sum_{ij=1}^{N}\int dx_{i}\int dx_{j}\frac{p_{i}\left(x_{i}\right)\dot{p}_{j}\left(x_{j}\right)}{\left|x_{i}-x_{j}\right|}.\end{aligned}$$

We then evaluate the expectation value in the first term. Defining the vector $\boldsymbol{x}\equiv\left(x_{1},...,x_{N}\right)$, we have

$$\begin{aligned}&\left\langle \hat{P}_{i}\frac{p_{k}\left(y_{k}\right)}{\left|\hat{x}_{i}-y_{k}\right|^{2}}+\frac{p_{k}\left(y_{k}\right)}{\left|\hat{x}_{i}-y_{k}\right|^{2}}\hat{P}_{i}\right\rangle \\ &= \int d\boldsymbol{x}\Psi\left(\boldsymbol{x}\right)^{*}\left(-i\hbar\partial_{x_{i}}\frac{p_{k}\left(y_{k}\right)}{\left|x_{i}-y_{k}\right|^{2}}\Psi\left(\boldsymbol{x}\right)\right)+\int d\boldsymbol{x}\Psi\left(\boldsymbol{x}\right)^{*}\frac{p_{k}\left(y_{k}\right)}{\left|x_{i}-y_{k}\right|^{2}}\left(-i\hbar\partial_{x_{i}}\Psi\left(\boldsymbol{x}\right)\right).\end{aligned}$$

Next, we integrate by parts multiple times, and use that

$$\frac{p_{k}\left(y_{k}\right)}{\left|x_{i}-y_{k}\right|^{2}}=-\partial_{x_{i}}\frac{p_{k}\left(y_{k}\right)}{\left|x_{i}-y_{k}\right|}, \tag{3.133}$$

to obtain

$$\begin{aligned}&\frac{i}{\hbar}\left\langle \hat{P}_{i}\frac{p_{k}\left(y_{k}\right)}{\left|\hat{x}_{i}-y_{k}\right|^{2}}+\frac{p_{k}\left(y_{k}\right)}{\left|\hat{x}_{i}-y_{k}\right|^{2}}\hat{P}_{i}\right\rangle \\ &= \int d\boldsymbol{x}\frac{p_{k}\left(y_{k}\right)}{\left|x_{i}-y_{k}\right|}\partial_{x_{i}}\left(\Psi\left(\boldsymbol{x}\right)^{*}\partial_{x_{i}}\Psi\left(\boldsymbol{x}\right)-\Psi\left(\boldsymbol{x}\right)\partial_{x_{i}}\Psi\left(\boldsymbol{x}\right)^{*}\right).\end{aligned}$$

This result can be connected to the continuity equation (which is satisfied by the SN theory):

$$\partial_{t}\rho+\nabla.\vec{j}=0, \tag{3.134}$$

where

$$\rho=\left|\Psi\right|^{2};\qquad\vec{j}=\frac{\hbar}{2im}\left(\Psi^{*}\nabla\Psi-\Psi\nabla\Psi^{*}\right). \tag{3.135}$$

We integrate over all variables except x_i (which we denote by $\boldsymbol{x}_{\neq i}$), obtaining

$$\begin{aligned}\int d\boldsymbol{x}_{\neq i}\left(\partial_{t}\rho+\nabla.\vec{j}\right) &= 0\\ &= \partial_{t}p_{i}\left(x_{i}\right)+\frac{\hbar}{2im}\int d\boldsymbol{x}_{\neq i}\sum_{j}\partial_{x_{j}}\left(\Psi^{*}\partial_{x_{j}}\Psi-\Psi\partial_{x_{j}}\Psi^{*}\right).\end{aligned}$$

For $j \neq i$,

$$\int dx_j \partial_{x_j} \left(\Psi^* \partial_{x_j} \Psi - \Psi \partial_{x_j} \Psi^* \right) = 0 \tag{3.136}$$

by integration by parts. Thus,

$$\partial_t p_i \left(x_i \right) = -\frac{\hbar}{2im} \int d\boldsymbol{x}_{\neq i} \partial_{x_i} \left(\Psi^* \partial_{x_i} \Psi - \Psi \partial_{x_i} \Psi^* \right) \tag{3.137}$$

so

$$\begin{aligned} & \frac{i}{\hbar} \left\langle \hat{P}_i \frac{p_k \left(y_k \right)}{\left| \hat{x}_i - y_k \right|^2} + \frac{p_k \left(y_k \right)}{\left| \hat{x}_i - y_k \right|^2} \hat{P}_i \right\rangle \\ = & \int dx_i \frac{p_k \left(y_k \right)}{\left| x_i - y_k \right|} \frac{-2im}{\hbar} \int d\boldsymbol{x}_{\neq i} \left(-\frac{\hbar}{2im} \partial_{x_i} \left(\Psi^* \partial_{x_i} \Psi - \Psi \partial_{x_i} \Psi^* \right) \right) \\ = & \frac{-2im}{\hbar} \int dx_i \frac{p_k \left(y_k \right) \dot{p}_i \left(x_i \right)}{\left| x_i - y_k \right|}. \end{aligned}$$

Substituting back into $d \left\langle \hat{E} \right\rangle / dt$,

$$\frac{d \left\langle \hat{E} \right\rangle}{dt} = (1 - \beta) Gm^2 \sum_{ji} \int dx_i \int dx_j \frac{p_i \left(x_i \right) \dot{p}_j \left(x_j \right)}{\left| x_j - x_i \right|} - \beta Gm^2 \sum_{ij=1}^{N} \int dx_i \int dx_j \frac{p_i \left(x_i \right) \dot{p}_j \left(x_j \right)}{\left| x_i - x_j \right|},$$

which is equal to 0 when

$$1 - \beta = \beta \tag{3.138}$$

or $\beta = 1/2$.

3.9 Appendix: Derivation of $p_0 \rightarrow \xi$ and $p_0 \leftarrow \xi$

In this Appendix, we derive equations (3.88) and (3.91) presented in subsection 3.4.3:

$$p_{0 \rightarrow \xi} \propto \exp \left[-\frac{1}{2} \int \frac{d\Omega}{2\pi} \frac{\left| \xi(\Omega) - \langle \hat{b}_2(\Omega) \rangle_0 \right|^2}{S_{A,A}} \right], \tag{3.139}$$

$$p_{0 \leftarrow \xi} \propto \exp \left[-\frac{1}{2} \int \frac{d\Omega}{2\pi} \frac{\left| \xi(\Omega) - \langle \hat{b}_2(\Omega) \rangle_\xi \right|^2}{S_{A,A}} \right]. \tag{3.140}$$

They represent the probabilities of obtaining a particular measurement record

$$\{ \xi \left(t \right) : \ 0 < t < \tau \} \tag{3.141}$$

over a period τ in the pre- and post-selection measurement prescriptions, respectively.

The probability of measuring $\xi(t)$ is

$$p_\xi = \left|{}_{out}\langle\xi|\hat{U}|0\rangle_{in}\right|^2, \tag{3.142}$$

where $\hat{U}$ is a shorthand for the pre-selection time evolution operator $\hat{U}_{|0\rangle_{in}}$ or the post selection evolution operator $\hat{U}_{|\xi\rangle_{out}}$, $|0\rangle_{in}$ is a vacuum state for the incoming light, and $|\xi\rangle_{out}$ is the state of the outgoing light corresponding to the measurement results $\xi(t)$. We then rewrite p_ξ to

$$p_\xi = \langle 0|\hat{U}^\dagger|\xi\rangle \langle\xi|\hat{U}|0\rangle, \tag{3.143}$$

where we have used the shorthand $|\xi\rangle$ for $|\xi\rangle_{out}$. $\hat{U}^\dagger |\xi\rangle \langle\xi| \hat{U}$ is a projection operator that can be written as a path integral (refer to p.2 of [15] for a derivation):

$$\hat{P} = \int \mathcal{D}k(t) \exp\left(i \int dt k(t) \left(\hat{b}_2(t) - \xi(t)\right)\right). \tag{3.144}$$

Notice that in the limit that the SN non-linearity vanishes, $\hat{P}$ agrees with the standard quantum mechanics projector onto the measurement results $\xi(t)$. This is due to the fact that when ω_{SN} vanishes, $\hat{b}_2$ becomes a linear operator which matches the prediction of standard quantum mechanics. Consequently, in the limit of $\omega_{SN} \to 0$, $p_{0\to\xi}$ and $p_{0\leftarrow\xi}$ recover the probabilities predicted by linear quantum mechanics.

Substituting $\hat{P}$ back into equation (3.142), we obtain

$$p_\xi = \int \mathcal{D}k(t) \left\langle 0\middle|\exp\left(i \int dt k(t) \hat{b}_2(t)\right)\middle|0\right\rangle \exp\left(-i \int dt k(t) \xi(t)\right). \tag{3.145}$$

Let us explicitly separate the mean of $\hat{b}_2(t)$ by defining $\hat{A}$ in the following way:

$$\hat{b}_2(t) \equiv \hat{A}(t) + \langle 0|\hat{b}_2(t)|0\rangle \equiv \hat{A}(t) + \left\langle \hat{b}_2(t)\right\rangle.$$

We can then rewrite p_ξ to

$$p_\xi = \int \mathcal{D}k(t) \left\langle 0\middle|\exp\left(i \int dt k(t) \hat{A}(t)\right)\middle|0\right\rangle \exp\left(-i \int dt k(t) \left(\xi(t) - \left\langle \hat{b}_2(t)\right\rangle\right)\right).$$

Next, we make use of the fact that $|0\rangle$ is a gaussian state to rewrite the above

expectation value as

$$p_\xi = \int \mathcal{D}k\,(t) \exp\left(-\frac{1}{2}\left\langle 0\left|\left(\int dt k\,(t)\,\hat{A}\,(t)\right)^2\right|0\right\rangle\right) \exp\left(-i\int dt k\,(t)\left(\xi\,(t) - \left\langle \hat{b}_2\,(t)\right\rangle\right)\right). \tag{3.146}$$

Expanding the first exponent, we obtain

$$p_\xi = \int \mathcal{D}k\,(t) \exp\left(-\frac{1}{2}\int dt \int dz k\,(t)\,k\,(z)\left\langle \hat{A}\,(t)\,\hat{A}\,(z)\right\rangle\right) \exp\left(-i\int dt k\,(t)\left(\xi\,(t) - \left\langle \hat{b}_2\,(t)\right\rangle\right)\right). \tag{3.147}$$

p_ξ is a functional Gaussian integral over $k\,(t)$, which we evaluate to

$$p_\xi \propto \exp\left(-\frac{1}{2}\int dt \int dz \left(\xi\,(t) - \left\langle \hat{b}_2\,(t)\right\rangle\right)\left\langle \hat{A}\,(t)\,\hat{A}\,(z)\right\rangle^{-1}\left(\xi\,(z) - \left\langle \hat{b}_2\,(z)\right\rangle\right)\right), \tag{3.148}$$

where $\left\langle \hat{A}\,(t)\,\hat{A}\,(z)\right\rangle^{-1}$ is the inverse of the function $\left\langle \hat{A}\,(t)\,\hat{A}\,(z)\right\rangle$. Assuming we have a time-stationary process, $\left\langle \hat{A}\,(t)\,\hat{A}\,(z)\right\rangle$ can be simplified to $\left\langle \hat{A}\,(t-z)\,\hat{A}\,(0)\right\rangle$ which allows us to take a Fourier transform and obtain

$$p_\xi \propto \exp\left(-\frac{1}{2}\int \frac{d\omega}{2\pi}\frac{\left|\xi\,(\omega) - \left\langle \hat{b}_2\,(\omega)\right\rangle\right|^2}{S_{A,A}\,(\omega)}\right). \tag{3.149}$$

Finally, we note that for post-selection $\left\langle 0|\hat{b}_2\,(t)\,|0\right\rangle$ is calculated with $\hat{b}_2\,(t)$ obtained from an effective Heisenberg picture with the boundary state fixed to be the recorded eigenstates by the measurement device: $|\xi\rangle$. For pre-selection, we obtain $\hat{b}_2\,(t)$ from an effective Heisenberg picture with the boundary state given to be the initial state of the light, vacuum.

3.10 Appendix: More details on calculating $\left\langle \hat{B}(\omega)\right\rangle_\xi$

In subsection 3.5.3, we calculated the spectrum of the outgoing light phase operator

$$\hat{b}_2\,(\omega) = \hat{A}\,(\omega) + \left\langle \hat{B}\,(\omega)\right\rangle_\xi, \tag{3.150}$$

where we have neglected the contribution from classical thermal noise, as it is not important for this Appendix. Both $\hat{A}$ and $\hat{B}$ are linear operators of the form

$$\hat{A}\,(t) = \hat{a}_2\,(t) + \int_{-\infty}^{\infty} L_A\,(t-z)\,\hat{a}_1\,(z)\,dz \tag{3.151}$$

$$\hat{B}\,(t) = \int_{-\infty}^{\infty} L_B\,(t-z)\,\hat{a}_1\,(z)\,dz. \tag{3.152}$$

We presented their exact expressions in Eqs. (3.77) and (3.79). Moreover, $\left\langle \hat{B}(\omega) \right\rangle_{\xi}$ is the expectation value of $\hat{B}$ over the outgoing light state $|\xi\rangle_{out}$ corresponding to the measured eigenstates of the outgoing light's phase. In the calculation of the spectrum, and in particular of $\left\langle \hat{B}(\omega) \right\rangle_{\xi}$, we stated without proof that if Eq. (3.109)

$$ {}_{in}\left\langle 0 \middle| \hat{R}(t)\, \hat{A}(z) \middle| 0 \right\rangle_{in} + {}_{in}\left\langle 0 \middle| \hat{A}(z)\, \hat{R}(t) \middle| 0 \right\rangle_{in} = 0 \tag{3.153} $$

is satisfied then

$$ {}_{out}\left\langle \xi \middle| \hat{R}(t) \middle| \xi \right\rangle_{out} \equiv \left\langle \hat{R}(t) \right\rangle_{\xi} = 0 $$

for all times t. $\hat{R}$ is defined by Eq. (3.107). In this Appendix, we present the proof.

We first rewrite $|\xi\rangle_{out}$ to

$$ |\xi\rangle_{out} = \hat{P}\,|0\rangle, \tag{3.154} $$

where

$$ \hat{P} \propto \int \mathcal{D}k\, e^{i\int dt\, k(t)\left(\hat{A}(t)-\eta(t)\right)} \tag{3.155} $$

projects the initial state of the light, vacuum $|0\rangle$, onto $|\xi\rangle_{out}$. This form of $\hat{P}$ can be derived by referring to p.2 of [15] and by making use of the fact that since $\left\langle \hat{B} \right\rangle_{\xi}$ is a c-number, a measured eigenstate of $\hat{b}_2(t)$, $|\xi(t)\rangle$, is also an eigenstate of $\hat{A}(t)$ with a different eigenvalue which we choose to call $\eta(t)$.

Substituting Eq. (3.154) into $\left\langle \hat{R}(t) \right\rangle_{\xi}$, we obtain

$$ \left\langle \hat{R}(t) \right\rangle_{\xi} = \left\langle 0 \middle| \hat{P}\hat{R}(t)\,\hat{P} \middle| 0 \right\rangle = -i\partial_{\mu} \left\langle 0 \middle| \hat{P} e^{i\mu\hat{R}} \hat{P} \middle| 0 \right\rangle \Big|_{\mu=0}. \tag{3.156} $$

Let us combine P and $e^{i\mu\hat{R}}$ into one exponential by repeated use of the Baker–Campbell–Hausdorff formula. We begin with $\hat{P}e^{i\mu\hat{R}}$,

$$ \hat{P}e^{i\mu\hat{R}} = \int \mathcal{D}k\, e^{i\int dt\, k(t)\left(\hat{A}(t)-\eta(t)\right)+i\mu\hat{R}} \exp\left(-\frac{\mu}{2} \int dz\, k(z) \left[\hat{A}(z), \hat{R}(t) \right] \right). $$

To evaluate the commutator, we make use of Eq. (3.107)

$$ \hat{R}(t) = \hat{B}(t) - \int_{-\infty}^{T} K(t-z)\, \hat{A}(z)\, dz. \tag{3.157} $$

Furthermore, since $A(t)$ and $B(t)$ are linear operators

$$\left[\hat{A}(z), \hat{B}(t)\right] = \int_{-\infty}^{\infty} L_B(t-z)\left[\hat{a}_2(t), \hat{a}_1(z)\right] dz \quad (3.158)$$

$$= -i\int_{-\infty}^{\infty} L_B(t-z)\,\delta(t-z)\,dz = -iL_B(0). \quad (3.159)$$

Substituting this result back into $\hat{P}e^{i\mu\hat{R}}$, we obtain

$$\hat{P}e^{i\mu\hat{R}} = \int \mathcal{D}k e^{i\int dtk(t)\left(\hat{A}(t)-\eta(t)\right)+i\mu\hat{R}} \exp\left(-\frac{i\mu L_B(0)}{2}\int dzk(z)\right). \quad (3.160)$$

Returning to $\hat{P}e^{i\mu\hat{R}}\hat{P}$, we have

$$\begin{aligned}
\hat{P}e^{i\mu\hat{R}}\hat{P} &= \int \mathcal{D}l \int \mathcal{D}k e^{i\int dtk(t)\left(\hat{A}(t)-\eta(t)\right)+i\mu\hat{R}} e^{i\int dzl(z)\left(\hat{A}(z)-\eta(z)\right)} \exp\left(-\frac{i\mu L_B(0)}{2}\int dzk(z)\right) \\
&= \int \mathcal{D}l \int \mathcal{D}k e^{i\int dzk(z)\left(\hat{A}(z)-\eta(z)\right)+i\int dzl(z)\left(\hat{A}(z)-\eta(z)\right)+i\mu\hat{R}} \\
&\quad \times \exp\left(-\frac{i\mu L_B(0)}{2}\int dzk(z)\right) \exp\left(\frac{\mu}{2}\int dzl(z)\left[\hat{A}(z), \hat{R}(t)\right]\right) \\
&= \int \mathcal{D}k_+ e^{i\int dzk_+(z)\left(\hat{A}(z)-\eta(z)\right)+i\mu\hat{R}} \int \mathcal{D}k_- \exp\left(-\frac{i\mu L_B(0)}{2}\int dzk_-(z)\right)
\end{aligned}$$

where we applied the Baker-Campbell-Hausdorff formula in the second line, and in the third line, we defined $k_+ = k(z) + l(z)$, and $k_- = k(z) - l(z)$.

Now,

$$\int \mathcal{D}k_- \exp\left(-\frac{i\mu L_B(0)}{2}\int dzk_-(z)\right) = \lim_{n\to\infty} \delta^n\left(\frac{\mu L_B(0)}{2}\right) \equiv \prod \delta\left(\frac{\mu L_B(0)}{2}\right) \quad (3.161)$$

so

$$\begin{aligned}
\partial_\mu \hat{P}e^{i\mu\hat{R}}\hat{P} &= \left(\partial_\mu \int \mathcal{D}k_+ e^{i\int dzk_+(z)\left(\hat{A}(z)-\eta(z)\right)+i\mu\hat{R}}\right) \times \prod \delta\left(\frac{\mu L_B(0)}{2}\right) \\
&\quad + \lim_{n\to\infty} n \int \mathcal{D}k_+ e^{i\int dzk_+(z)\left(\hat{A}(z)-\eta(z)\right)+i\mu\hat{R}} \times \delta'\left(\frac{\mu L_B(0)}{2}\right)\delta^{n-1}\left(\frac{\mu L_B(0)}{2}\right).
\end{aligned}$$

When μ is set to 0, the second term will vanish because $\delta'(\mu L_B(0)/2)$ vanishes at $\mu = 0$ (as can be easily determined by writing the dirac-delta function as a zero mean Gaussian with a vanishing variance). Consequently, we only need to study the first term.

Let take the expectation of $\partial_\mu \hat{P} e^{i\mu\hat{R}} \hat{P}$ over vacuum,

$$\partial_\mu \left\langle 0 \middle| \hat{P} e^{i\mu\hat{R}} \hat{P} \middle| 0 \right\rangle = \partial_\mu \int \mathcal{D}k_+ \left\langle 0 \middle| e^{i\int dz k_+(z)\hat{A}(z) + i\mu\hat{R}} \middle| 0 \right\rangle e^{-i\int dz k_+(z)\eta(z)} \times \prod \delta\left(\frac{\mu L_B(0)}{2}\right).$$

We now analyze the first term in the integrand. Since $|0\rangle$ is a Gaussian state, the expectation over $|0\rangle$ can be simplified to

$$\begin{aligned}\left\langle 0 \middle| e^{i\int dz k_+(z)\hat{A}(z) + i\mu\hat{R}} \middle| 0 \right\rangle &= \exp\left(-\frac{1}{2}\mu^2 \left\langle R^2 \right\rangle\right) \\ &\times \exp\left(-\frac{1}{2}\mu \left\langle \hat{R} \times \int dz k_+(z)\, \hat{A}(z) \right\rangle + \left\langle \int dz k_+(z)\, \hat{A}(z) \times \hat{R} \right\rangle\right) \\ &\times \exp\left(-\frac{1}{2}\left\langle \left(dz k_+(z)\, \hat{A}(z)\right)^2 \right\rangle\right).\end{aligned}$$

The second exponential is equal to unity by the assumption given by Eq. (3.109). Thus,

$$\left\langle 0 \middle| e^{i\int dz k_+(z)\hat{A}(z) + i\mu\hat{R}} \middle| 0 \right\rangle = \exp\left(-\frac{1}{2}\mu^2 \left\langle R^2 \right\rangle\right) \exp\left(-\frac{1}{2}\left\langle \left(dz k_+(z)\, \hat{A}(z)\right)^2 \right\rangle\right).$$

Once we differentiate over μ and then set it to 0, this product vanishes, giving

$$\langle 0|\hat{R}|0\rangle = \partial_\mu \left\langle 0 \middle| \hat{P} e^{i\mu\hat{R}} \hat{P} \middle| 0 \right\rangle\Big|_0 = 0 \tag{3.162}$$

as desired.

Bibliography

[1] Markus Aspelmeyer, Tobias J. Kippenberg, and Florian Marquardt. Cavity optomechanics. *Rev. Mod. Phys.*, 86:1391–1452, Dec 2014.

[2] S. M. Barnett. *Methods in theoretical quantum optics*. Clarendon Oxford University Press, Oxford Oxford New York, 2002.

[3] A. Bassi and K. Hejazi. No-faster-than-light-signaling implies linear evolutions. A re-derivation. *ArXiv e-prints*, November 2014.

[4] Angelo Bassi, Kinjalk Lochan, Seema Satin, Tejinder P Singh, and Hendrik Ulbricht. Models of wave-function collapse, underlying theories, and experimental tests. *Reviews of Modern Physics*, 85(2):471, 2013.

[5] Steven Carlip. Is Quantum Gravity Necessary? *Class.Quant.Grav.*, 25:154010, 2008.

[6] Yanbei Chen. Macroscopic quantum mechanics: theory and experimental concepts of optomechanics. *Journal of Physics B: Atomic, Molecular and Optical Physics*, 46(10):104001, 2013.

[7] L. Diósi. Models for universal reduction of macroscopic quantum fluctuations. *Phys. Rev. A*, 40:1165–1174, Aug 1989.

[8] L. Diósi. A universal master equation for the gravitational violation of quantum mechanics. *Physics Letters A*, 120(8):377 – 381, 1987.

[9] C. C. Gan, C. M. Savage, and S. Z. Scully. Optomechanical tests of a schrödinger-newton equation for gravitational quantum mechanics. *Phys. Rev. D*, 93:124049, Jun 2016.

[10] N Gisin and M Rigo. Relevant and irrelevant nonlinear schrodinger equations. *Journal of Physics A: Mathematical and General*, 28(24):7375, 1995.

[11] Domenico Giulini and André Großardt. Centre-of-mass motion in multiparticle schrödinger–newton dynamics. *New Journal of Physics*, 16(7):075005, 2014.

[12] André Großardt, James Bateman, Hendrik Ulbricht, and Angelo Bassi. Optomechanical test of the schrödinger-newton equation. *Phys. Rev. D*, 93:096003, May 2016.

[13] B.L. Hu and E. Verdaguer. Stochastic Gravity: Theory and Applications. *Living Rev.Rel.*, 11:3, 2008.

[14] D Kafri, JM Taylor, and GJ Milburn. A classical channel model for gravitational decoherence. *New Journal of Physics*, 16(6):065020, 2014.

[15] Farid Khalili, Stefan Danilishin, Haixing Miao, Helge Müller-Ebhardt, Huan Yang, and Yanbei Chen. Preparing a mechanical oscillator in non-gaussian quantum states. *Phys. Rev. Lett.*, 105:070403, Aug 2010.

[16] Pierre Meystre. A short walk through quantum optomechanics. *Annalen der Physik*, 525(3):215–233, 2013.

[17] C. Moller. *Les Theories Relativistes de la Gravitation*. CNRS, Paris, 1962.

[18] Stefan Nimmrichter and Klaus Hornberger. Stochastic extensions of the regularized Schrödinger-Newton equation. *Phys.Rev.*, D91(2):024016, 2015.

[19] Don N Page and CD Geilker. Indirect evidence for quantum gravity. *Physical Review Letters*, 47(14):979, 1981.

[20] L.-M. Peng, G. Ren, S. L. Dudarev, and M. J. Whelan. Debye–Waller Factors and Absorptive Scattering Factors of Elemental Crystals. *Acta Crystallographica Section A*, 52(3):456–470, May 1996.

[21] Roger Penrose. On gravity's role in quantum state reduction. *General relativity and gravitation*, 28(5):581–600, 1996.

[22] Joseph Polchinski. Weinberg's nonlinear quantum mechanics and the einstein-podolsky-rosen paradox. *Physical Review Letters*, 66(4):397, 1991.

[23] B Reznik and Y Aharonov. Time-symmetric formulation of quantum mechanics. *Physical Review A*, 52(4):2538, 1995.

[24] L. Rosenfeld. On quantization of fields. *Nuclear Physics*, 40(0):353 – 356, 1963.

[25] Christoph Simon, Vladimír Bužek, and Nicolas Gisin. No-signaling condition and quantum dynamics. *Phys. Rev. Lett.*, 87:170405, Oct 2001.

[26] P. C. E. Stamp. Rationale for a Correlated Worldline Theory of Quantum Gravity. *New J. Phys.*, 17(6):065017, 2015.

[27] Max Tegmark and Harold S. Shapiro. Decoherence produces coherent states: An explicit proof for harmonic chains. *Phys. Rev. E*, 50:2538–2547, Oct 1994.

[28] Eric E. Ungar and Jeffrey A. Zapfe. Structural damping. pages 579–609, 2007.

[29] Huan Yang, Haixing Miao, Da-Shin Lee, Bassam Helou, and Yanbei Chen. Macroscopic quantum mechanics in a classical spacetime. *Phys. Rev. Lett.*, 110:170401, Apr 2013.

Chapter 4

DIFFERENT INTERPRETATIONS OF QUANTUM MECHANICS MAKE DIFFERENT PREDICTIONS IN NON-LINEAR QUANTUM MECHANICS, AND SOME DO NOT VIOLATE THE NO-SIGNALING CONDITION

B. Helou, and Y. Chen, 2017, arXiv:1709.06639

Abstract

Nonlinear modifications of quantum mechanics have a troubled history. They were initially studied for many promising reasons: resolving the measurement problem, testing the limits of standard quantum mechanics, and reconciling it with gravity. Two results substantially undermined the credibility of non-linear theories. Some have been experimentally refuted, and more importantly, all deterministic non-linear theories can be used for superluminal communication. However, these results are unconvincing because they overlook the fact that the distribution of measurement results predicted by non-linear quantum mechanics depends on the interpretation of quantum mechanics that one uses. For instance, although the Everett and Copenhagen interpretations agree on the expression of Born's rule for the outcomes of multiple measurements in linear quantum mechanics, they disagree in non-linear quantum mechanics. We present the range of expressions of Born's rule that can be obtained by applying different formulations of quantum mechanics to a class of non-linear quantum theories. We then determine that many do not allow for superluminal communication but only two seem to have a reasonable justification. The first is the Everett interpretation, and the second, which we name *causal-conditional*, states that a measurement broadcasts its outcome to degrees of freedom in its future light-cone, who update the wavefunction that their non-linear Hamiltonian depends on according to this new information.

4.1 Introduction

Non-linear quantum mechanics (NLQM) has long been considered as a possible generalization of standard quantum mechanics (sQM) [1, 2, 3], for three main reasons. First, the measurement process is controversial. If we assume that linear quantum mechanics explains all processes, then it is very difficult to explain wavefunction collapse [4]. Phenomenological non-linear, stochastic, and experimentally falsifiable extensions of quantum mechanics (QM) have been proposed to explain the measurement process [5], and upper bounds on the parameters of such theo-

ries have been obtained in [5, 6, 7]. Second, we would like to test the domain of validity of sQM. One possible feature to test is linearity. Experimental tests of certain non-linear theories have been performed in [8, 9, 10, 11, 12], and all have returned negative results. Third, non-linear and deterministic theories of QM have been proposed to combine quantum mechanics with gravity. For instance, the Schroedinger-Newton theory describes a classical spacetime which is sourced by quantum matter [13], and the correlated worldlines theory is a quantum theory of gravity which postulates that gravity correlates quantum trajectories in the path integral [14].

NLQM became a much less credible theory after 1990 because Gisin showed that deterministic NLQM could allow for superluminal communication [15]. The no-signaling condition states that one cannot send information faster than the speed of light, and is a cornerstone of the special theory of relativity. The community regards the condition as being inviolable. Gisin's work was quickly followed by others with similar conclusions [16, 17]. Additional work then showed that under general conditions NLQM allows for superluminal communication [18, 19].

In [6], we showed that NLQM suffers from another serious conceptual issue: Born's rule cannot be uniquely extended from sQM to NLQM. Born's rule provides a prescription for predicting the distribution of measurement results in a particular experiment, and has, so far, passed all experimental tests. Any non-linear theory must make predictions that become equivalent to Born's rule in sQM when the non-linearity vanishes.

As in sQM, measurements in NLQM pose significant conceptual difficulties. Fortunately, in sQM, these difficulties do not result in practical challenges. Whether the experimentalist is an Everettian or a proponent of wavefunction collapse does not matter, as in both cases they can safely use Born's rule to predict the distribution of measurement results. This is no longer true in NLQM. Different interpretations of quantum mechanics result in different predictions for the outcome of an experiment, and so result in different expressions for Born's rule.

In this article, we search for interpretations of quantum mechanics that do not violate the no-signaling condition when are applied to NLQM. Since there could be interpretations that haven't been discovered, our approach won't be to extend all known interpretations to NLQM. Instead, we will extend the mathematical expression of Born's rule in a general way to NLQM, without regards to interpretation. After finding causal prescriptions, we speculate about their interpretation.

Note that our analysis doesn't cover all possible non-linear theories. We only wish

to show that non-linear quantum mechanics does not necessarily violate the no-signaling condition. More importantly, how to write down a general non-linear modification of quantum mechanics is still an open question. For example, the class of non-linear theories proposed by Weinberg in [3] doesn't include P.C.E. Stamp's proposal in [14]. We also do not, *a priori*, place any physical constraints on the class of non-linear theories we study. We only place one mathematical constraint: a single Dirichlet boundary condition is enough to completely specify a solution.

This article is outlined as follows. By introducing the formalism for multiple measurements in sQM, we show that linearity prevents two parties from communicating with each other faster than the speed of light. We then motivate the dependence of NLQM on the formulation of quantum mechanics by providing a simple example involving a single measurement. By extending the notion of a time-evolution operator to NLQM, we generate extensions of Born's rule in the context of multiple measurements. Afterwards, we discuss what well-known formulations of quantum mechanics, such as the Everett interpretation, predict for the distribution of measurement results in NLQM. We then present all possible prescriptions that do not violate the no-signaling condition. Finally, we propose and discuss a sensible prescription, which we name *causal-conditional*, that doesn't violate the no-signaling condition. It states that a measurement broadcasts its outcome to degrees of freedom in its future light-cone, who update the wavefunction that their non-linear Hamiltonian depends on according to this new information.

4.2 Multiple measurements in sQM and the no-signaling condition

In Fig. 4.1, we show the setup that is typically used to show that NLQM violates the no-signaling condition. Charlie prepares a collection of identical arbitrary 2-particle states $|\rangle$, and then sends them to Alice and Bob, such that they each hold one part of each of the states $|\Psi_{ini}\rangle$. Alice performs measurements on her ensemble of particles at time t_1, and then Bob on his at a later time t_2. We assume that Alice's measurements are space-like separated from Bob's, and so their particles do not interact from t_1 till t_2.

4.2.1 Born's rule for multiple measurements

Denote the probability that Alice measures α in some basis A_a, and Bob measures β in some basis B_b by $p(\alpha, \beta|\, A_a, B_b)$. For example, if the particles were spins, A_a could be the $\hat{\sigma}_z$ eigenstates, $|\uparrow\rangle, |\downarrow\rangle$, and B_b the $\hat{\sigma}_x$ eigenstates $|\pm\rangle = (|\uparrow\rangle \pm |\downarrow\rangle)/\sqrt{2}$. We will first determine $p(\alpha, \beta|\, A_a, B_b)$ according to sQM, and then discuss the different ways of generalizing it to NLQM in the next section.

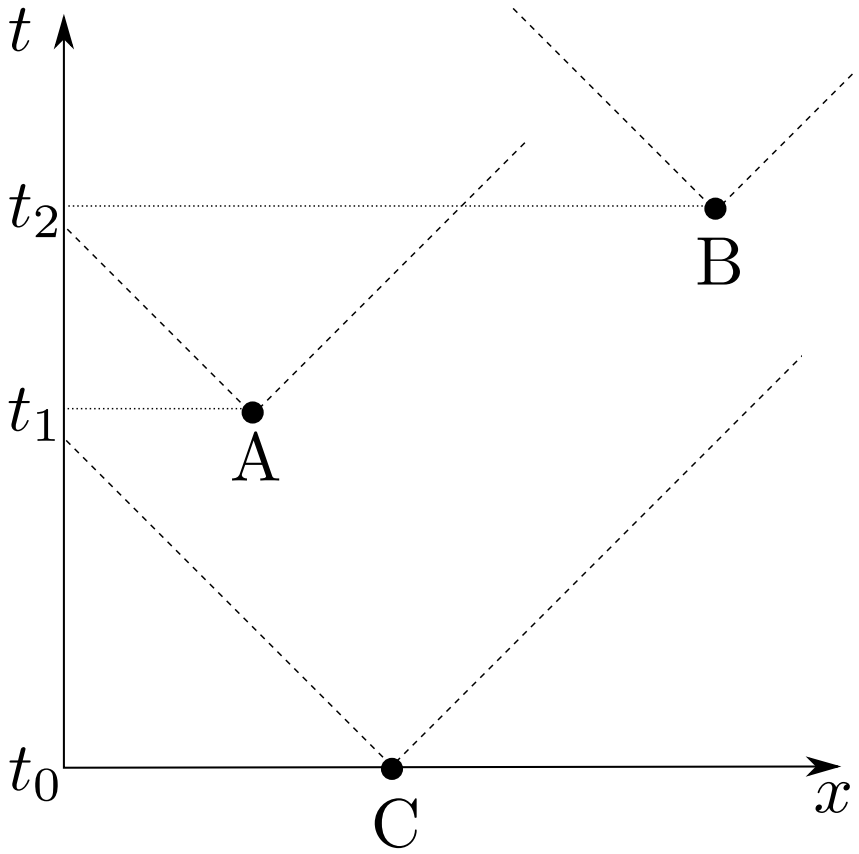

Figure 4.1: A spacetime diagram showing multiple measurement events. Event C describes the preparation of an ensemble of identical 2-particle states $|\Psi_{ini}\rangle$ by Charlie. Event A (B) describes Alice (Bob) measuring her (his) particles. The dashed lines show the light cone centered around each event.

In sQM, $p\left(\alpha,\beta|\, A_a, B_b\right)$ is given by

$$p\left(\alpha,\beta|\, A_a, B_b\right) = \langle\alpha,\beta|\alpha,\beta\rangle\,, \tag{4.1}$$

where $|\alpha,\beta\rangle$ is the unnormalized joint quantum state of Alice and Bob at t_2, conditioned on the measurement results α and β:

$$\left|\Psi_{c|\alpha,\beta}\right\rangle = \left(\hat{I}_A \otimes \hat{P}_\beta\right) \hat{U}\left(t_2, t_1\right) \left(\hat{P}_\alpha \otimes \hat{I}_B\right) \hat{U}\left(t_1, t_0\right) |\Psi_{ini}\rangle\,, \tag{4.2}$$

where $\hat{I}_A$ ($\hat{I}_B$) is the identity operator acting on Alice's (Bob's) particle, $\hat{U}(t,z)$ is the total time evolution operator for both Alice and Bob's particles from times z till t. The projectors are $\hat{P}_\alpha = |\alpha\rangle\langle\alpha|$ and $\hat{P}_\beta = |\beta\rangle\langle\beta|$. To simplify the formalism, we only work with pure states. Our analysis is general because $|\Psi_{ini}\rangle$ can always be enlarged to include the initial state of the environment.

Alice and Bob's measurement events are spacelike separated, so from t_1 till t_2, the interaction Hamiltonian between Alice's and Bob's particle is zero, and $\hat{U}(t_2, t_1)$ is separable

$$\hat{U}(t_2, t_1) \equiv \hat{A}(t_2, t_1)\hat{B}(t_2, t_1). \tag{4.3}$$

$\hat{A}$ acts on Alice's particle's Hilbert space, and $\hat{B}$ on Bob's. We can then rewrite Eq. (4.2) to

$$\left|\Psi_{c|\alpha,\beta}\right\rangle = \left(\hat{I} \otimes \hat{P}_\beta\right) \hat{A}(t_2, t_1)\hat{B}(t_2, t_1) \left(\hat{P}_\alpha \otimes \hat{I}\right) \hat{U}\left(t_1, t_0\right) \left|\Psi_{ini}\right\rangle, \tag{4.4}$$

which we substitute into Eq. (4.1)

$$p\left(\alpha, \beta\right| A_a, B_b) = \left\langle \left| \hat{U}^\dagger(t_1, t_0)\hat{P}_\alpha \hat{B}^\dagger(t_2, t_1)\hat{P}_\beta \hat{B}(t_2, t_1)\hat{P}_\alpha \hat{U}(t_1, t_0) \right| \right\rangle, \tag{4.5}$$

where we've used that $\hat{A}(t_2, t_1)$ commutes with $\hat{P}_\beta$. Since Alice and Bob's measurement events are spacelike separated, $\hat{P}_\alpha$ and $\hat{P}_\beta$ commute,

$$\left[\hat{P}_\alpha, \hat{P}_\beta\right] = 0, \tag{4.6}$$

which we use to simplify Eq. (4.5) to

$$p\left(\alpha, \beta\right| A_a, B_b) = \left\langle \left| \hat{U}^\dagger(t_1, t_0)\hat{B}^\dagger(t_2, t_1)\hat{P}_\beta \hat{B}(t_2, t_1)\hat{P}_\alpha \hat{U}(t_1, t_0) \right| \right\rangle. \tag{4.7}$$

4.2.2 The no-signaling condition

Superluminal communication from Alice to Bob is possible when

$$p\left(\beta\right| A_a, B_b) = \sum_\alpha p\left(\alpha, \beta\right| A_a, B_b) \tag{4.8}$$

is influenced by Alice's choice of a measurement basis in a deterministic way. Since Bob can easily estimate $p\left(\beta\right| A_a, B_b)$, he can determine the basis Alice chose for her measurement results, which can form the foundation of a communication strategy. For instance, both Alice and Bob can agree that a particular choice of Alice's measurement basis could be associated with sending the bit 0, while another choice could be associated with the bit 1.

In sQM, superluminal communication can never occur because, using Eq. (4.7),

$$\begin{aligned} p\left(\beta\right| A_a, B_b) &= \left\langle \left| \hat{U}^\dagger(t_1, t_0)\hat{B}^\dagger(t_2, t_1)\hat{P}_\beta \hat{B}(t_2, t_1) \left(\sum_\alpha \hat{P}_\alpha\right) \hat{U}(t_1, t_0) \right| \right\rangle & (4.9) \\ &= \left\langle \left| \hat{U}^\dagger(t_1, t_0)\hat{B}^\dagger(t_2, t_1)\hat{P}_\beta \hat{B}(t_2, t_1)\hat{U}(t_1, t_0) \right| \right\rangle, & (4.10) \end{aligned}$$

is clearly independent of A_a. We've shown that $p(\beta|\, A_a, B_b) = p(\beta|\, B_b)$, so sQM doesn't violate the no-signaling condition.

4.3 Ambiguity of Born's rule in NLQM

In this section, we discuss the ambiguity of Born's rule in NLQM. We first present an example with one measurement, and then present a general formalism for generating prescriptions for calculating the distribution of the outcomes of an arbitrary number of measurements at arbitrary spacetime points.

4.3.1 A simple example

For experiments with a single measurement, sQM states that the probability of measuring an outcome f is

$$p_{i\to f} = \left|\langle f|\hat{U}|i\rangle\right|^2, \tag{4.11}$$

where $|f\rangle$ is the pointer state associated with the outcome f. The expression (4.11) is usually interpreted in the following way. A preparation device prepares the system in $|i\rangle$, which evolves for some period of time under the time-evolution operator $\hat{U}$. The system then interacts with the measurement device. What happens next depends on one's interpretation of quantum-mechanics. An Everettian would state that decoherence splits the wavefunction into numerous branches that are approximately classical. On the other hand, a proponent of objective collapse would state that, due to stochastic modifications of the Schroedinger equation that become important when a microscopic system interacts with a macroscopic one, the wavefunction collapses onto $|f\rangle$ with probability $p_{i\to f}$. As in Ref. [6], we will refer to the formulation of Born's rule based on $p_{i\to f}$ as *pre-selection*.

Eq. (4.11) admits even more interpretations. For instance, it can be rewritten as

$$p_{i\leftarrow f} = \left|\langle i|\hat{U}^\dagger|f\rangle\right|^2, \tag{4.12}$$

which can be interpreted as $|f\rangle$ evolves backwards in time to $\hat{U}^\dagger|f\rangle$ and is then projected by the preparation device to the state $|i\rangle$. We will refer to the formulation of Born's rule based on $p_{i\leftarrow f}$ as *post-selection*.

In NLQM, the time evolution operator depends on the state it acts on. As a result, Eqs. (4.11) and (4.12) become

$$p^{NL}_{i\to f} = |\langle f|\mathcal{U}_i i\rangle|^2, \qquad p^{NL}_{i\leftarrow f} \propto \left|\left\langle i|\mathcal{U}^\dagger_f f\right\rangle\right|^2, \tag{4.13}$$

where, under some non-linear dynamics, $|\mathcal{U}_i i\rangle$ is the time-evolved $|i\rangle$ and $\left|\mathcal{U}_f^\dagger f\right\rangle$ is the backwards time-evolved $|f\rangle$. The superscript NL explicitly indicates that NLQM is being used. Moreover, the proportionality sign in $p^{NL}_{i\leftarrow f}$ follows from $\sum_f \left|\left\langle i|\mathcal{U}_f^\dagger f\right\rangle\right|^2$ being not, in general, normalized to unity. $p^{NL}_{i\rightarrow f}$ and $p^{NL}_{i\leftarrow f}$ are not necessarily equal, and so Born's rule cannot be uniquely extended to NLQM.

4.3.2 Ambiguity in the boundary condition driving the non-linear time evolution

By extending Eq. (4.4) to NLQM, we can extend Born's rule, given by Eq. (4.1), to NLQM. However, because NLQM is non-linear, a time-evolution operator doesn't exist. Nonetheless, inspired by the state-dependent Heisenberg picture introduced in [6], we will show that we can define a *boundary-dependent time-evolution operator*, and that the choice of a boundary condition is the essential degree of freedom for extending Born's rule to NLQM.

For some theories in NLQM[1], running time-evolution requires solving the non-linear Schroedinger equation which contains a linear term, $\hat{H}_L$, and a nonlinear term $\hat{V}_{NL}$:

$$i\hbar\partial_t |\psi\rangle = \left(\hat{H}_L + \hat{V}_{NL}\left(\psi(x,t)\right)\right)|\psi\rangle\,. \tag{4.14}$$

$\hat{V}_{NL}\left(\psi(x,t)\right)$ is a shorthand for a non-linear potential that depends on the wavefunction $|\psi\left(t\right)\rangle$ expressed in some (possibly multi-dimensional) basis x. For instance, the Schroedinger-Newton equation for a single non-relativistic particle of mass m interacting with its own gravitational field is given by

$$i\hbar\partial_t |\psi\rangle = \left(\hat{H}_L - m^2 G\int d^3\boldsymbol{x}\frac{\left|\psi\left(\boldsymbol{x},t\right)\right|^2}{|\hat{\boldsymbol{x}}-\boldsymbol{x}|}\right)|\psi\rangle\,, \tag{4.15}$$

where $\psi\left(\boldsymbol{x},t\right)$ is the state $|\psi\rangle$ expressed in the position basis $|\boldsymbol{x}\rangle$.

We chose to write the nonlinear Schroedinger equation in the form of Eq. (4.14) to illustrate its similarity to the standard Schroedinger equation. Once we specify the boundary conditions, we can have Eq. (4.14) be formally equivalent to a linear Schroedinger equation. We will assume that a single Dirichlet boundary condition is sufficient to solve Eq. (4.14), and that its solution with the boundary condition

[1] As mentioned in the introduction, we will not investigate all possible non-linear theories. In particular we only consider theories with the form of Eq. (4.14), and whose solution can be uniquely specified with one Dirichlet boundary condition.

$|\psi(T)\rangle = |\phi\rangle$ is $|\varphi(t)\rangle$. Consequently, the linear Schroedinger equation

$$i\hbar\partial_t |\psi\rangle = \left(\hat{H}_L + \hat{V}_{NL}\left(\varphi(x,t)\right)\right)|\psi\rangle \tag{4.16}$$

is formally identical to Eq. (4.14) with the boundary-condition $|\psi(T)\rangle = |\phi\rangle$. Heuristically, in the context of Eq. (4.16), we can interpret $\varphi(x,t)$ as a time-dependent classical drive. Eq. (4.16) has a time-evolution operator associated with it, which we denote by $\hat{U}_{\phi(T)}$. The subscript is to emphasize that the time-evolution operator is associated with the boundary condition $|\psi(T)\rangle = |\phi\rangle$. We can now write the solution to Eq. (4.14) as

$$|\psi\left(t\right)\rangle = \hat{U}_{\phi(T)}\left(t,T\right)|\phi\rangle\,. \tag{4.17}$$

We are ready to present the extension of Eqs. (4.1) and (4.4) to NLQM:

$$p^{NL}\left(\alpha,\beta|\,A_a,B_b\right) = \frac{1}{\mathcal{N}}\langle\alpha,\beta|\alpha,\beta\rangle\,, \tag{4.18}$$

where if Alice and Bob's measurement events are spacelike separated

$$\left|\Psi_{c|\alpha,\beta}\right\rangle = \hat{P}_\beta\hat{A}_{\phi_2^A(T_2^A)}\left(t_2,t_1\right)\hat{B}_{\phi_2^B(T_2^B)}\left(t_2,t_1\right)\hat{P}_\alpha\hat{U}_{\phi_1(T_1)}\left(t_1,t_0\right)|\Psi_{ini}\rangle\,, \tag{4.19}$$

and $\mathcal{N} = \sum_{\alpha,\beta}\langle\Psi_c\,|\,\alpha,\beta\,|\,\Psi_c\,|\,\alpha,\beta\rangle$ ensures that $\sum_{\alpha,\beta}p^{NL}\left(\alpha,\beta|\,A_a,B_b\right)$ is normalized to unity. Moreover, $\hat{U}_{\phi_1(T_1)}\left(t_1,t_0\right)$ is the time-evolution operator from t_0 till t_1 and is associated with the boundary $|\psi(T_1)\rangle = |\phi_1\rangle$. $\hat{A}_{\phi_2^A(T_2)}\left(t_2,t_1\right)$ ($\hat{B}_{\phi_2^B(T_2)}\left(t_2,t_1\right)$) is the time-evolution operator associated with the boundary condition $|\psi(T_2^A)\rangle = |\phi_2^A\rangle$ ($|\psi(T_2^B)\rangle = |\phi_2^B\rangle$), and acts on Alice's (Bob's) particle from t_1 till t_2. The time-evolution of Alice and Bob's joint system from t_1 till t_2 is separable because Alice's particle's future light-cone at t_1 does not overlap with Bob's particle's past light-cone at t_2. As a result, their total interaction Hamiltonian, which includes contributions from the linear Hamiltonian $\hat{H}_L$ and from the non-linear potential $\hat{V}_{NL}$, must be zero. Note that, by construction, Eq. (4.19) recovers the predictions of sQM when the non-linearity $\hat{V}_{NL}$ vanishes.

If the events A and B were time-like separated, then there are numerous schemes for extending the time evolution of Alice and Bob's particles to NLQM. Call the solutions to Eq. (4.14) with the boundary conditions $|\psi(T_2^A)\rangle = |\phi_2^A\rangle$, $|\psi(T_2^B)\rangle = |\phi_2^B\rangle$ and $|\psi(T_2^{AB})\rangle = |\phi_2^{AB}\rangle$ as $|\varphi^A(t)\rangle$, $|\varphi^B(t)\rangle$ and $|\varphi^{AB}(t)\rangle$ respectively. We can

then write the non-linear potential $\hat{V}_{NL}$ in Eq. (4.16) in the following general way:

$$\hat{V}_{NL} = \hat{V}_A\left(\varphi^A(x,t)\right) \otimes \hat{I}_B + \hat{I}_A \otimes \hat{V}_B\left(\varphi^B(x,t)\right) + \hat{V}_{int}\left(\varphi^{AB}(x,t)\right), \tag{4.20}$$

where $\hat{V}_A$ ($\hat{V}_B$) is the free non-linear Hamiltonian acting on Alice's (Bob's) particle, and $\hat{V}_{int}$ is the non-linear interaction potential. However, we find it difficult to justify why each term in $\hat{V}_{NL}$ would be generated by a different boundary condition when Alice and Bob's particles are allowed to directly communicate and interact. We will impose $\phi_2^A = \phi_2^B = \phi_2^{AB}$ and $T_2^A = T_2^B = T_2^{AB}$ when the measurement events A and B are timelike separated. We summarize our chosen form of $\left|\Psi_{c|\alpha,\beta}\right\rangle$ by

$$\left|\Psi_{c|\alpha,\beta}\right\rangle = \begin{cases} \hat{P}_\beta \hat{U}_{\phi_2(T_2)}(t_2,t_1)\,\hat{P}_\alpha \hat{U}_{\phi_1(T_1)}(t_1,t_0)\left|\Psi_{ini}\right\rangle & \text{A \& B timelike,} \\ \hat{P}_\beta \hat{A}_{\phi_2^A(T_2^A)}(t_2,t_1)\,\hat{B}_{\phi_2^B(T_2^B)}(t_2,t_1)\,\hat{P}_\alpha \hat{U}_{\phi_1(T_1)}(t_1,t_0)\left|\Psi_{ini}\right\rangle & \text{A \& B spacelike.} \end{cases}$$

The introduction of arbitrary boundary conditions $|\phi_1\rangle$ at T_1 and $|\phi_2\rangle$ at T_2 might appear artificial, but isn't. Each formulation of quantum mechanics predicts different boundary conditions after a measurement. For instance, in Eq. (4.14), an interpretation of quantum mechanics with wavefunction collapse states that $|\phi_1\rangle = |\alpha\rangle$ and $T_1 = t_1$, while the Everett interpretation states that $|\phi_1\rangle$ is the initial state of the universe and T_1 is when the universe began. Refer to section 4.1 for more details. In sQM, we do not have to worry if and how the wavefunction collapses because the time-evolution operator is well-defined independently of the wavefunction it acts on. However, in NLQM, each boundary condition generates a different time-evolution operator, and so how we formulate quantum mechanics matters in NLQM.

4.3.3 Extending the formalism to relativistic quantum mechanics

We can rigorously study superluminal communication only in quantum field theory, where the total Hamiltonian consists of free and interaction (between different fields) energy densities

$$\hat{H} = \int d^3\boldsymbol{x}\hat{H}_0(\boldsymbol{x}) + \int d^3\boldsymbol{x}\hat{H}_{int}(\boldsymbol{x}). \tag{4.21}$$

Assigning spatial locations for quantum degrees of freedom is crucial for placing constraints on $\hat{H}$ to ensure that it is causal. Let $\hat{\mathcal{H}}_{int}$ be the interaction energy density in an interaction picture with respect to $\int d^3\boldsymbol{x}\hat{H}_0(\boldsymbol{x})$, and then $\hat{\mathcal{H}}_{int}$ commutes over spacelike distances [20]

$$\left[\hat{\mathcal{H}}_{int}(t_x,\boldsymbol{x}),\, \hat{\mathcal{H}}_{int}(t_y,\boldsymbol{y})\right] = 0, \qquad c\left(t_{\boldsymbol{x}} - t_{\boldsymbol{y}}\right)^2 - |\boldsymbol{x}-\boldsymbol{y}|^2 < 0. \tag{4.22}$$

We generalize $\hat{H}$ to include a dependence on a wavefunction:

$$\hat{H}^{NL}(t) = \int d^3\boldsymbol{x}\hat{H}_0\left(\boldsymbol{x}, \left|\Psi_{\Phi(T)}(t)\right\rangle\right) + \int d^3\boldsymbol{x}\hat{H}_{int}\left(\boldsymbol{x}, \left|\Psi_{\Phi(T)}(t)\right\rangle\right), \tag{4.23}$$

where $\left|\Psi_{\Phi(T)}(t)\right\rangle$ is the solution to the non-linear Schroedinger equation

$$i\hbar\partial_t |\Psi(t)\rangle = \left(\int d^3\boldsymbol{x}\hat{H}_0(\boldsymbol{x}, |\Psi(t)\rangle) + \int d^3\boldsymbol{x}\hat{H}_{int}(\boldsymbol{x}, |\Psi(t)\rangle)\right)|\Psi(t)\rangle \tag{4.24}$$

with the boundary condition $|\Psi(t=T)\rangle = |\Phi\rangle$. We further generalize $\hat{H}^{NL}$ by allowing for different boundary conditions at each location

$$\hat{H}^{NL}(t) = \int d^3\boldsymbol{x}\hat{H}_0\left(\boldsymbol{x}, \left|\Psi_{\Phi_T(\boldsymbol{x})}(t)\right\rangle\right) + \int d^3\boldsymbol{x}\hat{H}_{int}\left(\boldsymbol{x}, \left|\Psi_{\Phi_T(\boldsymbol{x})}(t)\right\rangle\right), \tag{4.25}$$

where $\left|\Psi_{\Phi_T(\boldsymbol{x})}(t)\right\rangle$ is the solution to Eq. (4.24) with boundary condition $|\Psi(t=T(\boldsymbol{x}))\rangle = |\Phi(\boldsymbol{x})\rangle$.

The relativistic non-linear generalization of $\left|\Psi_{c|\alpha,\beta}\right\rangle$ in Eq. (4.2) is

$$\left|\Psi_{c|\alpha,\beta}\right\rangle = \hat{P}_\beta \hat{U}_{\Phi_T^{(1)}(\boldsymbol{x})}(t_2, t_1)\hat{P}_\alpha \hat{U}_{\Phi_T^{(0)}(\boldsymbol{x})}(t_1, t_0)|\Psi_{ini}\rangle, \tag{4.26}$$

where $\boldsymbol{x} \in \mathbb{R}^3$, and $\hat{U}^{(0)}_{\Phi_T(t,\boldsymbol{x})}$ ($\hat{U}^{(1)}_{\Phi_T(t,\boldsymbol{x})}$) is the time-evolution operator associated with the boundary condition $\left|\Psi\left(t=T^{(0)}(\boldsymbol{x})\right)\right\rangle = \left|\Phi^{(0)}(\boldsymbol{x})\right\rangle$ ($\left|\Psi\left(t=T^{(1)}(\boldsymbol{x})\right)\right\rangle = \left|\Phi^{(1)}(\boldsymbol{x})\right\rangle$).

4.4 The no-signaling condition in NLQM

As explained in section 2.1, Alice cannot communicate with Bob superluminally if $p^{NL}(\beta|A_a, B_b) = \sum_\alpha p^{NL}(\alpha, \beta|\, A_a, B_b)$ is independent of Alice's choice of measurement basis A_a. The normalization factor in $p^{NL}(\alpha, \beta|\, A_a, B_b)$ (which we've shown explicitly in Eq. (4.18)) won't affect our analysis and can be safely ignored for the remainder of this article[2].

Similarly to how we derived Eq. (4.7), $p^{NL}(\alpha, \beta|A_a, B_b)$ can be simplified to (ignor-

[2]If the unnormalized $p^{NL}(\beta|A_a, B_b)$ is independent of the basis A_a for all β, then its normalization, $\sum_\beta p^{NL}(\beta|A_a, B_b)$, will also be independent of A_a. Moreover, it is obvious when the normalization could help: $p^{NL}(\beta|A_a, B_b)$ is of the form $\left(\sum_\alpha f(\alpha)\right) g(\beta)$ where f depends only on α and g only on β. If such a scenario occurs, we will mention that the normalization eliminates the dependence of $p^{NL}(\beta|A_a, B_b)$ on A_a.

ing the irrelevant normalization factor)

$$p^{NL}\left(\alpha,\beta|A_a,B_b\right)=\left\langle\left|\hat{U}^{\dagger}_{\phi_1(T_1)}(t_1,t_0)\hat{B}^{\dagger}_{\phi_2^B(T_2^B)}\left(t_2,t_1\right)\hat{P}_\beta\hat{B}_{\phi_2^B(T_2^B)}\left(t_2,t_1\right)\hat{P}_\alpha\hat{U}_{\phi_1(T_1)}(t_1,t_0)\right|\right\rangle, \tag{4.27}$$

where we have used Eqs. (4.6), (4.18) and (4.19). Before we perform a general analysis for arbitrary boundary states ϕ_1, ϕ_2^A and ϕ_2^B, we provide some examples.

4.4.1 Some example formulations

An interpretation that states that the wavefunction collapses after a measurement predicts

$$p^{NL}_{collapse}\left(\alpha,\beta|A_a,B_b\right)=\left\langle\hat{U}^{\dagger}_{(t_0)}(t_1,t_0)\hat{B}^{\dagger}_{\phi_\alpha(t_2)}\left(t_2,t_1\right)\hat{P}_\beta\hat{B}_{\phi_\alpha(t_2)}\left(t_2,t_1\right)\hat{P}_\alpha\hat{U}_{(t_0)}(t_1,t_0)\right\rangle,$$

where the expectation value is taken over $|\rangle$ and $|\phi_\alpha\rangle\equiv\hat{P}_\alpha\hat{U}_{(t_0)}(t_1,t_0)\,|\rangle$. When we calculate $p^{NL}_{collapse}\left(\beta|A_a,B_b\right)$, we have to sum over α but since ϕ_α depends on α, the sum doesn't solely apply on $\hat{P}_\alpha$:

$$p^{NL}_{collapse}\left(\beta|A_a,B_b\right)=\left\langle\hat{U}^{\dagger}_{(t_0)}(t_1,t_0)\sum_\alpha\left(\hat{B}^{\dagger}_{\phi_\alpha(t_2)}\left(t_2,t_1\right)\hat{P}_\beta\hat{B}_{\phi_\alpha(t_2)}\left(t_2,t_1\right)\hat{P}_\alpha\right)\hat{U}_{(t_0)}(t_1,t_0)\right\rangle.$$

Consider another choice for Alice's measurement basis: A_d, corresponding to an observable with eigenstates $|\delta\rangle$ and projection operators $\hat{D}_\delta$, then

$$p^{NL}_{collapse}\left(\beta|A_d,B_b\right)=\left\langle\hat{U}^{\dagger}_{(t_0)}(t_1,t_0)\sum_\delta\left(\hat{B}^{\dagger}_{\varphi_\delta(t_2)}\left(t_2,t_1\right)\hat{P}_\beta\hat{B}_{\varphi_\delta(t_2)}\left(t_2,t_1\right)\hat{D}_\delta\right)\hat{U}_{(t_0)}(t_1,t_0)\right\rangle,$$

where $|\varphi_\delta\rangle\equiv\hat{D}_\delta\hat{U}_{(t_0)}(t_1,t_0)\,|\rangle$. In general, $p^{NL}_{collapse}\left(\beta|A_a,B_b\right)$ and $p^{NL}_{collapse}\left(\beta|A_d,B_b\right)$ aren't equal and so a formulation based on immediate wavefunction collapse violates the no-signaling condition. It also violates another tenet of special relativity: the statistics of measurement outcomes is not the same in all reference frames. Refer to the Appendix for more details.

On the other hand, a formulation of quantum mechanics in which collapse doesn't occur, such as the many-worlds interpretation, states

$$p^{NL}_{M.W.}\left(\alpha,\beta|A_a,B_b\right)=\left\langle\hat{U}^{\dagger}_{\Phi_{ini}(t_{ini})}(t_1,t_0)\hat{B}^{\dagger}_{\Phi_{ini}(t_{ini})}\left(t_2,t_1\right)\hat{P}_\beta\hat{B}_{\Phi_{ini}(t_{ini})}\left(t_2,t_1\right)\hat{P}_\alpha\hat{U}_{\Phi_{ini}(t_{ini})}(t_1,t_0)\right\rangle, \tag{4.28}$$

where the expectation value is taken over $|\rangle$, t_{ini} is when the universe began and $|\Phi_{ini}\rangle$ is the initial state of the universe and so is independent of α and β. When

calculating $p^{NL}_{M.W.}(\beta|A_a, B_b)$, the sum over α can be directly applied on $\hat{P}_\alpha$ resulting in the identity operator, and so many-worlds does *not* violate the no-signaling condition. In the case of fundamental semi-classical gravity, Eq. (4.28) has already been ruled out [22].

In section 3.2, we discussed the prescriptions pre-selection and post-selection in the context of a single measurement. For the multiple measurements setup shown in Fig. 4.1, pre-selection takes ϕ_1 and ϕ_2 to be the initial state of the experiment $|\Psi_{ini}\rangle$ and $T_2 = T_1 = t_0$. Post-selection takes ϕ_1 and ϕ_2 to be the final state of the experiment $|\alpha, \beta\rangle$ and $T_1 = T_2 = t_2$. Post-selection violates the no-signaling condition because both ϕ_1 and ϕ_2 depend on the measurement outcomes α and β. Pre-selection doesn't violate the no-signaling condition. However, although [6] treated it as a phenomenological prescription, it is equivalent to the Everett interpretation[3].

4.4.2 A general analysis

From Eq. (4.27), we calculate $p^{NL}(\beta|A_a, B_b)$ to be

$$p^{NL}(\beta|A_a, B_b) = \left\langle \sum_\alpha \left(\hat{U}^\dagger_{\phi_1(T_1)}(t_1, t_0) \hat{B}^\dagger_{\phi_2^B(T_2^B)}(t_2, t_1) \hat{P}_\beta \hat{B}_{\phi_2^B(T_2^B)}(t_2, t_1) \hat{P}_\alpha \hat{U}_{\phi_1(T_1)}(t_1, t_0) \right) \right\rangle,$$

and $p^{NL}(\alpha|A_a, B_b)$ to be

$$p^{NL}(\alpha|A_a, B_b) = \left\langle \sum_\beta \left(\hat{U}^\dagger_{\phi_1(T_1)}(t_1, t_0) \hat{B}^\dagger_{\phi_2^B(T_2^B)}(t_2, t_1) \hat{P}_\beta \hat{B}_{\phi_2^B(T_2^B)}(t_2, t_1) \hat{P}_\alpha \hat{U}_{\phi_1(T_1)}(t_1, t_0) \right) \right\rangle,$$

where for both probabilities, the expectation value is taken over $|\rangle$. The no-signaling condition is violated if $p^{NL}(\beta|A_a, B_b)$ depends on A_a or if $p^{NL}(\alpha|A_a, B_b)$ depends on B_b.

Notice that if ϕ_1 depends on α then $p^{NL}(\beta|A_a, B_b)$ depends on A_a and so $p^{NL}(\beta|A_a, B_b) \neq p^{NL}(\beta|B_b)$. Similarly, if ϕ_1 depends on β then $p^{NL}(\alpha|A_a, B_b)$ depends on B_b. Consequently, ϕ_1 must be independent of α and β. Similarly, ϕ_2^B must also be independent of α and β. On the other hand, ϕ_2^A is unconstrained, and so our analysis doesn't result in a unique prescription. Nonetheless, we find it difficult to justify why ϕ_1 and ϕ_2^B would be anything other than the initial state of the experiment or of

[3] Choosing $|\phi_1\rangle$ and $|\phi_2\rangle$ to be the initial states of an experiment is not a well-defined procedure. Consider again the setup shown in Fig. 4.1, where Charlie prepared $|\Psi_{ini}\rangle$. He must have manipulated some state, which we call $|\Psi'_{ini}\rangle$, to prepare $|\Psi_{ini}\rangle$. If we choose $|\Psi'_{ini}\rangle$ to be the initial state of the experiment, then pre-selection predicts that $|\phi_1\rangle = |\phi_2\rangle = |\Psi'_{ini}\rangle$. This argument could be repeated back to the initial state of the universe. As a result, pre-selection seems to be equivalent to the Everett interpretation.

the universe. If we choose all boundary states to be the initial state of the universe, then we recover the Everett interpretation. In the next section, we discuss another reasonable prescription for assigning boundary states.

4.5 Causal-conditional: A sensible prescription that doesn't violate the no-signaling condition

In this section, we propose and discuss a prescription, which we name *causal-conditional*, for assigning boundary states to time-evolution operators in a way that doesn't violate the no-signaling condition. The causal-conditional prescription updates the boundary states of degrees of freedom lying in the future light cone of a particular measurement. We will be conservative and not explicitly assign a mechanism for this process, be it objective collapse or emergent behavior after the wavefunction branches. We only specify that the predictions of causal-conditional are mathematically equivalent to sQM with causal feedback following each measurement event.

To precisely explain the causal-conditional prescription, we will present, using the language of quantum field theory introduced in section 3.3, the quantum state of a general collection of degrees of freedom at an arbitrary time t_f. We'll assume that their initial state at time t_0 is $|\Psi_{ini}\rangle$ and that N measurements have occurred up to the final time t_f. The (unnormalized) conditional state at t_f is

$$|\Psi_c\rangle = \hat{U}_N \hat{P}\left(t_N, \boldsymbol{x}_N\right) \hat{U}_{N-1} \ldots \hat{P}\left(t_1, \boldsymbol{x}_1\right) \hat{U}_0 \left|\Psi_{ini}\right\rangle, \tag{4.29}$$

where $\hat{P}\left(t', \boldsymbol{y}\right)$ is a projection operator associated with a measurement at the spacetime location $(t', \boldsymbol{y})$ and $\hat{U}_i$, for $0 \leq i \leq N$, is the time-evolution operator from t_{i-1} till t_i. After some explanation, we provide $\hat{U}_i$'s exact expression in Eq. (4.30).

According to the causal-conditional prescription, a degree of freedom modifies the boundary condition that the non-linearity at its spacetime location depends on (as in Eq. (4.25)) when it receives information about a measurement outcome. This information propagates along the future light cone of a measurement event. Assume that for some $1 \leq i \leq N$, a degree of freedom at $\boldsymbol{x}$ receives information, at times $s_1^{(i)}, \ldots, s_{m_i}^{(i)}$ between t_{i-1} and t_i, about m_i measurement outcomes, then

$$\hat{U}_i = \hat{U}_{\Phi_T^{(i)}\left(s_{m_i}^{(i)}, \boldsymbol{x}\right)}\left(t_i, s_{m_i}^{(i)}\right) \ldots \hat{U}_{\Phi_T^{(i)}\left(s_1^{(i)}, \boldsymbol{x}\right)}\left(s_2^{(i)}, s_1^{(i)}\right) \hat{U}_{\Phi_T^{(i)}(t_{i-1}, \boldsymbol{x})}\left(s_1^{(i)}, t_{i-1}\right). \tag{4.30}$$

Note that we have extended the definition of the boundary state $|\Phi\left(\boldsymbol{x}\right)\rangle$ to include a dependence on time: $|\Phi\left(t, \boldsymbol{x}\right)\rangle$. Moreover, no measurements occurred before t_1 so

$\hat{U}_0 = \hat{U}_{\Phi_T^{(0)}(t_0,\boldsymbol{x})}(t_1, t_0)$.

The causal-conditional prescription chooses the boundary states as follows. For $t_0 \leq t < t_1$, no measurements have occurred, so $\left|\Phi^{(0)}(t,\boldsymbol{x})\right\rangle = |\Psi_{ini}\rangle$ for all t and the boundary time is $T^{(0)}(\boldsymbol{x}) = t_0$. For $1 \leq i \leq N$, $T^{(i)}(\boldsymbol{x}) = t_i$. The $\left|\Phi^{(i)}(t,\boldsymbol{x})\right\rangle$ are defined sequentially from $i = 1$ till $i = N$:

$$\left|\Phi^{(1)}(t,\boldsymbol{x})\right\rangle \equiv \hat{\mathcal{P}}_{(t,\boldsymbol{x})}(t_1,\boldsymbol{x}_1)\,\hat{U}_{\Phi_T^{(0)}(t,\boldsymbol{x})}(t_1,t_0)\,|\Psi_{ini}\rangle\,, \tag{4.31}$$

$$\left|\Phi^{(2)}(t,\boldsymbol{x})\right\rangle \equiv \hat{\mathcal{P}}_{(t,\boldsymbol{x})}(t_2,\boldsymbol{x}_2)\,\hat{U}_{\Phi_T^{(1)}(t,\boldsymbol{x})}(t_2,t_1)\left|\Phi^{(1)}(t,\boldsymbol{x})\right\rangle, \tag{4.32}$$

$$\vdots \quad \vdots \quad \vdots$$

$$\left|\Phi^{(N)}(t,\boldsymbol{x})\right\rangle \equiv \hat{\mathcal{P}}_{(t,\boldsymbol{x})}(t_N,\boldsymbol{x}_N)\,\hat{U}_{\Phi_T^{(N-1)}(t,\boldsymbol{x})}(t_N,t_{N-1})\left|\Phi^{(N-1)}(t,\boldsymbol{x})\right\rangle, \tag{4.33}$$

for all $t \geq t_0$ and where h. We illustrate the assignment of boundary states after the first two measurements in Fig. 4.2.

Finally, note that our scheme is similar to Adrian Kent's proposal in [21]. He argued that if the non-linear time evolution depends only on local states, which are obtained by conditioning only on measurements in the past light cone of a degree of freedom, then superluminal communication is not possible.

4.5.1 An example

Consider the setup shown in Fig. 4.3, which is a more elaborate version of Fig. 4.1. The thought experiment now includes two additional parties: Dylan who prepares an ensemble of two particles in the state $\left|\Psi'_{ini}\right\rangle$ and then sends them to Charlie, and Eve who performs a measurement outside the future light cone of Alice on Bob's particle at time t_3. We've added Dylan to demonstrate that we don't need to know $\left|\Psi'_{ini}\right\rangle$ to predict the distribution of outcomes for measurements lying in the future light cone of Dylan's measurement. We've added Eve to show that even for a complicated configuration of measurement events, our prescription does not violate the no-signaling condition.

We begin our analysis with the predictions of sQM for the final unnormalized state of the experiment conditioned on Charlie, Alice, Bob and Eve measuring γ, α, β and ϵ with corresponding measurement eigenstates $|\Psi_{ini}\rangle$, $|\alpha\rangle$, $|\beta\rangle$ and $|\epsilon\rangle$, and corresponding measurement bases C_c, A_a, B_b and E_e, respectively:

$$|\psi_c\rangle = \hat{P}_\epsilon \hat{U}(t_3,t_2)\hat{P}_\beta \hat{U}(t_2,t_1)\hat{P}_\alpha \hat{U}(t_1,t_0)\hat{P}_\gamma \hat{U}(t_0,t_D)\left|\Psi'_{ini}\right\rangle. \tag{4.34}$$

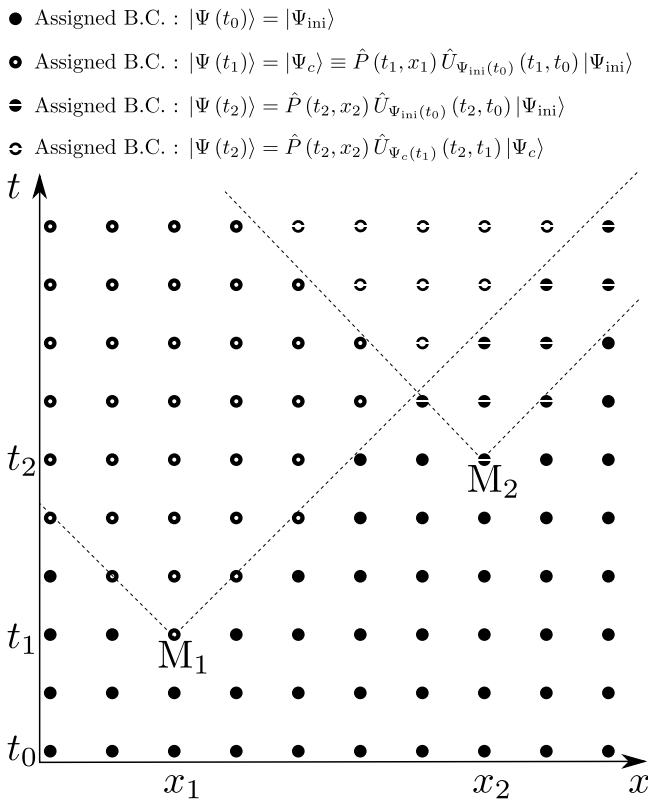

Figure 4.2: Assignment of boundary conditions after two measurements according to the causal-conditional prescription. M_1 and M_2 are two measurement events at spacetime locations (t_1, x_1) and (t_2, x_2), respectively, and the dashed lines show the light cones centered around each of them. To keep the figure uncluttered, we work with a one-dimensional quantum field, and we have discretized space and time into 10 points each. Each degree of freedom of the field is represented by a dot on the figure. How we fill the dot depends on what boundary condition (B.C.), which is indicated on the legend at the top of the figure, is assigned to the time-evolution of the wavefunction that the non-linear Hamiltonian at the spatial location of the dot depends on (see section 3.3 for more details). Note that the initial state of the field is $|\Psi_{ini}\rangle$.

The projection operators are

$$\hat{P}_\gamma = |\Psi_{ini}\rangle\langle\Psi_{ini}|, \quad \hat{P}_\alpha = |\alpha\rangle\langle\alpha|, \quad \hat{P}_\beta = |\beta\rangle\langle\beta|, \quad \hat{P}_\epsilon = |\epsilon\rangle\langle\epsilon|. \tag{4.35}$$

The structure of $|\psi_c\rangle$ can be simplified by noticing that Alice's measurement's future light cone doesn't overlap with Bob and Eve's measurement events' past light cone. We obtain

$$|\psi_c\rangle = \hat{P}_\epsilon \hat{A}(t_3, t_2)\, \hat{E}\hat{P}_\beta \hat{A}(t_2, t_1)\, \hat{B}\hat{P}_\alpha \hat{U}\hat{P}_\gamma \hat{V} \left|\Psi'_{ini}\right\rangle, \tag{4.36}$$

where to keep the notation concise, we have made the following definitions

$$\hat{V} \equiv \hat{U}(t_0, t_D); \qquad \hat{U} \equiv \hat{U}(t_1, t_0), \tag{4.37}$$

and $\hat{B}$ and $\hat{E}$ are the time-evolution operators for Bob and Eve's measured degrees of freedom from t_1 till t_2 and from t_2 till t_3, respectively.

According to the causal-conditional prescription, $|\psi_c\rangle$ extends to NLQM in the following way:

$$\begin{aligned} |\psi_c\rangle &= \hat{P}_\epsilon \hat{A}_{\alpha(t_1)}(t_3, t_2)\, \hat{E}_{\phi_3(t_2)}\hat{P}_\beta \hat{A}_{\alpha(t_1)}(t_2, t_1)\, \hat{B}_{\Psi_{ini}(t_0)}\hat{P}_\alpha \hat{U}_{\Psi_{ini}(t_0)}\hat{P}_\gamma \hat{V}_{\Psi'_{ini}(t_D)} \left|\Psi'_{ini}\right\rangle & (4.38)\\ &\propto \hat{A}_{\alpha(t_1)}(t_3, t_2)\, \hat{A}_{\alpha(t_1)}(t_2, t_1)\, \hat{P}_\epsilon \hat{E}_{\phi_3(t_2)}\hat{P}_\beta \hat{B}_{\Psi_{ini}(t_0)}\hat{P}_\alpha \hat{U}_{\Psi_{ini}(t_0)} |\Psi_{ini}\rangle, & (4.39) \end{aligned}$$

where

$$|\phi_3\rangle = \hat{P}_\beta \hat{A}_{\Psi_{ini}(t_0)}(t_2, t_1)\, \hat{B}_{\Psi_{ini}(t_0)}\hat{U}_{\Psi_{ini}(t_0)} |\Psi_{ini}\rangle. \tag{4.40}$$

We have also used that Alice's particle doesn't interact with the second particle after t_1 and so $\hat{A}$ commutes with $\hat{B}$, $\hat{E}$, $\hat{P}_\beta$ and $\hat{P}_\epsilon$. Bob's past light cone does not include Alice's measurement event, but includes Charlie's, so $|\Psi_{ini}\rangle$ is the boundary state associated with Bob's particle's time-evolution operator $\hat{B}$. Moreover, Eve's past light cone includes Bob's measurement event, so the conditional state $|\phi_3\rangle$ is the boundary state associated with $\hat{E}$. Notice that $\hat{A}$ in $|\phi_3\rangle$ is associated with the boundary state Ψ_{ini}. Refer to Fig. 4.4 for more details.

Eq. (4.39) doesn't violate the no-signaling condition and contains genuine non-linear time evolution, such as $\hat{U}_{\Psi_{ini}(t_0)}|\Psi_{ini}\rangle$. Moreover, notice that measurements within the past light cone of Charlie, like that of Dylan's, do not affect our analysis. Indeed, preparation events are always in the past light cone of the final measurements of an experiment because the measured particles' speed is upper bounded by the speed of light. Consequently, experimentalists do not need to know about measurements

occurring outside their experimental setup to calculate the predictions of the causal-conditional prescription.

We show that our proposed prescription does not violate the no-signaling condition by looking at the marginal probabilities, $p(\alpha|C,\mathcal{B})$, $p(\beta|C,\mathcal{B})$ and $p(\epsilon|C,\mathcal{B})$, conditioned on Charlie measuring $|\Psi_{ini}\rangle$ and on the measurement bases $\mathcal{B} \equiv \{C_c, A_a, B_b, E_e\}$. The probability of obtaining the measurement results α, β, ϵ, and that Charlie measures $|\Psi_{ini}\rangle$ is given by the norm of $|\Psi_c\rangle$:

$$\begin{aligned} p^{NL}(\alpha,\beta,\epsilon,C|\mathcal{B}) &= \left|\left\langle \Psi_{ini}\middle|\hat{V}_{\Psi'_{ini}(t_D)}\middle|\Psi'_{ini}\right\rangle\right|^2 \times \\ &\quad \left\langle \Psi_{ini}\middle|\hat{U}^{\dagger}_{\Psi_{ini}(t_0)}\hat{B}^{\dagger}_{\Psi_{ini}(t_0)}\hat{P}_{\beta}\hat{E}^{\dagger}_{\phi_3(t_2)}\hat{P}_{\epsilon}\hat{E}_{\phi_3(t_2)}\hat{P}_{\beta}\hat{B}_{\Psi_{ini}(t_0)}\hat{P}_{\alpha}\hat{U}_{\Psi_{ini}(t_0)}\middle|\Psi_{ini}\right\rangle, \end{aligned}$$

We are interested in $p^{NL}(\alpha,\beta,\epsilon|C,\mathcal{B})$, so we have to divide by

$$p^{NL}(C|\mathcal{B}) = \sum_{\alpha,\beta,\epsilon} p^{NL}(\alpha,\beta,\epsilon,C|\mathcal{B}) = \left|\left\langle \Psi_{ini}\middle|\hat{V}_{\Psi'_{ini}(t_D)}\middle|\Psi'_{ini}\right\rangle\right|^2. \tag{4.41}$$

We obtain

$$p^{NL}(\alpha,\beta,\epsilon|C,\mathcal{B}) = \left\langle \Psi_{ini}\middle|\hat{U}^{\dagger}_{\Psi_{ini}(t_0)}\hat{B}^{\dagger}_{\Psi_{ini}(t_0)}\hat{P}_{\beta}\hat{E}^{\dagger}_{\phi_3(t_2)}\hat{P}_{\epsilon}\hat{E}_{\phi_3(t_2)}\hat{P}_{\beta}\hat{B}_{\Psi_{ini}(t_0)}\hat{P}_{\alpha}\hat{U}_{\Psi_{ini}(t_0)}\middle|\Psi_{ini}\right\rangle. \tag{4.42}$$

Can Alice send signals to Bob or Eve, or vice versa? We first calculate $p^{NL}(\beta|C,\mathcal{B})$:

$$p^{NL}(\beta|C,\mathcal{B}) = \left\langle \Psi_{ini}\middle|\hat{U}^{\dagger}_{\Psi_{ini}(t_0)}\hat{B}^{\dagger}_{\Psi_{ini}(t_0)}\hat{P}_{\beta}\hat{B}_{\Psi_{ini}(t_0)}\hat{U}_{\Psi_{ini}(t_0)}\middle|\Psi_{ini}\right\rangle, \tag{4.43}$$

which doesn't depend on A_a. Next, we calculate Eve's distribution of measurement results:

$$p^{NL}(\epsilon|C,\mathcal{B}) = \left\langle \Psi_{ini}\middle|\hat{U}^{\dagger}_{\Psi_{ini}(t_0)}\hat{B}^{\dagger}_{\Psi_{ini}(t_0)}\sum_{\beta}\left(\hat{P}_{\beta}\hat{E}^{\dagger}_{\phi_3(t_2)}\hat{P}_{\epsilon}\hat{E}_{\phi_3(t_2)}\hat{P}_{\beta}\right)\hat{B}_{\Psi_{ini}(t_0)}\hat{U}_{\Psi_{ini}(t_0)}\middle|\Psi_{ini}\right\rangle, \tag{4.44}$$

so Alice cannot send superluminal signals to Eve. Bob and Eve's measurement events are time-like separated so it is acceptable that they can communicate amongst each other. Finally, Bob and Eve cannot communicate to Alice superluminally because

$$p^{NL}(\alpha|C,\mathcal{B}) = \left\langle \Psi_{ini}\middle|\hat{U}^{\dagger}_{\Psi_{ini}(t_0)}\hat{P}_{\alpha}\hat{U}_{\Psi_{ini}(t_0)}\middle|\Psi_{ini}\right\rangle \tag{4.45}$$

doesn't depend on B_b and E_e.

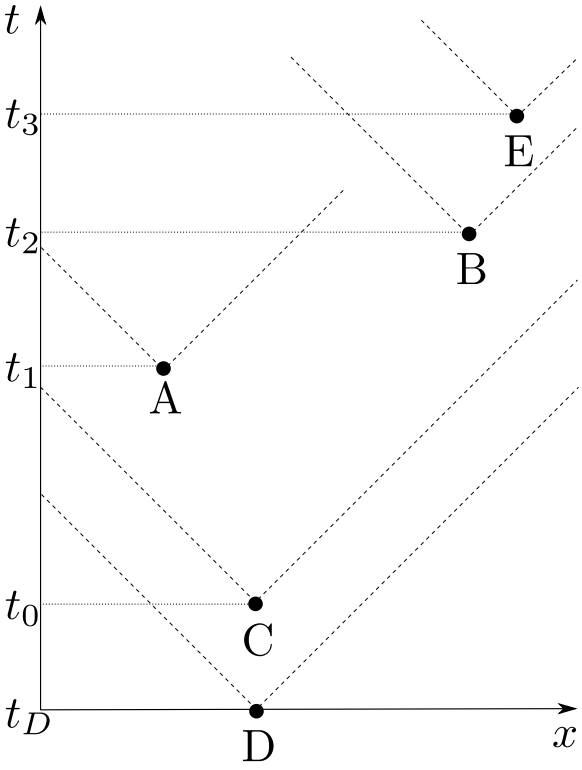

Figure 4.3: A setup similar to that described by Fig. 4.1, but more elaborate. Event D is Dylan preparing the state $|\Psi'_{ini}\rangle$, Event *C* is Charlie measuring the eigenstate $|\Psi_{ini}\rangle$. Event A (B) describes Alice (Bob) measuring her (his) particles. Bob then sends his particle to be measured by Eve at event E. The dashed lines show the light cone centered around each event.

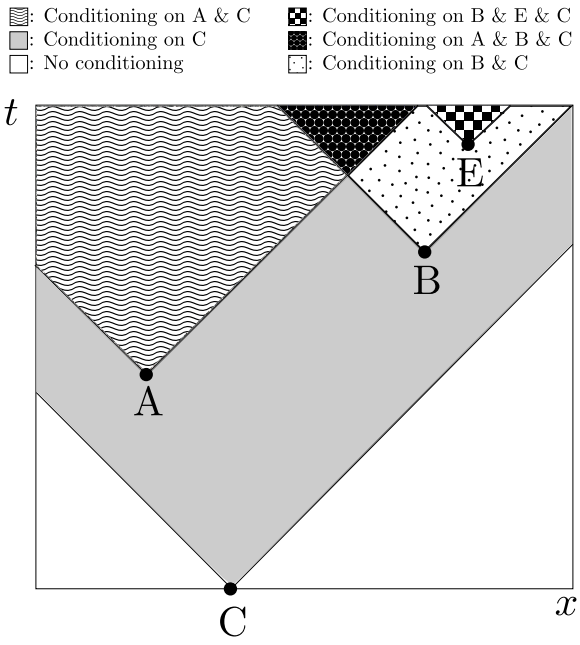

Figure 4.4: Partioning of spacetime into different regions according to which boundary state is associated with time evolution. There are 4 measurement events: C, A, B and E, that we've arranged identically as in Fig. 4.3. We didn't include Event D to limit clutter. The 4 events result in 6 regions. The boundary state associated with the non-linear time-evolution operator of each region is the time-evolved initial state of the experiment conditioned on measurement events presented in the legend at the top of the figure.

4.5.2 Proof that the causal-conditional prescription doesn't violate the no-signaling condition

We prove that the prescription discussed in this section does not violate the no-signaling condition. We first present a heuristic argument. The causal-conditional prescription is mathematically equivalent to linear quantum mechanics with causal feedback, and so doesn't violate the no-signaling condition. In particular, whenever a measurement occurs, the wavefunction that the non-linear potential depends on isn't modified instantaneously. Instead, a measurement transmits its outcome along its future light cone. Degrees of freedom that receive this information update their boundary state accordingly.

We now present a rigorous argument. Consider a general measurement configuration

as viewed in some reference frame. The unnormalized conditional state after the final measurement is

$$|\psi_c\rangle = \hat{U}_1 \hat{P}_1(\alpha_1) \ldots \hat{U}_f \hat{P}_f(\alpha_f) |ini\rangle, \tag{4.46}$$

where $|ini\rangle$ is the initial state of all degrees of freedom before the first measurement, $\hat{P}_i(\alpha_i)$ is the projection operator (with outcome α_i) associated with the ith measurement, and the $\hat{U}_1$, $\hat{U}_2$, ..., $\hat{U}_f$ are boundary-dependent time-evolution operators.

Assume that Bob performs, at time t_B, one of these measurement. We will show that Bob's probability of measuring a particular outcome β,

$$p(\beta|\Omega) = \sum_{\alpha_1,\ldots,\alpha_f}{}' \left\langle ini \middle| \hat{U}_1^\dagger \hat{P}_1(\alpha_1) \ldots \hat{P}_{f-1}(\alpha_{f-1}) \hat{U}_f^\dagger \hat{P}_f(\alpha_f) \hat{U}_f \hat{P}_{f-1}(\alpha_{f-1}) \ldots \hat{P}_1(\alpha_1) \hat{U}_1 \middle| ini \right\rangle, \tag{4.47}$$

where Ω is the set of all chosen measurement bases, is independent of measurements after t_B, and outside Bob's measurement's past light cone. Note that the sum is over all measurement outcomes except Bob's. All measurements occurring after t_B do not matter because we can directly sum over them. Let's first sum over α_f. We obtain

$$p(\beta|\Omega) = \sum_{\alpha_1,\ldots,\alpha_{f-1}}{}' \left\langle ini \middle| \hat{U}_1^\dagger \hat{P}_1(\alpha_1) \ldots \hat{U}_{f-1}^\dagger \hat{P}_{f-1}(\alpha_{f-1}) \hat{U}_{f-1} \ldots \hat{P}_1(\alpha_1) \hat{U}_1 \middle| ini \right\rangle \tag{4.48}$$

because the final measurement does not lie in the past light cone of any other measurement, and so no time-evolution operator would depend on α_f. We can repeat this procedure for all other measurements events after t_B.

For this part of the proof, we label the projection operator corresponding to Bob's measurement by $\hat{P}_\beta$ and assume that n measurements precede Bob's. Let $\tilde{\Omega} \subset \Omega$ be the set of measurements bases chosen by Bob and all experimentalists performing measurements before Bob. After summing over all the outcomes of all measurements performed after Bob's, we then obtain that

$$p(\beta|\tilde{\Omega}) = \sum_{\alpha_1,\ldots,\alpha_n} \left\langle ini \middle| \hat{U}_1^\dagger \hat{P}_1(\alpha_1) \ldots \hat{P}_n(\alpha_n) \hat{U}_{n+1}^\dagger \hat{P}_\beta \hat{U}_{n+1} \hat{P}_n(\alpha_n) \ldots \hat{P}_1(\alpha_1) \hat{U}_1 \middle| ini \right\rangle. \tag{4.49}$$

Consider the measurement occurring closest to t_B, and that is outside Bob's measurement's past light cone, as shown in Fig. 4.5. Assume it corresponds to the ith measurement event, and so according to the causal-conditional prescription, the time-evolution operators $\hat{U}_{i+1}$, ..., $\hat{U}_{n+1}$ contain boundary terms dependent on

α_i. Let's explicitly separate each of them into two components: $\hat{U}_j \equiv \hat{V}_j \hat{W}_j$ for $i+1 \leq j \leq n+1$ and where $\hat{V}_j$ doesn't depend on the boundary α_i whereas $\hat{W}_j$ does. The $\hat{W}_j$ also evolve degrees of freedom inside the ith measurement's future light cone. Consequently, the $\hat{W}_j$ commute with the $\hat{V}_j$, allowing us to simplify the expectation value in Eq. (4.49) to

$$\left\langle \hat{U}_1^\dagger \hat{P}_1(\alpha_1) \ldots \hat{U}_i^\dagger \hat{P}_i(\alpha_i) \hat{V}_{i+1}^\dagger \ldots \hat{P}_n(\alpha_n) \hat{V}_{n+1}^\dagger \hat{W}^\dagger \hat{P}_\beta \hat{W} \hat{V}_{n+1} \hat{P}_n(\alpha_n) \ldots \hat{V}_{i+1} \hat{P}_i(\alpha_i) \hat{U}_i \ldots \hat{P}_1(\alpha_1) \hat{U}_1 \right\rangle,$$

where the expectation value is taken over $|ini\rangle$ and $\hat{W} \equiv \hat{W}_{n+1} \ldots \hat{W}_{i+1}$. Since $\hat{W}^\dagger$ commutes with $\hat{P}_\beta$, it can be moved to the right of it where it will act on $\hat{W}$ and result in the identity matrix. Similarly, $\hat{P}_i(\alpha_i)$ can be moved to the right of $\hat{P}_\beta$ and we obtain

$$p\left(\beta|\tilde{\Omega}\right) = \sum_{\alpha_1,\ldots,\alpha_n} \left\langle \hat{U}_1^\dagger \hat{P}_1(\alpha_1) \ldots \hat{U}_i^\dagger \hat{V}_{i+1}^\dagger \ldots \hat{P}_n(\alpha_n) \hat{V}_{n+1}^\dagger \hat{P}_\beta \hat{V}_{n+1} \hat{P}_n(\alpha_n) \ldots \hat{V}_{i+1} \hat{P}_i(\alpha_i) \hat{U}_i \ldots \hat{P}_1(\alpha_1) \hat{U}_1 \right\rangle$$

The sum over α_i can then be directly applied on $\hat{P}_i(\alpha_i)$ allowing us to eliminate it. As a result, $p\left(\beta|\tilde{\Omega}\right)$ is independent of basis chosen during the ith measurement.

The above argument can be applied sequentially and in reverse chronological order to eliminate $p\left(\beta|\tilde{\Omega}\right)$'s dependence on all bases associated with measurements outside Bob's measurement's past light cone. Although we conducted our analysis in a particular reference frame, and so assuming a particular ordering of events, our arguments could be applied to any other reference frame (modulo a relabeling of spacetime points). We would always arrive to the same conclusion: the causal-conditional prescription does not violate the no-signaling condition.

4.6 Conclusions

We have shown that modifying linear quantum mechanics is not as simple as adding terms in the Hamiltonian that depend on the wavefunction. One must also make a choice on how to interpret measurements and the evolution of the wavefunction. By breaking linearity, different formulations of quantum mechanics, such as the Everett and Copenhagen interpretations, no longer make equivalent predictions.

By introducing the notion of a time-evolution operator that depends on the specified boundary conditions for the quantum state of the system that is being time-evolved, we were able to explore the range of possible prescriptions for assigning probabilities to measurement outcomes in NLQM. For a certain class of non-linear theories, we showed that two reasonable prescriptions do not violate the no-signaling condition. The first is the Everett interpretation, and the second, which we named *causal-*

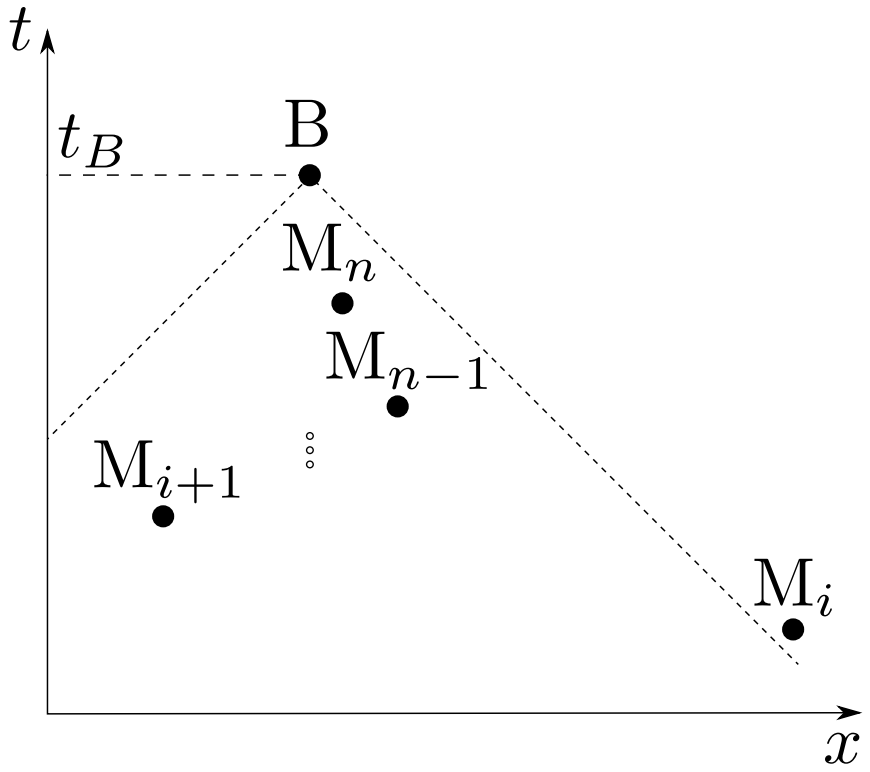

Figure 4.5: A general configuration of measurements, labeled by M_j where $1 \leq j \leq n$, occurring before an event B, which describes Bob performing a measurement. The dashed lines shows the past light cone of event B.

conditional, states that a measurement event at a particular spacetime point $\boldsymbol{X}$ updates the boundary state associated with the time evolution operator of quantum degrees of freedom lying in the future light cone of $\boldsymbol{X}$. The predictions of causal-conditional are mathematically equivalent to standard quantum mechanics with causal feedback. A measurement applies a feedback force (the details of which are determined by the non-linear theory of interest) on degrees of freedom lying in the future light cone of that measurement event.

Ackowledgments

We thank Craig Savage, Sabina Scully, Tian Wang, Maneeli Derakhshani, Yiqiu Ma, Haixing Miao, Sean Carroll and Ashmeet Singh for useful discussions. We also thank Antoine Tilloy for pointing out important issues with how we explained certain concepts. This research is supported by NSF grants PHY-1404569 and PHY-1506453, as well as the Institute for Quantum Information and Matter, a Physics Frontier Center.

Appendix: The statistics of measurement outcomes in different reference frames

We first review why sQM predicts, in all reference frames, identical statistics for measurement results. We then show that this is no longer true in NLQM if we adopt an interpretation where the wavefunction instantaneously collapses across all of space. Finally, we discuss why the causal-conditional prescription predicts, in different reference frames, identical statistics for measurement outcomes.

Consider the multiple measurements configuration shown in Fig. (4.1) where Alice and then Bob measure their respective particles, as viewed in some reference frame that what we'll refer to as the *lab frame*. In this frame, the probability of Alice measuring α and Bob measuring β, $p\left(\alpha,\beta|\, A_a, B_b\right)$ is given by Eqs. (4.1, 4.2). To conveniently transform $p\left(\alpha,\beta|\, A_a, B_b\right)$ from one reference frame to another, we will express $p\left(\alpha,\beta|\, A_a, B_b\right)$ in a Heisenberg picture. Define

$$\hat{P}_\alpha\left(\boldsymbol{x}_A, t_1\right) \equiv \hat{U}^\dagger\left(t_1, t_0\right)\hat{P}_\alpha\hat{U}\left(t_1, t_0\right), \quad \hat{P}_\beta\left(\boldsymbol{x}_B, t_2\right) \equiv \hat{U}^\dagger\left(t_2, t_0\right)\hat{P}_\beta\hat{U}\left(t_2, t_0\right), \tag{4.50}$$

where we've explicitly denoted the location of Alice's measurement at $\boldsymbol{x}_A$ and of Bob's at $\boldsymbol{x}_B$. Since $\hat{P}_\alpha\left(\boldsymbol{x}_A, t_1\right)$ and $\hat{P}_\beta\left(\boldsymbol{x}_B, t_2\right)$ commute, we can rewrite $p\left(\alpha,\beta|A_a, B_b\right)$ to

$$p\left(\alpha,\beta|\, A_a, B_b\right) = \left\langle\Psi_{ini}\middle|\hat{P}_\beta\left(\boldsymbol{x}_B, t_2\right)\hat{P}_\alpha\left(\boldsymbol{x}_A, t_1\right)\middle|\Psi_{ini}\right\rangle. \tag{4.51}$$

Consider now a Lorentz-transformation Λ from the lab frame to any other frame. On the Hilbert space of Alice and Bob's particles', Λ is realized by an operator $\hat{V}\left(\Lambda\right)$. For instance, $\hat{V}\left(\Lambda\right)$ transforms a momentum eigenstate of a spinless particles to $\hat{V}\left(\Lambda\right)|\boldsymbol{k}\rangle = |\Lambda\boldsymbol{k}'\rangle$, where $|\boldsymbol{k}\rangle$ is covariantly normalized to $\langle\boldsymbol{k}|\boldsymbol{k}'\rangle = \langle\Lambda\boldsymbol{k}|\Lambda\boldsymbol{k}'\rangle$ [20]. We re-express $p\left(\alpha,\beta|A_a, B_b\right)$ in terms of wavefunctions and projection operators viewed in a different frame

$$\begin{aligned} p\left(\alpha,\beta|A_a, B_b\right) &= \left\langle\Lambda\Psi_{ini}\middle|\hat{V}\left(\Lambda\right)\hat{P}_\beta\left(\boldsymbol{x}_B, t_2\right)\hat{V}^\dagger\left(\Lambda\right)\hat{V}\left(\Lambda\right)\hat{P}_\alpha\left(\boldsymbol{x}_A, t_1\right)\hat{V}^\dagger\left(\Lambda\right)\middle|\Lambda\Psi_{ini}\right\rangle \\ &= \left\langle\Lambda\Psi_{ini}\middle|\hat{P}_\beta\left(\Lambda^\mu_\nu x^\nu_B\right)\hat{P}_\alpha\left(\Lambda^\mu_\nu x^\nu_A\right)\middle|\Lambda\Psi_{ini}\right\rangle, \end{aligned} \tag{4.52, 4.53}$$

where $|\Lambda\Psi\rangle \equiv \hat{V}\left(\Lambda\right)|\Psi\rangle$ for any $|\Psi\rangle$, x^ν_A is the 4-vector $\left(\boldsymbol{x}_A, t_1\right)$ and x^ν_B is $\left(\boldsymbol{x}_B, t_2\right)$. If we assume that the measured results do not change under Lorentz transformations (*e.g.* photodetector clicks[4]), then Eq. (4.53) is just the probability of measuring α

[4]For a Klein-Gordon field $\hat{\phi}$, the measured observable would be

$$\int_V \hat{j}^\nu . d\Sigma_\nu, \quad \hat{j}^\nu\left(x^\mu\right) = i\left[\partial^\nu\hat{\phi}_-\left(x^\mu\right)\right]\hat{\phi}_+\left(x^\mu\right) + h.c, \tag{4.54}$$

and β in a different reference frame. Therefore, in sQM, the statistics of measurement outcomes are the same in all reference frames.

The extension of $p(\alpha, \beta|\, A_a, B_b) = \left\langle \Psi_{c|\alpha,\beta} | \Psi_{c|\alpha,\beta} \right\rangle$, as calculated by an observer in the lab frame, to NLQM coupled with an interpretation of QM with wavefunction collapse is

$$\left| \Psi^{collapse}_{c|\alpha,\beta} \right\rangle = \hat{P}_\beta \hat{U}_{\Phi_\alpha(t_1)}(t_2, t_1)\, \hat{P}_\alpha \hat{U}_{\Psi_{ini}(t_0)}(t_1, t_0)\, |\Psi_{ini}\rangle\,, \tag{4.55}$$

where $\hat{U}_{\Psi_{ini}(t_0)}(t_1, t_0)$ is the time-evolution operator associated with the boundary condition $|\Psi(t_0)\rangle = |\Psi_{ini}\rangle$, and $\hat{U}_{\Phi_\alpha(t_1)}(t_2, t_1)$ is associated with the condition $|\Psi(t_1)\rangle = |\Phi_\alpha\rangle$ where

$$|\Phi_\alpha\rangle = \hat{P}_\alpha \hat{U}_{\Psi_{ini}(t_0)}(t_1, t_0)\, |\Psi_{ini}\rangle\,. \tag{4.56}$$

The extension of the Heisenberg picture projection operators in Eq. (4.50) to NLQM is

$$\hat{P}^{collapse}_\alpha(\boldsymbol{x}_A, t_1) \equiv \hat{U}^\dagger_{\Psi_{ini}(t_0)}(t_1, t_0)\, \hat{P}_\alpha \hat{U}_{\Psi_{ini}(t_0)}(t_1, t_0), \quad \hat{P}^{collapse}_\beta(\boldsymbol{x}_B, t_2) \equiv \hat{U}^\dagger_2 \hat{P}_\beta \hat{U}_2, \tag{4.57}$$

$$\hat{U}_2 \equiv \hat{U}_{\Phi_\alpha(t_1)}(t_2, t_1)\, \hat{U}_{\Psi_{ini}(t_0)}(t_1, t_0)\,. \tag{4.58}$$

Consequently, the extension of Eq. (4.53) to NLQM is

$$p^{collapse}(\alpha, \beta|\, A_a, B_b) = \left\langle \Lambda\Psi_{ini} \middle| \hat{P}^{collapse}_\beta\left(\Lambda^\mu_\nu x^\nu_B\right) \hat{P}^{collapse}_\alpha\left(\Lambda^\mu_\nu x^\nu_A\right) \middle| \Lambda\Psi_{ini} \right\rangle. \tag{4.59}$$

Let's consider a Lorentz transformation $\tilde{\Lambda}$ that takes the lab frame to one where Bob measures his particles before Alice measures hers. An observer in that frame would calculate that the probability that Alice measures α and Bob measures β is

$$\begin{aligned}
\tilde{p}^{collapse}(\alpha, \beta|\, A_a, B_b) &= \left\langle \tilde{\Lambda}\Psi_{ini} \middle| \tilde{P}^{collapse}_\alpha(\tilde{x}_A)\, \tilde{P}^{collapse}_\beta(\tilde{x}_B) \middle| \tilde{\Lambda}\Psi_{ini} \right\rangle, \quad \tilde{x}_{A,B} \equiv \tilde{\Lambda}^\mu_\nu x^\nu_{A,B}, \\
\tilde{P}^{collapse}_\beta(\tilde{x}_B) &= \hat{U}^\dagger_{\tilde{\Lambda}\Psi_{ini}(t_0)}\left(\tilde{x}^0_B, \tilde{t}_0\right) \hat{P}_\beta \hat{U}_{\tilde{\Lambda}\Psi_{ini}(t_0)}\left(\tilde{x}^0_B, \tilde{t}_0\right), \quad \tilde{P}^{collapse}_\alpha(\tilde{x}_A) = \tilde{U}^\dagger_2 \hat{P}_\alpha \tilde{U}_2, \\
\tilde{U}_2 &\equiv \hat{U}_{\tilde{\Phi}_\beta\left(\tilde{x}^0_B\right)}\left(\tilde{x}^0_A, \tilde{x}^0_B\right) \hat{U}_{\tilde{\Lambda}\Psi_{ini}(t_0)}\left(\tilde{x}^0_B, \tilde{t}_0\right), \\
\left|\tilde{\Phi}_\beta\right\rangle &= \hat{P}_\beta \hat{U}_{\tilde{\Lambda}\Psi_{ini}(t_0)}\left(\tilde{x}^0_B, \tilde{t}_0\right) \left|\tilde{\Lambda}\Psi_{ini}\right\rangle,
\end{aligned}$$

where $\tilde{t}_0$ is when the experiment began in this new frame. Although $p^{collapse}(\alpha, \beta|A_a, B_b)$

where V is the spacetime volume occupied by the photodetector during a single measurement run, and $\hat{\phi}_+$ and $\hat{\phi}_-$ are the positive and negative frequency components of $\hat{\phi}$, respectively [23].

can be re-written to

$$p^{collapse}\left(\alpha,\beta|A_a,B_b\right)=\left\langle\tilde{\Lambda}\Psi_{ini}\middle|\hat{P}_{\alpha}^{collapse}\left(\tilde{x}_A\right)\hat{P}_{\beta}^{collapse}\left(\tilde{x}_B\right)\middle|\tilde{\Lambda}\Psi_{ini}\right\rangle, \tag{4.60}$$

it isn't in general equal to $\tilde{p}^{collapse}\left(\alpha,\beta|A_a,B_b\right)$ because $\hat{P}_{\beta}^{collapse}\left(\tilde{x}_B\right)$ depends on Φ_α while $\tilde{P}_{\beta}^{collapse}\left(\tilde{x}_B\right)$ doesn't. Similarly, $\tilde{P}_{\alpha}^{collapse}\left(\tilde{x}_A\right)$ depends on $\tilde{\Phi}_\beta$ while $\hat{P}_{\alpha}^{collapse}\left(\tilde{x}_A\right)$ doesn't. In other words, $\hat{V}\left(\tilde{\Lambda}\right)$ doesn't connect Φ_α, Φ_β and Ψ_{ini} to each other.

The fact that $p^{collapse}\left(\alpha,\beta|A_a,B_b\right)$ isn't the same in all reference frame isn't surprising. and can be understood heuristically when we view the non-linearity as a feedback force that changes acausally after the wavefunction collapses. Consider the following non-linear interaction energy density

$$\hat{V}_{NL}\left(\boldsymbol{x}\right)=\left\langle\Psi\left(t\right)\middle|\hat{O}\middle|\Psi\left(t\right)\right\rangle\hat{M}\left(\boldsymbol{x}\right), \tag{4.61}$$

where $\hat{O}$ is Lorentz-invariant ($\hat{V}^{\dagger}\left(\Lambda\right)\hat{O}\hat{V}\left(\Lambda\right)=\hat{O}$ for any transformation Λ), and we assume that $\hat{M}\left(x\right)$ transforms as $\hat{M}\left(\Lambda x\right)$ under Λ (so as to maintain the the requirement that the total interaction Hamiltonian density $\hat{H}_{int}\left(x\right)$ transforms as $\hat{H}_{int}\left(\Lambda x\right)$ - see sec. 5.5 of [20]). We can then view $F\left(t\right)\equiv\left\langle\Psi\left(t\right)\middle|\hat{O}\middle|\Psi\left(t\right)\right\rangle$ as a classical feedback force on $\hat{M}$.

When a measurement occurs, $\Psi(t)$ instantaneously changes, and so $F\left(t\right)$ acting on $\hat{M}\left(\boldsymbol{x}\right)$ for all $\boldsymbol{x}\in\mathbb{R}^3$ changes instantaneously too. The problem is that the spatial surface of time simultaneity is the not the same in all reference frames. In the case of multiple spacelike-separated measurement events, we'd get that $F\left(t\right)$ changes differently in different frames depending on the ordering of the measurement events in that frame. On the other hand, for the causal-conditional prescription, $F\left(t\right)$ would change causally after any measurement, and so there are no issues.

Bibliography

[1] Bialynicki-Birula I and Mycielski J 1976 Nonlinear wave mechanics *Annals of Physics* **100** 1 62.

[2] de Broglie L 1960 *Non-linear wave mechanics, A causal interpretation* (Elsevier Pub. Co.).

[3] Weinberg S 1989 Testing quantum mechanics *Annals of Physics* **194** 2 336.

[4] Bassi A and Ghirardi G 2000 A general argument against the universal validity of the superposition principle *Phys. Lett.* A **275** 373.

[5] Bassi A, Lochan K, Satin S, Singh T and Ulbricht H 2013 Models of wave-function collapse, underlying theories, and experimental tests *Rev. Mod. Phys.* **85** 2 471.

[6] Helou B, Luo J, Yeh H.-C., Shao C.-g., Slagmolen B. J., McClelland D. E. and Chen, Y 2016 Measurable signatures of quantum mechanics in a classical spacetime *Preprint* quant-ph/1612.06310.

[7] Vinante A, Bahrami M, Bassi A, Usenko O, Wijts G and Oosterkamp, T. H. 2016 Upper bounds on spontaneous wave-function collapse models using millikelvin-cooled nanocantilevers *Phys. Rev. Lett.* **116** 9 090402.

[8] Shull C. G., Atwood D. K., Arthur J and Horne M. A. 1980 Search for a nonlinear variant of the Schrodinger equation by neutron interferometry *Phys. Rev. Lett.* **44** 12 765.

[9] Bollinger J. J., Heinzen D. J., Itano W, Gilbert S. L. and Wineland D. J. 1989 Test of the linearity of quantum mechanics by rf spectroscopy of the $^{9}Be^{+}$ ground state *Phys. Rev. Lett.* **63** 10 1031.

[10] Chupp T. E. and Hoare R. J. 1990 Coherence in freely precessing ^{21}Ne and a test of linearity of quantum mechanics *Phys. Rev. Lett.* **64** 19 2261.

[11] Walsworth R. L., Silvera I. F., Mattison E. M. and Vessot R. F. C. 1990 Test of the linearity of quantum mechanics in an atomic system with a hydrogen maser *Phys. Rev. Lett.* **64** 22 2599.

[12] Majumder P. K., Venema B. J., Lamoreaux S. K., Heckel B. R. and Fortson E. N. 1990 Test of the linearity of quantum mechanics in optically pumped ^{201}Hg *Phys. Rev. Lett.* **65** 24 2931.

[13] Yang H, Miao H, Lee D, Helou B and Chen Y 2013 Macroscopic Quantum Mechanics in a Classical Spacetime *Phys. Rev. Lett.* **110** 17 170401.

[14] Stamp P. C. E. 2015 Rationale for a Correlated Worldline Theory of Quantum Gravity *New J. Phys.* **17** 6 065017.

[15] Gisin N 1990 Weinberg's non-linear quantum mechanics and supraluminal communications *Phys. Lett.* A **143** 1-2 1.

[16] Polchinski J 1991 Weinberg's nonlinear quantum mechanics and the Einstein-Podolsky-Rosen paradox *Phys. Rev. Lett.* **66** 4 397.

[17] M. Czachor 1991 Mobility and non-separability *Foundations of Physics Letters* **4** 4 351.

[18] Simon C, Bužek V and Gisin N 2001 No-signaling condition and quantum dynamics *Phys. Rev. Lett.* **87** 17 170405.

[19] Mielnik B 2001 Nonlinear quantum mechanics: a conflict with the Ptolomean structure? *Phys. Lett.* A **289** 1-2 1.

[20] Duncan A 2012 The conceptual framework of quantum field theory *Oxford* Eqs. 5.77 and 6.51.

[21] Kent A 2005 Nonlinearity without superluminality *Phys. Rev.* A **72** 1 012108.

[22] Don N. Page and C. D. Geilker. Indirect evidence for quantum gravity. *Phys. Rev. Lett.*, 47:979–982, Oct 1981.

[23] Belinda H. Pang, Yanbei Chen, and Farid Ya. Khalili. Universal decoherence under gravity: A perspective through the equivalence principle. *Phys. Rev. Lett.*, 117:090401, Aug 2016.

Chapter 5

MEASURABLE SIGNATURES OF A CAUSAL THEORY OF QUANTUM MECHANICS IN A CLASSICAL SPACETIME

5.1 Introduction

With the recent advances in quantum optomechanics, it is now feasible for such a platform to test alternative theories of quantum mechanics. There have been many proposals, and some experiments, for optomechanics to test alternative theories of quantum mechanics. In this article, we focus on fundamental semi-classical gravity, where the space-time geometry is sourced by the quantum expectation value of the stress energy tensor

$$G_{\mu\nu} = 8\pi \left\langle \Phi \middle| \hat{T}_{\mu\nu} \middle| \Phi \right\rangle \tag{5.1}$$

with $G = c = 1$, and where $G_{\mu\nu}$ is the Einstein tensor of a (3+1)-dimensional classical spacetime. $\hat{T}_{\mu\nu}$ is the operator representing the energy-stress tensor, and $|\Phi\rangle$ is the wave function of all (quantum) matter and fields that evolve within this classical spacetime.

There have been many proposals for optomechanics to test the predictions of Eq. (5.1) [2, 3, 5]. In this article, we propose a new version of the Schroedinger-Newton theory that does not violate causality. We also calculate its predictions in a low-frequency optomechanics experiment.

In particular, we will argue that once we fix the initial state of a system, its monitored evolution under a large class of Non-Linear Quantum Mechanics (NLQM) theories (of which Eq. (5.1) is a part of) is equivalent to evolution under a particular quantum feedback scheme. Since quantum feedback can be causal, we show that adding measurements to Eq. (5.1) doesn't necessarily mean the theory violates the no-signaling condition. Eq. (5.1) can be thought of as changing the dynamics of a quantum mechanical system by applying a causal feedback force everywhere in spacetime. Since this force is causal, it means that the applied force at location (t, x) can only depend on measurement results in the past light cone of (t, x), and so the expectation value in Eq. (5.1) would be over a state $|\Phi\rangle$ that is conditioned only on measurement results in the past light cone of (t, x). We also illustrate the mapping between NLQM and feedback with concrete examples. Finally, we calculate the signature of this causal theory of fundamental semi-classical gravity in a torsion pendulum experiment.

5.2 NLQM is formally equivalent to quantum feedback

We will show that a large set of non-linear quantum mechanical theories are formally equivalent to linear quantum feedback. This mapping has two main advantages. First, it allows us to leverage the tools developed for linear quantum mechanics to understand NLQM. Second, since we understand when quantum feedback is causal, we can come up with strategies to incorporate measurements in NLQM without violating the no-signaling condition.

Specifically, the class of non-linear quantum mechanical theories that we consider has the following evolution equation:

$$i\hbar\partial_t \left|\psi\left(t\right)\right\rangle = \hat{H}_{NLQM} \left|\psi\left(t\right)\right\rangle \tag{5.2}$$

where the non-linear Hamiltonian is

$$\hat{H}_{NLQM} = \hat{H}_L + \sum_i \beta_i \phi\left(x_i, t, \psi\left(t\right)\right) \hat{V}_i. \tag{5.3}$$

$\hat{H}_L$ is the linear part of $\hat{H}$, and doesn't depend on the wavefunction. The second term represents a classical field that couples to our quantum system through $\hat{V}_i$ at positions x_i. The classical field follows its own equation of motion:

$$\mathcal{L}\phi\left(x, t\right) = S\left(x, t, \psi\left(t\right)\right) \tag{5.4}$$

where $\mathcal{L}$ is a differential operator and $S\left(x, t, \psi\left(t\right)\right)$ is a source term that, in general, depends on $\psi\left(t\right)$. The β_i are constants. We wrote the non-linear Hamiltonian in the form of Eq. (5.3) because it clearly separates out the nonlinearity to a single parameter, ϕ. This separation will make it easier to understand the mapping from NLQM to quantum feedback. Once we solve for ϕ and substitute back into $\hat{H}_{NLQM}$, we will show that evolution under $\hat{H}_{NLQM}$ can be thought of as evolution under a linear Hamiltonian. Note that the sum $\sum_i$ could in general contain an integral. An example non-linear theory is fundamental semi-classical gravity in the Newtonian limit, which is typically called the Schroedinger-Newton theory. The non-linear Hamiltonian for a free particle of mass m is

$$\hat{H}_{SN} = -m \int d\boldsymbol{x} \phi\left(\boldsymbol{x}, \psi\left(t\right)\right) \left|\boldsymbol{x}\right\rangle \left\langle\boldsymbol{x}\right| \tag{5.5}$$

and the classical gravitational field follows the equation of motion

$$\nabla^2 \phi\left(\boldsymbol{x}, t\right) = 4\pi G m \left|\psi\left(\boldsymbol{x}, t\right)\right|^2. \tag{5.6}$$

5.2.1 No measurements

We first show that for Eq. (5.2), the unmonitored dynamics of the wavefunction, once we fix its initial state, are the same as the dynamics of a wavefunction evolving under a linear time-dependent Hamiltonian. Eq. (5.2) is a special case of evolution under a time-dependent Hamiltonian

$$i\hbar\partial_t \left|\psi\left(t\right)\right\rangle = \hat{H}\left(t\right)\left|\psi\left(t\right)\right\rangle \tag{5.7}$$

where

$$\hat{H}\left(t\right) = \hat{H}_0 + \sum_i \alpha_i\left(t\right)\hat{O}_i \tag{5.8}$$

and $\hat{H}_0$ is time-independent. Once we fix an initial state for Eq. (5.2) then we can solve Eqs. (5.2-5.4) and obtain ϕ. If we pick $\alpha_i\left(t\right)$ to be equal to $\phi\left(x_i, t, \psi\left(t\right)\right)$ and $\hat{O}_i$ equal to $\hat{V}_i$ then the evolution of the initial state under Eq. (5.2) is identical to the evolution of the same initial state under Eq. (5.7). Therefore, once we fix an initial state, we can use the tools of time-dependent quantum mechanics to examine Eq. (5.2). Moreover, we are assured that Eq. (5.2) has the same properties as Eq. (5.7), such as satisfying the no-signaling condition.

5.2.1.1 An example

We will give a simple example illustrating how NgLQM without measurement can produce dynamics that are equivalent to those of time-dependent linear quantum mechanics. Let's assume that Alice is at position x_A and has a spin that evolves under the linear Hamiltonian

$$\hat{H}_A = E\hat{\sigma}_z^{(A)}, \tag{5.9}$$

where $\hat{\sigma}_z^{(A)}$ is Alice's spin's Pauli z matrix. The spin also couples to a classical field:

$$\hat{V}_{NL}^{(A)}\left(t\right) = \hbar\omega_A\phi\left(x_A, t\right)\hat{\sigma}_x^{(A)} \tag{5.10}$$

where $\omega_A \in \mathbb{R}$ and $\hat{\sigma}_x^{(A)}$ is the Pauli x matrix. Let's assume that $\phi\left(x_A, t\right)$ is

$$\phi\left(x_A, t\right) = \left\langle\psi\left(t\right)\middle|\hat{\sigma}_z^{(A)}\middle|\psi\left(t\right)\right\rangle. \tag{5.11}$$

Given the initial state of Alice's spin $\left|\psi_{ini}^{A}\right\rangle$, Eq. (5.10) is equivalent to a time-dependent linear Hamiltonian. In particular, Alice can calculate $\phi\left(x_A, t\right)$ by solving

$$i\hbar\partial_t \left|\psi\left(t\right)\right\rangle = \left(\hat{H}_A + \hat{V}_{NL}^{(A)}\left(t\right)\right)\left|\psi\left(t\right)\right\rangle \tag{5.12}$$

with the boundary condition

$$|\psi(t_{ini})\rangle = \left|\psi^A_{ini}\right\rangle . \tag{5.13}$$

With $\phi(x_A, t)$ Alice can then construct an experiment with a Hamiltonian that is equivalent to $\hat{H}_A + \hat{V}^{(A)}_{NL}(t)$. She would just have to apply a magnetic field along the z direction with time-dependence given by $-\hbar\gamma\phi(x_A, t)/(2\omega_A)$, where γ is the gyromagnetic ratio of Alice's particle.

5.2.2 Adding measurements

If we monitor the quantum system we are investigating, then $|\psi(t)\rangle$ depends on the measurement record because the unitary evolution of $|\psi(t)\rangle$ is interrupted by projection operators. Specifically, if n observables, $\hat{Y}_1$ through $\hat{Y}_n$, are measured at times t_1 through t_n, then $|\psi(t)\rangle$ is (up to a normalization factor)

$$|\psi(t)\rangle \propto \hat{U}_{\varphi_n}(t, t_n)\,\hat{P}_n ... \hat{P}_2 \hat{U}_{\varphi_1}(t_2, t_1)\,\hat{P}_1 \hat{U}_{\varphi_0}(t_1, t_0)\,|\psi(t_0)\rangle \tag{5.14}$$

where for $i = 1...n$, $\hat{P}_i$ projects $\hat{Y}_i$ at time t_i to its eigenstate with eigenvalue y_i. Each evolution operator $\hat{U}_\varphi(\tilde{t}_1, \tilde{t}_0)$ evolves a wavefunction from $\tilde{t}_0$ till $\tilde{t}_1$ under Eq. (5.2) and the boundary condition

$$|\psi(\tilde{t}_0)\rangle = |\varphi\rangle . \tag{5.15}$$

As explained in Ref. [4], the boundary state $|\varphi\rangle$ could depend arbitrarily on the measurements results $\{y_i\}$. For example, according to the Everett intepretation, all boundary states are the initial state of the universe. On the other hand, the Copenhagen interpretation states that the boundary states should incorporate all measurements up the current time.

Similarly to Eq. (5.14), the wavefunction under feedback, $\left|\psi_{fb}(t)\right\rangle$, is (up to a normalization factor)

$$\left|\psi_{fb}(t)\right\rangle \propto \hat{U}_{fb}(t, t_n)\,\hat{P}_n ... \hat{P}_2 \hat{U}_{fb}(t_2, t_1)\,\hat{P}_1 \hat{U}_{fb}(t_1, t_0)\,|\psi(t_0)\rangle , \tag{5.16}$$

where we've denoted the measurement record by

$$\boldsymbol{y} = \begin{pmatrix} y_n & \dots & y_2 & y_1 \end{pmatrix}^T , \tag{5.17}$$

and $\hat{U}_{fb}$ is the time evolution operator associated with feedback and a time-

independent Hamiltonian $\hat{H}_0$:

$$\hat{U}_{fb}(z_2, z_1) = \exp\left(-\frac{i}{\hbar}\left(\hat{H}_0(z_2 - z_1) + \sum_j \int_{z_1}^{z_2} dz \alpha_j(z, \boldsymbol{y})\hat{O}_i\right)\right). \tag{5.18}$$

α is the time-dependent feedback force applied on the degree of freedom associated with $\hat{O}_i$. Note that since we've allowed the αs to depend on the entire measurement record $\boldsymbol{y}$, we haven't restricted the feedback scheme to be causal (we will do so in Sec. 5.2.3).

Once the initial state $|\psi(t_0)\rangle$ is fixed, we will show that Eq. (5.16) can match any evolution under the non-linear Hamiltonian (5.3). Let's assume that till time t, a feedback scheme successfully matches the non-linear evolution under Eq. (5.14). We will show that this feedback scheme can continue to match the non-linear evolution until time z, which we assume is when the next measurement occurs. Under NLQM,

$$\left|\psi_{NLQM}(z)\right\rangle \propto \hat{P}(z) \exp\left(-\frac{i}{\hbar}\left(\hat{H}_L(z - t) + \sum_j \int_t^z dl \phi\left(x_j, l, \tilde{\psi}(l), \boldsymbol{y}\right)\hat{V}_i\right)\right)|\psi(t)\rangle \tag{5.19}$$

where $\hat{P}(z)$ is the projection operator associated with the measurement at time z. $\tilde{\psi}(l)$ for $t \leq l \leq z$ is the solution of Eq. (5.2) with the boundary condition

$$\left|\tilde{\psi}(t)\right\rangle = |\varphi\rangle, \tag{5.20}$$

where the boundary state$|\varphi\rangle$ depends on the interpretation of quantum mechanics that one uses[1]. Moreover, it might seem odd that we've associated a unitary evolution operator to the non-linear Hamiltonian (5.3) but, as discussed in Sec. 5.2.1, once we solve for $\tilde{\psi}(t)$, we can think of $\hat{H}_{NLQM}$ as a time-dependent Hamiltonian.

Under linear quantum mechanics and feedback, the state at time z is

$$\left|\psi_{fb}(z)\right\rangle \propto \hat{P}(z)\hat{U}_{fb}(z_2, z_1)|\psi(t)\rangle. \tag{5.21}$$

If we choose $\hat{H}_0$ to be $\hat{H}_L$, the $\hat{O}_i$ to be the $\hat{V}_i$ and the α_js to be equal to the ϕ_j then

$$\left|\psi_{fb}(z)\right\rangle = \left|\psi_{NLQM}(z)\right\rangle. \tag{5.22}$$

[1]It might seem surprising that the boundary state is not $|\psi(t)\rangle$ but we remind the user that this is a feature of NLQM: different interpretations of quantum mechanics lead to different predictions in NLQM [4].

The first two conditions can be easily met. To meet to third condition, we have to first solve for $\tilde{\psi}(l)$ for $t \leq l \leq z$, which will allow us to calculate the classical field ϕ by using Eq. (5.4). The feedback force is then crafted to be the same as ϕ.

We've shown that once we fix the initial state, a monitored system evolving under NLQM indistinguishable from a monitored system evolving under a linear Hamiltonian and feedback. Moreover, even if we don't know the initial state, evolution under quantum feedback could asympotactically approach the non-linear quantum evolution because a monitored system tends to eventually be driven by measurements, and forgets its initial state.

5.2.3 Causal NLQM

It is widely believed that adding measurements to NLQM breaks causality. We will exploit the equivalence between NLQM and quantum feedback to show that we can incorporate measurements in NLQM in a causal way.

Feedback is causal if the applied force at time t and location x depends only on the measurement results an experimentalist can collect. These are the results of measurement events in the past light cone of (t, x). Therefore, for NLQM to be causal, the classical field $\phi(x, t)$ that appears in Eq. (5.3) can only depend on the y_i collected in the past light cone of (t, x).

To allow only measurements in the past light cone of (x, t), we rewrite Eq. (5.4) to

$$\mathcal{L}\phi(x, t) = S(x, t, \lambda(t, x)) \tag{5.23}$$

where $|\lambda(t, x)\rangle$ is a modified $|\psi\rangle$, given by Eq. (5.14), that only incorporates measurements in the past light cone. If the n measurements occur at locations z_1 through z_n then

$$|\lambda(t, x)\rangle \propto \hat{U}_{\rightarrow}(t, t_n)\,\hat{\mathcal{P}}_{(t,x)}(t_n, z_n)\ldots\hat{\mathcal{P}}_{(t,x)}(t_2, z_2)\,\hat{U}_{\rightarrow}(t_2, t_1)\,\hat{\mathcal{P}}_{(t,x)}(t_1, z_1)\,\hat{U}_{\rightarrow}(t_1, t_0)\,|\psi(t_0)\rangle \tag{5.24}$$

where $\hat{\mathcal{P}}_{(t,x)}(t', z)$ is $\hat{P}(t', z)$ if (t, x) lies in (t', z)'s future light cone, and the identity operator otherwise:

$$\hat{\mathcal{P}}_{(t,x)}(t', z) = \begin{cases} \hat{P}(t', z) & t - t' - \frac{|z-x|}{c} \geq 0 \\ \hat{I} & \text{otherwise} \end{cases} \tag{5.25}$$

where $\hat{P}(t', z)$ denotes a projection at time t' and location z. Moreover, $\hat{U}_{\rightarrow}(t_2, t_1)$ denotes evolution under Eq. (5.2) from time t_1 till t_2. The $\rightarrow$ denotes that the

boundary state is chosen to be the state that $\hat{U}_{\rightarrow}(t_2, t_1)$ acts on. For example, in $\hat{U}_{\rightarrow}(t_2, t_1)|\varphi\rangle$, the boundary state is chosen to be φ. We will call this prescription *causal-conditional*.

5.2.3.1 An example

We revisit the example setup in Sec. 5.2.1.1, but now extend it to two parties: Alice and Bob, as is shown in Fig. 5.1. We'll assume that Alice and Bob are localized at positions x_A and x_B. We will illustrate what happens when Alice measures her spin at time t_1. The associated measurement event is M_A.

For both NLQM and feedback, let's assume that they both have the same linear part of the Hamiltonian

$$\hat{H}_L \equiv \hat{H}_A + \hat{H}_B. \tag{5.26}$$

According to the causal-conditional prescription, the non-linear Hamiltonian is

$$\hat{V}_{NL}^{(A)}(\lambda_A, t) = \hbar\omega_A \left\langle \lambda_A(t) \middle| \hat{\sigma}_z^{(B)} \middle| \lambda_A(t) \right\rangle \hat{\sigma}_x^{(A)}, \tag{5.27}$$

$$\hat{V}_{NL}^{(B)}(\lambda_B, t) = \hbar\omega_B \left\langle \lambda_B(t) \middle| \hat{\sigma}_z^{(B)} \middle| \lambda_B(t) \right\rangle \hat{\sigma}_x^{(B)} \tag{5.28}$$

where $\lambda_{A/B}(t)$ incorporates all measurements in the past light cone of $\left(t, x_{A/B}\right)$. We can think of $|\lambda_A(t)\rangle$ ($|\lambda_B(t)\rangle$) as the joint Alice-Bob quantum state as perceived by Alice (Bob) with all the information she (he) could have gathered at time t.

In our simple example, only one measurement occurred at (t_1, x_A). Therefore, only two λs are sufficient to completely describe $\hat{V}_{NL}^{(A)}$ and $\hat{V}_{NL}^{(B)}$. The first, which we call $|\lambda_0(t)\rangle$, is the solution of

$$i\hbar\partial_t |\psi(t)\rangle = \left(\hat{H}_L + \hat{V}_{NL}^{(A)}(\psi(t), t) + \hat{V}_{NL}^{(B)}(\psi(t), t)\right)|\psi(t)\rangle \tag{5.29}$$

with the initial condition

$$|\psi(t_0)\rangle = |\psi_{ini}\rangle. \tag{5.30}$$

$|\psi_{ini}\rangle$ is the initial state of Alice and Bob's spins. The second, which we call $|\lambda_1(t)\rangle$, is the solution of Eq. (5.29) under the initial condition

$$|\psi(t_1)\rangle = \frac{\hat{P}_\alpha^{(A)}|\lambda_0(t_1)\rangle}{\left\langle \lambda_0(t_1) \middle| \hat{P}_\alpha^{(A)} \middle| \lambda_0(t_1) \right\rangle} \tag{5.31}$$

where $\hat{P}_\alpha^{(A)}$ is the projection operator associated with Alice's measurement, which

we assume has a measurement result of α.

We can now write down the non-linear potential as a function of time only:

$$\hat{V}_{NL}^{(A)}(t) = \begin{cases} \hbar\omega_A \left\langle \lambda_0(t) \middle| \hat{\sigma}_z^{(A)} \middle| \lambda_0(t) \right\rangle \hat{\sigma}_x^{(A)} & t_0 \le t \le t_1 \\ \hbar\omega_A \left\langle \lambda_1(t) \middle| \hat{\sigma}_z^{(A)} \middle| \lambda_1(t) \right\rangle \hat{\sigma}_x^{(A)} & t > t_1 \end{cases}, \tag{5.32}$$

$$\hat{V}_{NL}^{(B)}(t) = \begin{cases} \hbar\omega_B \left\langle \lambda_0(t) \middle| \hat{\sigma}_z^{(B)} \middle| \lambda_0(t) \right\rangle \hat{\sigma}_x^{(B)} & t_0 \le t \le t_1 + \frac{|x_B - x_A|}{c} \\ \hbar\omega_B \left\langle \lambda_1(t) \middle| \hat{\sigma}_z^{(B)} \middle| \lambda_1(t) \right\rangle \hat{\sigma}_x^{(B)} & t > t_1 + \frac{|x_B - x_A|}{c} \end{cases}. \tag{5.33}$$

Stated in this way, we can now think of the total Hamiltonian

$$\sum_{i=A,B} \left(E\hat{\sigma}_z^{(i)} + \hat{V}_{NL}^{(i)}(t) \right) \tag{5.34}$$

as a linear time-dependent Hamiltonian. Since it is separable, we can assign an evolution operator for each of Alice and Bob's spins:

$$\hat{U}_i(t, t') \quad i = A, B \tag{5.35}$$

and the unnormalized quantum state at time $t > t_1 + |x_B - x_A|/c$ is

$$|\psi(t)\rangle \propto \hat{U}_B(t, t_1)\, \hat{U}_A(t, t_1)\, \hat{P}_\alpha^{(A)} \hat{U}_B(t_1, t_0)\, \hat{U}_A(t_1, t_0)\, |\psi_{ini}\rangle . \tag{5.36}$$

Alice and Bob can forge their own feedback schemes that would produce a wave-function evolution that is identical to $|\psi(t)\rangle$. In particular, they'd base their feedback strategy on two options: Alice (Bob) can apply a feedback force on $\hat{\sigma}_x^{(A)}$ ($\hat{\sigma}_x^{(B)}$) that is equal to either $\hbar\omega_A \left\langle \lambda_0(t) \middle| \hat{\sigma}_z^{(A)} \middle| \lambda_0(t) \right\rangle$ ($\hbar\omega_B \left\langle \lambda_0(t) \middle| \hat{\sigma}_z^{(B)} \middle| \lambda_0(t) \right\rangle$) or $\hbar\omega_A \left\langle \lambda_1(t) \middle| \hat{\sigma}_z^{(A)} \middle| \lambda_1(t) \right\rangle$ ($\hbar\omega_B \left\langle \lambda_1(t) \middle| \hat{\sigma}_z^{(B)} \middle| \lambda_1(t) \right\rangle$). The two feedback strategies would have the following two feedback potentials associated with them

$$\hat{V}_{fb,0}^{(A/B)} = \hbar\omega_{A/B} \left\langle \lambda_0(t) \middle| \hat{\sigma}_z^{(A/B)} \middle| \lambda_0(t) \right\rangle \hat{\sigma}_x^{(A/B)}, \tag{5.37}$$

$$\hat{V}_{fb,1}^{(A/B)} = \hbar\omega_{A/B} \left\langle \lambda_1(t) \middle| \hat{\sigma}_z^{(A/B)} \middle| \lambda_1(t) \right\rangle \hat{\sigma}_x^{(A/B)}. \tag{5.38}$$

Alice and Bob would alternate between the two feedback strategies in such a way that they'd reproduce $\hat{V}_{NL}^{(A)}(t)$ and $\hat{V}_{NL}^{(B)}(t)$.

To calculate $\left\langle \lambda_0(t) \middle| \hat{\sigma}_z^{(A/B)} \middle| \lambda_0(t) \right\rangle$ and $\left\langle \lambda_1(t) \middle| \hat{\sigma}_z^{(A/B)} \middle| \lambda_1(t) \right\rangle$, Alice and Bob would first solve Eq. (5.29) for $|\lambda_0(t)\rangle$. Once they do so, they will apply $\hat{V}_{fb,0}^{(A)}$ and $\hat{V}_{fb,0}^{(B)}$

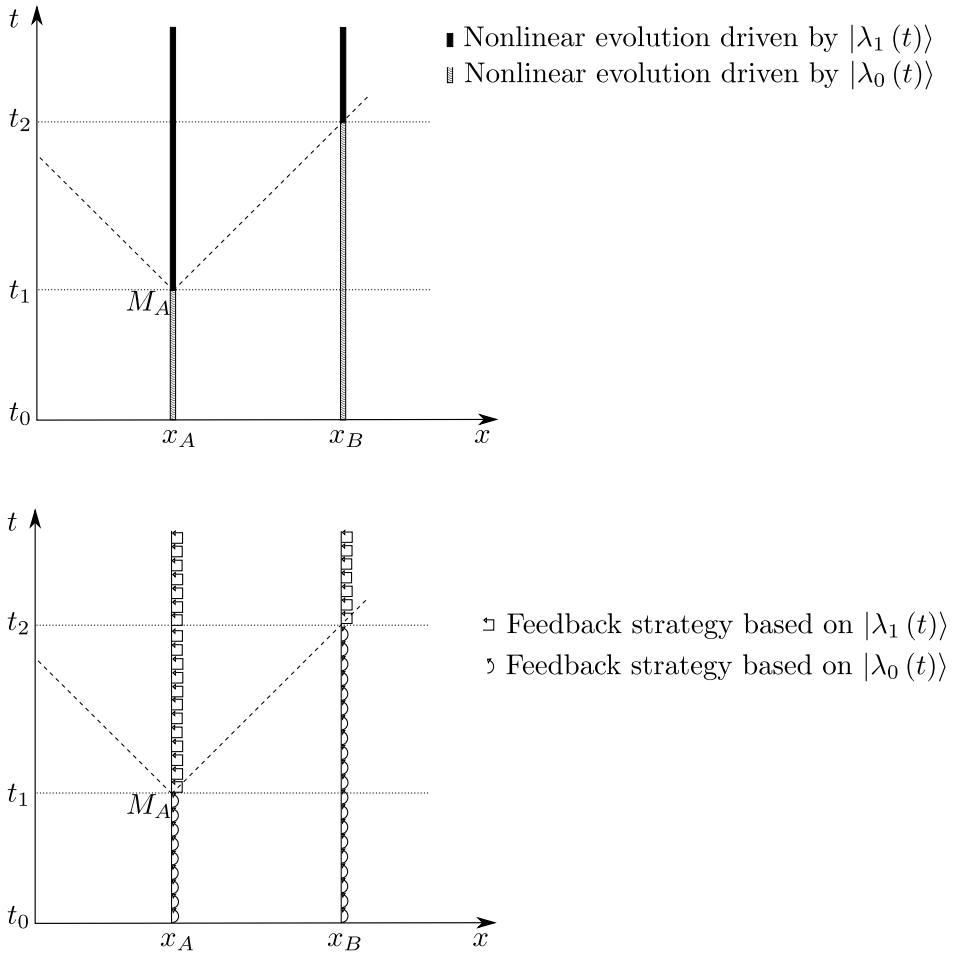

Figure 5.1: Showing how causal NLQM and causal feedback are equivalent in a simple example. At time t_1, Alice performs a measurement. The corresponding measurement event is denoted byM_A. The result of the measurement is broadcast along M_A's future light cone. It reaches Bob at time $t_2 = t_1 + |x_B - x_A|/c$. In the NLQM picture, at time t_2, the classical field at x_B suddenly changes to incorporate information about Alice's measurement result. In the quantum feedback picture, Bob switches his feedback strategy at t_2 to incorporate information about Alice's measurement result. $|\lambda_1(t)\rangle$ and $|\lambda_0(t)\rangle$ are obtained from solving a non-linear Schroedinger equation with initial conditions given by (5.30) and (5.31), respectively.

till time t_1. Once Alice obtains her measurement result, she would solve Eq. (5.29) to obtain $|\lambda_1(t)\rangle$ and switch her feedback potential from $\hat{V}^{(A)}_{fb,0}$ to $\hat{V}^{(A)}_{fb,1}$. Alice would also share her measurement result with Bob, who would receive the result at time $t_1 + |x_B - x_A|/c$, at which point he would change his feedback scheme from $\hat{V}^{(B)}_{fb,0}$ to $\hat{V}^{(B)}_{fb,1}$.

5.3 An example of continuously monitored optomechanical systems

We will provide a concrete example of how the causal-conditional prescription is equivalent to causal feedback.

5.3.1 Setup

We will consider two parties, Alice and Bob, that are separated by a distance Δx_{AB} and that respectively monitor an optomechanical setup that is non-linearly coupled to a classical field. We will show that the evolution equation governing their setups is exactly identical to a particular feedback scheme that Alice and Bob could implement. Therefore, although their setups evolve non-linearly, Alice and Bob cannot communicate with each other superluminally.

Each of Alice and Bob's setups, shown in Fig. 5.2, evolves under the following Hamiltonian

$$\hat{H}^{(i)} = \hat{H}_L^{(i)} + \hat{V}_\phi^{(i)}(t), \tag{5.39}$$

where $i = A, B$ and $\hat{H}_L^{(i)}$ is the linear part of the Hamiltonian

$$\hat{H}_L^{(i)} = \hat{H}_{tm}^{(i)} + \hat{H}_{probe}^{(i)} + \hat{V}_I^{(i)}. \tag{5.40}$$

$\hat{H}_{tm}^{(i)}$ is the test mass' free Hamiltonian:

$$\hat{H}_{tm}^{(i)} = \frac{\hat{P}_i^2}{2m} + \frac{1}{2}m\omega^2\hat{x}_i^2, \tag{5.41}$$

and $\hat{H}_{probe}^{(i)}$ is the driving light's free Hamiltonian:

$$\hat{H}_{probe}^{(i)} \approx \int_{-\infty}^{\infty} \frac{d\omega}{2\pi}\hbar\omega\hat{a}_i^\dagger(\omega_0+\omega)\,\hat{a}_i(\omega_0+\omega). \tag{5.42}$$

Note that we are working with the 2-photon formalism and the driving optical fields' frequency is ω_0. $\hat{V}_I^{(i)}$ is the linearized interaction Hamiltonian of light with the test mass:

$$\hat{V}_I^{(i)} = -\hbar\alpha\hat{x}_i\hat{a}_{i,1}(x_i), \tag{5.43}$$

where x_A (x_B) is the center of mass location of Alice's (Bob's) test mass (quantum fluctuations negligibly perturb x_A and x_B), and

$$\alpha = 8I_{in}\frac{\hbar\omega_0}{c^2}, \tag{5.44}$$

where I_{in} is the driving laser's intensity.

It will be convenient to enter into an interaction picture with $\hat{H}^{(A)}_{probe}+\hat{H}^{(B)}_{probe}$ removed. $\hat{H}^{(A)}_{probe}+\hat{H}^{(B)}_{probe}$ just propagate the optical fields forward. $\hat{V}_I$ becomes

$$\hat{V}_I(i)(t) = -\hbar\alpha\hat{x}\hat{a}_{i,1}(x_i - t/c) \qquad i = A, B \tag{5.45}$$

where $\hat{a}_{i,1}(x_i - t/c)$ is the incoming optical degree of freedom at location $x_i - t/c$.

We'll assume that the non-linear interaction is given by

$$\hat{V}^{(i)}_{\phi} = \hbar\phi(x_i, t)\,\hat{x}_i \tag{5.46}$$

where ϕ obeys the field equation

$$\mathcal{L}\phi(x,t) = \kappa_A \langle\lambda(t,x)|\hat{x}_A|\lambda(t,x)\rangle\,\delta(x - x_A) + \kappa_B \langle\lambda(t,x)|\hat{x}_B|\lambda(t,x)\rangle\,\delta(x - x_B) \tag{5.47}$$

where $|\lambda(t,x)\rangle$ is $|\psi(t)\rangle$ with all projection operators corresponding to measurement events at (t', z) replaced by $\hat{\mathcal{P}}_{(t,x)}(t', z)$ (see Eqs. (5.24-5.25)). For simplicity, we will assume that the differential operator $\mathcal{L}$'s Green's function is the retarded Green's function:

$$G_{\mathcal{L}}(x,t;x',t') = \delta\left(t - \left(t' + \frac{|x - x'|}{c}\right)\right) \tag{5.48}$$

so

$$\phi(x,t) = \sum_{i=A,B} \kappa_i \left\langle \lambda\left(t - \frac{|x - x_i|}{c}, x_i\right)\middle|\hat{x}_i\middle|\lambda\left(t - \frac{|x - x_i|}{c}, x_i\right)\right\rangle. \tag{5.49}$$

Substituting back into $\hat{V}^{(i)}_{\phi}$ for $i = A, B$, we obtain

$$\begin{aligned}\hat{V}^{(A)}_{\phi}/\hbar &= \kappa_A \langle\lambda(t,x_A)|\hat{x}_A|\lambda(t,x_A)\rangle\,\hat{x}_A \\ &\quad + \kappa_B \left\langle \lambda\left(t - \frac{\Delta x_{AB}}{c}, x_B\right)\middle|\hat{x}_B\middle|\lambda\left(t - \frac{\Delta x_{AB}}{c}, x_B\right)\right\rangle \hat{x}_A\end{aligned} \tag{5.50}$$

and

$$\begin{aligned}\hat{V}^{(B)}_{\phi}/\hbar &= \kappa_A \left\langle \lambda\left(t - \frac{\Delta x_{AB}}{c}, x_A\right)\middle|\hat{x}_A\middle|\lambda\left(t - \frac{\Delta x_{AB}}{c}, x_A\right)\right\rangle \hat{x}_B \\ &\quad + \kappa_B \langle\lambda(t,x)|\hat{x}_B|\lambda(t,x)\rangle\,\hat{x}_A.\end{aligned} \tag{5.51}$$

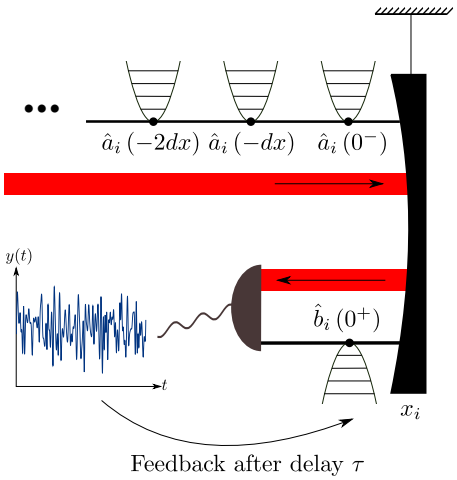

Figure 5.2: Alice and Bob's optomechanical setups. Note that $i = A, B$.

5.3.2 Stochastic Schroedinger Equation

Denote Alice and Bob test masses' center of mass joint quantum state at time t by $|\psi(t)\rangle$. We will obtain a differential equation for $|\psi(t)\rangle$ by following three steps. We first unitarily evolve $|\psi(t)\rangle$ under the linear part of the Hamiltonian $\hat{H}^{(A)} + \hat{H}^{(B)}$. Second, we evolve $|\psi(t)\rangle$ under the non-linear part of the Hamiltonian, $\hat{V}_\phi^{(A)} + \hat{V}_\phi^{(B)}$. Third, we project the outgoing light into eingenstates corresponding to Alice and Bob's measurement results at time t. Note that to leading order we are allowed to separate the first and second step.

We first unitarily evolve $|\psi(t)\rangle$ till time $t + dt$ under $\hat{H}^{(A)} + \hat{H}^{(B)}$. Denote the corresponding evolution operator by $\hat{U}_L$:

$$\hat{U}_L = e^{-i\left(\hat{H}_{tm}^{(A)} + \hat{H}_{tm}^{(B)}\right)dt/\hbar} \exp\left(i \sum_{j=A,B} \alpha_j \hat{x}_j \hat{a}_{j,1} \left(x_j - t/c\right) dt\right) + O\left(dt^2\right). \tag{5.52}$$

$\hat{U}_L$ will act on $|\psi(t)\rangle \otimes |0\rangle \otimes |0\rangle$ where $|0\rangle \otimes |0\rangle$ is the joint quantum state of the light driving Alice and Bob's test masses at time t. We've assumed the driving light to be in vacuum. Since $\exp\left(i \sum_{j=A,B} \alpha_j \hat{x}_j \hat{a}_{j,1} \left(x_j - t/c\right) dt\right)$ is a shift operator, it is convenient expand $|0\rangle \otimes |0\rangle$ into eigenstates of $\hat{a}_{A,2}$ and $\hat{a}_{B,2}$ and then shift them by $-\alpha_A \hat{x}_A dt$ and $-\alpha_B \hat{x}_B dt$, respectively. We obtain that

$$\hat{U}_L |\psi(t), 0, 0\rangle = \hat{U}_{tm} \int \frac{dq_A}{\pi^{1/4}} \frac{dq_B}{\pi^{1/4}} \exp\left(-\sum_{i=A,B} \left(q_i - \alpha_j \hat{x}_j dt\right)^2 /2\right) |\psi(t), q_A, q_B\rangle, \tag{5.53}$$

where $|\psi, l, k\rangle$ is a shorthand for $|\psi\rangle \otimes |l\rangle \otimes |k\rangle$, with $|l\rangle$ ($|k\rangle$) an eigenstate of $\hat{a}_{A,2}$

$(\hat{a}_{B,2})$, and

$$\hat{U}_{tm} \equiv e^{-i\left(\hat{H}_{tm}^{(A)}+\hat{H}_{tm}^{(B)}\right)dt/\hbar}. \tag{5.54}$$

We then evolve $\hat{U}_L \left|\psi\left(t\right),0,0\right\rangle$ under

$$\hat{U}_{NL} \equiv \exp\left(-i\sum_j \frac{\hat{V}_\phi^{(j)}}{\hbar}dt\right) \tag{5.55}$$

$$= \exp\left(-i\sum_{j,k=A,B}\kappa_j\left\langle\lambda\left(t-\frac{\left|x_k-x_j\right|}{c},x_j\right)\middle|\hat{x}_j\middle|\lambda\left(t-\frac{\left|x_k-x_j\right|}{c},x_j\right)\right\rangle\hat{x}_j dt\right) \tag{5.56}$$

and obtain that the fully evolved wavefunction is

$$\hat{U}\left|\psi\left(t\right),0,0\right\rangle = \hat{U}_{NL}\hat{U}_{tm}\int\frac{dq_A}{\pi^{1/4}}\frac{dq_B}{\pi^{1/4}}\exp\left(-\sum_{i=A,B}\left(q_i-\alpha_j\hat{x}_j dt\right)^2/2\right)\left|\psi\left(t\right),q_A,q_B\right\rangle. \tag{5.57}$$

Finally, we apply the projection operators corresponding to Alice and Bob's measurements of the phase quadrature of the outgoing light. Denote these operators by

$$\hat{P}_j\left(t,x_j\right) \equiv \delta\left(\hat{a}_{j,2}\left(x_j-t/c\right)-y_j\left(t\right)\right) \tag{5.58}$$

where $j = A,B$ and $y_A\left(t\right)$ $(y_B\left(t\right))$ is Alice's (Bob's) measurement result at time t. Applying $\hat{P}_A\left(t,x_A\right)\hat{P}_B\left(t,x_B\right)$ on the LHS of Eq. (5.57), we obtain that

$$\left|\psi\left(t+dt\right)\right\rangle \propto \hat{U}_{NL}\hat{U}_{tm}\exp\left(-\sum_{i=A,B}\left(y_i\left(t\right)-\alpha_j\hat{x}_j dt\right)^2/2\right)\left|\psi\left(t\right)\right\rangle. \tag{5.59}$$

$y_A\left(t\right)$ and $y_B\left(t\right)$ follow a stochastic evolution which we can quantify by noting that in the Heisenberg picture,

$$\hat{b}_{i,2}\left(t\right) = \alpha_i\hat{x}_i\left(t\right)+\hat{a}_2\left(t\right), \qquad i = A,B \tag{5.60}$$

so $y_A\left(t\right)$ and $y_B\left(t\right)$ are the Gaussian random processes

$$y_i\left(t\right) = \alpha_i\left\langle\hat{x}_i\right\rangle\left(t\right)+\frac{dW_i\left(t\right)}{\sqrt{2}dt}, \tag{5.61}$$

$$dy_i\left(t\right) = \alpha_i\left\langle\hat{x}_i\right\rangle\left(t\right)dt+\frac{dW_i\left(t\right)}{\sqrt{2}} \tag{5.62}$$

where $i = A,B$ and the dW_i are Wiener increments.

To get a Stochastic Schroedinger equation, we will have to expand all the exponentials in Eq. (5.59) to order dt. We obtain

$$\begin{aligned}
&d\left|\psi\left(t\right)\right\rangle \\
&= -i\sum_{j=A,B}\frac{\hat{H}_{tm}^{(j)}}{\hbar}\left|\psi\left(t\right)\right\rangle dt + \sum_{j=A,B}\frac{\alpha_j^2}{2}\left(\hat{x}_j - \left\langle\hat{x}_j\right\rangle\left(t\right)\right)^2\left|\psi\left(t\right)\right\rangle dt - \\
&\sum_{j=A,B}\alpha_j\left(\hat{x}_j - \left\langle\hat{x}_j\right\rangle\left(t\right)\right)\left|\psi\left(t\right)\right\rangle\frac{dW_j\left(t\right)}{\sqrt{2}} - i\times \\
&\sum_{j,k=A,B}\kappa_j\left\langle\lambda\left(t-\frac{\left|x_k-x_j\right|}{c},x_j\right)\middle|\hat{x}_j\middle|\lambda\left(t-\frac{\left|x_k-x_j\right|}{c},x_j\right)\right\rangle\hat{x}_j\left|\psi\left(t\right)\right\rangle dt
\end{aligned} \tag{5.63}$$

where we've substituted Eq. (5.61) into Eq. (5.59), Taylor-expanded the exponentials to leading order in dt, and we've used that $dW_i^2 = dt$ for $i = A, B$. $\left|\lambda\left(t,x\right)\right\rangle$ can be interpreted as the estimate of an observer at (t,x) of $\left|\psi\left(t\right)\right\rangle$, given that the observer has access to the entire measurement record in the past light cone of (t,x).

We can also obtain a stochastic Schroedinger equation for $\left|\lambda\left(t,x_A\right)\right\rangle$ and $\left|\lambda\left(t,x_B\right)\right\rangle$. Consider $\left|\lambda\left(t,x_A\right)\right\rangle$, it only incorporates measurements in the past light cone of (t,x_A). This means that after $t - \Delta x_{AB}/c$ we no longer assume that Bob's test mass is monitored, it just follows its own free evolution. It also means as we change t, $\left|\lambda\left(t,x_A\right)\right\rangle$ for instance, follows a different stochastic Schroedinger equation, because with each time increment dt, we receive information about Bob's measurement results in the past at time $t + dt - \Delta x_{AB}/c$. Let $\left|\lambda_z\left(t,x\right)\right\rangle$ represent a quantum trajectory that at time $z = t$ equals $\left|\lambda\left(t,x\right)\right\rangle$. $\left|\lambda_z\left(t,x_A\right)\right\rangle$ follows the stochastic Schroedinger equation

$$\begin{aligned}
&d\left|\lambda_z\left(t,x_A\right)\right\rangle \\
&= -i\sum_{j=A,B}\frac{\hat{H}_{tm}^{(j)}}{\hbar}\left|\lambda_z\left(t,x_A\right)\right\rangle dt + \frac{\alpha_A^2}{2}\left(\hat{x}_A - \left\langle\hat{x}_A\right\rangle_\lambda\left(z\right)\right)^2\left|\lambda_z\left(t,x_A\right)\right\rangle dt \\
&+\frac{\alpha_B^2}{2}\left(\hat{x}_B - \left\langle\hat{x}_B\right\rangle_\lambda\left(z\right)\right)^2\tilde{\theta}_{(t,x_A)}\left(z,x_B\right)\left|\lambda_z\left(t,x_A\right)\right\rangle dt \\
&-\alpha_A\left(\hat{x}_A - \left\langle\hat{x}_A\right\rangle_\lambda\left(z\right)\right)\left|\lambda_z\left(t,x_A\right)\right\rangle\frac{dW_A\left(z\right)}{\sqrt{2}} \\
&-\alpha_B\left(\hat{x}_B - \left\langle\hat{x}_B\right\rangle_\lambda\left(z\right)\right)\tilde{\theta}_{(t,x_A)}\left(z,x_B\right)\left|\lambda_z\left(t,x_A\right)\right\rangle\frac{dW_B\left(z\right)}{\sqrt{2}} \\
&-i\sum_{j,k=A,B}\kappa_j\left\langle\lambda\left(t-\frac{\left|x_k-x_j\right|}{c},x_j\right)\middle|\hat{x}_j\middle|\lambda_z\left(t-\frac{\left|x_k-x_j\right|}{c},x_j\right)\right\rangle\hat{x}_j\left|\lambda_z\left(t,x_A\right)\right\rangle dt
\end{aligned} \tag{5.64}$$

where $\langle \quad \rangle_\lambda(z)$ is to remind the reader that an expectation value is taken over $\lambda_z(t, x_A)$ at time z, and $\tilde{\theta}_{(t,x)}(t', y)$ is non-zero only if (t', y) is in the past light cone of (t, x):

$$\tilde{\theta}_{(t,x)}(t', y) = \begin{cases} 1 & t - t' - \frac{|y-x|}{c} \geq 0 \\ 0 & \text{otherwise} \end{cases}. \tag{5.65}$$

A similar expression exists for $|\lambda_z(t, x_B)\rangle$.

A concise way to represent Eq. (5.64) is

$$d|\lambda_z(t, x_A)\rangle = \begin{cases} (-i\mathcal{H}(z) + \mathcal{L}(z))|\lambda_z(t, x_A)\rangle & z \leq t - \Delta x_{AB}/c \\ (-i\mathcal{H}(z) + \mathcal{L}_A(z))|\lambda_z(t, x_A)\rangle & z > t - \Delta x_{AB}/c \end{cases} \tag{5.66}$$

$\mathcal{H}$ is a unitary differential operator, $\mathcal{L}$ is a differential operator that incorporates both Alice and Bob's measurements and $\mathcal{L}_A$ incorporates just Alice's measurements. In particular,

$$\begin{aligned} \mathcal{H}(z) &= \left(\sum_{j=A,B} \frac{\hat{H}^{(j)}_{tm}}{\hbar} + \sum_{j,k=A,B} \kappa_j \left\langle \lambda_z\left(t - \frac{|x_k - x_j|}{c}, x_j\right) \middle| \hat{x}_j \middle| \lambda_z\left(t - \frac{|x_k - x_j|}{c}, x_j\right) \right\rangle \hat{x}_j \right) dt \\ \mathcal{L}(z) &= \mathcal{L}_A(z) + \mathcal{L}_B(z) \qquad (5.67) \\ \mathcal{L}_i(z) &= \frac{\alpha_i^2}{2}(\hat{x}_i - \langle \hat{x}_i \rangle(z))^2 dt - \alpha_i(\hat{x}_i - \langle \hat{x}_i \rangle_\lambda(z)) \frac{dW_i(z)}{\sqrt{2}} \quad i = A, B. \qquad (5.68) \end{aligned}$$

We can then calculate that for any Hermitian operator $\hat{O}$ that (for example)

$$d\langle \hat{O} \rangle_\lambda = i\langle [\mathcal{H}, \hat{O}] \rangle_\lambda + \langle \{\hat{O}, \tilde{\mathcal{L}}\} \rangle_\lambda + \langle \tilde{\mathcal{W}} \hat{O} \tilde{\mathcal{W}} \rangle_\lambda \tag{5.69}$$

where the expectation value is with respect to for example $|\lambda_z(t, x_A)\rangle$, and

$$\tilde{\mathcal{L}} = \begin{cases} \mathcal{L} & z \leq t - \Delta x_{AB}/c \\ \mathcal{L}_A & z > t - \Delta x_{AB}/c \end{cases}. \tag{5.70}$$

Moreover,

$$\begin{aligned} \tilde{\mathcal{W}} &= \begin{cases} \mathcal{W}_A + \mathcal{W}_B & z \leq t - \Delta x_{AB}/c \\ \mathcal{W}_A & z > t - \Delta x_{AB}/c \end{cases} \qquad (5.71) \\ \mathcal{W}_i &= -\alpha_i(\hat{x}_i - \langle \hat{x}_i \rangle_\lambda) \quad i = A, B. \qquad (5.72) \end{aligned}$$

5.3.2.1 Analogy to feedback

We will show that the Stochastic Schroedinger equation (5.63) is indistinguishable from evolution under a linear Hamiltonian and feedback. Tracking the evolution of $|\psi(t)\rangle$ doesn't tell us if Alice and Bob's test masses are evolving under a non-linear quantum-mechanical theory, or if Alice and Bob are applying feedback forces on their test masses. The last term in Eq. (5.63) can be interpreted as a feedback force. Alice (Bob) can calculate $|\lambda(t, x_A)\rangle$ and $|\lambda(t - \Delta x_{AB}/c, x_B)\rangle$ ($|\lambda(t, x_B)\rangle$ and $|\lambda(t - \Delta x_{AB}/c, x_A)\rangle$) and then craft a feedback scheme that would mimic Eq. (5.50) (Eq. (5.51)).

5.4 Signature of SN with the causal-conditional prescription

In this section, we calculate the signature of the Schroedinger-Newton theory in a torsion pendulum experiment. As derived in Ref. [8], when an object has its center of mass' displacement fluctuations much smaller than fluctuations of the internal motions of its constituent atoms, then its center of mass, has the following non-linear Hamiltonian

$$\hat{H}_{cm} = \frac{\hat{p}^2}{2M} + \frac{1}{2}M\omega_{cm}^2\hat{x}^2 + \frac{1}{2}M\omega_{SN}^2(\hat{x} - \langle\hat{x}\rangle)^2 \tag{5.73}$$

where M is the test mass' mass, ω_{cm} is the center of mass' resonant frequency and ω_{SN} is a frequency scale that is determined by the matter distribution of the object. For materials with single atoms sitting close to lattice sites, we have

$$\omega_{SN} = \sqrt{\frac{Gm}{6\sqrt{\pi}\Delta x_{zp}^3}} \tag{5.74}$$

where m is the mass of the atom, and $\Delta x_{zp}$is the standard deviation of the crystal's constituent atoms' displacement from their equilibrium position along each spatial direction due to quantum fluctuations [5]. We will show if the phase quadrature of the outgoing light is measured, then the Schroedinger-Newton theory will predict a deviation from the predictions of standard quantum mechanics in the fluctuations of measured observable at the frequency

$$\omega_q \equiv \sqrt{\omega_{cm}^2 + \omega_{SN}^2}. \tag{5.75}$$

Hereafter, with the analogy of NLQM to quantum feedback established in subsequent sections, we will treat the total system-environment Hamiltonian as a quantum feedback (linear) Hamiltonian. Consequently, we can present the torsion pendulum's

(unconditional) equations of motion in the Heisenberg picture:

$$\partial_t \hat{x} = \frac{\hat{p}}{M}, \tag{5.76}$$

$$\partial_t \hat{p} = -M\omega_{cm}^2 \hat{x} - \gamma_m \hat{p} - M\omega_{SN}^2 \left(\hat{x} - \langle \hat{x} \rangle\right) + \alpha \hat{a}_1 + \hat{f}_{zp} + f_{cl}, \tag{5.77}$$

$$\hat{b}_1 = \hat{a}_1, \tag{5.78}$$

$$\hat{b}_2 = \hat{a}_2 + \frac{\alpha}{\hbar}\hat{x}, \tag{5.79}$$

where α is defined in Eq. (5.44), $\hat{a}_{1,2}$ are the perturbed incoming quadrature light fields around a large steady state, and similarly $\hat{b}_{1,2}$ are the perturbed outgoing light field quadratures (refer to section 2 of [1] for details). $f_{cl}(t)$ is the classical thermal bath fluctuation force. In a single realization of the experiment, it is a deterministic force but its correlation function has an ensemble average of (in the high-temperature limit)

$$\overline{f_{cl}(t) f_{cl}(t')} = 2m\gamma_m k_B T \delta(t - t') \tag{5.80}$$

where T is the thermal bath's equilibrium temperature, and $\gamma_m = \omega_{cm}/Q$ is the oscillator's damping rate and Q is the test mass' quality factor. $\hat{f}_{zp}(t)$ is the quantum thermal bath's fluctuation force originating from the zero-point fluctuations of the bath's modes. are given by Since the torsion pendulum is strongly driven by the driving light, the quantum fluctuations of $\alpha\hat{a}_1$ dominate over $\hat{f}_{zp}$ and $\hat{f}_{zp}$ will be ignored for the rest of this section.

From Eq. (7.43), it is clear that $\hat{x}(t)$ has a non-zero expectation value. We remove this expectation value by linearizing the system. We replace any operator $\hat{o}(t)$ with its expected value and a small perturbed part (note that we use the same $\hat{o}$ to denote its perturbed part):

$$\hat{o}(t) \longrightarrow \langle \hat{o}(t) \rangle + \hat{o}(t). \tag{5.81}$$

By using Eqs. (7.43-5.77) and that $\langle \hat{a}_1 \rangle = \left\langle \hat{f}_{zp} \right\rangle = 0$, we determine that

$$M\left(\partial_t^2 + \gamma_m + \omega_{cm}^2\right) \langle \hat{x}(t) \rangle = f_{cl}(t) \tag{5.82}$$

which can be Fourier transformed to determine that

$$\langle \hat{x}(\omega) \rangle = G_{cm}(\omega) f_{cl}(\omega) \tag{5.83}$$

where $G_{cm}(\omega)$ is the classical response function of $\hat{x}$ to external forces

$$G_{cm}(\omega) \equiv M^{-1}\left(\omega_{cm}^2 - \omega^2 - i\omega\gamma_m\right)^{-1}. \tag{5.84}$$

Therefore, in the time-domain,

$$\hat{x}(t) \rightarrow \int_{-\infty}^{t} G_{cm}(t-z)\, f_{cl}(z)\, dz + \hat{x}(t), \tag{5.85}$$

$$\hat{b}_2(t) \rightarrow \frac{\alpha}{\hbar}\int_{-\infty}^{t} G_{cm}(t-z)\, f_{cl}(z)\, dz + \hat{b}_2(t). \tag{5.86}$$

We then move to the Fourier domain for the linearized center of mass position operator

$$\hat{x}(\omega) = G_q(\omega)\left(\alpha\hat{a}_1(\omega) + \hat{f}_{fb}(\omega)\right) \tag{5.87}$$

where $G_q(\omega)$ is the response function of $\hat{x}$ to external forces

$$G_q(\omega) \equiv M^{-1}\left(\omega_q^2 - \omega^2 - i\omega\gamma_m\right)^{-1}, \tag{5.88}$$

and, in anticipation to the analogy to feedback, we've defined (in the Fourier domain)

$$\hat{f}_{fb}(\omega) \equiv C(\omega)\,\hat{b}_2(\omega) \tag{5.89}$$

where $C(\omega)$ is a complex function that needs to be chosen in such a way that

$$\left\langle \hat{f}_{fb}(\omega)\right\rangle = M\omega_{SN}^2\langle\hat{x}\rangle. \tag{5.90}$$

Furthermore, from Eq. (5.77), the non-linear force that we are mapping to the formalism of feedback, $M\omega_{SN}^2\langle\hat{x}\rangle$ appears as a c-number, whereas we've introduced it as an operator in Eq. (5.87). This is because when our system is monitored, $\langle\hat{x}\rangle$ is a conditional mean that depends on the measurement record. As a result, a feedback force that is proportional to $\langle\hat{x}(t)\rangle$ is promoted to a quantum operator in the Heisenberg picture because the measurement record is stochastic and some its randomness comes from the quantum fluctuations of the measured operator $\hat{b}_2$ given by Eq. (5.79). More details about feedback forces in the Heisenberg picture can be found in Chapter 5 of Ref. [7].

To obtain the conditional mean of $\hat{x}$, we will show that all we need to calculate is the projection of $\hat{x}(t)$ with no feedback, which we call $\hat{x}_0(t)$, onto the subspace spanned by the $\hat{b}_2(z)$ with no feedback, which we call $\hat{b}_2^{(0)}(z)$, for $z \leq t$. $\hat{x}_0$ and $\hat{b}_2^{(0)}$ are

$$\hat{x}_0(\omega) = G_q(\omega)\left(\alpha\hat{a}_1(\omega) + f_{cl}(\omega)\right), \tag{5.91}$$

$$\hat{b}_2^{(0)} = \hat{a}_2 + \frac{\alpha}{\hbar}\hat{x}_0 \tag{5.92}$$

so that

$$\hat{x}(\omega) = \hat{x}_0(\omega) + G_q(\omega)\hat{f}_{fb}(\omega), \tag{5.93}$$

$$\hat{b}_2(\omega) = \hat{b}_2^{(0)}(\omega) + \frac{\alpha}{\hbar}G_q(\omega)\hat{f}_{fb}(\omega). \tag{5.94}$$

As is shown in Ref. [6], causally projecting $\hat{x}_0$ onto $\hat{b}_2^{(0)}$ entails expressing $\hat{x}_0$ as

$$\hat{x}_0(\omega) = K(\omega)\hat{b}_2^{(0)}(\omega) + \hat{R}_0(\omega) \tag{5.95}$$

with $K(t)$ chosen in such a way that

$$\left\langle \hat{R}_0(t)\hat{b}_2^{(0)}(t') \right\rangle = 0 \tag{5.96}$$

for all $t' \leq t$. Eq. (5.96) guarantees that the inverse Fourier transform of $K(\omega)\hat{b}_2^{(0)}(\omega)$ is

$$\int_{-\infty}^{t} K(t-z)\hat{b}_2^{(0)}(z)\,dz. \tag{5.97}$$

Substituting Eq. (5.95) and Eq. (5.89) into Eq. (5.93), we obtain

$$\hat{x}(\omega) = K(\omega)\hat{b}_2^{(0)}(\omega) + G_q(\omega)C(\omega)\hat{b}_2(\omega) + \hat{R}_0(\omega). \tag{5.98}$$

Using Eq, (5.94) and Eq. (5.89), we can express $\hat{b}_2^{(0)}$ in terms of $\hat{b}_2$:

$$\hat{b}_2^{(0)}(\omega) = \left(1 - \frac{\alpha}{\hbar}G_q(\omega)C(\omega)\right)\hat{b}_2(\omega). \tag{5.99}$$

Substituting back into Eq. (5.98), we obtain

$$\begin{aligned}\hat{x}(\omega) &= \left(K(\omega)\left(1 - \frac{\alpha}{\hbar}G_q(\omega)C(\omega)\right) + G_q(\omega)C(\omega)\right)\hat{b}_2(\omega) + \hat{R}_0(\omega) \\ &\equiv \mathcal{X}(\omega)\hat{b}_2(\omega) + \hat{R}_0(\omega).\end{aligned} \tag{5.100}$$

Assuming that $\hat{b}_2$ and $\hat{b}_2^{(0)}$ are causally related, then Eq. (5.96) implies that

$$\left\langle \hat{R}_0(t)\hat{b}_2^{(0)}(t') \right\rangle = 0 \tag{5.101}$$

for all $t' \leq t$. As explained in Ref. [6], this entails that

$$\langle \hat{x}(t) \rangle = \int_{-\infty}^{t} \mathcal{X}(t-z)b_2(z)\,dz. \tag{5.102}$$

Therefore, using Eq. (5.90), we must have that

$$\frac{C(\omega)}{M\omega_{SN}^2} = \mathcal{X}(\omega) \tag{5.103}$$

which, using the definition of $\mathcal{X}(\omega)$, implies

$$C(\omega) = \left(\frac{1}{M\omega_{SN}^2} + \left(\frac{\alpha}{\hbar}K(\omega) - 1\right) G_q(\omega)\right)^{-1} K(\omega). \tag{5.104}$$

Note that we need to ensure that $C(t)$ contains no delta functions because causal feedback can only depend on the measurement result up to the time when the feedback is applied.

Substituting Eq. (5.104) into Eq. (5.94), and using Eq. (5.86), we determine that the unlinearized $\hat{b}_2$ is

$$\hat{b}_2(\omega) = \left(1 + \frac{\alpha K(\omega)/\hbar}{G_q^{-1}(\omega)/(M\omega_{SN}^2) - 1}\right) \hat{b}_2^{(0)}(\omega) + \frac{\alpha}{\hbar} G_{cm}(\omega) f_{cl}(\omega). \tag{5.105}$$

To calculate the spectrum of $\hat{b}_2$, we use that, as shown in Ref. [6], K is

$$K(\omega) = \sqrt{2}\frac{\hbar}{\alpha} i\sqrt{\Omega - \omega_q^2}\frac{\omega - \Omega_3}{(\omega - \Omega_1)(\omega - \Omega_2)} \tag{5.106}$$

where

$$\Omega \equiv \sqrt{\omega_q^4 + \frac{\alpha^4}{\hbar^2 m^2}}, \tag{5.107}$$

$$\Omega_{1,2} \equiv \left(\pm\sqrt{\Omega + \omega_q^2} - i\sqrt{\Omega - \omega_q^2}\right)/\sqrt{2}. \tag{5.108}$$

If $\omega_{SN} \gg \omega_{cm}$, $Q \gg 1$ and a weakly driven test mass

$$\omega_{SN} \gg \frac{\alpha}{\hbar m}, \tag{5.109}$$

we can show that $\hat{b}_2(\omega)$'s one-sided spectrum is around ω_q (after taking an ensemble average)

$$1 + \beta\Gamma^2 - \left(1 + 4\frac{(\omega - \omega_q)^2}{\Delta^2}\right)^{-1} \tag{5.110}$$

which is a dip of width

$$\Delta \equiv \frac{\alpha}{M\hbar\omega_q}, \tag{5.111}$$

and $\beta\Gamma^2$ is the thermal noise background around ω_q:

$$\beta \equiv \frac{\alpha^2}{M\hbar\gamma_m\omega_q}, \tag{5.112}$$

$$\Gamma^2 \equiv 2\frac{k_B T_0}{\hbar\omega_q}\frac{\gamma_m^2\omega_q^2}{\gamma_m^2\omega_q^2 + \omega_{SN}^4}. \tag{5.113}$$

Bibliography

[1] Yanbei Chen. Macroscopic quantum mechanics: theory and experimental concepts of optomechanics. *Journal of Physics B: Atomic, Molecular and Optical Physics*, 46(10):104001, 2013.

[2] C. C. Gan, C. M. Savage, and S. Z. Scully. Optomechanical tests of a schrödinger-newton equation for gravitational quantum mechanics. *Phys. Rev. D*, 93:124049, Jun 2016.

[3] André Großardt, James Bateman, Hendrik Ulbricht, and Angelo Bassi. Optomechanical test of the schrödinger-newton equation. *Phys. Rev. D*, 93:096003, May 2016.

[4] B. Helou and Y. Chen. Different interpretations of quantum mechanics make different predictions in non-linear quantum mechanics, and some do not violate the no-signaling condition. *ArXiv e-prints*, September 2017.

[5] Bassam Helou, Jun Luo, Hsien-Chi Yeh, Cheng-gang Shao, B. J. J. Slagmolen, David E. McClelland, and Yanbei Chen. Measurable signatures of quantum mechanics in a classical spacetime. *Phys. Rev. D*, 96:044008, Aug 2017.

[6] Helge Müller-Ebhardt, Henning Rehbein, Chao Li, Yasushi Mino, Kentaro Somiya, Roman Schnabel, Karsten Danzmann, and Yanbei Chen. Quantum-state preparation and macroscopic entanglement in gravitational-wave detectors. *Phys. Rev. A*, 80:043802, Oct 2009.

[7] Howard M. Wiseman and Gerard J. Milburn. *Quantum Measurement and Control*. Cambridge University Press, 2009.

[8] Huan Yang, Haixing Miao, Da-Shin Lee, Bassam Helou, and Yanbei Chen. Macroscopic quantum mechanics in a classical spacetime. *Phys. Rev. Lett.*, 110:170401, Apr 2013.

Chapter 6

EFFECTIVE MODES FOR LINEAR GAUSSIAN OPTOMECHANICS. I. SIMPLIFYING THE DYNAMICS

Abstract

For a linear optomechanical system with a finite number of internal modes that interacts with an environment with an infinite number of internal modes, we show that the interaction can be reduced to one with finite degrees of freedom. Specifically, the optomechanical interaction can be considered as a scattering process, during which Heisenberg operators of the incoming environment modes, plus the n initial optomechanical modes (which correspond to $2n$ operators), are linearly transformed into the Heisenberg operators of the outgoing environment modes, plus the n final optomechanical modes. In general, one can divide the incoming environment modes into n interacting incoming modes and an infinity of non-interacting incoming modes (with operators from different modes commuting with each other), and the outgoing environment modes into n interacting outgoing modes and an infinity of non-interacting outgoing modes (with operators from different modes commuting with each other). The final optomechanical modes and the operators of the n interacting outgoing modes depend only on the n interacting incoming modes and the initial optomechanical modes. On the other hand, operators of the outgoing non-interacting modes only depend on the incoming non-interacting modes. In this way, the optomechanical interaction can be regarded as only taking place between the interacting modes and the optomechanical system. Constructions of such interacting modes have been proposed in other works to analyze quantum engineering protocols in simple optomechanical setups, but in this paper we demonstrate that such interacting modes exist in general. We note that since the annililation operators of the interacting modes can depend on both the annihilation and creation operators of the original incoming modes, the interacting modes can be squeezed, and so contain excitations, even when the initial state of the environment is at vacuum. As a result, even though the interacting and non-interacting modes do not scatter into each other, they may be statistically correlated, in a way that depends on the initial state of the environment.

6.1 Introduction

Optomechanics studies the interaction of light with mechanical systems through radiation pressure, and has many applications. Optomechanical setups can be a high precision sensor of, for example, gravitational waves [2], or a transducer which converts signals in the microwave regime to the optical regime [1]. They can also

be used to test alternative theories of quantum mechanics such as collapse models [9].

All of these applications are mediated through light. Pulsed light has been of interest lately because of proposals to prepare mechanical systems in non-Gaussian quantum states. Hofer *et al.* proposed a scheme for entangling the center of mass mode of a test mass with an outgoing light mode [5]. Vanner *et al.* developed a toolset for transforming a test mass' quantum state into any desired target state [10], and Galland *et al.* proposed a post-selection scheme for preparing a test mass in a single phonon state [3] which Hong *et al.* experimentally realized in Ref. [6].

Pulsed optomechanics has two appealing features. It can be resilient to thermal loss, because a protocol's duration can be designed to be much shorter than the timescale of thermal dissipation. Moreover, because of the pulses' finite duration, protocols which are unstable in the continuous wave regime (such as those involving blue-detuned light) are stable in pulsed optomechanics.

The pulses' finite duration also entails that the initial state of the mechanics could matter, and so the Fourier regime would be less useful because operators at different frequencies would no longer be independent. We will have to construct a new set of convenient effective modes.

Effective modes have been proposed in Refs. [5, 10, 3] to help analyze their proposed quantum engineering protocols. In this article, we show that these effective modes interact only with the system modes, and that no other environment degree of freedom interacts with these modes or the system modes. We also present a general method for constructing a set of effective modes which summarize the interaction of a system of interest with the environment. If the joint system and environment Hamiltonian is linear (equivalently, quadratic), then we can show that a system with n degrees of freedom interacts only with n effective ingoing modes which evolve into n effective outgoing modes, as is shown in Fig. 6.1.

This article is outlined as follows. In Sec. 6.2, we rigorously justify how the effective modes were used in Ref. [5]. This example will serve as an introduction to the general formalism presented in Sec. 6.3.

6.2 Effective modes for an optomechanical setup driven by pulsed blue-detuned light

In Ref. [5], Hofer *et al.* propose a protocol for entangling a mechanical oscillator with an outgoing light pulse. We show their proposed setup in Fig. 6.2 where a blue-detuned pulse impinges on a cavity with one movable mirror.

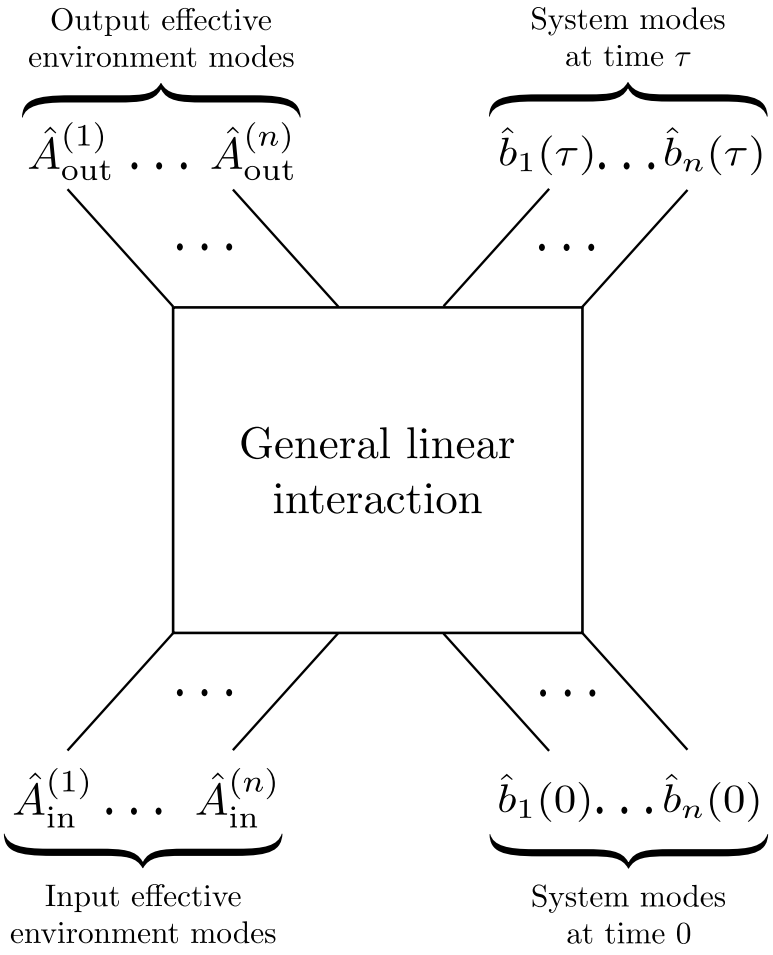

Figure 6.1: An optomechanical system with n degrees of freedom interacts with n effective input modes, $\hat{A}^{(1)}_{in}$ through $\hat{A}^{(n)}_{in}$, which evolve into n effective output modes, $\hat{A}^{(1)}_{out}$ through $\hat{A}^{(n)}_{out}$. The operators $\hat{b}_1$ through $\hat{b}_n$ represent system degrees of freedom.

In general, investigating the entanglement of an outgoing light pulse with the center of mass mode of a test mass at a particular time is in general difficult because the light modes form a continuum. For example, Miao *et al.* perform sophisticated calculations in Ref. [8] to obtain the total entanglement between a mechanical mode and the outgoing light modes, and to obtain the effective optical mode that the test mass is most entangled with.

For the simple setup shown in Fig. 6.2, Hofer *et al.* postulate that the test mass interacts with a single effective optical ingoing and outgoing mode, $\hat{A}^{(H)}_{in}$ and $\hat{A}^{(H)}_{out}$

respectively, where

$$\hat{A}_{in}^{(H)} = \sqrt{\frac{2G}{1-e^{-2G\tau}}}\int_0^\tau dt\; e^{-Gt}\hat{a}_{in}(t) \tag{6.1}$$

$$\hat{A}_{out}^{(H)} = \sqrt{\frac{2G}{e^{2G\tau}-1}}\int_0^\tau dt\; e^{Gt}\hat{a}_{out}(t)\,. \tag{6.2}$$

τ is the length of the pulse, $\hat{a}_{out}(t)$ are the outgoing light modes, and

$$G \equiv \frac{\alpha^2}{\kappa}. \tag{6.3}$$

α is the enhanced optomechanical coupling (and is defined by Eq. (2) of [5]), and κ is the light amplitude decay rate from the cavity. Note that we've ignored thermal noise, and we are in a rotating frame of $+\omega_m$ for the mechanical mode and $-\omega_m$ for the cavity and incoming light modes (refer to section II.A of [5] for more details). ω_m is the mechanical oscillator's resonant frequency. Moreover, we assume that we are in the resolved sideband regime $\alpha \ll \omega_m \ll \kappa$. This regime allows us to apply the rotating wave approximation which approximates the interaction Hamiltonian between the center of mass mode, $\hat{a}_m$, and the cavity mode, $\hat{a}_c$, to

$$\hbar\alpha\left(\hat{a}_m\hat{a}_c + \hat{a}_m^\dagger\hat{a}_c^\dagger\right). \tag{6.4}$$

Since $\alpha \ll \omega_m \ll \kappa$, the cavity is then adiabatically eliminated.

Hofer *et al.* claim that at time τ the mechanical oscillator is only entangled with $\hat{A}_{out}$. They show that $\hat{A}_{in}$ and $\hat{A}_{out}$ satisfy the following equations of motion

$$\hat{A}_{out} = -e^{G\tau}\hat{A}_{in} - i\sqrt{e^{2G\tau}-1}\hat{a}_m^\dagger(0), \tag{6.5}$$

$$\hat{a}_m(\tau) = e^{G\tau}\hat{a}_m(0) + i\sqrt{e^{2G\tau}-1}\hat{A}_{in}^\dagger, \tag{6.6}$$

which represent pure two-mode squeezing between the mechanical oscillator and the outgoing light mode $\hat{A}_{out}$. However, they do not show that no other effective output mode than $\hat{A}_{out}$ interacts with $\hat{A}_{in}$ or $\hat{a}_m$. In this section, we prove that $\hat{a}_m$ and $\hat{A}_{in}$ interact with each other and with nothing else .

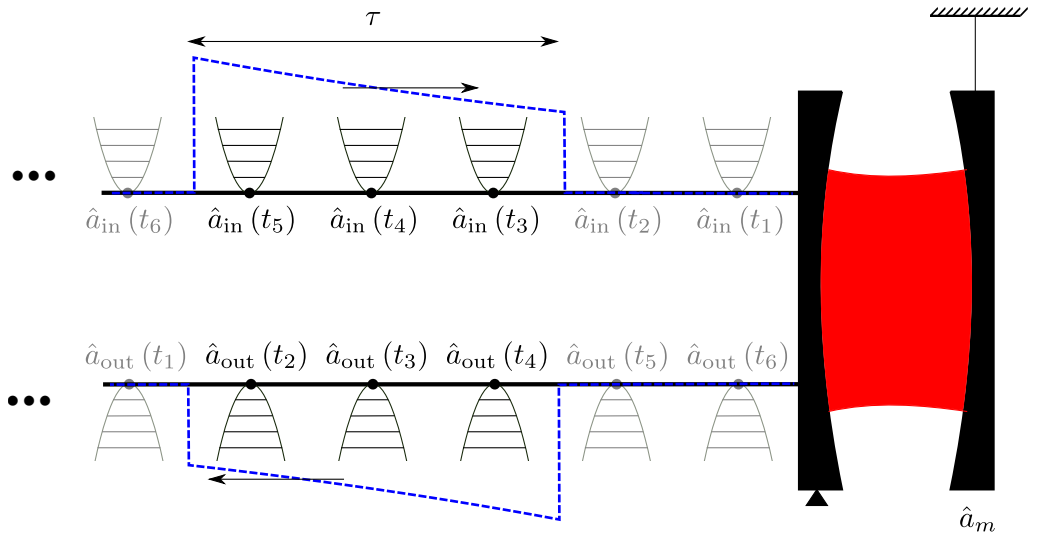

Figure 6.2: The setup proposed by Hofer *et al.* in Ref. [5]. The cavity has a single movable mirror with a center of mass mode denoted by $\hat{a}_m$. The incoming light pulse, shown in dashed blue, is blue-detuned and of length τ. Note that the ingoing and outgoing light modes, $\hat{a}_{in}(t)$ and $\hat{a}_{out}(t)$ respectively, form a continuum but we show them as discrete modes for simplicity.

6.2.1 Structure of the equations of motion

We start the proof with the (approximate) equations of motion for the modes $\hat{a}_m(t)$ and $\hat{a}_{out}(t)$:

$$\partial_t \hat{a}_m(t) = \frac{\alpha^2}{\kappa}\hat{a}_m(t) + i\frac{\alpha\sqrt{2}}{\sqrt{\kappa}}\hat{a}_{in}^\dagger(t), \tag{6.7}$$

$$\hat{a}_{out}(t) = \left(1 - \frac{\sqrt{2}}{\sqrt{\kappa}}\right)\hat{a}_{in}(t) - i\frac{\alpha\sqrt{2}}{\sqrt{\kappa}}\hat{a}_m^\dagger(t). \tag{6.8}$$

Since these differential equations are linear, they imply that both $\hat{a}_m(t)$ and $\hat{a}_{out}(t)$ are linear combinations of the incoming light $\hat{a}_{in}(t)$ and the initial state of the mechanical oscillator $\hat{a}_m(0)$. As a result, we can write the solution to Eqs. (6.7-6.8) in matrix form:

$$\boldsymbol{w} = M\boldsymbol{v}, \tag{6.9}$$

where $\boldsymbol{w}$ contains the outgoing light modes and the center of mass mode at time τ,

$$\boldsymbol{w} = \begin{pmatrix} \tilde{a}_{out}(0) \\ \tilde{a}_{out}(dt) \\ \vdots \\ \tilde{a}_{out}(\tau) \\ \hline \hat{a}_m^\dagger(\tau) \end{pmatrix} \equiv \begin{pmatrix} \hat{\boldsymbol{a}}_{out} \\ \hline \hat{a}_m^\dagger(\tau) \end{pmatrix}. \tag{6.10}$$

$\boldsymbol{v}$ contains the input light and the mechanics at the initial time $t = 0$,

$$\boldsymbol{v} = \begin{pmatrix} \tilde{a}_{in}(0) \\ \tilde{a}_{in}(dt) \\ \vdots \\ \tilde{a}_{in}(\tau) \\ \hline \hat{a}_m^\dagger(0) \end{pmatrix} \equiv \begin{pmatrix} \hat{\boldsymbol{a}}_{in} \\ \hline \hat{a}_m^\dagger(0) \end{pmatrix}. \tag{6.11}$$

Note that to simplify the exposition of the proof, we've discretized the dynamics by dividing the period τ into N time steps of length $dt = \tau/N$. The limit $N \to \infty$ can be easily taken at the end of the proof. The $\tilde{a}_{in}$ and $\tilde{a}_{out}$ are normalized with $1/\sqrt{dt}$

$$\tilde{a}_{in} \equiv \hat{a}_{in}/\sqrt{dt}, \quad \tilde{a}_{out} \equiv \hat{a}_{out}/\sqrt{dt}, \tag{6.12}$$

so that their commutation relation is normalized to unity (see Eq. (6.18)).

The matrix M describes the transformation of $\boldsymbol{v}$ into $\boldsymbol{w}$, as is depicted in Fig. 6.3. To obtain the entries of M, we need to solve for $\hat{a}_m^\dagger(\tau)$ and $\hat{a}_{out}(t)$. Because the equations of motion (6.7-6.8) are linear, $\hat{a}_m^\dagger(\tau)$ and $\hat{a}_{out}(t)$ are of the form

$$\hat{a}_m^\dagger(\tau) = \beta \hat{a}_m^\dagger(0) + \int_0^\tau dt\; g^*(t)\, \hat{a}_{in}(t), \tag{6.13}$$

$$\hat{a}_{out}(t) = h(t)\, \hat{a}_m^\dagger(0) + \int_0^t dz\; T(t,z)\, \hat{a}_{in}(z). \tag{6.14}$$

Consequently, M's structure is

$$M \equiv \begin{pmatrix} T & \vec{h} \\ \vec{g}^\dagger & \beta \end{pmatrix}, \tag{6.15}$$

where T shows how part of the outgoing fields are mixtures of the incoming fields, $\vec{h}$ and $\vec{g}$ show the 2-mode squeezing between the light and the mechanics, and β is the portion of $\hat{a}_m(0)$ that appears in $\hat{a}_m(\tau)$. Note that β is a scalar, $T \in \mathbb{M}_{N\times N}$ is

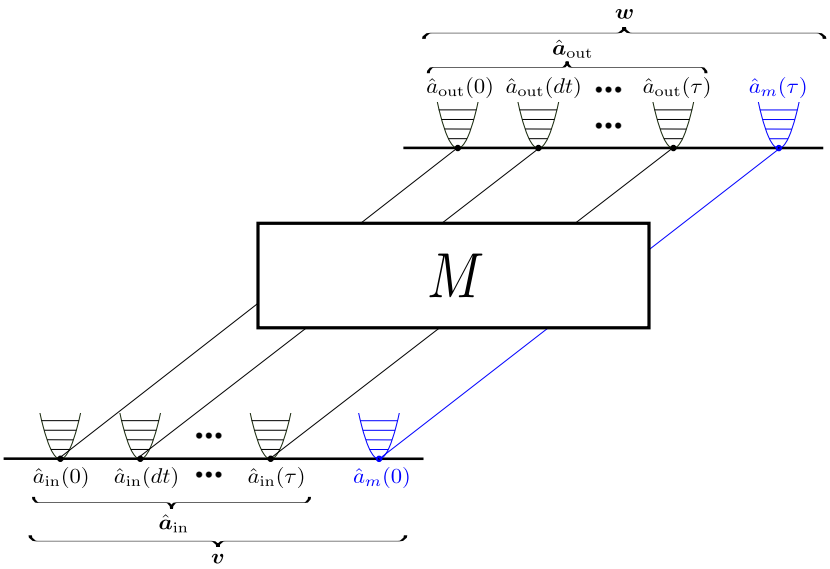

Figure 6.3: The transformation of input degrees of freedom to output degrees of freedom under the matrix M.

an $N \times N$ matrix, and $\vec{h}$, $\vec{g}$ are N-sized column vectors. We pick the convention of writing matrices in capital letters, vectors in lower case form with an overhead arrow, and scalars in greek letters.

6.2.2 The effective modes that simplify M's structure

In general, M's structure is complicated and it would seem like $\hat{a}_m$ interacts with uncountably many modes. We will show that a simple narrative, that of a mechanical mode and an optical mode interacting with each other and with nothing else, is possible.

Consider a new set of input and output modes, which we name $\hat{c}_{in}$ and $\hat{c}_{out}$ respectively, that are a linear combination of the $\tilde{a}_{in}$s and $\tilde{a}_{out}$s:

$$\hat{\boldsymbol{c}}_{in} \equiv \begin{pmatrix} \hat{c}_{in}(1) \\ \hat{c}_{in}(2) \\ \vdots \\ \hat{c}_{in}(N) \end{pmatrix} = V\hat{\boldsymbol{a}}_{in}, \tag{6.16}$$

$$\hat{\boldsymbol{c}}_{out} \equiv \begin{pmatrix} \hat{c}_{out}(1) \\ \hat{c}_{out}(2) \\ \vdots \\ \hat{c}_{out}(N) \end{pmatrix} = U\hat{\boldsymbol{a}}_{out}, \tag{6.17}$$

where U and V are *unitary* $N \times N$ matrices. They are unitary because we impose that the effective modes $\hat{c}_{out}$ and $\hat{c}_{in}$ are separate degrees of freedom, just as $\hat{a}_{out}$ and $\hat{a}_{in}$ are:

$$\begin{aligned}\left[\left(\hat{\boldsymbol{c}}_{out/in}\right)_i, \left(\hat{\boldsymbol{c}}_{out/in}\right)_j^\dagger\right] &= \left[\left(\hat{\boldsymbol{a}}_{out/in}\right)_i, \left(\hat{\boldsymbol{a}}_{out/in}\right)_j^\dagger\right] \\ &= \delta_{ij} \end{aligned} \tag{6.18}$$

for $1 \leq i, j \leq N$. By substituting $\hat{\boldsymbol{c}}_{in}$ and $\hat{\boldsymbol{c}}_{out}$ into Eq. (6.9) and using the expression for M in Eq. (6.15), we find that

$$\begin{pmatrix} \hat{\boldsymbol{c}}_{out} \\ \hat{a}_m^\dagger(\tau) \end{pmatrix} = \begin{pmatrix} UTV^\dagger & U\vec{h} \\ \vec{g}^\dagger V^\dagger & \beta \end{pmatrix} \begin{pmatrix} \hat{\boldsymbol{c}}_{in} \\ \hat{a}_m^\dagger(0) \end{pmatrix}. \tag{6.19}$$

$\hat{a}_m(0)$ and only a single optical mode interact with each other and with nothing else if Eq. (6.19) is of the form

$$\left(\begin{array}{c} \hat{A}_{out} \\ \hline \hat{a}_m^\dagger(\tau) \\ \hline \hat{c}_{out}(2) \\ \vdots \\ \hat{c}_{out}(N) \end{array}\right) = \left(\begin{array}{cc|c} \theta & \phi & 0 \\ \gamma & \beta & 0 \\ \hline 0 & 0 & W \end{array}\right) \left(\begin{array}{c} \hat{A}_{in} \\ \hline \hat{a}_m^\dagger(0) \\ \hline \hat{c}_{in}(2) \\ \vdots \\ \hat{c}_{in}(N) \end{array}\right), \tag{6.20}$$

where θ, ϕ, γ are scalars and W is a $(N-1) \times (N-1)$ matrix and

$$\hat{c}_{in}(1) \equiv \hat{A}_{in}, \quad \hat{c}_{out}(1) \equiv \hat{A}_{out}. \tag{6.21}$$

The second term on the RHS of Eq. (6.13) implies that $\hat{a}_m(0)$ interacts with just one effective input mode, so we postulate that:

$$\hat{A}_{in} = \mathcal{N}_{in}^{-1} \int_0^\tau dt\; g^*(t)\, \hat{a}_{in}(t), \tag{6.22}$$

$$\mathcal{N}_{in} \equiv \sqrt{\int_0^\tau dt\;\; |g(t)|^2}, \tag{6.23}$$

where $\mathcal{N}_{in}$ ensures that $\hat{A}_{in}$'s commutation relation is normalized to unity. In Appendix 6.5 (see Eqs. (6.113) and (6.117)), we show that Eq. (6.18) entails that

$$T\vec{g} = \beta^*\vec{h}, \tag{6.24}$$

$$\vec{h}^\dagger T \propto \vec{g}^\dagger, \tag{6.25}$$

so from Eq. (6.14),

$$\hat{A}_{out} = \mathcal{N}_{out}^{-1} \int_0^\tau dt\ h^*(t)\, \hat{a}_{out}(t), \tag{6.26}$$

$$\mathcal{N}_{out} \equiv \sqrt{\int_0^\tau dt\ |h(t)|^2} \tag{6.27}$$

interacts only with $\hat{a}_m(0)$ and $\hat{A}_{in}$.

If we show that no other effective output mode than $\hat{A}_{out}$ interacts with $\hat{a}_m(0)$ and $\hat{A}_{in}$, then we would have proven that the test mass' center of mass mode and one optical mode interact with each other and nothing else. Consider a mode

$$\hat{O} \equiv \int_0^\tau dt\, l^*(t)\, \hat{a}_{out}(t) \tag{6.28}$$

that commutes with $\hat{A}_{out}$, so in the discrete limit

$$\vec{l}^\dagger \vec{h} = 0. \tag{6.29}$$

When combined with Eq. (6.14), this means that $\hat{O}$ cannot depend on $\hat{a}_m(0)$. Eq. (6.14) also tells us that $\hat{O}$ depends on the effective input mode $\vec{l}^\dagger T \hat{\boldsymbol{a}}_{in}$, which commutes with $\hat{A}_{in} \propto \vec{g}^\dagger \hat{\boldsymbol{a}}_{in}$ because of Eq. (6.24).

From Eqs. (6.19), (6.22) and (6.26), the effective modes follow the equations of motion

$$\left(\begin{array}{c} \hat{A}_{out} \\ \hline \hat{a}_m^\dagger(\tau) \\ \hat{c}_{out}(2) \\ \vdots \\ \hat{c}_{out}(N) \end{array}\right) = \left(\begin{array}{ccc} \theta & \left\|\vec{h}\right\| & 0 \\ \|\vec{g}\| & \beta & 0 \\ \hline 0 & 0 & W \end{array}\right) \left(\begin{array}{c} \hat{A}_{in} \\ \hline \hat{a}_m^\dagger(0) \\ \hat{c}_{in}(2) \\ \vdots \\ \hat{c}_{in}(N) \end{array}\right), \tag{6.30}$$

where W is an $(N-1)\times(N-1)$ matrix,

$$\|\vec{v}\| \equiv \vec{v}^\dagger v \xrightarrow[limit]{continuous} \int_0^\tau dt\, |v(t)|^2 \tag{6.31}$$

for any vector $\vec{v}$, and

$$\theta = \frac{\vec{h}^\dagger}{\left\|\vec{h}\right\|} T \frac{\vec{g}}{\|\vec{g}\|} \tag{6.32}$$

which, by using Eq. (6.24), we simplify to

$$\theta = \beta^* \|\vec{h}\| / \|\vec{g}\| \,. \tag{6.33}$$

By imposing that $\hat{A}_{out}$ and $\hat{a}_m^\dagger(\tau)$ satisfy the same commutation relations as $\hat{A}_{in}$ and $\hat{a}_m^\dagger(0)$, we conclude that $\|\vec{h}\| = \|\vec{g}\|$, and that $\|\vec{g}\| = \sqrt{|\beta|^2 - 1}$. The physics we are interested in is neatly summarized by

$$\hat{A}_{out} = e^{-i\delta}\left(|\beta|\,\hat{A}_{in} + \sqrt{|\beta|^2 - 1}e^{i\delta}\hat{a}_m^\dagger(0)\right) \tag{6.34}$$

$$\hat{a}_m(\tau) = e^{-i\delta}\left(|\beta|\,\hat{a}_m(0) + \sqrt{|\beta|^2 - 1}e^{i\delta}\hat{A}_{in}^\dagger\right), \tag{6.35}$$

where $\delta \equiv \arg\beta$. Eqs. (6.34 - 6.35) describe two-mode squeezing with a squeezing parameter $re^{-i\arg\beta}$. r can be formally solved for with the equations

$$\cosh r = |\beta|\,, \quad \sinh r = \sqrt{|\beta|^2 - 1}. \tag{6.36}$$

Notice that to derive the effective modes, we never had to calculate T. Moreover, if we are only interested in obtaining the equations of motion of the effective modes, then we only need to know β.

Note that in Appendices 6.5 and 6.6, we follow two different approaches to show why $\hat{a}_m$ and a single effective optical mode interact with each other and nothing else. Appendix 6.5 derives the effective modes from the constraints they have to satisfy. Appendix 6.6 uses group theory to prove the existence of a single effective optical mode.

We can use the above results to quickly obtain the effective modes mentioned in Ref. [5]. We first extract $h(t)$ and $g(t)$ by solving for $\hat{a}_m(t)$ and $\hat{a}_{out}(t)$. Using Eqs. (6.7) and (6.8),

$$\begin{aligned}
\hat{a}_m(\tau) &= e^{G\tau}\hat{a}_m(0) + i\sqrt{2G}\int_0^\tau dt\; e^{-G(t-\tau)}\hat{a}_{in}^\dagger(t), \\
\hat{a}_{out}(t) &= -i\sqrt{2G}e^{Gt}\hat{a}_m^\dagger(0) - 2G\int_0^t dz\; e^{-Gz}\hat{a}_{in}(z) \\
&\quad + \left(1 - \frac{\sqrt{2}}{\sqrt{\kappa}}\right)\hat{a}_{in},
\end{aligned}$$

and so

$$\beta = e^{G\tau}, \quad h(t) = -i\sqrt{2G}e^{Gt}, \quad g(t) = i\sqrt{2G}e^{-G(t-\tau)}, \tag{6.37}$$

with

$$\|\vec{h}\| \quad = \|\vec{g}\| = \sqrt{|\beta|^2 - 1} = \quad \sqrt{e^{2G\tau} - 1}. \tag{6.38}$$

Using Eqs. (6.22) and (6.26), we determine that

$$\hat{A}_{in} \quad = \quad \frac{-i\sqrt{2G}}{\sqrt{1 - e^{-2G\tau}}} \int_0^\tau dt \; e^{-Gt} \hat{a}_{in}(t) \tag{6.39}$$

$$\hat{A}_{out} \quad = \quad \frac{i\sqrt{2G}}{\sqrt{e^{2G\tau} - 1}} \int_0^\tau dt \; e^{Gt} \hat{a}_{out}(t), \tag{6.40}$$

which agree with Eqs. (6.1) and (6.2) up to an irrelevant phase factor. Moreover, the equations of motion for these effective modes are

$$\hat{A}_{out} \quad = \quad e^{G\tau} \hat{A}_{in} + \sqrt{e^{2G\tau} - 1} \hat{a}_m^\dagger(0), \tag{6.41}$$

$$\hat{a}_m(\tau) \quad = \quad e^{G\tau} \hat{a}_m(0) + \sqrt{e^{2G\tau} - 1} \hat{A}_{in}^\dagger, \tag{6.42}$$

which agree with the results of Ref. [5].

6.2.3 Applying our framework to heralded single-phonon preparation

Ref. [3] shows that a weak blue-detuned pulse can be used to prepare a mechanical oscillator's center of mass mode $\hat{a}_m$ in a Fock state. As indicated by Eqs. (6.41-6.42), the pulse squeezes $\hat{a}_m$ with $\hat{A}_{out}$. Ref. [3] assumes that $\hat{a}_m$ is initially almost in vacuum and that the pulse is weak, so $\hat{a}_m(\tau)$ and $\hat{A}_{out}$'s joint quantum state is approximately $|0,0\rangle + \epsilon\,|1,1\rangle$. The outgoing light is measured by a photodetector. If it clicks we infer that the center of mass mode must be in $|1\rangle$. Such a measurement scheme is usually difficult to analyze analytically because the detector measures a nonlinear operator, the photon number operator. Fortunately, in the case of the simplified setup discussed in [3], the analysis can be done analytically because the effective modes given by Eqs. (6.39-6.40) have a simple form. In this section, we rigorously derive the results of [3].

The (unnormalized) conditional state of an optomechanical setup under continuous measurement is formally given by

$$|\psi_c\rangle = \hat{P}_n \hat{\mathcal{U}}_n \ldots \hat{P}_2 \hat{\mathcal{U}}_2 \hat{P}_1 \hat{\mathcal{U}}_1 \, |\psi_{ini}\rangle, \tag{6.43}$$

where $|\psi_{ini}\rangle$ is the initial state of the system and environment. We take the initial state of the incoming light to be vacuum. $\hat{\mathcal{U}}_i$ is the unitary time evolution operator from t_{i-1} to t_i, and $\hat{P}_i$ is the projection operator corresponding to a click or no click

at time t_i. To simplify our analysis, we've taken the discrete limit and assumed that t_i and t_{i-1} are separated by a time interval dt. Moreover, we ignore the possibility of multiple clicks at the same time because in the continuum limit the probability of two clicks at the same time is 0.

We express the projection operators in the Heisenberg picture:

$$\hat{P}_i^H = \left(\hat{\mathcal{U}}_i ... \hat{\mathcal{U}}_1\right)^\dagger \hat{P}_i \left(\hat{\mathcal{U}}_i ... \hat{\mathcal{U}}_1\right), \tag{6.44}$$

which allows us to rewrite Eq. (6.43) to

$$|\psi_c\rangle = \hat{\mathcal{U}}_\tau \hat{P}_n^H ... \hat{P}_2^H \hat{P}_1^H |\psi_{ini}\rangle, \tag{6.45}$$

where $\hat{\mathcal{U}}_\tau$ is the total time evolution operator from $t = 0$ till $t = \tau$:

$$\hat{\mathcal{U}}_\tau = \hat{\mathcal{U}}_n ... \hat{\mathcal{U}}_2 \hat{\mathcal{U}}_1. \tag{6.46}$$

The Heisenberg projection operator associated with a single click at time t_i is

$$\begin{aligned} \hat{\mathcal{P}}_{t_i} &= (|0\rangle\langle 0|)(\tau) \otimes .... \otimes (|0\rangle\langle 0|)(t_{i+1}) \otimes (|1\rangle\langle 1|)(t_i) \\ &\quad \otimes (|0\rangle\langle 0|)(t_{i-1}) \otimes .... \otimes (|0\rangle\langle 0|)(0) \\ &= \hat{a}_{out}^\dagger(t_i) \left(|0\rangle\langle 0| \otimes \hat{I}_m\right)_H \hat{a}_{out}(t_i), \end{aligned}$$

where $\hat{I}_m$ is the identity operator associated with the mechanical center of mass mode. $\left(|0\rangle\langle 0| \otimes \hat{I}_m\right)_H$ is a shorthand for the projection operator (in the Heisenberg picture) associated with no clicks for the duration of the experiment. We then express $\hat{a}_{out}(t_i)$ in terms of the effective modes defined by Eq. (6.17):

$$\hat{a}_{out}(t_i) = \sum_j u_{jt_i} \hat{c}_{out}(j), \tag{6.47}$$

where u_{jt_i} is a scalar and $1 \leq j \leq N$. Substituting $\hat{a}_{out}(t_i)$ into $\hat{\mathcal{P}}_{t_i}$, we obtain

$$\hat{\mathcal{P}}_{t_i} = \sum_l u_{lt_i} \hat{a}_{out}^\dagger(t_i) \left(|0\rangle\langle 0| \otimes \hat{I}_m\right)_H \hat{c}_{out}(l). \tag{6.48}$$

Using Eq. (6.45), the conditional state associated with a click at time t_i is

$$\left|\psi_{t_i}\right\rangle = \hat{\mathcal{U}}_\tau \hat{\mathcal{P}}_{t_i} |\psi_{ini}\rangle. \tag{6.49}$$

The optical part of $|\psi_{ini}\rangle$ is vacuum so when $\hat{c}_{out}(l)$ acts on $|\psi_{ini}\rangle$, only the $l = 1$ term, $\hat{A}_{out}$, which is a linear combination of optical annihilation operators and a mechanical creation operator, will result in a non-null state. As indicated by Eq. (6.30), the remainder of the effective optical modes consist of only annihilation operators, so they will not affect our analysis and will be ignored.

Let us assume that the center of mass mode is initially in vacuum, then when the $\hat{a}_m^\dagger(0)$ component of $\hat{A}_{out}$, given by Eq. (6.34), acts on $|\psi_{ini}\rangle$, it yields:

$$\begin{aligned}\hat{\mathcal{P}}_{t_i}|\psi_{ini}\rangle &= u_{1t_i}\sqrt{|\beta|^2-1} \\ &\quad \times\hat{a}_{out}^\dagger(t_i)\left(|0\rangle\langle 0|\otimes\hat{I}_m\right)_H\hat{a}_m^\dagger(0)|\psi_{ini}\rangle \\ &= u_{1t_i}\sqrt{|\beta|^2-1} \\ &\quad \times\hat{a}_{out}^\dagger(t_i)\left(|0\rangle\langle 0|\otimes\hat{I}_m\right)_H|1,0\rangle\,. \end{aligned} \tag{6.50}$$

We then expand $\hat{I}_m$,

$$\begin{aligned}\left(|0\rangle\langle 0|\otimes\hat{I}_m\right)_H &= \sum_l\frac{1}{l!}\left(\hat{a}_m^\dagger(\tau)\right)^l \\ &\quad (|0,0\rangle\langle 0,0|)_H\,\hat{a}_m^l(\tau)\,. \end{aligned} \tag{6.51}$$

Substituting Eq. (6.51) in Eq. (6.50), when $\hat{a}_m^l(\tau)$ acts on $|1,0\rangle$, it can contain at most one mechanical annihilation operator. Therefore, using Eq. (6.35), $\hat{a}_m^l(\tau)|1,0\rangle$ simplifies to

$$\begin{aligned}\hat{a}_m^l(\tau)|1,0\rangle &= \left(|\beta|^2-1\right)^{l/2}\sqrt{l!} \\ &\quad \times\left(|1,l\rangle+\frac{\beta^*}{\sqrt{l\left(|\beta|^2-1\right)}}|0,l-1\rangle\right). \end{aligned} \tag{6.52}$$

Eq. (6.35) indicates that $\hat{a}_m(\tau)$ and $\hat{A}_{out}$ are 2-mode squeezed with a squeezing

parameter $re^{-i\arg\beta}$. Therefore, $|0,0\rangle_H = \hat{\mathcal{U}}_\tau |0,0\rangle$ is

$$|0,0\rangle_H = \sum_s d_s |s,s\rangle \tag{6.53}$$

$$d_s = (-1)^s e^{-is\arg\beta} \frac{(\tanh r)^s}{\cosh r} \tag{6.54}$$

$$= e^{-is\arg\beta} \frac{\left(|\beta|^2 - 1\right)^{s/2}}{|\beta|^{s+1}}. \tag{6.55}$$

When $\langle 0,0|_H$ acts on $\hat{a}_m^l(\tau)|1,0\rangle$, given by Eq. (6.52), only the $l = 1$ term remains:

$$\langle 0,0|_H \hat{a}_m^l(\tau)|1,0\rangle = \delta_{l1} e^{-i\arg\beta} \left(-e^{-2i\arg\beta}\tanh^2 r + 1\right), \tag{6.56}$$

where we used Eq. (6.36) to express everything in terms of r. Substituting Eq. (6.56) back into $\hat{\mathcal{P}}_{t_i}|\psi_{ini}\rangle$, we obtain

$$\hat{\mathcal{P}}_{t_i}|\psi_{ini}\rangle = u_{1t_i} e^{-i\arg\beta} \left(-e^{-2i\arg\beta}\tanh^2 r + 1\right) \sinh r \times \hat{a}_{out}^\dagger(t_i)\, \hat{a}_m^\dagger(\tau)|0,0\rangle_H . \tag{6.57}$$

Substituting $\hat{\mathcal{P}}_{t_i}|\psi_{ini}\rangle$ into Eq. (6.49), we obtain

$$|\psi_c\rangle \propto \hat{\mathcal{U}}_\tau \hat{a}_{out}^\dagger(t_i)\, \hat{a}_m^\dagger(\tau)|0,0\rangle_H \tag{6.58}$$

$$= \hat{\mathcal{U}}_\tau \hat{a}_{out}^\dagger(t_i)\, \hat{a}_m^\dagger(\tau)\, \hat{\mathcal{U}}_\tau^\dagger |0,0\rangle \tag{6.59}$$

$$= |1,1\rangle . \tag{6.60}$$

The mechanical state is in the first Fock state, as expected. Notice that $|\psi_c\rangle$ doesn't depend on t_i. The probability of a click at time t_i is

$$\langle\psi_{ini}|\hat{\mathcal{P}}_{t_i}|\psi_{ini}\rangle = |u_{1t_i}|^2 \left|-e^{-2i\arg\beta}\tanh^2 r + 1\right|^2 \sinh^2 r. \tag{6.61}$$

For $\arg\beta = 0$ (as in Ref. [3]), we have

$$\langle\psi_{ini}|\hat{\mathcal{P}}_{t_i}|\psi_{ini}\rangle = |u_{1t_i}|^2 \frac{\sinh^2 r}{\cosh^4 r}. \tag{6.62}$$

To calculate the probability of obtaining a single click over the period τ, we integrate over t_i:

$$\text{Prob}\,(1\text{ click}) = \frac{\sinh^2 r}{\cosh^4 r}, \tag{6.63}$$

where we have used that (in the continuum limit)

$$\int_0^\tau dt\, |u_1(t)|^2 = 1 \tag{6.64}$$

because (as explained in Sec. 6.2.2) the transformation matrix relating $\hat{\boldsymbol{a}}_{out}$ and $\hat{\boldsymbol{c}}_{out}$ is unitary, so its rows and columns are normalized to 1.

Finally, we note that a similar analysis can be performed to show that the test mass' quantum state conditioned on n clicks is $|n\rangle$, and the probability of measuring n clicks is $|d_n|^2 = \tanh^{2n} r/\cosh^2 r$. In addition, the conditional scheme described in Ref. [3] can be extended to setups driven by two tones (instead of just a blue-detuned or red-detuned laser). For instance, consider the setup described in Ref. [7], where a cavity is driven by two tones with frequencies centered around the cavity's resonant frequency. In the good cavity limit, where the cavity linewidth is much smaller than the mechanical resonant frequency, the authors show that the optomechanical Hamiltonian can be approximated to be squeezing between a squeezed mechanical operator and the driving light. As a result, the analysis performed in Ref. [3] and in this section also applies to the setup considered in Ref. [7]. The only difference is that the mechanical ladder operators would have to be replaced with squeezed ladder operators.

6.3 Effective modes for general setups

In this section, we show that a general system with n degrees of freedom interacts with only n effective environment modes, as shown in Fig. 6.1. For instance, the cavity optomechanical setup shown in Fig. 6.2 has $n = 2$ degrees of freedom: the cavity field (assuming it isn't adiabatically eliminated) and the test mass' center of mass mode. This system would interact with only $n = 2$ effective modes.

We first introduce the notation and present the general structure of equations of motion in linear optomechanics. We then show that the system modes and n effective environment modes interact with each other and nothing else. Finally, although the constructed effective modes simplify the dynamics between the system and its environment, we show that they do not, in general, simplify the structure of the entanglement between the system and its environment.

6.3.1 Setup

Consider a general linear transformation of a collection of modes $\boldsymbol{v}$ to $\boldsymbol{w}$ via M:

$$\boldsymbol{w} = M\boldsymbol{v}, \tag{6.65}$$

with

$$\boldsymbol{w} = \begin{pmatrix} \tilde{a}_{out}(t_1) \\ \vdots \\ \tilde{a}_{out}(t_N = \tau) \\ \tilde{a}^{\dagger}_{out}(t_1) \\ \vdots \\ \tilde{a}^{\dagger}_{out}(t_N = \tau) \\ \hline \hat{b}_1(\tau) \\ \vdots \\ \hat{b}_n(\tau) \\ \hat{b}^{\dagger}_1(\tau) \\ \vdots \\ \hat{b}^{\dagger}_n(\tau) \end{pmatrix} \equiv \begin{pmatrix} \hat{\boldsymbol{a}}_{out} \\ \hline \hat{\boldsymbol{b}}_{\tau} \end{pmatrix}, \tag{6.66}$$

where τ is any time after the experiment began, $\tilde{a}_{out}$ and $\tilde{a}_{in}$ is defined in Eq. (6.12), and $\hat{b}_1$ through $\hat{b}_n$ are the ladder operators corresponding to the degrees of freedom of the optomechanical system of interest. $\hat{\boldsymbol{a}}_{out}$ contains the output optical modes and is an N-size vector (because we've discretized time into N intervals), and $\hat{\boldsymbol{b}}_{\tau}$ is an n-size vector. $\boldsymbol{v}$ contains the input optical modes and the system modes evaluated at the initial time of the experiment t_1:

$$\boldsymbol{v} = \begin{pmatrix} \tilde{a}_{in}(t_1) \\ \vdots \\ \tilde{a}_{in}(\tau) \\ \tilde{a}^{\dagger}_{in}(t_1) \\ \vdots \\ \tilde{a}^{\dagger}_{in}(\tau) \\ \hline \hat{b}_1(t_1) \\ \vdots \\ \hat{b}_n(t_1) \\ \hat{b}^{\dagger}_1(t_1) \\ \vdots \\ \hat{b}^{\dagger}_n(t_1) \end{pmatrix} \equiv \begin{pmatrix} \hat{\boldsymbol{a}}_{in} \\ \hline \hat{\boldsymbol{b}}_0 \end{pmatrix}. \tag{6.67}$$

M is not an arbitrary matrix because we require that the output light modes be separate degrees of freedom in the same way that the input light modes are. We

must have

$$M\Omega M^\dagger = \Omega, \tag{6.68}$$

where the commutation matrix $\Omega_{kl} \equiv \left[v_k, v_l^\dagger\right]$ is given by

$$\Omega = \begin{pmatrix} J_N & 0 \\ 0 & J_n \end{pmatrix}. \tag{6.69}$$

For any positive integer z, J_z is

$$J_z \equiv \begin{pmatrix} I_z & 0 \\ 0 & -I_z \end{pmatrix}, \tag{6.70}$$

where I_z is the identity matrix of size z.

In contrast to Eq. (6.10), we have included both annihilation and creation ladder operators in Eq. (6.65). In general, we cannot, as in Eq. (6.4), apply a rotating wave approximation that would reduce the optomechanical interaction to only the beamsplitter or squeezing interaction. Moreover, we have assumed that the environment consists only of optical modes. Thermal noise can be incorporated by having an explicit model of the thermal bath as a collection of harmonic oscillators. Such models are usually used to derive the Langevin equations of motion [4]. The thermal bath ladder operators can be included in $\hat{\boldsymbol{a}}_{in}$, and their time-evolved counterparts in $\hat{\boldsymbol{a}}_{out}$. If we include them, then the effective modes we derive in this section would be super-modes consisting of both light and bath ladder operators.

We can decompose M into four blocks:

$$M \equiv \begin{pmatrix} T & H \\ G & B \end{pmatrix}, \tag{6.71}$$

where $T \in \mathbb{M}_{2N\times 2N}$ relates the output optical fields to the input optical fields, $B \in \mathbb{M}_{2n\times 2n}$ relates the system modes at τ to their initial state $\hat{\boldsymbol{b}}_0$, $H \in \mathbb{M}_{2N\times 2n}$ specifies the dependence of $\hat{\boldsymbol{a}}_{out}$ on $\hat{\boldsymbol{b}}_0$, and $G \in \mathbb{M}_{2n\times 2N}$ specifies the dependence of $\hat{\boldsymbol{b}}_\tau$ on the input modes $\hat{\boldsymbol{a}}_{in}$. Because $\boldsymbol{v}$ and $\boldsymbol{w}$ contain ladder operators and their adjoints, T must have the following structure

$$T \equiv \begin{pmatrix} T_1 & T_2 \\ T_2^* & T_1^* \end{pmatrix} \in \mathbb{M}_{2N\times 2N}, \tag{6.72}$$

where $T_1 \in \mathbb{M}_{N\times N}$ indicates how the input optical fields get mixed amongst each

other, and T_2 carries information about their multi-mode squeezing. Similarly, H and G must have the following structure:

$$H = \begin{pmatrix} \vec{h}_1 & \dots & \vec{h}_n & \tilde{h}_1 & \dots & \tilde{h}_n \end{pmatrix}, \tag{6.73}$$

$$G^\dagger = \begin{pmatrix} \vec{g}_1 & \dots & \vec{g}_n & \tilde{g}_1 & \dots & \tilde{g}_n \end{pmatrix}, \tag{6.74}$$

where $\tilde{s}$ denotes the dual of a vector $\vec{s}$

$$\tilde{s} \equiv K_N \vec{s}^*,$$

with

$$K_N \equiv \begin{pmatrix} 0 & I_N \\ I_N & 0 \end{pmatrix} \tag{6.75}$$

a 'switching' matrix that switches the top and bottom halves of $\vec{s}$.

6.3.2 The effective modes that simplify M's structure

From Eqs. (6.65) and (6.71), the system modes interact with the n effective input modes $G\hat{\boldsymbol{a}}_{in}$. In general, $G\hat{\boldsymbol{a}}_{in}$ does not form a conjugate set of modes, as their commutation relation is not equal to J_n. Consequently, we will choose the n effective input modes to be

$$\hat{\boldsymbol{A}}_{in} = \boldsymbol{S}_v^\dagger G \hat{\boldsymbol{a}}_{in} \tag{6.76}$$

where $\hat{\boldsymbol{A}}_{in}$ contains the annihilation and creation operators of n effective modes, and $\boldsymbol{S}_v$ ensures that

$$\left[\hat{\boldsymbol{A}}_{in}, \hat{\boldsymbol{A}}_{in}^\dagger\right] = J_n, \tag{6.77}$$

so

$$\boldsymbol{S}_v^\dagger G J_N G^\dagger \boldsymbol{S}_v = J_n. \tag{6.78}$$

Note that since bottom half of $\hat{\boldsymbol{A}}_{in}$ has to be the hermitian conjugate of the top half, $\boldsymbol{S}_v$ has to be of the form

$$\boldsymbol{S}_v = \begin{pmatrix} S_v & K_n S_v^* \end{pmatrix}, \tag{6.79}$$

where S_v is an $N \times N$ matrix.

In practice, we can construct $\boldsymbol{S}_v^\dagger$ with a symplectic Gram-Schmidt procedure. We

pick the first effective input mode to be

$$\left(\hat{\boldsymbol{A}}_{in}\right)_1 = \mathcal{N}_{in,1}^{-1}\vec{g}_1^{\dagger}\hat{\boldsymbol{a}}_{in}, \quad \left(\hat{\boldsymbol{A}}_{in}\right)_1^{\dagger} = \mathcal{N}_{in,1}^{-1}\tilde{g}_1^{\dagger}\hat{\boldsymbol{a}}_{in}, \tag{6.80}$$

$$\mathcal{N}_{in,1}^{-1} = \sqrt{\left|\vec{g}_1^{\dagger}J_N\vec{g}_1\right|}, \tag{6.81}$$

where we've assumed that $\vec{g}_1^{\dagger}J_N\vec{g}_1 > 0$. If it isn't, then $\tilde{g}_1^{\dagger}J_N\tilde{g}_1$ must be positive, and $\mathcal{N}_{in,1}^{-1}\tilde{g}_1^{\dagger}\hat{\boldsymbol{a}}_{in}$ corresponds to an annihilation operator with its conjugate given by $\mathcal{N}_{in,1}^{-1}\vec{g}_1^{\dagger}\hat{\boldsymbol{a}}_{in}$. To construct the second effective mode, we find a vector, $\vec{l}_2$ that is a linear combination of $\vec{g}_1$, $\tilde{g}_1$ and $\vec{g}_2$, and that J_N-orthogonal to $\vec{g}_1$ and $\tilde{g}_1$:

$$\vec{l}^{\dagger}J_N\vec{g}_1 = 0, \quad \vec{l}^{\dagger}J_N\tilde{g}_1 = 0. \tag{6.82}$$

We then continue this process until we've exhausted all the rows of G.

In Appendix 6.7 (see Eqs. (6.153) and (6.156)), we show that Eq. (6.68) implies that

$$H^{\dagger}J_NT = \left(H^{\dagger}J_NH - J_n\right)B^{-1}G, \tag{6.83}$$

$$TJ_NG^{\dagger} = -HJ_nB^{\dagger}. \tag{6.84}$$

The first of these equations tells us that the n effective output modes in

$$\hat{\boldsymbol{A}}_{out} = \boldsymbol{S}_u^{\dagger}H^{\dagger}J_N\hat{\boldsymbol{a}}_{out} \tag{6.85}$$

depend only on the system modes and $\hat{\boldsymbol{A}}_{in} = \boldsymbol{S}_v^{\dagger}G\hat{\boldsymbol{a}}_{in}$. Similarly to $\boldsymbol{S}_v$, $\boldsymbol{S}_u$ is a $2n \times 2n$ matrix that ensures that

$$\left[\hat{\boldsymbol{A}}_{out}, \hat{\boldsymbol{A}}_{out}^{\dagger}\right] = J_n. \tag{6.86}$$

Note that $\boldsymbol{S}_u$ has to be of the form

$$\boldsymbol{S}_u = \begin{pmatrix} S_u & -K_nS_u^* \end{pmatrix}, \tag{6.87}$$

where S_u is an $N \times N$ matrix, because the bottom half of $\hat{\boldsymbol{A}}_{out}$ has to be the hermitian conjugate of the top half, and J_N introduces a minus sign to the bottom half of $\hat{\boldsymbol{a}}_{in}$.

If we can show that no other effective output modes than $\hat{\boldsymbol{A}}_{out}$ interact with the system modes and $\hat{\boldsymbol{A}}_{in}$, then we've realized the desired narrative of n system modes and n effective optical modes interacting with each other and nothing else. Consider

a mode

$$\hat{O} \equiv \vec{l}^{\dagger} \hat{\boldsymbol{a}}_{out} \tag{6.88}$$

that commutes with $\hat{\boldsymbol{A}}_{out}$, then

$$\vec{l}^{\dagger} J_N^2 H = 0 = \vec{l}^{\dagger} H \tag{6.89}$$

as $\boldsymbol{S}_u$ is invertible. Using Eqs. (6.65) and (6.71), we deduce that $\hat{O}$ doesn't depend on the system modes. Furthermore, $\hat{O}$ depends on the effective input mode $\vec{l}^{\dagger} T^{\dagger} \hat{\boldsymbol{a}}_{in}$, which commutes with $\hat{\boldsymbol{A}}_{in}$ because of Eqs. (6.76) and (6.84).

The system modes and $\hat{\boldsymbol{A}}_{in}$ and $\hat{\boldsymbol{A}}_{out}$ interact in the following way:

$$\left(\begin{array}{c} \hat{\boldsymbol{A}}_{out} \\ \hat{\boldsymbol{b}}_{\tau} \\ \hline \hat{\boldsymbol{C}}_{out} \end{array}\right) = \left(\begin{array}{c|c} M_n & 0 \\ \hline 0 & M_{other} \end{array}\right) \left(\begin{array}{c} \hat{\boldsymbol{A}}_{in} \\ \hat{\boldsymbol{b}}_{0} \\ \hline \hat{\boldsymbol{C}}_{in} \end{array}\right), \tag{6.90}$$

where $\hat{\boldsymbol{C}}_{in}$ and $\hat{\boldsymbol{C}}_{out}$ are effective modes of the environment that commute with $\hat{\boldsymbol{A}}_{in}$ and $\hat{\boldsymbol{A}}_{out}$, respectively. M_{other} tells us how the $\hat{\boldsymbol{C}}_{in}$ evolve into the $\hat{\boldsymbol{C}}_{out}$, and doesn't affect the system modes' dynamics. M_n is

$$M_n = \begin{pmatrix} \boldsymbol{S}_u^{\dagger} H^{\dagger} J_N T J_N G^{\dagger} \boldsymbol{S}_v J_n & \boldsymbol{S}_u^{\dagger} H^{\dagger} J_N H \\ G J_N G^{\dagger} \boldsymbol{S}_v J_n & B \end{pmatrix}, \tag{6.91}$$

where we've used Eqs. (6.65) and (6.71), and we've used that since $\boldsymbol{S}_v^{\dagger} G$ in Eq. (6.76) is a symplectic matrix, we have that

$$\left(\boldsymbol{S}_v^{\dagger} G\right)^{-1} = J_N G^{\dagger} \boldsymbol{S}_v J_n. \tag{6.92}$$

By using Eq. (6.84),we can remove M_n's dependence on T:

$$M_n = \begin{pmatrix} -\boldsymbol{S}_u^{\dagger} H^{\dagger} J_N H J_n B^{\dagger} \boldsymbol{S}_v J_n & \boldsymbol{S}_u^{\dagger} H^{\dagger} J_N H \\ G J_N G^{\dagger} \boldsymbol{S}_v J_n & B \end{pmatrix}. \tag{6.93}$$

Moreover, we can use Eq. (6.154) to eliminate M_n's dependence on G, and Eqs. (6.83) and (6.84) to eliminate M_n's dependence on H. We obtain

$$M_n = \begin{pmatrix} -\boldsymbol{S}_u^{\dagger} \left(J_n - B^{\dagger} J_n B\right) J_n B^{\dagger} \boldsymbol{S}_v J_n & \boldsymbol{S}_u^{\dagger} \left(J_n - B^{\dagger} J_n B\right) \\ \left(J_n - B J_n B^{\dagger}\right) \boldsymbol{S}_v J_n & B \end{pmatrix}. \tag{6.94}$$

Finally, we note that Appendix 6.7 offers an alternative derivation of the effective modes. We derive the effective modes from the constraints they have to satisfy.

6.3.3 Discussion

The effective modes we have developed in this article simplify the structure of the dynamics, as shown in Fig. 6.1. However, in general they do not simplify the structure of the entanglement between the optomechanical system and its environment. We argue for this statement with a simple example.

Consider the hypothetical configuration of effective modes shown in Fig. 6.4, where the system degrees of freedom interact only with the effective modes $\hat{A}_{in}^{(1)}$ through $\hat{A}_{in}^{(n)}$ in a beam-splitter type interaction that swaps the states of the system and effective environment modes. Assume that the initial state of $\hat{b}_1$ through $\hat{b}_n$ is vacuum, so $\hat{A}_{out}^{(1)}$ through $\hat{A}_{out}^{(n)}$ will be in vacuum.

$\hat{b}_1(\tau)$ through $\hat{b}_n(\tau)$ will inherit the state of $\hat{A}_{in}^{(1)}$ through $\hat{A}_{in}^{(n)}$, which could be entangled with $\hat{A}_{in}^{(n+1)}$ through $\hat{A}_{in}^{(N)}$, because the effective modes are, in general, of the form

$$\hat{A}_{in} = \int_0^\tau dt L(t)\,\hat{a}_{in}(t) + \int_0^\tau dt K(t)\,\hat{a}_{in}^\dagger(t), \tag{6.95}$$

where $L(t)$ and $K(t)$ are arbitrary functions.

As a result, even though the system degrees of freedom do not interact with $\hat{A}_{in}^{(n+1)}$ through $\hat{A}_{in}^{(N)}$, they could still be entangled with them. Our formalism does not, in general, say anything about the entanglement of the system of interest with the environment.

6.4 Conclusions

We showed that any linear optomechanical system interacts with a finite number of effective environment modes. If the system has n degrees of freedom, we showed how to construct n effective input modes and n effective output modes that interact with the system. Modes of the environment orthogonal to these effective modes interact with each other and with nothing else.

This article isn't the first to propose such effective modes. For example, Hofer *et al.* used them in Ref. [5] to analyze a protocol for entangling a mechanical center of mass mode with an outgoing effective optical mode, and Galland *et al.* used them in Ref. [3] to analyze a protocol for heralded single-phonon preparation. However, they did not show that no other environment mode interacts with the system or the proposed effective modes. We do so in this article. We also showed that such a

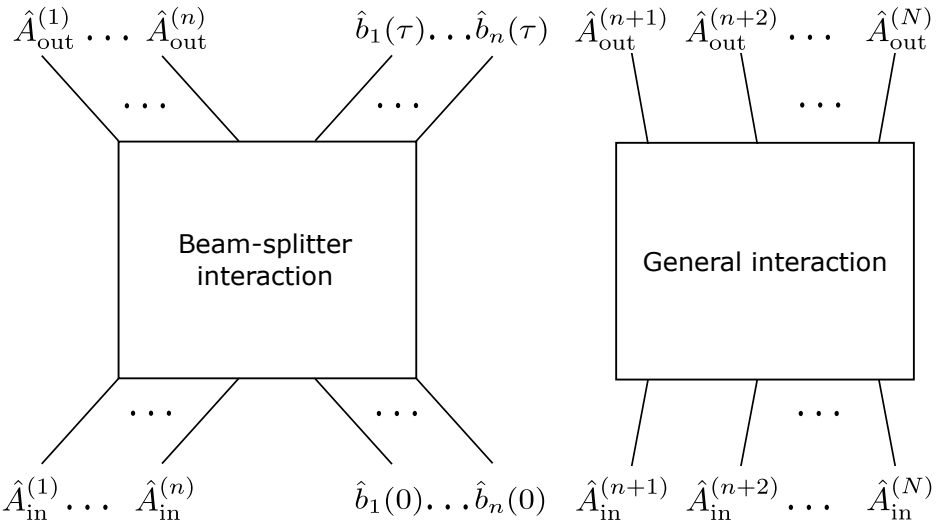

Figure 6.4: A diagram showing a hypothetical beam-splitter interaction that swaps the quantum states of the system degrees of freedom, $\hat{b}_1$ through $\hat{b}_n$, with that of the effective modes it interacts with: $\hat{A}^{(1)}_{in}$ through $\hat{A}^{(n)}_{in}$. The remainder of the effective modes are assumed to have an arbitrary interaction amongst themselves.

formalism can also be used to study heralded phonon states in a cavity driven by two tones.

Finally, we found that the usefulness of our proposed effective modes might be limited to simple setups because the modes are a linear combination of both annihilation and creation ladder operators. As a result, even when the original environment modes are in vacuum, the effective modes' ground state could be a complicated multi-mode squeezed vacuum. For the same reason, the system modes could be entangled with modes orthogonal to the constructed effective modes, even though they do not interact with them. In part II, we will show that a finite number of effective environment modes are entangled with a linear Gaussian optomechanical system.

Acknowledgments

We thank Haixing Miao, Yiqiu Ma, Mikhail Korobko, Farid Khalili, Alessio Serafini, and Klemens Hammerer for useful discussions. This research is supported by NSF grants PHY-1404569 and PHY-1506453, as well as the Institute for Quantum Information and Matter, a Physics Frontier Center.

6.5 Appendix: Constructing effective modes that simplify the dynamics of a cavity optomechanical setup interacting with a single sideband of light

To realize the desired narrative of $\hat{a}_m(0)$ and only a single optical mode interacting with each other and with nothing else, we must satisfy the four conditions implied by Eq. (6.20):

1. $\hat{a}_m(\tau)$ couples to a single input optical mode, which we call $\hat{A}_{in} \equiv \hat{c}_{in}(1)$:
$$\vec{g}^\dagger V \propto \begin{pmatrix} 1 & 0 & \dots & 0 \end{pmatrix}; \tag{6.96}$$
2. Only one outgoing light mode, which we call $\hat{A}_{out} \equiv \hat{c}_{out}(1)$, couples to $\hat{a}_m(0)$:
$$U\vec{h} \propto \begin{pmatrix} 1 & 0 & \dots & 0 \end{pmatrix}^T; \tag{6.97}$$
3. $\hat{A}_{out}$ couples to a single input mode, $\hat{A}_{in}$:
$$\text{First row of } UTV^\dagger \propto \begin{pmatrix} 1 & 0 & \dots & 0 \end{pmatrix}; \tag{6.98}$$
4. Only $\hat{A}_{out}$, and no other outgoing optical mode, couples to $\hat{A}_{in}$:
$$\text{First column of } UTV^\dagger \propto \begin{pmatrix} 1 & 0 & \dots & 0 \end{pmatrix}^T. \tag{6.99}$$

6.5.1 Satisfying the constraints

6.5.1.1 Meeting constraints 1 and 2

If we define
$$U \equiv \begin{pmatrix} \vec{u}_1^\dagger \\ \vdots \\ \vec{u}_N^\dagger \end{pmatrix}, \; V \equiv \begin{pmatrix} \vec{v}_1^\dagger \\ \vdots \\ \vec{v}_N^\dagger \end{pmatrix}, \tag{6.100}$$
we can rewrite constraint (6.97) to
$$U\vec{h} \;=\; \begin{pmatrix} \vec{u}_1^\dagger \vec{h} \\ \vec{u}_2^\dagger \vec{h} \\ \vdots \\ \vec{u}_N^\dagger \vec{h} \end{pmatrix} \propto \begin{pmatrix} 1 \\ 0 \\ \vdots \\ 0 \end{pmatrix}.$$

As a result, we require $\vec{u}_2, ..., \vec{u}_N$ to be orthogonal to $\vec{h}$. Since U is unitary, this implies

$$\vec{u}_1 = e^{i\phi_u}\vec{h}/\left\|\vec{h}\right\|, \tag{6.101}$$

where ϕ_u is a phase factor that we are free to choose, and $\|\vec{h}\|$ is the 2-norm of the vector $\vec{h}$

$$\left\|\vec{h}\right\| \equiv \sqrt{\vec{h}^\dagger\vec{h}}. \tag{6.102}$$

Similarly, if

$$\vec{v}_1 = e^{i\phi_v}\vec{g}/\|\vec{g}\|, \tag{6.103}$$

then the constraint (6.96) is met. ϕ_v is another phase factor that we are free to choose.

6.5.1.2 Meeting constraints 3 and 4

We've fixed $\hat{A}_{in}$ and $\hat{A}_{out}$ up to a phase factor but there are two more constraints to meet. Meeting the third and fourth constraints, given by Eqs. (6.98) and (6.99), require

$$UTV^\dagger = \begin{pmatrix} \vec{u}_1^\dagger T\vec{v}_1 & \dots & \vec{u}_1^\dagger T\vec{v}_N \\ \vdots & \ddots & \vdots \\ \vec{u}_N^\dagger T\vec{v}_1 & \dots & \vec{u}_N^\dagger T\vec{v}_N \end{pmatrix} \tag{6.104}$$

$$= \left(\begin{array}{c|c} \theta & 0 \\ \hline 0 & \text{anything} \end{array}\right) \tag{6.105}$$

for some scalar θ. Consequently, $\vec{v}_2, ..., \vec{v}_N$ must be orthogonal to $T^\dagger\vec{u}_1$, and $\vec{u}_2, ..., \vec{u}_N$ must be orthogonal to $T\vec{v}_1$. Since U and V are unitary matrices, this implies

$$\vec{v}_1 \propto T^\dagger\vec{u}_1, \quad \vec{u}_1 \propto T\vec{v}_1. \tag{6.106}$$

Eqs. (6.101) and (6.103) constrain $\vec{u}_1$ and $\vec{v}_1$ to be proportional to $\vec{h}$ and $\vec{g}$ respectively, so

$$\vec{g} \propto T^\dagger\vec{h}, \tag{6.107}$$

$$\vec{h} \propto T\vec{g}. \tag{6.108}$$

It would seem that Eqs. (6.107-6.108) cannot be met in general. Fortunately, by investigating the structure of M, we will show that $\vec{h}$ and $\vec{g}$ are connected in

such a way that Eqs. (6.107-6.108) can be satisfied. M is not allowed to be an arbitrary matrix because we require that the output light modes be separate degrees of freedom. Specifically, the modes contained in $\boldsymbol{w}$ must have the same commutation relation as those in $\boldsymbol{v}$:

$$\begin{aligned}\left[w_i, w_j^\dagger\right] &= \sum_{k,l=1}^{N} M_{ik} M_{jl}^* \left[v_k, v_l^\dagger\right] \equiv M_{ik}\Omega_{kl}M_{lj}^\dagger \\ &= \left[v_k, v_l^\dagger\right] = \Omega_{ij} \end{aligned} \tag{6.109}$$

where $1 \leq i, j \leq N$, the commutation matrix $\Omega_{kl} \equiv \left[v_k, v_l^\dagger\right]$ is

$$\Omega \equiv \begin{pmatrix} I_N & 0 \\ 0 & -1 \end{pmatrix} \tag{6.110}$$

and I_N is the identity matrix of size N. Eq. (6.109) can be conveniently written in matrix form

$$M\Omega M^\dagger = \Omega. \tag{6.111}$$

Notice that M is a SU(N,1) transformation. In Appendix 6.6, we use this to prove that $\hat{a}_m$ and a single optical mode interact with each other and with nothing else.

By using Eq. (6.111) and the explicit form for M given by Eq. (6.15), we can easily show that

$$TT^\dagger - \vec{h}\vec{h}^\dagger = I_N, \tag{6.112}$$

$$T\vec{g} - \beta^*\vec{h} = 0, \tag{6.113}$$

$$\vec{g}^\dagger\vec{g} - |\beta|^2 = -1. \tag{6.114}$$

Eq. (6.113) automatically satisfies constraint (6.108). As for constraint (6.107), using Eq. (6.112), we have

$$TT^\dagger\vec{h} = \left(I_N + \vec{h}\vec{h}^\dagger\right)\vec{h} = \vec{h}\left(1 + \left\|\vec{h}\right\|^2\right). \tag{6.115}$$

Using Eq. (6.113), we establish that

$$TT^\dagger\vec{h} \propto T\vec{g}. \tag{6.116}$$

T, which encodes the dependence of the outgoing optical fields on the ingoing optical fields, is a causal matrix and so is a lower triangular matrix. Moreover, at

each instant of time, part of the input field at the current time is reflected from the cavity, and so T's diagonal entries are non-zero. Consequently, T is invertible and Eq. (6.116) is equivalent to

$$T^{\dagger}\vec{h} \propto \vec{g}, \tag{6.117}$$

which satisfies the constraint (6.107).

6.6 Appendix: An alternative proof based on group theory

We can prove that the optomechanical system discussed in Sec. 6.2 interacts with a finite number of environment modes with a proof that makes use of group theory. Notice that Ω, defined by Eq. (6.110), has the form of a generalized Minkowski metric, SU(N,1), with N spatial dimensions. Using Eq. (6.111), we conclude that M is a generalized Lorentz transformation. Consequently, M can be decomposed into a pair of pure spatial rotations and a pure boost:

$$M = R_1 B(\chi) R_2, \tag{6.118}$$

where R_1 and R_2 are unitary matrices, and

$$B(\chi) = \begin{pmatrix} \cosh\chi & 0 & \dots & 0 & -e^{i\phi}\sinh\chi \\ 0 & 1 & 0 & \dots & 0 \\ \vdots & \vdots & \ddots & \vdots & \vdots \\ 0 & .... & 0 & 1 & 0 \\ -e^{-i\phi}\sinh\chi & 0 & \dots & 0 & \cosh\chi \end{pmatrix} \tag{6.119}$$

is a boost matrix. Then,

$$\left(R_1^{-1}\boldsymbol{w}\right) = B(\chi)(R_2\boldsymbol{v}), \tag{6.120}$$

and the first mode of $\left(R_1^{-1}\boldsymbol{w}\right)$ is pure two-mode squeezed with the mechanics. Moreover, the first mode of $(R_2\boldsymbol{v})$ and the test mass' center of mass mode interact with each other and with nothing else.

6.7 Appendix: Constructing effective modes that simplify the dynamics of a general optomechanical setup

We will construct a new set of input and output modes, which we call $\hat{c}_{in}$ and $\hat{c}_{out}$ respectively, in such a way that only n input and n output modes interact with the

system. Let these effective modes be linear combinations of the $\hat{a}_{in}$s and $\hat{a}_{out}$s:

$$\hat{\boldsymbol{c}}_{in} \equiv \begin{pmatrix} \hat{c}_{in}(1) \\ \vdots \\ \hat{c}_{in}(N) \\ \hat{c}^{\dagger}_{in}(1) \\ \vdots \\ \hat{c}^{\dagger}_{in}(N) \end{pmatrix} = V\hat{\boldsymbol{a}}_{in}, \tag{6.121}$$

$$\hat{\boldsymbol{c}}_{out} \equiv \begin{pmatrix} \hat{c}_{out}(1) \\ \vdots \\ \hat{c}_{out}(N) \\ \hat{c}^{\dagger}_{out}(1) \\ \vdots \\ \hat{c}^{\dagger}_{out}(N) \end{pmatrix} = U\hat{\boldsymbol{a}}_{out}, \tag{6.122}$$

where U and V are $2N \times 2N$ matrices. To ensure that the $\hat{\boldsymbol{c}}_{out}$ and $\hat{\boldsymbol{c}}_{in}$ are commuting degrees of freedom (just as $\hat{\boldsymbol{a}}_{out}$ and $\hat{\boldsymbol{a}}_{in}$ are), we require

$$UJ_NU^{\dagger} = VJ_NV^{\dagger} = J_N, \tag{6.123}$$

where we've defined J_N in Eq. (6.70). In addition, since the bottom halves of $\hat{\boldsymbol{c}}_{in}$ and $\hat{\boldsymbol{c}}_{out}$ are adjoints of the top halves, the structure of V must be

$$V = \begin{pmatrix} V_1 & V_2 \\ V_2^* & V_1^* \end{pmatrix}. \tag{6.124}$$

$V_1 \in \mathbb{M}_{N\times N}$ contains the contribution of annihilation operators $\hat{a}_{in}$ to $\hat{c}_{in}$, while V_2 contains the contribution of creation operators $\hat{a}^{\dagger}_{in}$ to $\hat{c}_{in}$. An analogous expression holds for the structure of U.

By substituting $\hat{\boldsymbol{c}}_{in}$ and $\hat{\boldsymbol{c}}_{out}$ into Eq. (6.65), we find that they satisfy

$$\begin{pmatrix} \hat{\boldsymbol{c}}_{out} \\ \hat{\boldsymbol{b}}_{\tau} \end{pmatrix} = \begin{pmatrix} UTV^{-1} & UH \\ GV^{-1} & B \end{pmatrix} \begin{pmatrix} \hat{\boldsymbol{c}}_{in} \\ \hat{\boldsymbol{b}}_{0} \end{pmatrix}, \tag{6.125}$$

where

$$V^{-1} = J_NV^{\dagger}J_N. \tag{6.126}$$

6.7.1 The constraints

To achieve the desired narrative of the system modes and only n effective optical modes interacting with each other, we must satisfy four requirements:

1. The modes contained in $\hat{\boldsymbol{b}}_\tau$ couple to only n effective input modes which, without loss of generality, we choose to be $\hat{c}_{in}(1)$ through $\hat{c}_{in}(n)$:

$$GV^{-1} = \left(\begin{array}{cccc|cccc} G_n & 0 & \dots & 0 & K_n G_n^* & 0 & \dots & 0 \end{array} \right), \tag{6.127}$$

   where G_n is of size $2n \times n$, and we've defined K_n in Eq. (6.75).

2. Only n effective output modes, $\hat{c}_{out}(1)$ through $\hat{c}_{out}(n)$, couple to $\hat{\boldsymbol{b}}_0$:

$$UH = \left(\begin{array}{cccc|cccc} H_n^T & 0 & \dots & 0 & \left(H_n^* K_n\right)^T & 0 & \dots & 0 \end{array} \right)^T, \tag{6.128}$$

   where H_n is of size $n \times 2n$.

3. $\hat{c}_{out}(1)$ through $\hat{c}_{out}(n)$ couple only to $\hat{c}_{in}(1)$ through $\hat{c}_{in}(n)$, and to no other effective input mode, so the rows of UTV^{-1} satisfy:

$$\begin{aligned} \text{The first } n \text{ rows} &= \left(\begin{array}{cccc} T_R & 0 & T_S & 0 \end{array} \right), \\ N+1 \text{ to } N+n \text{ rows} &= \left(\begin{array}{cccc} T_S^* & 0 & T_R^* & 0 \end{array} \right), \end{aligned}$$

   where $T_R,\ T_S$ are $n \times n$ matrices.

4. $\hat{c}_{out}(1)$ through $\hat{c}_{out}(n)$, and no other effective output modes, couple to $\hat{c}_{in}(1)$ through $\hat{c}_{in}(n)$, so the columns of UTV^{-1} satisfy:

$$\begin{aligned} \text{The first } n \text{ columns} &= \left(\begin{array}{c} T_R \\ 0 \\ T_S^* \\ 0 \end{array} \right), \\ \text{The } N+1 \text{ to } N+n \text{ columns} &= \left(\begin{array}{c} T_S \\ 0 \\ T_R^* \\ 0 \end{array} \right). \end{aligned}$$

We summarize requirements 3 and 4 by

$$UTV^{-1} = \left(\begin{array}{c|c|c|c} T_R & 0 & T_S & 0 \\ \hline 0 & \text{anything} & 0 & \text{anything} \\ \hline T_S^* & 0 & T_R^* & 0 \\ \hline 0 & \text{anything} & 0 & \text{anything} \end{array}\right). \tag{6.129}$$

6.7.2 Meeting the constraints

To show how to meet requirements (6.127), (6.128) and (6.129), it will be convenient to make the following definitions:

$$U \equiv \left(\begin{array}{c} \vec{u}_1^\dagger \\ \vdots \\ \vec{u}_n^\dagger \\ \hline \tilde{u}_1^\dagger \\ \vdots \\ \tilde{u}_n^\dagger \end{array}\right), \quad V \equiv \left(\begin{array}{c} \vec{v}_1^\dagger \\ \vdots \\ \vec{v}_n^\dagger \\ \hline \tilde{v}_1^\dagger \\ \vdots \\ \tilde{v}_n^\dagger \end{array}\right) \tag{6.130}$$

with the dual vector $\tilde{v}_i$ defined by $K_N \vec{v}_i^*$ (and similarly for $\tilde{u}_i$). U and V have this form because the bottom halves of $\hat{c}_{in}$ and $\hat{c}_{out}$ are adjoints of the upper halves. With these definitions, and using Eq. (6.123), we must have that with respect to the operation

$$\langle \vec{x}, \vec{y} \rangle \equiv \vec{x}^\dagger J_N \vec{y}, \tag{6.131}$$

all the $\vec{v}_j$s and $\tilde{v}_j$s are orthogonal to each other, the $\vec{v}_i$ are normalized to unity and the $\tilde{v}_i$ are normalized to -1. If two vectors are orthogonal to each other with respect to this operation, we will say that they are J_N-orthogonal.

6.7.2.1 Meeting the first and second constraints

The entries of GV^{-1} are

$$\left(\begin{array}{ccc|ccc} \vec{g}_1^\dagger J_N \vec{v}_1 & \dots & \vec{g}_1^\dagger J_N \vec{v}_N & -\vec{g}_1^\dagger J_N \tilde{v}_1 & \dots & -\vec{g}_1^\dagger J_N \tilde{v}_N \\ \vdots & \ddots & \vdots & \vdots & \ddots & \vdots \\ \tilde{g}_n^\dagger J_N \vec{v}_1 & \dots & \tilde{g}_n^\dagger J_N \vec{v}_N & -\tilde{g}_n^\dagger J_N \tilde{v}_1 & \dots & -\tilde{g}_n^\dagger J_N \tilde{v}_N \end{array}\right).$$

Meeting constraint (6.127) means that GV^{-1} would be of the form

$$\left(\begin{array}{ccc|ccc|ccc|ccc} \vec{g}_1^\dagger J_N \vec{v}_1 & \dots & \vec{g}_1^\dagger J_N \vec{v}_n & 0 & \dots & 0 & -\vec{g}_1^\dagger J_N \tilde{v}_1 & \dots & -\vec{g}_1^\dagger J_N \tilde{v}_n & 0 & \dots & 0 \\ \vdots & \ddots & \vdots & \vdots & \ddots & \vdots & \vdots & \ddots & \vdots & \vdots & \ddots & \vdots \\ \tilde{g}_n^\dagger J_N \vec{v}_1 & \dots & \tilde{g}_n^\dagger J_N \vec{v}_n & 0 & \dots & 0 & -\tilde{g}_n^\dagger J_N \tilde{v}_1 & \dots & -\tilde{g}_n^\dagger J_N \tilde{v}_n & 0 & \dots & 0 \end{array}\right).$$

Thus, we require that the $\vec{v}_{n+1}, ..., \vec{v}_N$ and their duals be J_N-orthogonal to the $\vec{g}$s. Since the $\vec{v}$s are J_N-orthogonal to each other and to their duals, a solution is that $\vec{v}_1$ through $\vec{v}_n$ are a linear combination of the $\vec{g}$s:

$$\left(\begin{array}{ccc} \vec{v}_1 & \dots & \vec{v}_n \end{array}\right) = \left(\begin{array}{cccccc} \vec{g}_1 & \dots & \vec{g}_n & \tilde{g}_1 & \dots & \tilde{g}_n \end{array}\right) S_v, \tag{6.132}$$

where S_v^T must be a full rank $n \times 2n$ matrix. The duals of $\vec{v}_1$,...,$\vec{v}_n$ are then given by

$$\left(\begin{array}{ccc} \tilde{v}_1 & \dots & \tilde{v}_n \end{array}\right) = \left(\begin{array}{cccccc} \vec{g}_1 & \dots & \vec{g}_n & \tilde{g}_1 & \dots & \tilde{g}_n \end{array}\right) K_n S_v^*. \tag{6.133}$$

Consequently,

$$\left(\begin{array}{cccccc} \vec{v}_1 & \dots & \vec{v}_n & \tilde{v}_1 & \dots & \tilde{v}_n \end{array}\right) = G^\dagger \boldsymbol{S}_v, \tag{6.134}$$

where

$$\boldsymbol{S}_v \equiv \left(\begin{array}{cc} S_v & K_n S_v^* \end{array}\right) \tag{6.135}$$

is a $2n \times 2n$ invertible matrix.

Similarly, we can show that constraint (6.128) requires

$$\left(\begin{array}{cccccc} \vec{u}_1 & \dots & \vec{u}_n & \tilde{u}_1 & \dots & \tilde{u}_n \end{array}\right) = J_N H \boldsymbol{S}_u \tag{6.136}$$

where

$$\boldsymbol{S}_u \equiv \left(\begin{array}{cc} S_u & -K_n S_u^* \end{array}\right) \tag{6.137}$$

is a $2n \times 2n$ invertible matrix.

6.7.2.2 Meeting the third and fourth constraints

We've fixed the effective input and output modes up to irrelevant phase factors and rotations, but we still need to satisfy Eq. (6.129). Specifically, we would like UTV^{-1}

to be of the form

$$UTV^{-1} \tag{6.138}$$

$$= \left(\begin{array}{ccc|ccc|ccc|ccc} \vec{u}_1^\dagger T J_N \vec{v}_1 & \dots & \vec{u}_1^\dagger T J_N \vec{v}_n & 0 & \dots & 0 & -\vec{u}_1^\dagger T J_N \tilde{v}_1 & \dots & -\vec{u}_1^\dagger T J_N \tilde{v}_n & 0 & \dots & 0 \\ \vdots & \vdots & \vdots & \vdots & \dots & \vdots & \vdots & \vdots & \vdots & \vdots & \dots & \vdots \\ \vec{u}_n^\dagger T J_N \vec{v}_1 & \dots & \vec{u}_n^\dagger T J_N \vec{v}_n & 0 & \dots & 0 & -\vec{u}_n^\dagger T J_N \tilde{v}_1 & \dots & -\vec{u}_n^\dagger T J_N \tilde{v}_n & 0 & \dots & 0 \\ \hline 0 & \dots & 0 & & & & 0 & \dots & 0 & & & \\ \vdots & \dots & \vdots & & \text{anything} & & \vdots & \dots & \vdots & & \text{anything} & \\ 0 & \dots & 0 & & & & 0 & \dots & 0 & & & \\ \hline \tilde{u}_1 T J_N \vec{v}_1 & \dots & \tilde{u}_1 T J_N \vec{v}_n & 0 & \dots & 0 & -\tilde{u}_1 T J_N \tilde{v}_1 & \dots & -\tilde{u}_1^\dagger T J_N \tilde{v}_n & 0 & \dots & 0 \\ \vdots & \vdots & \vdots & \vdots & \dots & \vdots & \vdots & \vdots & \vdots & \vdots & \dots & \vdots \\ \tilde{u}_n^\dagger T J_N \vec{v}_1 & \dots & \tilde{u}_n T J_N \vec{v}_n & 0 & \dots & 0 & -\tilde{u}_n T J_N \tilde{v}_1 & \dots & -\tilde{u}_n T J_N \tilde{v}_n & 0 & \dots & 0 \\ \hline 0 & \dots & 0 & & & & 0 & \dots & 0 & & & \\ \vdots & \dots & \vdots & & \text{anything} & & \vdots & \dots & \vdots & & \text{anything} & \\ 0 & \dots & 0 & & & & 0 & \dots & 0 & & & \end{array}\right).$$

Consequently,

1. We require the upper left blue block to be 0:

$$\begin{aligned} \vec{u}_1^\dagger T J_N \vec{v}_{n+1} &= \dots = \vec{u}_1^\dagger T J_N \vec{v}_N = 0, \\ &\vdots \quad \vdots \quad \vdots \\ \vec{u}_n^\dagger T J_N \vec{v}_{n+1} &= \dots = \vec{u}_n^\dagger T J_N \vec{v}_N = 0, \end{aligned}$$

and so we must have that $\vec{v}_{n+1} \dots \vec{v}_N$ are J_N-orthogonal to the vectors $T\vec{u}_1^\dagger \dots T^\dagger \vec{u}_n$. Since $\vec{v}_1 \dots \vec{v}_n$ and their duals are J_N-orthogonal to $\vec{v}_{n+1} \dots \vec{v}_N$, we want $T^\dagger \vec{u}_i$ for $1 \leq i \leq n$ to be a linear combination of the $\vec{v}_i$s and $\tilde{v}_i$s:

$$T^\dagger \begin{pmatrix} \vec{u}_1 & \dots & \vec{u}_n \end{pmatrix} = \begin{pmatrix} \vec{v}_1 & \dots & \vec{v}_n & \tilde{v}_1 & \dots & \tilde{v}_n \end{pmatrix} R_v, \tag{6.139}$$

where $R_v \in \mathbb{M}_{2n \times n}$. Imposing that the lower blue block be 0 requires

$$\begin{aligned} \tilde{u}_1^\dagger T J_N \vec{v}_{n+1} &= \dots = \tilde{u}_1^\dagger T J_N \vec{v}_N = 0, \\ &\vdots \quad \vdots \quad \vdots \\ \tilde{u}_n^\dagger T J_N \vec{v}_{n+1} &= \dots = \tilde{u}_n^\dagger T J_N \vec{v}_N = 0, \end{aligned}$$

so we must have

$$\begin{aligned} & T^\dagger \begin{pmatrix} \tilde{u}_1 & \dots & \tilde{u}_n \end{pmatrix} \\ = & \begin{pmatrix} \vec{v}_1 & \dots & \vec{v}_n & \tilde{v}_1 & \dots & \tilde{v}_n \end{pmatrix} \tilde{R}_v, \end{aligned} \tag{6.140}$$

where $\tilde{R}_v \in \mathbb{M}_{2n\times n}$ must be equal to

$$\tilde{R}_v = K_n R_v^*. \tag{6.141}$$

Combining Eq. (6.140) with Eq. (6.139), we require

$$T^\dagger \begin{pmatrix} \vec{u}_1 & \dots & \vec{u}_n & \tilde{u}_1 & \dots & \tilde{u}_n \end{pmatrix} \equiv \begin{pmatrix} \vec{v}_1 & \dots & \vec{v}_n & \tilde{v}_1 & \dots & \tilde{v}_n \end{pmatrix} \boldsymbol{R}_v, \tag{6.142}$$

where

$$\boldsymbol{R}_v \equiv \begin{pmatrix} R_v & K_n R_v^* \end{pmatrix} \tag{6.143}$$

must be a $2n \times 2n$ invertible matrix.

2. We require the upper right green block to be 0:

$$\begin{aligned} \vec{u}_1^\dagger T J_N \tilde{v}_{n+1} &= \dots = \vec{u}_1^\dagger T J_N \tilde{v}_N = 0, \\ \vdots & \vdots \quad \vdots \\ \vec{u}_n^\dagger T J_N \tilde{v}_{n+1} &= \dots = \vec{u}_n^\dagger T J_N \tilde{v}_N = 0. \end{aligned}$$

For the lower right green block to be 0, we need

$$\begin{aligned} \tilde{u}_1^\dagger T J_N \tilde{v}_{n+1} &= \dots = \tilde{u}_1^\dagger T J_N \tilde{v}_N = 0, \\ \vdots & \vdots \quad \vdots \\ \tilde{u}_n T J_N \tilde{v}_{n+1} &= \dots = \tilde{u}_n T J_N \tilde{v}_N = 0. \end{aligned}$$

All these constraints are satisfied by Eq. (6.142).

3. We require the upper red block to be 0:

$$\begin{aligned} \vec{u}_{n+1}^\dagger T J_N \vec{v}_1 &= \dots = \vec{u}_N^\dagger T J_N \vec{v}_1 = 0, \\ \vdots & \vdots \quad \vdots \\ \vec{u}_{n+1}^\dagger T J_N \vec{v}_n &= \dots = \vec{u}_N^\dagger T J_N \vec{v}_n = 0. \end{aligned}$$

Thus, we require that the $T J_N \vec{v}_i$s be a linear combination of the $J_N \vec{u}_j$ and $J_N \tilde{u}_j$

for $1 \leq j \leq n$:

$$\begin{aligned} & TJ_N \begin{pmatrix} \vec{v}_1 & \dots & \vec{v}_n \end{pmatrix} \\ = \; & J_N \begin{pmatrix} \vec{u}_1 & \dots & \vec{u}_n & \tilde{u}_1 & \dots & \tilde{u}_n \end{pmatrix} R_u \end{aligned} \tag{6.144}$$

where R_u is $M_{2n\times n}$. Imposing that the lower red block be 0 requires

$$\begin{aligned} \tilde{u}_{n+1} T J_N \vec{v}_1 &= \dots = \tilde{u}_N T J_N \vec{v}_1 = 0, \\ &\vdots \quad \vdots \quad \vdots \\ \tilde{u}_{n+1} T J_N \vec{v}_n &= \dots = \tilde{u}_N T J_N \vec{v}_n = 0. \end{aligned}$$

Eq. (6.144) already satisfies these requirements.

4. We require the upper magenta block to be 0:

$$\begin{aligned} \vec{u}^{\dagger}_{n+1} T J_N \tilde{v}_1 &= \dots = \vec{u}^{\dagger}_N T J_N \tilde{v}_1 = 0. \\ &\vdots \quad \vdots \quad \vdots \\ \vec{u}^{\dagger}_{n+1} T J_N \tilde{v}_n &= \dots = \vec{u}^{\dagger}_N T J_N \tilde{v}_n = 0, \end{aligned}$$

so the $TJ_N\tilde{v}_j$s must be a linear combination of the $J_N\vec{u}_j$ and $J_N\tilde{u}_j$ for $1 \leq j \leq n$:

$$\begin{aligned} & TJ_N \begin{pmatrix} \tilde{v}_1 & \dots & \tilde{v}_n \end{pmatrix} \\ = \; & J_N \begin{pmatrix} \vec{u}_1 & \dots & \vec{u}_n & \tilde{u}_1 & \dots & \tilde{u}_n \end{pmatrix} \tilde{R}_u, \end{aligned} \tag{6.145}$$

where $\tilde{R}_u$ must be equal to $K_n R^*_u$. Combining this constraint with Eq. (6.144), we have

$$\begin{aligned} & TJ_N \begin{pmatrix} \vec{v}_1 & \dots & \vec{v}_n & \tilde{v}_1 & \dots & \tilde{v}_n \end{pmatrix} \\ = \; & J_N \begin{pmatrix} \vec{u}_1 & \dots & \vec{u}_n & \tilde{u}_1 & \dots & \tilde{u}_n \end{pmatrix} \boldsymbol{R}_u, \end{aligned} \tag{6.146}$$

where

$$\boldsymbol{R}_u \equiv \begin{pmatrix} R_u & K_n R^*_u \end{pmatrix} \tag{6.147}$$

must be an invertible $2n \times 2n$ matrix. Imposing that the lower magenta block

be 0 requires

$$\begin{aligned} \tilde{u}_{n+1}^{\dagger} T J_N \tilde{v}_1 &= \ldots. = \tilde{u}_N^{\dagger} T J_N \tilde{v}_1 = 0 \\ &\vdots \quad \vdots \quad \vdots \\ \tilde{u}_{n+1}^{\dagger} T J_N \tilde{v}_{2n} &= \ldots. = \tilde{u}_N^{\dagger} T J_N \tilde{v}_n = 0 \end{aligned}$$

Eq. (6.144) already satisfies these requirements.

Combining constraint (6.142) with constraints (6.134) and (6.136) implies

$$\begin{aligned} & T^{\dagger} J_N \begin{pmatrix} \vec{h}_1 & \ldots & \vec{h}_n & \tilde{h}_1 & \ldots & \tilde{h}_n \end{pmatrix} \boldsymbol{S}_u \\ = & \begin{pmatrix} \vec{g}_1 & \ldots & \vec{g}_n & \tilde{g}_1 & \ldots & \tilde{g}_n \end{pmatrix} \boldsymbol{S}_v \boldsymbol{R}_v. \end{aligned} \tag{6.148}$$

Since $\boldsymbol{S}_u$ is invertible, we rewrite Eq. (6.148) to

$$T^{\dagger} J_N H \equiv G^{\dagger} \boldsymbol{S}_v \boldsymbol{R}_v \boldsymbol{S}_u^{-1}. \tag{6.149}$$

Furthermore, combining constraint (6.146) with constraints (6.134) and (6.136) implies

$$\begin{aligned} & T J_N \begin{pmatrix} \vec{g}_1 & \ldots & \vec{g}_n & \tilde{g}_1 & \ldots & \tilde{g}_n \end{pmatrix} \boldsymbol{S}_v \\ = & J_N \begin{pmatrix} \vec{h}_1 & \ldots & \vec{h}_n & \tilde{h}_1 & \ldots & \tilde{h}_n \end{pmatrix} \boldsymbol{S}_u \boldsymbol{R}_u. \end{aligned} \tag{6.150}$$

Since $\boldsymbol{S}_v$ is invertible, we rewrite Eq. (6.150) to

$$T J_N G^{\dagger} = H \boldsymbol{S}_u \boldsymbol{R}_u \boldsymbol{S}_v^{-1}. \tag{6.151}$$

6.7.2.3 Meeting constraints 3 and 4

Since $\boldsymbol{R}_u$ and $\boldsymbol{R}_v$ are not arbitrary matrices and must be of the form given by Eqs. (6.147) and (6.143) respectively, it would seem that Eq. (6.149) and Eq. (6.151) cannot be met in general. By investigating the structure of M, we will show that H and G are connected in such a way that we can satisfy both Eq. (6.149) and Eq. (6.151).

By substituting Eq. (6.71) into Eq. (6.68), we obtain

$$TJ_NT^\dagger + HJ_nH^\dagger = J_N, \tag{6.152}$$
$$TJ_NG^\dagger + HJ_nB^\dagger = 0, \tag{6.153}$$
$$GJ_NG^\dagger + BJ_nB^\dagger = J_n. \tag{6.154}$$

Eq. (6.153) automatically satisfies constraint (6.151) if

$$\boldsymbol{R}_u = -\boldsymbol{S}_u^{-1} J_n B^\dagger \boldsymbol{S}_v. \tag{6.155}$$

This equality can be met because the RHS of Eq. (6.155) has the same form as $\boldsymbol{R}_u$ in Eq. (6.147).

We can also meet constraint (6.149). We use Eqs. (6.152)-(6.154) to show that the $T^\dagger J_N \vec{h}_i$s are a linear combination of the $\vec{g}$s :

$$T^\dagger J_N H = G^\dagger \left(B^\dagger\right)^{-1} \left(H^\dagger J_N H - J_n\right), \tag{6.156}$$

where we assumed that B is invertible. Thus, we can meet Eq. (6.149) if

$$\boldsymbol{R}_v = \boldsymbol{S}_v^{-1} \left(B^\dagger\right)^{-1} \left(H^\dagger J_N H - J_n\right) \boldsymbol{S}_u. \tag{6.157}$$

Note that the RHS of the above equation can be shown to be of the same form as that of $\boldsymbol{R}_v$ in Eq. (6.143).

In summary, the n effective input modes that the system interacts with are

$$\begin{pmatrix} \hat{c}_{in}(1) \\ \vdots \\ \hat{c}_{in}(n) \end{pmatrix} = \begin{pmatrix} \vec{v}_1 \\ \vdots \\ \vec{v}_n \end{pmatrix} \hat{\boldsymbol{a}}_{in} = S_v^\dagger G \hat{\boldsymbol{a}}_{in}, \tag{6.158}$$

and the n effective output modes are

$$\begin{pmatrix} \hat{c}_{out}(1) \\ \vdots \\ \hat{c}_{out}(n) \end{pmatrix} = \begin{pmatrix} \vec{u}_1 \\ \vdots \\ \vec{u}_n \end{pmatrix} \hat{\boldsymbol{a}}_{out} = S_u^\dagger H^\dagger J_N \hat{\boldsymbol{a}}_{out}, \tag{6.159}$$

where S_u and S_v are $2n \times n$ matrices that need to be picked in such a way that the $\vec{u}$s and $\vec{v}$s are J_N-orthogonal, respectively.

Bibliography

[1] Reed W Andrews, Robert W Peterson, Tom P Purdy, Katarina Cicak, Raymond W Simmonds, Cindy A Regal, and Konrad W Lehnert. Bidirectional and efficient conversion between microwave and optical light. *Nature Physics*, 10(4):321, 2014.

[2] LIGO Scientific Collaboration and Virgo Collaboration. Observation of gravitational waves from a binary black hole merger. *Phys. Rev. Lett.*, 116:061102, Feb 2016.

[3] Christophe Galland, Nicolas Sangouard, Nicolas Piro, Nicolas Gisin, and Tobias J. Kippenberg. Heralded single-phonon preparation, storage, and readout in cavity optomechanics. *Phys. Rev. Lett.*, 112:143602, Apr 2014.

[4] C. W. Gardiner. *Quantum noise : a handbook of Markovian and non-Markovian quantum stochastic methods with applications to quantum optics*. Springer, Berlin New York, 2004.

[5] Sebastian G. Hofer, Witlef Wieczorek, Markus Aspelmeyer, and Klemens Hammerer. Quantum entanglement and teleportation in pulsed cavity optomechanics. *Phys. Rev. A*, 84:052327, Nov 2011.

[6] Sungkun Hong, Ralf Riedinger, Igor Marinković, Andreas Wallucks, Sebastian G. Hofer, Richard A. Norte, Markus Aspelmeyer, and Simon Gröblacher. Hanbury brown and twiss interferometry of single phonons from an optomechanical resonator. *Science*, 2017.

[7] Andreas Kronwald, Florian Marquardt, and Aashish A. Clerk. Arbitrarily large steady-state bosonic squeezing via dissipation. *Phys. Rev. A*, 88:063833, Dec 2013.

[8] Haixing Miao, Stefan Danilishin, and Yanbei Chen. Universal quantum entanglement between an oscillator and continuous fields. *Phys. Rev. A*, 81:052307, May 2010.

[9] Stefan Nimmrichter, Klaus Hornberger, and Klemens Hammerer. Optomechanical sensing of spontaneous wave-function collapse. *Phys. Rev. Lett.*, 113:020405, Jul 2014.

[10] M. R. Vanner, M. Aspelmeyer, and M. S. Kim. Quantum state orthogonalization and a toolset for quantum optomechanical phonon control. *Phys. Rev. Lett.*, 110:010504, Jan 2013.

Chapter 7

EFFECTIVE MODES FOR LINEAR GAUSSIAN OPTOMECHANICS. II. SIMPLIFYING THE ENTANGLEMENT STRUCTURE BETWEEN A SYSTEM AND ITS ENVIRONMENT

Abstract

We show that a general linear optomechanical system with n degrees of freedom, and that is driven by arbitrarily many environment bosonic modes in Gaussian states, is entangled with only n effective environment modes. We provide a cavity optomechanical system as an example, and quantify its entanglement with the environment. We also discuss potential applications. A simple entanglement structure allows us to derive and understand the one-shot quantum Cramer Rao bound in a simple way, and allows to provide bounds on how well we can perform different state-preparation tasks. If we limit the effective modes to consist of only optical modes (which experimentalists can probe), then we cannot make any general statements about the entanglement structure of an optomechanical system with its optical bath. Nonetheless, the correlation between a system and its optical bath has a simple structure. A system with n degrees of freedom is correlated with only n effective optical modes, which in turn are only correlated to another n effective optical modes. This correlation chain continues *ad infinitum*.

7.1 Introduction

The present series of articles explores new bases in which to view linear optomechanical systems driven by environment modes in Gaussian states. The most widely used bases are the time and Fourier bases, which have simple interpretations. For example, the incoming optical bath mode in the time basis, $\hat{a}_{in}(t)$, represents the light mode that interacts with an optomechanical system at time t. We can also assign some meaning to Fourier operators (as defined by the two-photon formalism [3]). Their spectrum represents the strength of fluctuations at a particular frequency. For example, the symmetrized expectation value of $\hat{a}^{\dagger}_{out,2}(\omega)\,\hat{a}_{out,2}(\omega)$, where $\hat{a}_{out,2}(\omega)$ is the outgoing phase-quadrature light operator with frequency ω, characterizes the degree of fluctuations that a homodyne detector would register at the frequency $\omega/2\pi$. Moreover, Fourier operators are useful because they are, at steady state, independent at different frequencies: $\left\langle \hat{a}^{\dagger}_{out,2}(\omega_1)\,\hat{a}_{out,2}(\omega_2)\right\rangle$ for $|\omega_1| \neq |\omega_2|$.

Hofer *et al.* and Galland *et al.* in Refs. [5, 4] constructed a special basis in their analysis of quantum optomechanical engineering protocols. We were intrigued

because it seemed like the optomechanical system they considered, and the effective environment modes they proposed, interact with each other and with nothing else. In part I, we investigated these modes in detail, and showed that they can be generalized: a linear optomechanical system's modes and a finite number of effective environment modes interact with each other and with nothing else. Nonetheless, we cannot in general limit our analysis to these effective modes, because the system could be entangled with effective modes it doesn't interact with. In this article, we will show that an optomechanical system with n degrees of freedom is entangled with only n environment modes.

We will first set up a general optomechanical system, and introduce the notation we will use throughout the article. In Sec. 7.2, we then present the phase-space Schmidt decomposition theorem, which will allow us to directly show that a system with n modes is entangled with n environment modes. We then provide a cavity optomechanical system as an example, and quantify its entanglement with the environment. In Sec. 7.4, we discuss potential applications. If we assume we can measure any environment mode, the simple entanglement structure of a general optomechanical setup makes it easy to understand the one-shot quantum Cramer Rao bound, and obtain bounds on well we can carry out different quantum state preparation tasks. Finally, in Sec. 7.5, we limit our analysis to effective modes that consist of only optical degrees of freedom, because experimentalists can only control and measure such modes. Although we cannot make general statements about the entanglement structure of an optomechanical system with its optical bath, we show that the correlation structure can be reduced to a 'chain'. A system with n degrees of freedom is correlated with only n effective optical modes, which in turn are only correlated to another n effective optical modes. The chain continues *ad infinitum*.

7.2 Setup and notation

Consider the general optomechanical system shown in Fig. 7.1. It consists of n degrees of freedom with corresponding quadratures

$$(\hat{x}_1,\ \hat{p}_1),\ \ldots,\ (\hat{x}_n,\ \hat{p}_n)\,. \tag{7.1}$$

This system interacts with an environment consisting of m bosonic fields through a linear (*i.e.* quadratic) Hamiltonian. We label the ladder operators corresponding to the degrees of freedom of each field by $\hat{a}_j^{(i)}$, where $1 \leq i \leq m$ labels the field and j (generally a continuous variable) indexes a particular harmonic oscillator of that field. To simplify the analysis in this article, we will take the discrete time limit of

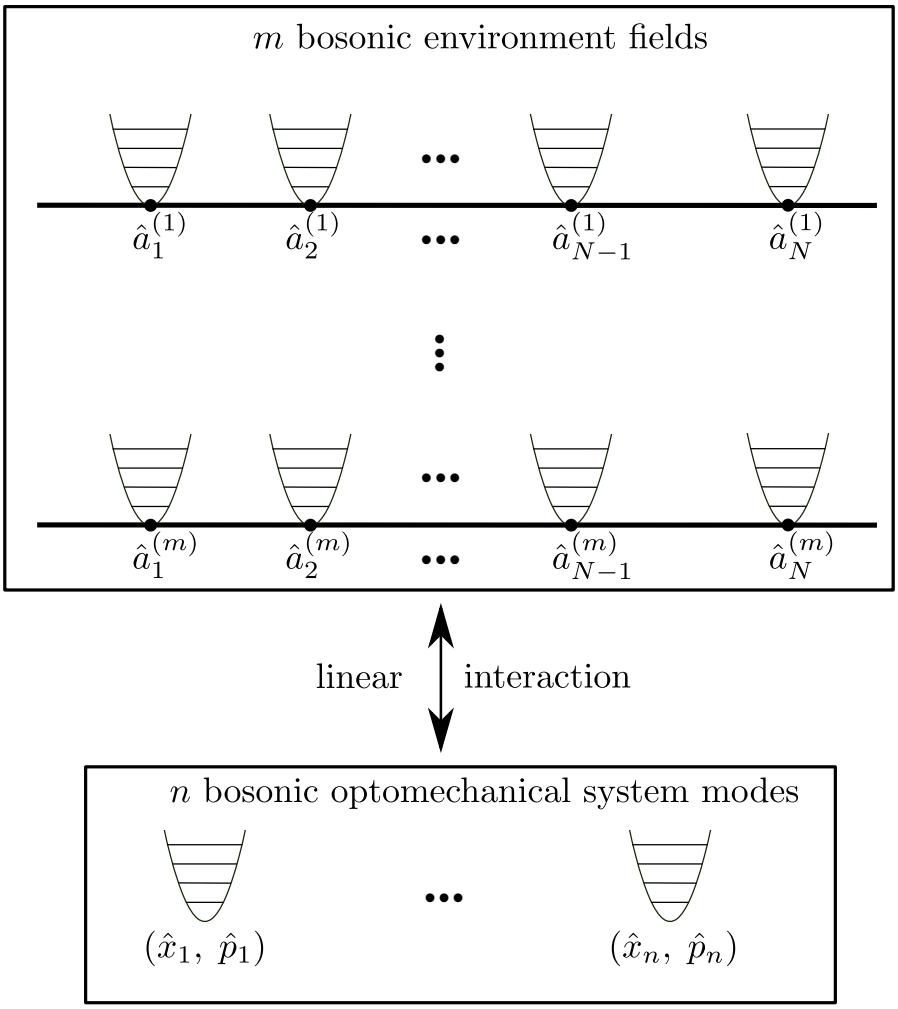

Figure 7.1: General optomechanical setup with n degrees of freedom interacting with m bosonic environment fields.

the dynamics by dividing the length of an experiment, τ, into N time steps of length $dt = \tau/N$. The limit $N \to \infty$ can be taken at the end of our analysis.

It will be convenient to normalize all operators such that their commutator is equal to $2i$. Denote the vector of dimensionless system quadratures by

$$\boldsymbol{v}_{sys} = \begin{pmatrix} \tilde{x}_1 & \tilde{p}_1 & \dots & \tilde{x}_n & \tilde{p}_n \end{pmatrix}^T . \tag{7.2}$$

$\boldsymbol{v}_{sys}$'s commutation matrix is

$$\left[\boldsymbol{v}_{sys}, \boldsymbol{v}_{sys}^T\right] = 2\begin{pmatrix} \sigma_y & 0 & 0 \\ 0 & \ddots & 0 \\ 0 & 0 & \sigma_y \end{pmatrix} \equiv 2i\Omega_{sys} \tag{7.3}$$

where σ_y is the $y-$Pauli matrix

$$\sigma_y = \begin{pmatrix} 0 & i \\ -i & 0 \end{pmatrix}, \tag{7.4}$$

and Ω_{sys} is

$$\Omega_{sys} = \bigoplus_{i=1}^{n} \begin{pmatrix} 0 & 1 \\ -1 & 0 \end{pmatrix}. \tag{7.5}$$

Similarly, we denote the vector of dimensionless environment quadratures by

$$\boldsymbol{v}_{env} = \begin{pmatrix} \boldsymbol{v}_{env,1} \\ \vdots \\ \boldsymbol{v}_{env,N} \end{pmatrix}, \tag{7.6}$$

$$\boldsymbol{v}_{env,j} = \begin{pmatrix} \tilde{a}^{(j)}_{1,1} & \tilde{a}^{(j)}_{1,2} & \tilde{a}^{(j)}_{2,1} & \tilde{a}^{(j)}_{2,2} & \dots & \tilde{a}^{(j)}_{N,1} & \tilde{a}^{(j)}_{N,2} \end{pmatrix}^T, \tag{7.7}$$

for $j = 1...m$. $\tilde{a}^{(i)}_{j,1}$ and $\tilde{a}^{(i)}_{j,2}$ are two orthogonal quadratures of the jth degree of freedom of the ith field:

$$\tilde{a}^{(i)}_{j,1} \equiv \frac{\tilde{a}^{(i)}_j + \left(\tilde{a}^{(i)}_j\right)^\dagger}{\sqrt{2}}, \quad \tilde{a}^{(i)}_{j,2} \equiv \frac{\tilde{a}^{(i)}_j - \left(\tilde{a}^{(i)}_j\right)^\dagger}{i\sqrt{2}}, \tag{7.8}$$

where $i = 1, ...m$ and $j = 1...N$. $\boldsymbol{v}_{env}$'s commutation matrix is

$$\left[\boldsymbol{v}_{env}, \boldsymbol{v}^T_{env}\right] = 2i\Omega_{env} \tag{7.9}$$

where similarly to Ω_{sys}, Ω_{env} is the direct sum of $m \times N$ σ_y/i. We combine $\boldsymbol{v}_{sys}$ and $\boldsymbol{v}_{env}$ into a vector $\boldsymbol{v}$:

$$\boldsymbol{v} \equiv \begin{pmatrix} \boldsymbol{v}_{sys} \\ \boldsymbol{v}_{env} \end{pmatrix}, \quad \left[\boldsymbol{v}, \boldsymbol{v}^T\right] \equiv 2i\Omega_{tot}, \tag{7.10}$$

where

$$\Omega_{tot} \equiv \begin{pmatrix} \Omega_{sys} & 0 \\ 0 & \Omega_{env} \end{pmatrix}. \tag{7.11}$$

For example, consider a cavity optomechanical setup with $n = 2$ modes, which we show in Fig. 7.2. $\tilde{x}_1$ and $\tilde{p}_1$ are the normalized center of mass position and

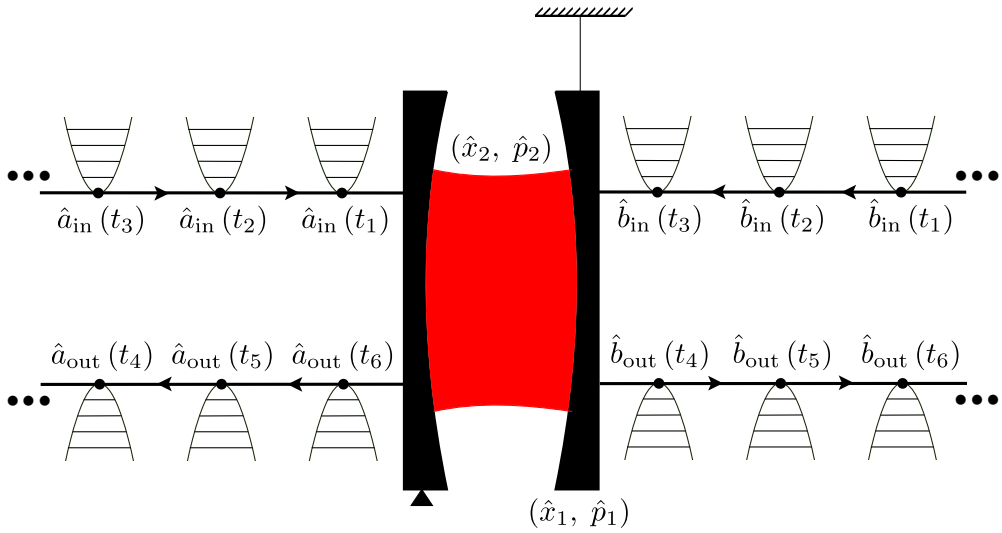

Figure 7.2: A cavity optomechanical setup. A test mass' center of mass position with corresponding quadratures $(\hat{x}_1,\ \hat{p}_1)$ is driven by the thermal bath field operators $\hat{b}_{in}\,(t)$. The cavity field with corresponding quadratures $(\hat{x}_2,\ \hat{p}_2)$ is driven by the optical field operators $\hat{a}_{in}\,(t)$. $\hat{a}_{in}\,(t)$ and $\hat{b}_{in}\,(t)$ then evolve into $\hat{a}_{out}\,(t)$ and $\hat{b}_{out}\,(t)$, respectively.

momentum operators of a test mass with resonant frequency ω_m and mass m

$$\tilde{x}_1 = \frac{\sqrt{2}\hat{x}_1}{\Delta x_{zp}}, \quad \tilde{p}_1 = \frac{\sqrt{2}\hat{p}_1}{\Delta p_{zp}}, \tag{7.12}$$

where

$$\Delta x_{zp} = \sqrt{\frac{\hbar}{2m\omega_m}}, \quad \Delta p_{zp} = \sqrt{\frac{\hbar m\omega_m}{2}}. \tag{7.13}$$

$\tilde{x}_2$ and $\tilde{p}_2$ are proportional to the amplitude and phase quadratures of the cavity field

$$\tilde{x}_2 = \hat{x}_2\sqrt{2}. \quad \tilde{p}_2 = \hat{p}_2\sqrt{2}. \tag{7.14}$$

The environment consists of the input optical field $\hat{a}_{in}\,(t)$ and its time-evolved counterpart $\hat{a}_{out}\,(t)$, and of the thermal bath field $\hat{b}_{in}\,(t)$ and its time-evolved counterpart $\hat{b}_{out}\,(t)$.

7.3 Entanglement structure

The phase-space Schmidt decomposition theorem [2, 1] allows to simplify the entanglement structure of a generic optomechanical system. We first state the theorem, and then show how its direct application simplifies the state of an optomechanical setup with n degrees of freedom to a collection of n independent two-mode squeezed

system-environment pairs (and the rest of the effective environment modes would be in vacuum). Finally, we quantify the entanglement of a cavity optomechanical setup with its environment.

7.3.1 Phase-space decomposition theorem

Because we assume that the dynamics are linear and that the environment is initially in a Gaussian state (which includes thermal states), the joint system-environment's quantum state, $|\Psi(t)\rangle$, is eventually pure and Gaussian for $t \gg t_i$ where t_i is the initial time of the experiment. As a result, $|\Psi(t)\rangle$ is fully characterized by its mean, and by its covariance matrix V. We will also assume that initially $\langle \boldsymbol{v} \rangle = 0$ which guarantees that for $t \gg t_i$, $\langle \boldsymbol{v}(t) \rangle \approx 0$. As a result, $|\Psi(t)\rangle$'s Wigner function is of the form

$$W(\vec{\nu}, t) = \frac{1}{\sqrt{\det(2\pi V(t))}} \exp\left(-\frac{1}{2}\vec{\nu}^T V(t)^{-1}\,\vec{\nu}\right), \tag{7.15}$$

where $\vec{\nu}$ is a real vector of the same dimension as $\boldsymbol{v}$, defined in Eq. (7.10), and $\vec{\nu}$'s ith entry, for $i = 1...n$, corresponds to the degree of freedom in the ith entry of $\boldsymbol{v}$. $V(t)$ is of the covariance matrix for $\boldsymbol{v}$

$$V(t) \;=\; \left\langle \boldsymbol{v}\boldsymbol{v}^T \right\rangle_s = \begin{pmatrix} \sigma_{sys}(t) & \sigma_c^T(t) \\ \sigma_c(t) & \sigma_{env}(t) \end{pmatrix} \tag{7.16}$$

where σ_{sys} is the system's covariance matrix, σ_{env} the environment's covariance matrix, and σ_c the cross-correlation between them:

$$\sigma_{sys}(t) \;\equiv\; \left\langle \boldsymbol{v}_{sys}\boldsymbol{v}_{sys}^T \right\rangle_s, \tag{7.17}$$

$$\sigma_c(t) \;\equiv\; \left\langle \boldsymbol{v}_{env}\boldsymbol{v}_{sys}^T \right\rangle_s, \tag{7.18}$$

$$\sigma_{env}(t) \;\equiv\; \left\langle \boldsymbol{v}_{env}\boldsymbol{v}_{env}^T \right\rangle_s, \tag{7.19}$$

where

$$\left\langle \hat{o}\hat{l} \right\rangle_s \equiv \left\langle \hat{o}\hat{l} + \hat{l}\hat{o} \right\rangle/2 \tag{7.20}$$

denotes a symmetric expectation over $|\Psi(t)\rangle$.

The phase-space Schmidt decomposition theorem [2, 1] states that we can substantially simplify the structure of V by choosing a different basis than $\boldsymbol{v}_{sys}$ for the n system modes and a different basis than $\boldsymbol{v}_{env}$ for the environment modes. In this new basis, all effective environment modes, except n of them, are in vacuum. The n environment modes that are not in vacuum are each in a two-mode squeezed state with an effective system mode.

Denote the new basis of system and environment modes by

$$\boldsymbol{w}_{sys} \equiv \begin{pmatrix} \hat{s}_{1,1} & \hat{s}_{1,2} & \dots & \hat{s}_{n,1} & \hat{s}_{n,2} \end{pmatrix}^T, \tag{7.21}$$

$$\boldsymbol{w} \equiv \begin{pmatrix} \boldsymbol{w}_{sys} \\ \boldsymbol{w}_{opt} \end{pmatrix}, \tag{7.22}$$

$$\boldsymbol{w}_{env} \equiv \begin{pmatrix} \hat{e}_{1,1} & \hat{e}_{1,2} & \hat{e}_{2,1} & \hat{e}_{2,2} & \dots \end{pmatrix}^T. \tag{7.23}$$

We choose the modes in $\boldsymbol{w}$ in such a way that they are linear combinations of the modes in $\boldsymbol{v}$:

$$\boldsymbol{w} = M\boldsymbol{v}, \quad M \equiv \begin{pmatrix} M_{sys} & 0 \\ 0 & M_{env} \end{pmatrix}. \tag{7.24}$$

Moreover, we constrain $\boldsymbol{w}$ to satisfy the same commutation relation as $\boldsymbol{v}$:

$$\left[\boldsymbol{w}, \boldsymbol{w}^T\right] = \left[\boldsymbol{v}, \boldsymbol{v}^T\right] = 2i\Omega_{tot}. \tag{7.25}$$

Using Eq. (8.44), Eq. (8.45) implies that $M\Omega_{tot}M^T = \Omega_{tot}$. Matrices that satisfy such a relation are called symplectic matrices. Similarly, we can also show that M_{sys} and M_{env} are symplectic matrices.

The theorem states that there exists an M such that

$$V_{\boldsymbol{w}} \equiv \left\langle \boldsymbol{w}\boldsymbol{w}^T \right\rangle_s = MVM^T \equiv \begin{pmatrix} C & S & 0 \\ S & C & 0 \\ 0 & 0 & I \end{pmatrix}, \tag{7.26}$$

$$C \equiv \begin{pmatrix} C_1 & 0 & \dots & 0 \\ 0 & C_2 & \dots & 0 \\ \vdots & \vdots & \ddots & 0 \\ 0 & 0 & \dots & C_n \end{pmatrix}, \quad C_k \equiv \begin{pmatrix} \nu_k & 0 \\ 0 & \nu_k \end{pmatrix}, \tag{7.27}$$

$$S \equiv \begin{pmatrix} S_1 & 0 & \dots & 0 \\ 0 & S_2 & \dots & 0 \\ \vdots & \vdots & \ddots & 0 \\ 0 & 0 & \dots & S_n \end{pmatrix}, \tag{7.28}$$

$$S_k \equiv \begin{pmatrix} \sqrt{\nu_k^2 - 1} & 0 \\ 0 & -\sqrt{\nu_k^2 - 1} \end{pmatrix}, \tag{7.29}$$

where I is the identity matrix, $\nu_k \geq 1$ and $1 \leq k \leq n$. In addition, notice that M_{sys}

is the symplectic diagonalizing matrix for σ_{sys}:

$$M_{sys}\sigma_{sys}M_{sys}^T = C, \tag{7.30}$$

so the ν_i for $1 \leq i \leq n$ are the symplectic eigenvalues of σ_{sys}. The Williamson theorem guarantees the existence of an M_{sys} that diagonalizes σ_{sys} into C [7].

7.3.2 A collection of two-mode squeezed states

The structure of $V_{\boldsymbol{w}}$ in Eq. (8.47) indicates that the system is entangled with only n effective environment modes. In particular, each of the effective modes described by $\boldsymbol{w}_{sys}$ forms a two-mode squeezed state with a mode in $\boldsymbol{w}_{env}$. This can directly be seen by forming the covariance matrix of one of the system effective degrees of freedom, say $\left(\hat{s}_{i,1},\ \hat{s}_{i.2}\right)$ for $1 \leq i \leq n$, with its correlated effective environment counterpart $\left(\hat{e}_{i,1},\ \hat{e}_{i,2}\right)$:

$$\sigma_i = \left\langle \begin{pmatrix} \hat{s}_{i,1} \\ \hat{s}_{i,2} \end{pmatrix} \begin{pmatrix} \hat{e}_{i,1} & \hat{e}_{i,2} \end{pmatrix} \right\rangle_s \tag{7.31}$$

$$= \begin{pmatrix} \nu_i & 0 & \lambda_i & 0 \\ 0 & \nu_i & 0 & -\lambda_i \\ \lambda_i & 0 & \nu_i & 0 \\ 0 & -\lambda_i & 0 & \nu_i \end{pmatrix}, \tag{7.32}$$

$$\lambda_i \equiv \sqrt{\nu_i^2 - 1}. \tag{7.33}$$

σ_i indicates that the modes $\hat{s}_i$ and $\hat{e}_i$ are two-mode squeezed of degree r_i where

$$\cosh 2r_i = \nu_i, \tag{7.34}$$

as we show in Fig. 7.3.

Because the system-environment state is Gaussian, we can quantify the entanglement between each effective system mode and its entangled effective environment partner. Consider the joint density matrix of such a pair, $\rho^{(i)}_{sys-env}$ where $i = 1 \ldots n$. Since $\rho^{(i)}_{sys-env}$ is Gaussian, it is separable if and only if its partial transpose with respect to the system is positive semidefinite. This is called the Peres–Horodecki criterion. Say σ_i, given by Eq. (7.31), is the covariance matrix associated with $\rho^{(i)}_{sys-env}$, then

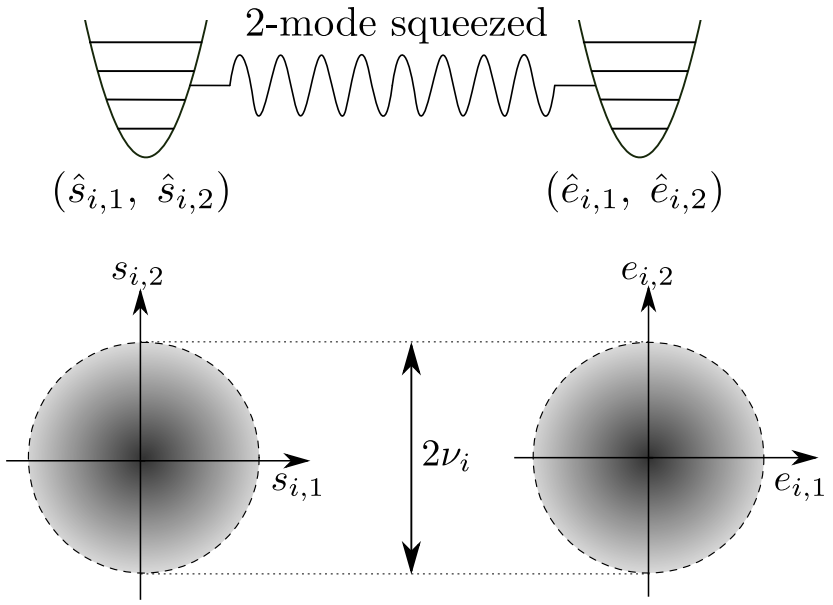

Figure 7.3: Two-mode squeezing between the modes $\hat{s}_i$ and $\hat{e}_i$ for $1 \leq i \leq n$. The bottom two graphs show the phase space distribution of both of these modes.

the Peres–Horodecki criterion is equivalent to

$$\tilde{\sigma}_i + \begin{pmatrix} \sigma_y & 0 \\ 0 & \sigma_y \end{pmatrix} \geq 0, \tag{7.35}$$

where

$$\tilde{\sigma}_i = \theta \sigma_i \theta, \quad \theta = \begin{pmatrix} 1 & 0 & 0 & 0 \\ 0 & -1 & 0 & 0 \\ 0 & 0 & 1 & 0 \\ 0 & 0 & 0 & 1 \end{pmatrix} \tag{7.36}$$

is the covariance matrix of the partial transpose of $\rho^{(i)}_{sys-env}$ with respect to one of its degrees of freedom.

The logarithmic negativity quantifies the violation of the Peres–Horodecki criterion. For the two-mode Gaussian state characterized by the covariance matrix $\tilde{\sigma}_i$, where $i = 1 \ldots n$, the logarithmic negativity is

$$\mathcal{N}_i = \max\left\{0, -\log \tilde{\eta}^{(i)}_-\right\} \tag{7.37}$$

$$= \max\left\{0, -\frac{1}{2}\log\left(2\nu_i\left(\nu_i - \sqrt{\nu_i^2 - 1}\right) - 1\right)\right\} \tag{7.38}$$

where $\tilde{\eta}^{(i)}_-$ is the smallest symplectic eigenvalue of $\tilde{\sigma}_i$.

7.3.3 An example

Consider the cavity optomechanical setup shown in Fig. 7.2. The test mass' free Hamiltonian is

$$\hat{H}_{tm} = \frac{\hat{P}^2}{2m} + \frac{1}{2} m\omega_m \hat{x}^2, \tag{7.39}$$

where m and ω_m are the test mass' mass and resonant frequency, respectively. The test mass interacts with the cavity field via the interaction Hamiltonian

$$\hat{H}_{int} = \hbar G_0 \hat{x}_1 \hat{a}^\dagger \hat{a}, \tag{7.40}$$

where $\hat{x}_1$ is the test mass' center of mass position, $\hat{a}$ is the cavity field annihilation operator (associated with the quadratures $\hat{x}_2$ and $\hat{p}_2$), and G_0 is the bare optomechanical coupling

$$G_0 = \frac{\omega_c}{L}. \tag{7.41}$$

ω_c is a resonant frequency of the cavity, which we assume is equal to the driving laser's frequency ω_0, and L is the length of the cavity. Moreover, the cavity field is lossy and is driven by a coherent laser:

$$\hat{H}_{drive} = i\hbar\sqrt{2\gamma}\left(\hat{a}_{in}\hat{a}^\dagger - \text{h.c.}\right) \tag{7.42}$$

where $\hat{a}_{in}$ is the ingoing optical field as is shown in Fig. 7.2.

At steady state, we can calculate $\sigma_{sys}^{s.s.}$, which is the covariance matrix for the normalized test mass modes, $\tilde{x}_1$ and $\tilde{p}_1$ as given by Eq. (7.12), and the normalized cavity modes, $\tilde{x}_2$ and $\tilde{p}_2$ as given by Eq. (7.14). Their linearized equations of motion, in an interaction picture with the cavity's free Hamiltonian and the $\hbar\omega_0$ part of the external continuum removed, and in terms of dimensionless parameters only

are

$$\partial_{\tilde{t}}\tilde{x}_1(\tilde{t}) = \tilde{p}_1(\tilde{t}), \tag{7.43}$$

$$\partial_{\tilde{t}}\tilde{p}_1(\tilde{t}) = -\tilde{x}_1(\tilde{t}) - \frac{\tilde{p}_1(\tilde{t})}{Q} - \sqrt{2}\Gamma_\Theta^{3/2}\tilde{x}_2(\tilde{t}) + \frac{\sqrt{2n}}{Q}\tilde{b}_{th}(\tilde{t}), \tag{7.44}$$

$$\partial_{\tilde{t}}\tilde{x}_2(\tilde{t}) = -\frac{\tilde{x}_2(\tilde{t})}{\Gamma_m} + \sqrt{\frac{2}{\Gamma_m}}\tilde{a}_{1,in}(\tilde{t}), \tag{7.45}$$

$$\partial_{\tilde{t}}\tilde{p}_2(\tilde{t}) = -\sqrt{2}\Gamma_\Theta^{3/2}\tilde{x}_1(\tilde{t}) - \frac{\tilde{p}_2(\tilde{t})}{\Gamma_m} + \sqrt{\frac{2}{\Gamma_m}}\tilde{a}_{2,in}(\tilde{t}), \tag{7.46}$$

where $\tilde{t} = t \times \omega_m$, ω_m and Q are the resonant frequency and the quality factor of the test mass, respectively, and

$$\Gamma_m = \frac{\omega_m}{\gamma}, \tag{7.47}$$

$$n = \frac{k_B T}{\hbar\omega_m}, \tag{7.48}$$

$$\Gamma_\Theta^3 = \frac{\hbar g^2/m}{\omega_m^3}, \quad g \equiv G_0\bar{a}. \tag{7.49}$$

Γ_m indicates the quality of the cavity, n is thermal occupation of the test mass and Γ_Θ is a measure of the measurement strength. $\bar{a}$ is the amplitude of the light inside the cavity

$$\bar{a} \equiv \langle\hat{a}\rangle = \sqrt{2I_0/\gamma\hbar\omega_0}. \tag{7.50}$$

We've assumed that the driving laser light has an intensity of I_0, and is in a coherent state. Moreover,

$$\tilde{a}_{1,in}(t) = \frac{\hat{a}_{1,in}(t)}{\sqrt{\omega_m}}, \quad \tilde{a}_{2,in}(t) = \frac{\hat{a}_{2,in}(t)}{\sqrt{\omega_m}} \tag{7.51}$$

are the dimensionless amplitude and phase quadratures of the incoming light. $\tilde{b}_{th}(t)$ is the dimensionless thermal fluctuation operator. Its correlation function is

$$\left\langle \tilde{b}_{th}(\tilde{t})\,\tilde{b}_{th}(\tilde{t}')\right\rangle = Q \times \delta(\tilde{t} - \tilde{t}'). \tag{7.52}$$

Following a procedure similar to that of section I of the supplemental information of [4], we can analytically calculate the system's steady state covariance matrix from Eqs. (7.43-7.46). The results are shown in Appendix 8.7.

By obtaining the symplectic eigenvalues of Eq. (7.102), we can use Eq. (7.38) to quantify how entangled each of the correlated system-environment pairs are. For $n = 1/2$ and $Q = 10^6$, we show the results in Fig. 7.4. Notice that the larger Γ_m and Γ_Θ are, the more information the environment contains about the optomechanical system. Moreover, most of the information about the optomechanical system leaks to only one environment mode as $\mathcal{N}_1 \ll \mathcal{N}_2$

7.4 Applications

If we assume that we can measure any environment mode then the phase-space Schmidt decomposition theorem makes it easy to devise optimal strategies for sensing and quantum state preparation tasks. Although this assumption is unrealistic, it provides us with tractable toy models that we can draw lessons from. Moreover, it allows us to obtain bounds on how well we can perform a certain task, and allows us to explore large parameter regimes with little computational cost.

We will first discuss how the phase-space Schmidt decomposition theorem provides a fresh and illuminating perspective on the one-shot Quantum Cramer-Rao Bound (QCRB). We then discuss two state preparation tasks: squeezing a system operator as much as possible, and maximizing the entanglement between two modes of our system.

7.4.1 Connection to one-shot QCRB

Simplifying the entanglement structure of a general optomechanical setup allows us to understand, in a simple way, the QCRB for estimating a single parameter. The QCRB sets fundamental limits on how well quantum systems can estimate classical parameters. For a single parameter θ that is coupled linearly to a quantum system through an operator $\hat{O}$:

$$\hat{H}_{int} = -\hat{O}\theta\delta(t), \tag{7.53}$$

the minimum estimation error on θ is (see Chapter 2 of [8])

$$\sigma_{\theta\theta}^{QCRB} = \frac{\hbar^2}{4\left\langle\psi\middle|\hat{O}^2\middle|\psi\right\rangle}, \tag{7.54}$$

where we've assumed that $\left\langle\psi\middle|\hat{O}\middle|\psi\right\rangle = 0$ and $|\psi\rangle$ is the state of the system at time t.

We will show how a linear optomechanical system can always saturate the bound $\sigma_{\theta\theta}^{QCRB}$ if we assume that we can measure any commuting environment modes. The proof will be both mathematically and conceptually simple because the phase-space decomposition theorem allows us to simplify the seemingly complicated joint

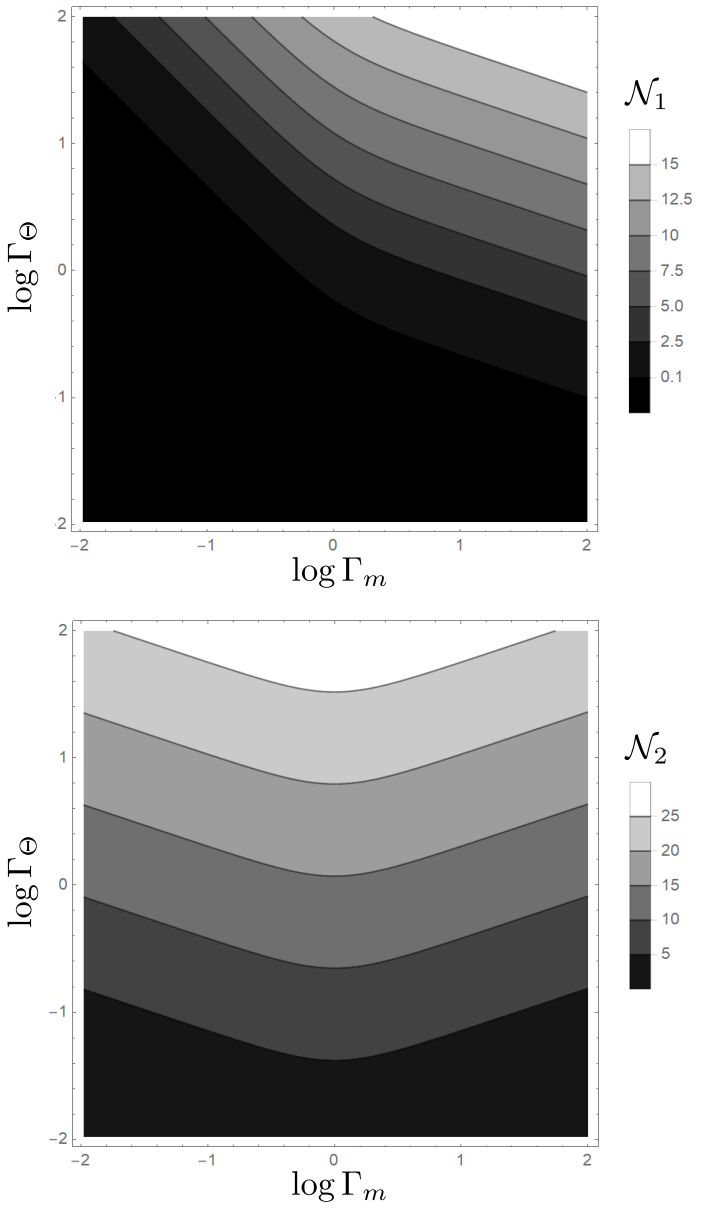

Figure 7.4: Quantifying the entanglement between the cavity optomechanical setup shown in Fig. 7.2 with its environment. $\mathcal{N}_1$ ($\mathcal{N}_2$) is the logarithmic negativity of the first (second) diagonalizing symplectic system mode of Eq. (7.102) with the effective environment mode it is correlated with. We set the equilibrium thermal occupation of the test mass to $1/2$ and the quality factor to 10^6.

quantum state of the system and environment to a collection of pure 2-mode squeezed states as shown in Fig. 7.3.

First, we decompose $\hat{O}$ into the system's symplectic modes:

$$\hat{O} = \sum_{i=1}^{n} \beta_i \left(\cos\phi_i \hat{s}_{i,1} + \sin\phi_i \hat{s}_{i,2} \right) \tag{7.55}$$

where the βs and ϕs are real, and we've assumed that our system has n degrees of freedom. Since each $\hat{s}_{i,1}$ and $\hat{s}_{i,2}$ pair, for $i = 1...n$, are independent and occupy a symmetric thermal state (see Fig. 7.3), we can redefine each $\hat{s}_{i,1}$ and $\hat{s}_{i,2}$ to

$$\hat{s}_{i,1}\big|_{new} = \cos\phi_i \hat{s}_{i,1} + \sin\phi_i \hat{s}_{i,2}, \tag{7.56}$$

$$\hat{s}_{i,2}\big|_{new} = \sin\phi_i \hat{s}_{i,1} + \cos\phi_i \hat{s}_{i,2}, \tag{7.57}$$

which allows us to conveniently express $\hat{O}$ as

$$\hat{O} = \sum_{i=1}^{n} \beta_i \hat{s}_{i,1}. \tag{7.58}$$

Substituting Eq. (7.58) into Eq. (7.53), we obtain

$$\hat{H}_{int} = \sum_{i=1}^{n} \hat{s}_{i,1} \times (\beta_i \theta)\, \delta(t). \tag{7.59}$$

Each $\hat{s}_{i,1}$, for $i = 1...n$, is independent from all the others, lives in a different Hilbert space, and interacts with an environment mode, $\hat{e}_i$, that is only correlated with $\hat{s}_i$ and with nothing else. As a result, it is better to think of the signal θ not as appearing in a single system, but as appearing in n distinct systems. Since each system is composed of a single optomechanical degree of freedom that is coupled to a single environment mode in a simple way, we can apply the same strategy for extracting the optimal amount of information about θ to all n systems.

Consider for example the ith system. Because of the simple correlation structure between $\hat{s}_i$ and $\hat{e}_i$, given by Eq. (7.31), any system observable can be estimated with the same accuracy: $1/\nu_i$. So the optimal estimation strategy is to maximize the signal. Consider the ith term in $\hat{H}_{int}$: $\beta_i \hat{s}_{i,1} \theta \delta(t)$. Such an interaction leaves $\hat{s}_{i,1}$ unchanged but shifts any operator $\hat{l}$ that doesn't commute with $\hat{s}_{i,1}$ by

$$\frac{i}{\hbar} \beta_i \left[\hat{l}, \hat{s}_{i,1} \right] \theta. \tag{7.60}$$

Since $\hat{s}_{i,2}$ is the conjugate operator of $\hat{s}_{i,1}$, it maximizes the norm of $\left[\hat{l}, \hat{s}_{i,1}\right]$ to 2. Consequently, $\hat{s}_{i,2}$ will be the operator we will estimate as accurately as possible.

As indicated by Eq. (7.31), $\hat{s}_{i,2}$ is correlated with only one environment operator, $\hat{e}_{i,2}$. Therefore, we measure $\hat{e}_{i,2}$ to estimate $\hat{s}_{i,2}$. The conditional mean of $\hat{s}_{i,2}$ given that $\hat{e}_{i,2}$ is measured to be e_i is

$$\left\langle \hat{s}_{i,2} \right\rangle_c = \frac{\left\langle \hat{s}_{i,2}\hat{e}_{i,2} \right\rangle_s}{\left\langle \hat{s}_{i,2}^2 \right\rangle} e_i = \frac{-\sqrt{\nu_i^2 - 1}}{\nu_i} e_i \tag{7.61}$$

and the conditional variance of $\hat{s}_{i,2}$ is

$$\left\langle \hat{s}_{i,2}^2 \right\rangle_c = \left\langle \hat{s}_{i,2}^2 \right\rangle - \frac{\left(\left\langle \hat{s}_{i,2}\hat{e}_{i,2} \right\rangle_s \right)^2}{\left\langle \hat{s}_{i,2}^2 \right\rangle} = \frac{1}{\nu_i}, \tag{7.62}$$

where we've used Eq. (7.31). As a result, for the ith system, our optimal unbiased estimator of θ is

$$Z_i = \left(\frac{i}{\hbar} \beta_i \left[\hat{s}_{i,2}, \hat{s}_{i,1} \right] \right)^{-1} \left\langle \hat{s}_{i,2} \right\rangle_c = \frac{\hbar}{2\beta_i} \left\langle \hat{s}_{i,2} \right\rangle_c \tag{7.63}$$

with a squared error of

$$\Delta Z_i = \frac{\hbar^2}{4\beta_i^2} \frac{1}{\nu_i}. \tag{7.64}$$

We now have a collection of n estimators, Z_1 through Z_n, for θ. We will optimally combine them to obtain a single estimator for θ:

$$Z = \left(\sum_{i=1}^{n} \alpha_i \right)^{-1} \sum_{i=1}^{n} \alpha_i Z_i \tag{7.65}$$

and choose the α_i such that ΔZ is minimized. We obtain, by using that Z_1 through Z_n are independent, that the minimum error is

$$\Delta Z_{min} = \left(\sum_{i=1}^{n} \Delta Z_i^{-1} \right)^{-1} \tag{7.66}$$

$$= \frac{\hbar^2}{4} \frac{1}{\sum_{i=1}^{n} \beta_i^2 \nu_i} = \frac{\hbar^2}{4 \left\langle \hat{O}^2 \right\rangle}, \tag{7.67}$$

where we've used Eqs. (7.58) and (7.64), and that $\left\langle \hat{s}_{i,1}^2 \right\rangle = \nu_i$. Notice that ΔZ_{min} is just the one-shot QCRB given by Eq. (7.54)

7.4.2 Optimal squeezing

Ref. [6] discusses a strategy for optimally choosing the optical environment modes to measure in order to squeeze a system operator as much as possible. Nonetheless, the phase-space Schmidt decomposition theorem makes it easy to obtain a bound on how well a particular operator can be squeezed, and allows us to efficiently sweep large parameter regimes.

Consider a system operator $\hat{O}$. We will obtain a lower bound on how well we can squeeze $\hat{O}$. To do so, we first project $\hat{O}$ onto the system symplectic basis:

$$\hat{O} = \vec{\alpha}.\boldsymbol{w}_{sys} \tag{7.68}$$

$$= \sum_{i=1}^{n} \left(\alpha_{i,1}\hat{s}_{i,1} + \alpha_{i,2}\hat{s}_{i,2}\right) \tag{7.69}$$

where we've assumed that our optomechanical system has n degrees of freedom. Each operator in the sum (8.52) is correlated with only a single environment mode. Therefore, optimally squeezing $\hat{O}$ is equivalent to optimally squeezing n operators with a simple correlation structure. This structure can be made trivial by normalizing each term in Eq. (8.52):

$$\hat{O} = \sum_{i=1}^{n} \sqrt{\alpha_{i,1}^2 + \alpha_{i,2}^2} \frac{\alpha_{i,1}\hat{s}_{i,1} + \alpha_{i,2}\hat{s}_{i,2}}{\sqrt{\alpha_{i,1}^2 + \alpha_{i,2}^2}}. \tag{7.70}$$

We then simplify each term in the sum (8.53) by using the same argument that we employed in Sec. 7.4.1. Since each $\hat{s}_{i,1}$ and $\hat{s}_{i,2}$ pair, for $i = 1...n$, are independent and occupy a symmetric thermal state, we can redefine each

$$\frac{\alpha_{i,1}\hat{s}_{i,1} + \alpha_{i,2}\hat{s}_{i,2}}{\sqrt{\alpha_{i,1}^2 + \alpha_{i,2}^2}} \tag{7.71}$$

to be $\hat{s}_{i,1}$. Therefore,

$$\hat{O} = \sum_{i=1}^{n} \sqrt{\alpha_{i,1}^2 + \alpha_{i,2}^2}\hat{s}_{i,1}. \tag{7.72}$$

By measuring $\hat{e}_{i,1}$, $\hat{s}_{i,1}$ is squeezed to $\left\langle \hat{s}_{i,1}^2 \right\rangle = 1/\nu_i$ so $\hat{O}$ can be optimally squeezing

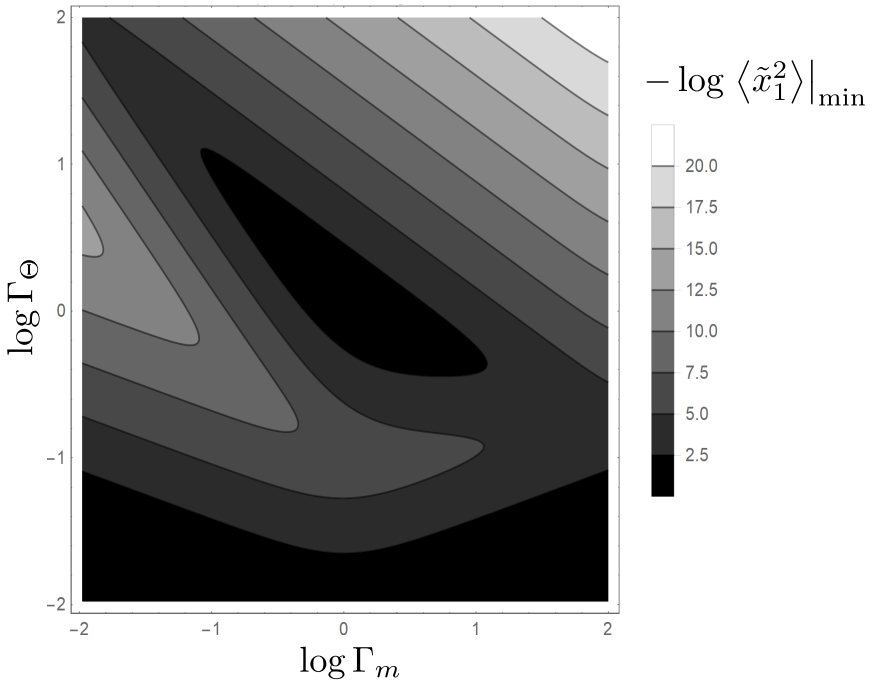

Figure 7.5: Optimal squeezing of $\tilde{x}_1$ for $Q = 10^6$, $n = 1/2$ and different values of Γ_m and Γ_Θ for the cavity optomechanical setup discussed in Sec. 7.3.3. We remind the reader that $\tilde{x}_1 = \sqrt{2}\hat{x}_1/\Delta x_{zp}$, where $\hat{x}_1$ is the center of mass position of the test mass, and $\Delta x_{zp} = \sqrt{\hbar/2m\omega_m}$ is its zero-point fluctuations. Moreover, Q is the test mass' quality factor, n is the test mass' thermal occupation number, $\Gamma_m = \omega_m/\gamma$, where γ is the cavity decay rate, and Γ_Θ is the dimensionless measurement strength $\Gamma_\Theta^3 = \hbar g^2/(m\omega_m^3)$.

to

$$\langle \hat{O}^2 \rangle|_{min} = \sum_{i=1}^{n} \frac{\alpha_{i,1}^2 + \alpha_{i,2}^2}{\nu_i}. \tag{7.73}$$

We provide an example based on the cavity optomechanical setup that we discussed in Sec. 7.3.3. In Fig. 7.5, we show how well the test mass' center of mass position can be squeezed for $Q = 10^6$, $n = 1/2$ and different values of the measurement strength and the cavity decay rate.

7.4.3 Maximizing the entanglement between the cavity and test mass

The phase-space Schmidt decomposition theorem makes it easy to determine how to measure the environment in order to optimally enhance the entanglement between two subsystems in an optomechanical setup. Without the theorem and because quantum mechanics allows us to only measure commuting observables, for each of the infinitely many environment modes that the system seems correlated with, we

have to pick the optimal quadrature to measure. As a result, the optimization problem is not tractable unless we apply the theorem and reduce the number of environmental modes to consider to just n (the number of system degrees of freedom). We illustrate this with an example based on the cavity optomechanical setup discussed in Sec. 7.3.3. We will show how to measure the environment in order to optimally enhance the entanglement between the cavity and the test mass' center of mass degree of freedom.

In the symplectic basis, the total system-environment covariance matrix has the simple structure

$$\sigma = \begin{pmatrix} \sigma_{sys} & \sigma_c \\ \sigma_c & \sigma_{env} \end{pmatrix} \tag{7.74}$$

where

$$\sigma_{sys} = \sigma_{env} = \begin{pmatrix} \nu_1 & & & \\ & \nu_1 & & \\ & & \nu_2 & \\ & & & \nu_2 \end{pmatrix},$$

$$\sigma_c = \begin{pmatrix} \sqrt{\nu_1^2 - 1} & & & \\ & -\sqrt{\nu_1^2 - 1} & & \\ & & \sqrt{\nu_2^2 - 1} & \\ & & & -\sqrt{\nu_2^2 - 1} \end{pmatrix}.$$

The system is coupled to only two environment modes, but we are limited to measuring commuting observables. Therefore, we are limited to measuring the two observables

$$\hat{e}_{\theta_1} \equiv \cos\theta_1 \hat{e}_{1,1} + \sin\theta_2 \hat{e}_{1,2}, \tag{7.75}$$

$$\hat{e}_{\theta_2} \equiv \cos\theta_2 \hat{e}_{2,1} + \sin\theta_2 \hat{e}_{2,2}, \tag{7.76}$$

where θ_1 and θ_2 are real numbers.

If we measured $\hat{e}_{\theta_1}$ and $\hat{e}_{\theta_2}$ then the conditional covariance matrix of the system is

$$\begin{aligned}\sigma(\theta_1,\theta_2) &= \sigma_{sys} \\ &\quad -\sigma_c^T(\theta_1,\theta_2)\begin{pmatrix} \nu_1 & \\ & \nu_2 \end{pmatrix}^{-1}\sigma_c(\theta_1,\theta_2) \qquad (7.77)\\ &= \begin{pmatrix} \sigma_1(\theta_1,\theta_2) & 0 \\ 0 & \sigma_2(\theta_1,\theta_2) \end{pmatrix}, \qquad (7.78)\end{aligned}$$

where and we've used that since $\hat{e}_{1,1}$ and $\hat{e}_{2,2}$ are independent

$$\Delta e_{\theta_1} = \nu_1 \qquad \Delta e_{\theta_2} = \nu_2, \tag{7.79}$$

and $\sigma_c(\theta_1,\theta_2)$ is the cross-correlation matrix between the system symplectic modes, $\boldsymbol{w}_{sys}$, and $\hat{e}_{\theta_1}$ and $\hat{e}_{\theta_2}$:

$$\begin{aligned}\sigma_c^T(\theta_1,\theta_2) &= \left\langle \boldsymbol{w}_{sys}\begin{pmatrix}\hat{e}_{\theta_1}\\ \hat{e}_{\theta_2}\end{pmatrix}\right\rangle \qquad (7.80)\\ &= \begin{pmatrix} \cos\theta_1\sqrt{\nu_1^2-1} & \\ -\sin\theta_1\sqrt{\nu_1^2-1} & \\ & \cos\theta_2\sqrt{\nu_2^2-1} \\ & -\sin\theta_2\sqrt{\nu_2^2-1}\end{pmatrix}. \qquad (7.81)\end{aligned}$$

Moreover, we can calculate that

$$\begin{aligned}\sigma_i(\theta_1,\theta_2) &= \begin{pmatrix} \nu_i - \cos^2\theta_i\xi_i & -\cos\theta_i\sin\theta_i\xi_i \\ -\cos\theta_i\sin\theta_i\xi_i & \nu_i - \sin^2\theta_i\xi_i\end{pmatrix} \qquad (7.82)\\ \xi_i &\equiv \nu_i^{-1}\left(\nu_i^2-1\right) \qquad (7.83)\end{aligned}$$

for $i = 1, 2$.

Finally, to evaluate the entanglement between the cavity and the test mass, we first revert back to the original basis, $\boldsymbol{v}_{sys}$ (which consists of the test mass' center of mass position and momentum, and the cavity's phase and amplitude quadratures):

$$\boldsymbol{v}_{sys} = M^{-1}\boldsymbol{w}_{sys}, \tag{7.84}$$

where M is the symplectic transformation that diagonalizes the system's covariance matrix in the $\boldsymbol{v}_{sys}$ basis. We then evaluate the logarithmic negativity, given by Eq.

(7.37), of the system covariant matrix in the $\boldsymbol{v}_{sys}$ basis, $M^{-1}\sigma_c(\theta_1,\theta_2)\left(M^{-1}\right)^T$, for different values of θ_1 and θ_2. We show example results for different values of Γ_m and Γ_Θ in Fig. 7.6. Notice that choosing the right commuting observables to measure is crucial and can result in a much stronger entanglement between the cavity and the test mass.

7.5 Correlation structure of a system with its optical bath

In optomechanics experiments, we can only control and measure optical degrees of freedom. We will show that even when we restrict effective environment modes to consist of only optical degrees of freedom, a system with n degrees of freedom is correlated with only n effective optical modes. However, these optical modes are correlated with the remainder of the optical bath. As a result, the system-environment quantum state doesn't reduce to a collection of n independent two-mode squeezed states. Instead, we will show that a system with n degrees of freedom is correlated with only n effective optical modes, which in turn are only correlated to another n effective optical modes. This correlation chain continues *ad infinitum,* as is illustrated in Fig. 7.7.

7.5.1 Bipartite and multipartite entanglement

We denote the outgoing optical modes' quadratures by

$$\hat{a}^{(i)}_{out,1}(t),\ \hat{a}^{(i)}_{out,2}(t) \tag{7.85}$$

where $i \in \mathbb{Z}^+$ indexes a particular optical field (there could be multiple optical fields interacting with the system) and $t \in \mathbb{R}$ represents time. Let us re-write each of the effective environment modes $\hat{e}_i$, which are the ladder operators corresponding to the quadratures given by Eq. (7.23), in a way that separates the optical environmental degrees of freedom:

$$\hat{e}_i = \alpha_i \hat{o}_i + \beta_i \hat{t}_i, \tag{7.86}$$

where $\hat{o}_i$ ($\hat{t}_i$) is a ladder operator that lives in the Hilbert space spanned by the optical modes $\hat{a}^{(i)}_{out,1}(t)$ and $\hat{a}^{(i)}_{out,2}(t)$ (non-optical environment modes). The α_i and β_i are complex numbers that we'd choose in such a way that $\left[\hat{o}_i,\ \hat{o}_i^\dagger\right] = 1$ and $\left[\hat{t}_i,\ \hat{t}_i^\dagger\right] = 1$, respectively.

We'll first show that only $\hat{o}_1$ through $\hat{o}_n$ are correlated with the system, where n is the number of system degrees of freedom. As we showed in Section 7.3, the system is only correlated with $\hat{e}_i$ and $\hat{e}_i^\dagger$ for $i = 1 \ldots n$, and so any mode that is orthogonal

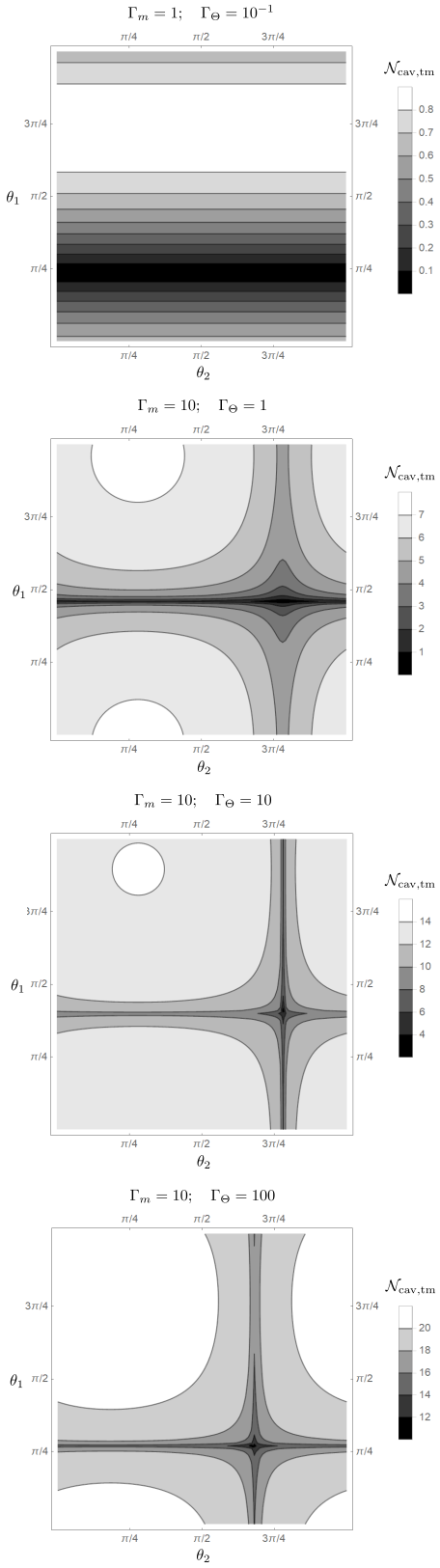

Figure 7.6: The logarithmic negativity between the cavity and the test mass for the setup discussed in Sec. 7.3.3, if we were to measure the two environment modes $\hat{e}_{\theta_1}$ and $\hat{e}_{\theta_2}$ given by Eqs. (7.75-7.76).

to (*i.e.* commutes with) them is not correlated with the system. An arbitrary optical mode $\hat{l}$ that is orthogonal to $\hat{o}_1$ through $\hat{o}_n$ will necessarily be orthogonal with $\hat{e}_1$ through $\hat{e}_n$, because $\hat{l}$ lives in a different Hilbert space than the $\hat{t}_i$.

We'll now show that, in general, the system is not only entangled with $\hat{o}_1 \dots \hat{o}_n$. Let $\boldsymbol{o}_c$ contain the effective optical modes that are correlated with the system:

$$\boldsymbol{o}_c = \begin{pmatrix} \hat{o}_{1,1} & \hat{o}_{1,2} & \dots & \hat{o}_{n,1} & \hat{o}_{n,2} \end{pmatrix}^T, \tag{7.87}$$

where $\hat{o}_{i,1}$ and $\hat{o}_{i,2}$ are the two quadratures associated with the mode $\hat{o}_i$ for $i = 1 \dots n$. Moreover, let $\boldsymbol{o}_i$ contain the modes that are independent from the system:

$$\boldsymbol{o}_i = \begin{pmatrix} \hat{o}_{n+1,1} & \hat{o}_{n+1,2} & \dots & \hat{o}_{N_{opt},1} & \hat{o}_{N_{opt},2} \end{pmatrix}^T. \tag{7.88}$$

N_{opt} is the total number of outgoing optical modes that interact with the system. The limit $N_{opt} \to \infty$ can be taken at any time. The covariance matrix between the system and the optical bath, as expressed in the effective modes basis $\{\hat{o}_i\}$, is

$$V_{sys-opt} = \begin{pmatrix} V_{sys} & C^T & 0 \\ C & B_1 & D^T \\ 0 & D & B_2 \end{pmatrix}, \tag{7.89}$$

where $V_{sys} = \left\langle \boldsymbol{v}_{sys} \boldsymbol{v}_{sys}^T \right\rangle_s$ with $\boldsymbol{v}_{sys}$ given by Eq. (7.2), $B_1 = \left\langle \boldsymbol{o}_c \boldsymbol{o}_c^T \right\rangle_s$, $C = \left\langle \boldsymbol{o}_c \boldsymbol{v}_{sys}^T \right\rangle_s$ and $B_2 = \left\langle \boldsymbol{o}_i \boldsymbol{o}_i^T \right\rangle_s$. $D = \left\langle \boldsymbol{o}_i \boldsymbol{o}_c^T \right\rangle_s$ is in general non-zero, and so the system is not only entangled with $\boldsymbol{o}_c$.

7.5.2 A correlation chain

We can further simplify the structure of Eq. (7.89) by choosing a new basis, $\tilde{\boldsymbol{o}}_i$, for the modes in $\boldsymbol{o}_i$ in such a way that they'd be independent from the modes in $\boldsymbol{o}_c$ (*i.e.* $\left\langle \boldsymbol{o}_i \boldsymbol{o}_c^T \right\rangle_s = 0$).

Let

$$\tilde{\boldsymbol{o}}_i = S_{opt-opt} \boldsymbol{o}_i, \tag{7.90}$$

where

$$S_{opt-opt} \equiv \begin{pmatrix} \vec{s}_{1,1}^T \\ \vec{s}_{1,2}^T \\ \vdots \\ \vec{s}_{\tilde{N},1}^T \\ \vec{s}_{\tilde{N},2}^T \end{pmatrix}, \tag{7.91}$$

is a symplectic transformation ensuring that $\left[\tilde{\boldsymbol{o}}_i, \tilde{\boldsymbol{o}}_i^T\right] = \left[\boldsymbol{o}_i, \boldsymbol{o}_i^T\right]$, and

$$\tilde{N} \equiv N_{opt} - n. \tag{7.92}$$

Moreover, we'll write D, which is defined in Eq. (7.89), in the following way:

$$D \equiv \begin{pmatrix} \vec{d}_{1,1} & \vec{d}_{1,2} & \dots & \vec{d}_{n,1} & \vec{d}_{n,2} \end{pmatrix}, \tag{7.93}$$

then

$$S_{opt-opt} D = \begin{pmatrix} \vec{s}_{1,1}^T \vec{d}_{1,1} & \vec{s}_{1,1}^T \vec{d}_{1,2} & \dots & \vec{s}_{1,1}^T \vec{d}_{n,1} & \vec{s}_{1,2}^T \vec{d}_{n,2} \\ \vec{s}_{1,2}^T \vec{d}_{1,1} & \vec{s}_{1,2}^T \vec{d}_{1,2} & \dots & \vec{s}_{1,2}^T \vec{d}_{n,1} & \vec{s}_{1,2}^T \vec{d}_{n,2} \\ \vdots & \vdots & \vdots & \vdots & \vdots \\ \vec{s}_{\tilde{N},1}^T \vec{d}_{1,1} & \vec{s}_{\tilde{N},1}^T \vec{d}_{1,2} & \dots & \vec{s}_{\tilde{N},1}^T \vec{d}_{n,1} & \vec{s}_{\tilde{N},2}^T \vec{d}_{n,2} \\ \vec{s}_{\tilde{N},2}^T \vec{d}_{1,1} & \vec{s}_{\tilde{N},2}^T \vec{d}_{1,2} & \dots & \vec{s}_{\tilde{N},2}^T \vec{d}_{n,1} & \vec{s}_{\tilde{N},2}^T \vec{d}_{n,2} \end{pmatrix}. \tag{7.94}$$

Fir $\boldsymbol{o}_c$ to be correlated with only n modes in $\tilde{\boldsymbol{o}}_i$, we would like this matrix to be of the form

$$\begin{pmatrix} \vec{s}_{1,1}^T \vec{d}_{1,1} & \vec{s}_{1,1}^T \vec{d}_{1,2} & \dots & \vec{s}_{1,1}^T \vec{d}_{n,1} & \vec{s}_{1,2}^T \vec{d}_{n,2} \\ \vdots & \vdots & \vdots & \vdots & \vdots \\ \vec{s}_{n,2}^T \vec{d}_{1,1} & \vec{s}_{n,2}^T \vec{d}_{1,2} & \dots & \vec{s}_{n,2}^T \vec{d}_{n,1} & \vec{s}_{n,,2}^T \vec{d}_{n,2} \\ 0 & 0 & 0 & 0 & 0 \\ \vdots & \vdots & \vdots & \vdots & \vdots \\ 0 & 0 & 0 & 0 & 0 \end{pmatrix}. \tag{7.95}$$

Eq. (7.95) indicates that $\vec{s}_{n+1,1}$, $\vec{s}_{n+1,2}$ through $\vec{s}_{\tilde{N},1}$, $\vec{s}_{\tilde{N},2}$ must be orthogonal to the vector space spanned by the $\vec{d}_{1,1}$, $\vec{d}_{1,2}$ through $\vec{d}_{n,1}$, $\vec{d}_{n,2}$. Since $S_{opt-opt}$ is a symplectic matrix then all the $\vec{s}_{n+1,1}$, $\vec{s}_{n+1,2}$ through $\vec{s}_{\tilde{N},1}$, $\vec{s}_{\tilde{N},2}$ are orthogonal to $\Omega_{opt}\vec{s}_{1,1}$, $\Omega_{opt}\vec{s}_{1,2}$ through $\Omega_{opt}\vec{s}_{n,1}, \Omega_{opt}\vec{s}_{n,2}$, where Ω_{opt} is a direct sum of $\tilde{N}$ σ_y/i. Therefore if D is full rank, then we can achieve Eq. (7.95) by constraining the $\vec{s}_{1,1}$, $\vec{s}_{1,2}$ through $\vec{s}_{n,1}$, $\vec{s}_{n,2}$ to span the entirety of the vector space spanned by $\Omega_{opt}\vec{d}_{1,1}$, $\Omega_{opt}\vec{d}_{1,2}$ through $\Omega_{opt}\vec{d}_{n,1}$, $\Omega_{opt}\vec{d}_{n,2}$. If we do so then, for example,

$$\vec{s}_{\tilde{N},1}^T \vec{d}_{1,1} = \vec{s}_{\tilde{N},1}^T \left(\sum_{i=1}^{n} \left(\alpha_i \Omega_{opt} \vec{s}_{i,1} + \beta_i \Omega_{opt} \vec{s}_{i,2} \right) \right), \tag{7.96}$$

is equal to 0.

The covariance matrix between the system and the effective optical modes

$$\begin{pmatrix} \boldsymbol{o}_c \\ \tilde{\boldsymbol{o}}_i \end{pmatrix} \equiv \begin{pmatrix} \boldsymbol{o}_c \\ \tilde{\boldsymbol{o}}_c \\ \tilde{\tilde{\boldsymbol{o}}}_i \end{pmatrix}, \tag{7.97}$$

where $\tilde{\boldsymbol{o}}_c$ contains the first n modes of $\tilde{\boldsymbol{o}}_i$, is

$$V_{sys-\widetilde{opt}} = \begin{pmatrix} V_{sys} & C^T & 0 & 0 \\ C & B_1 & C_2^T & 0 \\ 0 & C_2 & B_2 & \left\langle \tilde{\boldsymbol{o}}_c \tilde{\tilde{\boldsymbol{o}}}_i^T \right\rangle_s \\ 0 & 0 & \left\langle \tilde{\tilde{\boldsymbol{o}}}_i \tilde{\boldsymbol{o}}_c^T \right\rangle_s & \left\langle \tilde{\tilde{\boldsymbol{o}}}_i \tilde{\tilde{\boldsymbol{o}}}_i^T \right\rangle_s \end{pmatrix}. \tag{7.98}$$

B_2 is equal to $\left\langle \tilde{\boldsymbol{o}}_c \tilde{\boldsymbol{o}}_c^T \right\rangle_s$ and C_2 is equal to $\left\langle \tilde{\boldsymbol{o}}_c \boldsymbol{o}_c^T \right\rangle_s$.

The same arguments that we used to simplify the structure of D in Eq. (7.89) allow us to simplify the structure of $\left\langle \tilde{\tilde{\boldsymbol{o}}}_i \tilde{\boldsymbol{o}}_c^T \right\rangle_s$ in Eq. (7.98). This process can be repeated until we express the optical modes in a basis that transforms the covariance matrix between the sytem and the optical into a tri-block-diagonal form:

$$V_{sys-new\ opt} = \begin{pmatrix} V_{sys} & C^T & 0 & 0 & 0 \\ C & B_1 & C_2^T & 0 & 0 \\ 0 & C_2 & B_2 & \ddots & 0 \\ 0 & 0 & \ddots & \ddots & C_{\tilde{N}/n}^T \\ 0 & 0 & 0 & C_{\tilde{N}/n} & B_{\tilde{N}/n} \end{pmatrix}, \tag{7.99}$$

where all the non-zero blocks are $n \times n$ matrices.

Eq. (7.98) tell us that, at its simplest, the correlation structure of an optomechanical system with its optical bath reduces to a chain of n-partite correlated systems, as is shown in Fig. 7.7. It also tells us that an optomechanical system is bipartite entangled with at most n optical modes, but could be multipartite-entangled with an infinite number of modes.

7.6 Conclusions

We've shown that a general linear optomechanical system with n degrees of freedom, and that is driven by arbitrarily many environment modes in Gaussian states, is entangled with only n effective environment modes. Simplifying the entanglement structure to this extent allows us to better understand how information leaks from the system to the environment. For a cavity optomechanical system at resonance,

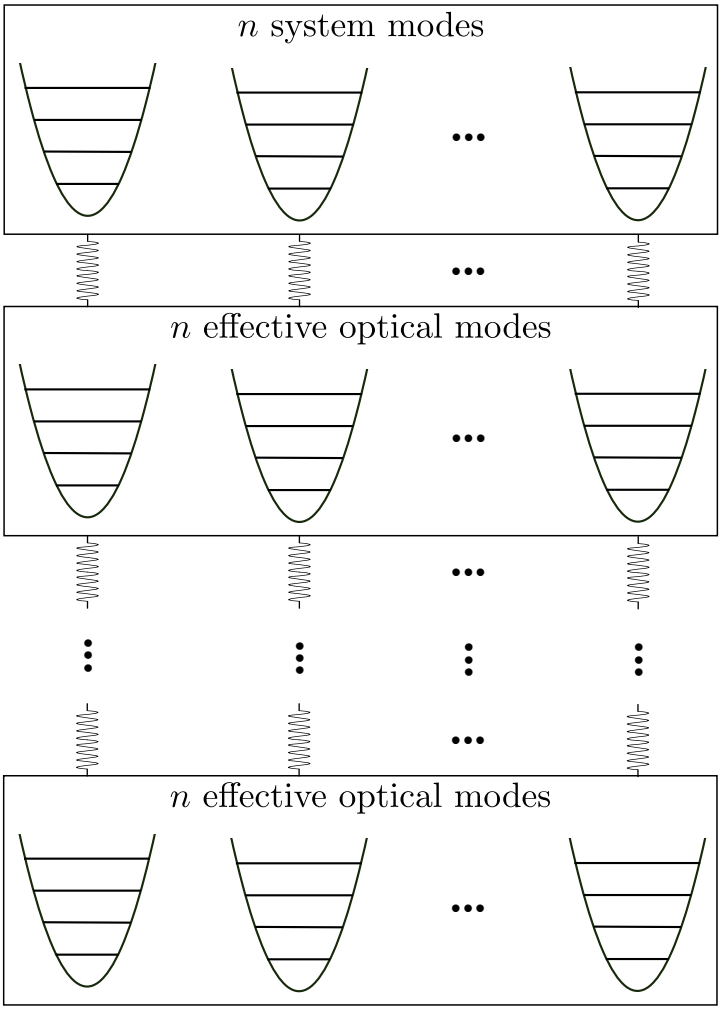

Figure 7.7: The correlation structure, at its simplest, of a general optomechanical system with its optical bath. The optomechanical system consists of n degrees of freedom, and is correlated with only n effective optical modes. These optical modes are also only correlated with n effective optical modes. This correlation 'chain' extends for the rest of the optical bath modes.

we've quantified how entangled the system is with its environment, and for a certain parameter regime, we've determined that information about the system mostly leaks to just one mode.

We then discussed how a simple entanglement structure, and the assumption that we can measure any commuting environment modes, allow us to easily devise optimal strategies for sensing and quantum state preparation tasks. For example, we derived the one-shot quantum Cramer-Rao bound in a conceptually simple way. Moreover, we provided bounds on how well we can squeeze different observables, and how well we can enhance the entanglement between the cavity and the test mass in a cavity optomechanical setup.

Finally, if we limit the effective environment modes to consist of only optical modes (which experimentalists can probe), then we cannot make any general statements about the entanglement structure of an optomechanical system with its optical bath. Nonetheless, the correlation between a system and its optical bath has a simple structure. A system with n degrees of freedom is correlated with only n effective optical modes, which in turn are only correlated to another n effective optical modes. This correlation chain continues *ad infinitum*.

Acknowledgments

We thank Haixing Miao, Yiqiu Ma, Mikhail Korobko and Farid Khalili for useful discussions. This research is supported by NSF grants PHY-1404569 and PHY-1506453, as well as the Institute for Quantum Information and Matter, a Physics Frontier Center.

Appendix: The covariance matrix for the example setup in Sec. 7.3.3

In this appendix, we show the steady state covariance matrix for the setup shown in Fig. 7.2. The optomechanical system's degrees of freedom are

$$\boldsymbol{x} = \begin{pmatrix} \tilde{x}_1 & \tilde{p}_1 & \tilde{a}_1 & \tilde{a}_2 \end{pmatrix}^T, \tag{7.100}$$

where $\tilde{x}_1$ and $\tilde{p}_1$ are the normalized test mass' center of mass position and momentum operators, respectively. The normalization factor is shown in Eq. (7.12). Moreover, $\tilde{a}_1$ and $\tilde{a}_2$ are the normalized cavity's amplitude and phase quadratures, respectively:

$$\tilde{a}_{1,2} = \sqrt{2}\hat{a}_{1,2} \tag{7.101}$$

where $\hat{a}_1$ and $\hat{a}_2$ are the cavity's amplitude and phase quadratures.

$\boldsymbol{x}$'s covariance matrix is

$$\sigma_{sys}^{s.s.} = \lambda \begin{pmatrix} 2\left(Q\Gamma_m\left(Q+\Gamma_m\right)\Gamma_\Theta^3 + n\lambda^{-1}\right) & 0 & -\sqrt{2}Q\Gamma_\Theta^{3/2}\Gamma_m^2 & \sigma_{\tilde{x}_1\tilde{p}_2}^{s.s.} \\ 0 & 2\left(Q^2\Gamma_m\Gamma_\Theta^3 + n\lambda^{-1}\right) & -\sqrt{2}Q\Gamma_\Theta^{3/2}\Gamma_m & \sigma_{\tilde{p}_1\tilde{p}_2}^{s.s.} \\ -\sqrt{2}Q\Gamma_\Theta^{3/2}\Gamma_m^2 & -\sqrt{2}Q\Gamma_\Theta^{3/2}\Gamma_m & \lambda^{-1} & Q\Gamma_\Theta^3\Gamma_m^3 \\ \sigma_{\tilde{x}_1\tilde{p}_2}^{s.s.} & \sigma_{\tilde{p}_1\tilde{p}_2}^{s.s.} & Q\Gamma_\Theta^3\Gamma_m^3 & \sigma_{\tilde{p}_2\tilde{p}_2}^{s.s.} \end{pmatrix}, \tag{7.102}$$

where

$$\begin{aligned}
\lambda^{-1} &\equiv \Gamma_m + \Gamma_m^2 Q + Q, \\
\sigma_{\tilde{x}_1\tilde{p}_2}^{s.s.} &= \sqrt{2}\Gamma_\Theta^{3/2}\Gamma_m\left(-Q\Gamma_m\left(2Q^2 + \Gamma_m\left(\Gamma_m^2+4\right)Q + 2\Gamma_m^2\right)\Gamma_\Theta^3 - \frac{2n(Q+\Gamma_m)}{\lambda}\right)\lambda, \\
\sigma_{\tilde{p}_1\tilde{p}_2}^{s.s.} &= \sqrt{2}Q\Gamma_\Theta^{3/2}\Gamma_m^2\left(Q\Gamma_m\left(2Q+\Gamma_m\right)\Gamma_\Theta^3\lambda + 2n\right), \\
\sigma_{\tilde{p}_2\tilde{p}_2}^{s.s.} &= \lambda\left(4Q^3\Gamma_m^3\Gamma_\Theta^6 + 4n\Gamma_m^4\Gamma_\Theta^3 + \Gamma_m^2 + 2Q\Gamma_m\left(\left(2\left(\left(\Gamma_\Theta^3+n\right)\Gamma_m^2 + 2n\right)\Gamma_\Theta^3 + 1\right)\Gamma_m^2 + 1\right)\right) \\
&\quad + \lambda\left(Q^2\left(\left(4n\left(\Gamma_m^2+1\right)\Gamma_\Theta^3 + \Gamma_m^2\left(2\left(\Gamma_m^2+4\right)\Gamma_\Theta^6 + 1\right) + 2\right)\Gamma_m^2 + 1\right)\right).
\end{aligned}$$

Moreover, γ is the cavity decay rate and is defined in Eq. (7.42), and

$$\Gamma_m = \frac{\omega_m}{\gamma}, \quad n = \frac{k_B T}{\hbar\omega_m}, \tag{7.103}$$

$$\Gamma_\Theta^3 = \frac{\hbar g^2/m}{\omega_m^3}, \quad g \equiv G_0\bar{a}. \tag{7.104}$$

where n is thermal occupation of the test mass and $\bar{a}$ is the amplitude of the light inside the cavity. G_0 is the coupling strength between the test mass and cavity (see

Eq. (7.40)).

Bibliography

[1] Gerardo Adesso. *Entanglement of Gaussian states*. PhD thesis, Salerno U., 2007.

[2] Alonso Botero and Benni Reznik. Modewise entanglement of gaussian states. *Phys. Rev. A*, 67:052311, May 2003.

[3] Carlton M. Caves and Bonny L. Schumaker. New formalism for two-photon quantum optics. i. quadrature phases and squeezed states. *Phys. Rev. A*, 31:3068–3092, May 1985.

[4] Christophe Galland, Nicolas Sangouard, Nicolas Piro, Nicolas Gisin, and Tobias J. Kippenberg. Heralded single-phonon preparation, storage, and readout in cavity optomechanics. *Phys. Rev. Lett.*, 112:143602, Apr 2014.

[5] Sebastian G. Hofer, Witlef Wieczorek, Markus Aspelmeyer, and Klemens Hammerer. Quantum entanglement and teleportation in pulsed cavity optomechanics. *Phys. Rev. A*, 84:052327, Nov 2011.

[6] H. Mueller-Ebhardt, H. Miao, S. Danilishin, and Y. Chen. Quantum-state steering in optomechanical devices. *ArXiv e-prints*, November 2012.

[7] John Williamson. On the algebraic problem concerning the normal forms of linear dynamical systems. *American Journal of Mathematics*, 58(1):141–163, 1936.

[8] H. M. Wiseman. *Quantum measurement and control*. Cambridge University Press, Cambridge, UK New York, 2010.

Chapter 8

ADIABATICALLY ELIMINATING A LOSSY CAVITY CAN RESULT IN GROSS UNDERESTIMATIONS OF THE CONDITIONAL VARIANCES OF AN OPTOMECHANICAL SETUP

8.1 Introduction

A cavity is a crucial component in many optomechanical setups. It can amplify the light that a test mass interacts with, it can drastically change how the test mass responds to the driving light (opening up applications such as cooling a test mass to its ground state), and it can improve the sensitivity of gravitational wave interferometers at different frequencies [5].

The theory of unmonitored quantum cavity-optomechanical systems is well understood. We know how a cavity modifies the dynamics of the test mass. When the cavity is sufficiently lossy, it doesn't alter the behavior of the test mass in any substantial qualitative way. We can eliminate the cavity from the dynamics, and focus only on the test mass. Such a procedure is called adiabatic elimination and it is common in the optomechanics literature. In connection to this, certain linear degrees of freedom can be non-adiabatically eliminated, even when the optomechanical system is monitored [10].

When we monitor an optomechanical system, its dynamics conditioned on the measurement results become more complicated. Nonetheless, over the past decade, our understanding of quantum control, and quantum state preparation and verification in continuously monitored setups has improved substantially[4, 6, 8]. These advances have also been used to describe the experiment in Ref. [9].

In this article, we show that adiabatic elimination accurately describes the conditional dynamics of an optomechanical system in a limited parameter regime. For the canonical cavity optomechanical setup, we numerically determined that adiabatic elimination is accurate when the measurement rate is slower than the cavity's bandwidth. We then analytically analyzed a simpler setup where we can measure any environment mode. This toy model showed us that if we measure the cavity optomechanical system too strongly, then the test mass is so strongly slaved to the environment that we become limited by the information that is locked in the cavity and which cannot be retrieved by measuring the environment.

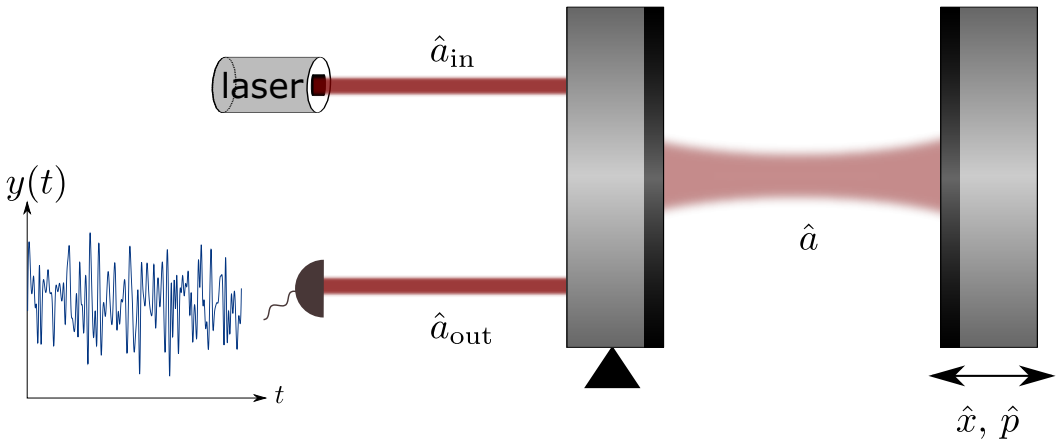

Figure 8.1: The cavity optomechanical setup we examine in this article. $y(t)$ is the measurement record collected by the experimentalist.

8.2 Unconditional dynamics of a cavity optomechanical setup

8.2.1 Setup

Consider the strawman optomechanical setup shown in Fig. 8.1, where a cavity with one movable mirror is pumped by an external source of light. We denote the test mass' center of mass position and momentum by $\hat{x}$ and $\hat{p}$, respectively. The ladder operator associated with the cavity field is $\hat{a}$, and we denote the ladder operators associated with the incoming (outgoing) light continuum by $\hat{a}_{in}$ ($\hat{a}_{out}$).

The Hamiltonian for the setup is

$$\hat{H}_I = \frac{\hat{p}^2}{2m} + \frac{1}{2}m\omega_m^2\hat{x}^2 + \hbar\left(\omega_c - \omega_0\right)\hat{a}^\dagger\hat{a} + \hbar G_0\hat{x}\hat{a}^\dagger\hat{a} + i\hbar\sqrt{2\gamma}\left(\hat{a}_{in}\left(t\right)\hat{a}^\dagger - \hat{a}_{in}^\dagger\left(t\right)\hat{a}\right), \tag{8.1}$$

where m and ω_m are the test mass' mass and resonant frequency, respectively. $G_0 = \omega_c/L$ is the bare optomechanical interaction strength, ω_c is a resonant frequency of the cavity and L is the length of the cavity. We are an interaction picture with the cavity's free Hamiltonian, and the $\hbar\omega_0$ part of the external continuum, removed. We denote by Δ the detuning between the laser and the cavity resonant frequency:

$$\Delta \equiv \omega_0 - \omega_c. \tag{8.2}$$

The test mass is also driven by a thermal fluctuation operator $\hat{f}_{th}$, with a correlation function of

$$\left\langle \hat{f}_{th}\left(t\right)\hat{f}_{th}\left(t'\right)\right\rangle = 2m\frac{\omega_m}{Q}k_B T\delta\left(t - t'\right), \tag{8.3}$$

where Q is the test mass' quality factor, and T the temperature of the thermal bath.

Since the laser emits light in a coherent state with a large amplitude, the fluctuations of $\hat{a}_{in}$ are small compared to its large classical amplitude. Since the cavity mode $\hat{a}$ is driven by $\hat{a}_{in}$, it will also have a large classical amplitude which allows us to linearize the interaction $\hat{x}\hat{a}^\dagger\hat{a}$ to

$$\hat{x}\left(|\overline{a}|^2 + \bar{a}^*\delta\hat{a} + \bar{a}\delta\hat{a}^\dagger\right) \tag{8.4}$$

where $\hat{a} = \delta\hat{a} + \bar{a}$ and

$$\bar{a} = \sqrt{\frac{2\gamma}{\gamma^2 + \Delta^2}\frac{I_0}{\hbar\omega_0}}. \tag{8.5}$$

γ is the half-bandwidth of the cavity and I_0 is the input laser intensity. Moreover, to simplify our analysis, we've chosen the convention that $\bar{a}$ is real and positive. For the remainder of the article, we will denote $\delta\hat{a}$ by $\hat{a}$.

To simplify the analysis in this article, we will present the cavity's and test mass' equations of motion in matrix form, and we will work with dimensionless parameters only:

$$\tilde{t} \equiv \omega_m t, \tag{8.6}$$

$$\tilde{x} = \frac{\hat{x}/\Delta x_{zp}}{\sqrt{2}}, \quad \tilde{p} \equiv \frac{\hat{p}/}{\sqrt{2}}, \tag{8.7}$$

$$\Delta x_{zp} \equiv \sqrt{\frac{\hbar}{2m\omega_m}}, \quad \equiv \sqrt{\frac{\hbar m\omega_m}{2}}, \tag{8.8}$$

$$\tilde{a}_{in} \equiv \hat{a}_{in}/\sqrt{\omega_m}, \quad \tilde{a}_{out} \equiv \hat{a}_{out}/\sqrt{\omega_m}, \quad \tilde{f}_{th} \equiv \frac{\hat{f}_{th}}{(\omega_m/Q)\sqrt{2mk_bT}}. \tag{8.9}$$

Let $\boldsymbol{x}$ denote the system's dimensionless degrees of freedom:

$$\boldsymbol{x} = \begin{pmatrix} \tilde{x} & \tilde{p} & \hat{a}_1 & \hat{a}_2 \end{pmatrix}^T, \tag{8.10}$$

and $\boldsymbol{n}$ denote the environment noise operators:

$$\boldsymbol{n} = \begin{pmatrix} \tilde{f}_{th} & \tilde{a}_{in,1} & \tilde{a}_{in,2} \end{pmatrix}^T. \tag{8.11}$$

$\boldsymbol{x}$'s equation of motion in the Heisenberg picture is

$$\partial_{\tilde{t}}\boldsymbol{x} = M\boldsymbol{x} + N\boldsymbol{n}, \tag{8.12}$$

where

$$M \equiv \begin{pmatrix} 0 & 1 & 0 & 0 \\ -1 & -1/Q & -\sqrt{2}\Gamma_\Theta^{3/2} & 0 \\ 0 & 0 & -\Gamma_\gamma^{-1} & -\Gamma_\Delta \\ -\sqrt{2}\Gamma_\Theta^{3/2} & 0 & \Gamma_\Delta & -\Gamma_\gamma^{-1} \end{pmatrix}, \tag{8.13}$$

$$N \equiv \begin{pmatrix} 0 & 0 & 0 \\ \sqrt{2n}/Q & 0 & 0 \\ 0 & \sqrt{2\Gamma_\gamma^{-1}} & 0 \\ 0 & 0 & \sqrt{2\Gamma_\gamma^{-1}} \end{pmatrix}, \tag{8.14}$$

and

$$\Gamma_\gamma = \frac{\omega_m}{\gamma} \quad , \Gamma_\Delta = \frac{\Delta}{\omega_m}, \quad n = \frac{k_B T}{\hbar \omega_m}, \tag{8.15}$$

$$\Gamma_\Theta^3 = \frac{\hbar g^2/m}{\omega_m^3}, \quad g \equiv G_0 \bar{a}. \tag{8.16}$$

Γ_Θ has the dimension of frequency and is a measure of the strength of the optomechanical interaction. n is the thermal occupation number of the test mass.

The outgoing light's equations of motion are

$$\boldsymbol{a}_{out} = A\boldsymbol{x} + B\boldsymbol{n} \tag{8.17}$$

where

$$\boldsymbol{a}_{out} \equiv \begin{pmatrix} \tilde{a}_{out,1}(\tilde{t}) & \tilde{a}_{out,2}(\tilde{t}) \end{pmatrix}^T, \tag{8.18}$$

$$A = \begin{pmatrix} 0 & 0 & \sqrt{2/\Gamma_\gamma} & 0 \\ 0 & 0 & 0 & \sqrt{2/\Gamma_\gamma} \end{pmatrix}, \quad B = -\begin{pmatrix} 0 & 1 & 0 \\ 0 & 0 & 1 \end{pmatrix}. \tag{8.19}$$

8.2.2 Adiabatically eliminating the cavity

When $\Gamma_\gamma \gg 1$, the cavity bandwidth is much larger than the mechanical resonant frequency and the cavity mode responds almost instantaneously to the motion of the test mass, so most analyzes of cavity optomechanics adiabatically eliminate the

cavity. Specifically, they set $\partial_{\tilde{t}}\hat{a}_{1,2}(\tilde{t}) = 0$ and solve for $\hat{a}_1$ and $\hat{a}_2$:

$$\hat{a}_1(\tilde{t}) \approx \frac{\sqrt{2\Gamma_\gamma}}{\Gamma_\Delta^2\Gamma_\gamma^2+1}\left(\tilde{a}_{in,1}(\tilde{t}) - \Gamma_\Delta\Gamma_\gamma\tilde{a}_{in,2}(\tilde{t}) + \Gamma_\Theta^{3/2}\Gamma_\Delta\Gamma_\gamma^{3/2}\tilde{x}(\tilde{t})\right), \tag{8.20}$$

$$\hat{a}_2(\tilde{t}) \approx \frac{\sqrt{2\Gamma_\gamma}}{\Gamma_\Delta^2\Gamma_\gamma^2+1}\left(\Gamma_\Delta\Gamma_\gamma\tilde{a}_{in,1}(\tilde{t}) + \tilde{a}_{in,2}(\tilde{t}) - \sqrt{\Gamma_\gamma}\Gamma_\Theta^{3/2}\tilde{x}(\tilde{t})\right). \tag{8.21}$$

We substitute these back into the equations of motion for $\tilde{x}$ and $\tilde{p}$ given by Eq. (8.12) and obtain

$$\partial_{\tilde{t}}\tilde{x}(\tilde{t}) = \tilde{p}(\tilde{t}), \tag{8.22}$$

$$\partial_{\tilde{t}}\tilde{p}(\tilde{t}) \approx -\frac{\tilde{p}(\tilde{t})}{Q} - \left(1 + \frac{2\Gamma_\Theta^3\Gamma_\Delta}{\Gamma_\Delta^2+\Gamma_\gamma^{-2}}\right)\tilde{x}(\tilde{t}) + \frac{2\Gamma_\Theta^{3/2}\Gamma_\gamma^{-3/2}}{\Gamma_\Delta^2+\Gamma_\gamma^{-2}}\left(\Gamma_\Delta\Gamma_\gamma\tilde{a}_{in,2}(\tilde{t}) - \tilde{a}_{in,1}(\tilde{t})\right) + \frac{\sqrt{2n}}{Q}\tilde{f}_{th}(\tilde{t}). \tag{8.23}$$

We can simplify Eqs. (8.22-8.23) by defining

$$\Gamma_q^2 \equiv 4\Gamma_\Theta^3\frac{\Gamma_\gamma^{-1}}{\Gamma_\gamma^{-2}+\Gamma_\Delta^2}, \tag{8.24}$$

and redefining the optical external continuum's amplitude and phase quadratures to

$$\tilde{a}_{out/in,1}(\tilde{t})\big|_{new} = \frac{\tilde{a}_{out/in,1}(\tilde{t}) - \Gamma_\Delta\Gamma_\gamma\tilde{a}_{out/in,2}(\tilde{t})}{\sqrt{1+\Gamma_\Delta^2\Gamma_\gamma^2}}, \tag{8.25}$$

$$\tilde{a}_{out/in,2}(\tilde{t})\big|_{new} = \frac{\tilde{a}_{out/in,2}(\tilde{t}) + \Gamma_\Delta\Gamma_\gamma\tilde{a}_{out/in,1}(\tilde{t})}{\sqrt{1+\Gamma_\Delta^2\Gamma_\gamma^2}}. \tag{8.26}$$

With these definitions, we simplify Eqs. (8.22-8.23) to

$$\partial_{\tilde{t}}\breve{\boldsymbol{x}} = \breve{M}\breve{\boldsymbol{x}} + \breve{N}\boldsymbol{n}, \tag{8.27}$$

where

$$\check{\boldsymbol{x}} = \begin{pmatrix} \tilde{x} & \tilde{p} \end{pmatrix}^T, \tag{8.28}$$

$$\check{M} \equiv \begin{pmatrix} 0 & 1 \\ -\left(1 + \Gamma_q^2 \Gamma_\Delta \Gamma_\gamma / 2\right) & -1/Q \end{pmatrix}, \tag{8.29}$$

$$\check{N} \equiv \begin{pmatrix} 0 & 0 & 0 \\ \sqrt{2n}/Q & -\Gamma_q & 0 \end{pmatrix}. \tag{8.30}$$

Notice that these equations resemble those of a test mass directly interacting with a driving laser's light. The test mass has a shifted eigenfrequency from ω_m to $\omega_m + \Gamma_q^2 \omega_m \Delta/(2\gamma)$, and it interacts with the light via an interaction strength of Γ_q.

The outgoing light's equations of motions are

$$\begin{aligned} \tilde{a}_{out,1}(\tilde{t})\big|_{new} &\approx \frac{1 - \Gamma_\Delta^2 \Gamma_\gamma^2}{1 + \Gamma_\Delta^2 \Gamma_\gamma^2} \tilde{a}_{in,1}(\tilde{t})\big|_{\text{new}} - \frac{2\Gamma_\Delta \Gamma_\gamma}{1 + \Gamma_\Delta^2 \Gamma_\gamma^2} \tilde{a}_{in,2}(\tilde{t})\big|_{\text{new}} \\ &\quad + 2\Gamma_\Delta \Gamma_\gamma \Gamma_q \tilde{x}(\check{t}), \end{aligned} \tag{8.31}$$

$$\begin{aligned} \tilde{a}_{out,2}(\tilde{t})\big|_{new} &\approx \frac{1 - \Gamma_\Delta^2 \Gamma_\gamma^2}{1 + \Gamma_\Delta^2 \Gamma_\gamma^2} \tilde{a}_{in,2}(\tilde{t})\big|_{\text{new}} + \frac{2\Gamma_\Delta \Gamma_\gamma}{1 + \Gamma_\Delta^2 \Gamma_\gamma^2} \tilde{a}_{in,1}(\tilde{t})\big|_{\text{new}} \\ &\quad - \Gamma_q \left(1 - \Gamma_\Delta^2 \Gamma_\gamma^2\right) \tilde{x}(t). \end{aligned} \tag{8.32}$$

8.2.3 Adiabatically eliminating a lossy cavity accurately describes the exact unconditional steady state dynamics

In this section, we show that adiabatically eliminating the cavity accurately describes the unconditional (*i.e.* unmonitored) dynamics of the test mass at steady state. We will set the detuning Δ to 0 (non no-zero detuning, adiabatic elimination is justified when $\Delta \ll \omega_m$ [4]), which simplifies Eq. (8.31-8.32) to

$$\begin{aligned} \tilde{a}_{out,1}(\tilde{t})\big|_{new} &\approx \tilde{a}_{in,1}(\tilde{t})\big|_{\text{new}}, \\ \tilde{a}_{out,2}(\tilde{t})\big|_{new} &\approx \tilde{a}_{in,2}(\tilde{t})\big|_{\text{new}} - \Gamma_q \tilde{x}(t). \end{aligned}$$

Eq. (8.12) describes the exact unconditional dynamics, and Eq. (8.27) describes the dynamics of the test mass when we adiabatically eliminate the cavity. Since these equations are linear and we've assumed that the thermal and optical bath degrees of freedom are in zero-mean Gaussian states, at steady state the state of the system is Gaussian and so is completely characterized by its first and second moments. For example, the unconditional Wigner function for the test mass and cavity at a time t

when the optomechanical setup's initial state is forgotten is of the form

$$W(x,p,a_1,a_2;t)=\frac{1}{\sqrt{\det\left(2\pi V_{\boldsymbol{xx}}(t)\right)}}\exp\left(-\frac{1}{2}\vec{x}^{T}V_{\boldsymbol{xx}}^{-1}(t)\,\vec{x}\right), \tag{8.33}$$

where $\vec{x}^{T}\equiv\begin{pmatrix} x & p & a_1 & a_2\end{pmatrix}$ and $V_{\boldsymbol{xx}}(t)$ is the symmetric expectation value of $\boldsymbol{x}(t)$, which follows the equation of motion (8.12), over the initial system-environment state$|\Psi_i\rangle$

$$\begin{aligned} V_{\boldsymbol{xx}}(t) &\equiv \left\langle \boldsymbol{x}(t).\boldsymbol{x}(t)^{T}\right\rangle_{s} \\ &\equiv \frac{1}{2}\left(\left\langle\Psi_i\middle|\boldsymbol{x}(t).\boldsymbol{x}(t)^{T}\middle|\Psi_i\right\rangle+\left\langle\Psi_i\middle|\boldsymbol{x}(t).\boldsymbol{x}(t)^{T}\middle|\Psi_i\right\rangle^{T}\right). \end{aligned} \tag{8.34}$$

Note that $\langle\Psi_i|\boldsymbol{x}(t)|\Psi_i\rangle=0$ because the thermal bath has zero mean and we've linearized the incoming light (around its large classical amplitude), and assumed the laser is in a coherent state.

We calculate the unconditional equation of motion for $V_{\boldsymbol{xx}}$ to be

$$\partial_t V_{\boldsymbol{xx}}(t) = MV_{\boldsymbol{xx}}(t)+V_{\boldsymbol{xx}}(t)M^{T}+NV_{\boldsymbol{nn}}N^{T}, \tag{8.35}$$

where $V_{\boldsymbol{nn}}\delta(t-t')$ is the covariance matrix of $\boldsymbol{n}(t)$ and $\boldsymbol{n}(t')$:

$$V_{\boldsymbol{nn}}\equiv\begin{pmatrix} Q\Gamma_{\gamma}^{-1} & 0 & 0\\ 0 & 1/2 & 0\\ 0 & 0 & 1/2\end{pmatrix}. \tag{8.36}$$

We will denote the variances of an operator $\hat{o}$ calculated with adiabatic elimination by $\mathcal{V}_{oo}$. $V_{\check{\boldsymbol{x}}\check{\boldsymbol{x}}}$ follows the equation of motion

$$\partial_t\mathcal{V}_{\check{\boldsymbol{x}}\check{\boldsymbol{x}}}(t)=\check{M}\mathcal{V}_{\check{\boldsymbol{x}}\check{\boldsymbol{x}}}(t)+\mathcal{V}_{\check{\boldsymbol{x}}\check{\boldsymbol{x}}}(t)\check{M}^{T}+\check{N}V_{\boldsymbol{nn}}\check{N}^{T},. \tag{8.37}$$

We can obtain the steady state unconditional covariance matrix by setting $\partial_t V_{\boldsymbol{xx}}$ in Eq. (8.12) and $\partial_t\mathcal{V}_{\check{\boldsymbol{x}}\check{\boldsymbol{x}}}(t)$ in Eq. (8.37) to 0. The resultant equations are called

continuous Lyapunov equations. For zero detuning, we obtain at steady state that

$$\mathcal{V}_{\check{\boldsymbol{x}}\check{\boldsymbol{x}}} = \begin{pmatrix} Q\Gamma_q^2/4 + n & 0 \\ 0 & Q\Gamma_q^2/4 + n \end{pmatrix}, \quad n \equiv \frac{k_b T}{\hbar\omega_m}, \tag{8.38}$$

$$V_{\check{\boldsymbol{x}}\check{\boldsymbol{x}}} \equiv \left\langle \check{\boldsymbol{x}}\,(t)\,.\check{\boldsymbol{x}}\,(t)^T \right\rangle_s \tag{8.39}$$

$$= \left(n + \frac{\Gamma_\Theta^3 \Gamma_\gamma Q^2}{\Gamma_\gamma + \Gamma_\gamma^2 Q + Q}\right) \begin{pmatrix} 1 + \frac{\Gamma_\Theta^3 \Gamma_\gamma^2 Q}{n\left(\Gamma_\gamma + \Gamma_\gamma^2 Q + Q\right) + \Gamma_\Theta^3 \Gamma_\gamma Q^2} & 0 \\ 0 & 1 \end{pmatrix}. \tag{8.40}$$

In the bad cavity limit, $\Gamma_\gamma \ll 1$, and for $Q \gg 1$, we obtain $V_{\check{\boldsymbol{x}}\check{\boldsymbol{x}}} \approx \mathcal{V}_{\check{\boldsymbol{x}}\check{\boldsymbol{x}}}$, with the leading error in $V_{\tilde{x}\tilde{x}} - \mathcal{V}_{\tilde{x}\tilde{x}}$ is $n\Gamma_\gamma^2$.

8.3 Numerics showing the breakdown of adiabatic elimination in describing conditional dynamics

Adiabatically eliminating a lossy cavity accurately describes the unconditional dynamics of the test mass at all measurement strengths Γ_Θ, but the approximation fails to describe the conditional dynamics for a large range of Γ_Θ. To arrive at this conclusion, we numerically calculated the steady state conditional variance of $\tilde{x}$, exactly and if the cavity were adiabatically eliminated, for a large range of Q, Γ_Θ and Γ_γ.

First, we'll numerically show that even if we always measure the outgoing light's phase quadrature $\hat{a}_{out,2}$ and don't optimize over which quadratures to measure, adiabatically eliminating the cavity breaks down for measurement rates larger than the cavity decay rate. In Fig. 8.2, we show $\mathcal{V}_{\tilde{x}\tilde{x}}^{phase}/V_{\tilde{x}\tilde{x}}^{phase}$ as a function of Γ_Θ for different values of Γ_γ, Q and n. $\mathcal{V}_{\tilde{x}\tilde{x}}^{phase}$ is the conditional variance of $\tilde{x}$ if the phase quadrature is always measured (*i.e.* $\theta\,(t)$ is set to $\pi/2$ in Eq. (8.66) for all times t) and if the cavity is adiabatically eliminated. $V_{\tilde{x}\tilde{x}}^{phase}$ is the exact conditional variance of $\tilde{x}$ if the phase quadrature is always measured. We observe that when $\Gamma_\gamma\Gamma_\Theta \approx 1/2$ (which corresponds to a measurement strength $\gtrsim$ the cavity half-bandwidth γ), adiabatically eliminating the cavity results in a large error in the conditional variance of $\tilde{x}$:

$$\mathcal{V}_{\tilde{x}\tilde{x}}^{phase} \approx V_{\tilde{x}\tilde{x}}^{phase}/2. \tag{8.41}$$

When we optimally choose the homodyne angle $\theta\,(t)$ in order to squeeze $\tilde{x}$ as much as possible (refer to Appendix 8.6 for how to do so), $\mathcal{V}_{\tilde{x}\tilde{x}}^{min} = V_{\tilde{x}\tilde{x}}^{min}/2$ (where the superscript *min* is to highlight the fact it is the minimum achievable conditional variance) when

$$\Gamma_\Theta \approx 0.7\Gamma_\gamma^{-0.97} Q^{-0.09}. \tag{8.42}$$

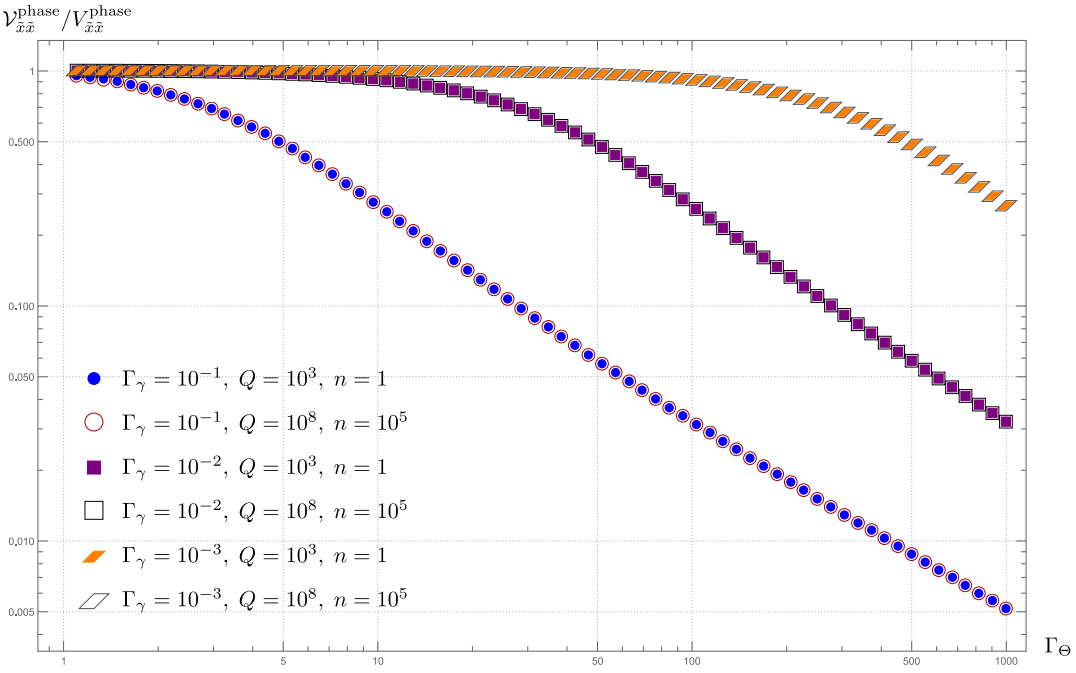

Figure 8.2: Predictions of the squeezing of $\tilde{x}$ after measuring the phase quadrature $\hat{a}_{out,2}$ of the outgoing light and at different measurement strengths Γ_Θ, when the cavity is adiabatically eliminated and when it isn't. When $\hat{a}_{out,2}$ is measured, $\mathcal{V}^{phase}_{\check{x}\check{x}}$ is the steady state conditional variance of $\tilde{x}$ if the cavity were adiabatically eliminated, and $V^{min}_{\tilde{x}\tilde{x}}$ the steady state conditional variance of $\tilde{x}$ under the full dynamics. The inset shows $\mathcal{V}^{phase}_{\check{x}\check{x}}$ at different measurement strengths. We chose the thermal occupation number n to be 1.

We determined this relationship through a large scale numerical analysis which we show in Fig. 8.3. Specifically, we've set $n = 1$, and we show $\mathcal{V}^{min}_{\tilde{x}\tilde{x}}/V^{min}_{\tilde{x}\tilde{x}}$ as a function of Γ_Θ for different values of Γ_γ, Q and n. In Fig. 8.4, we also plot $\mathcal{V}^{min}_{\tilde{x}\tilde{x}}/V^{min}_{\tilde{x}\tilde{x}}$ against Γ_Θ for different combinations Γ_γ, Q and n.

8.4 Insights from a simplified version of the problem

To analytically obtain insights on why adiabatic elimination fails, we will assume that we can measure any environmental mode, including thermal fluctuation operators. This assumption is useful because it will allow us to use the phase-space Schmidt decomposition theorem, which makes it easy to obtain tractable expressions for the conditional variances of our system.

Since in an actual experiment we only have access to optical degrees of freedom, we will set $n = 0$ throughout this section, so that optical noise is the primary source of uncertainty in the test mass' center of mass position and momentum. Equivalently, when $n = 0$, most of the information we can recover about the test mass will be

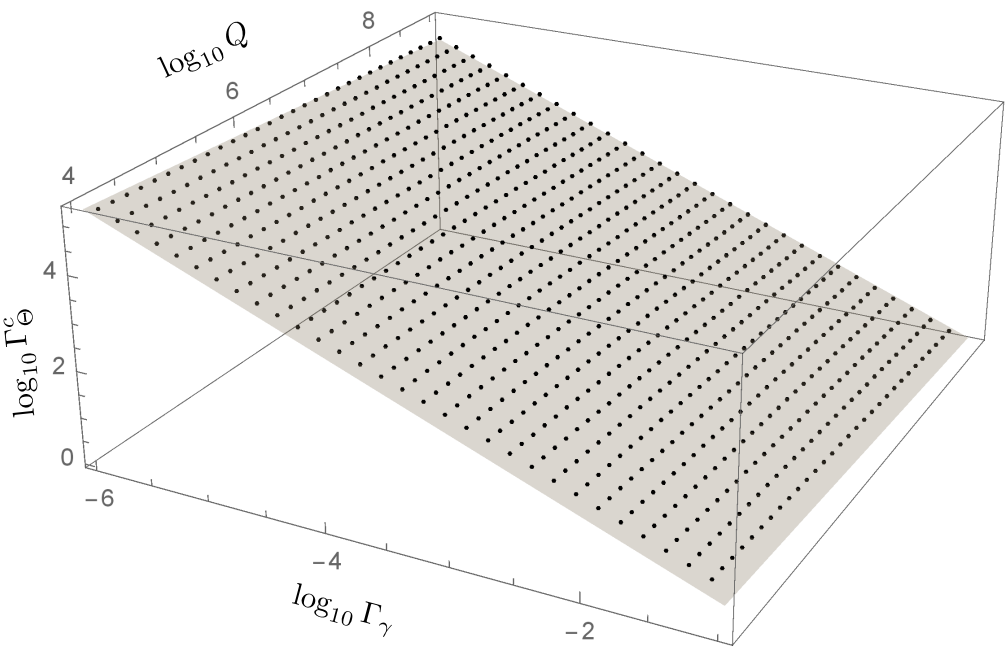

Figure 8.3: Simulation results of the critical measurement strength, Γ_Θ^c, when the optimal squeezing variance for $\tilde{x}$ according to the exact dynamics is half of that as when the cavity is adiabatically eliminated. Each black dot represents Γ_Θ^c for a different choice of Γ_γ and Q in the range $10^{-1} \leq \Gamma_\gamma \leq 10^{-6}$ and $10^4 \leq Q \leq 10^9$. We chose the thermal occupation number n to be 1. The gray surface is fit to guide the eye, and is equal to $-0.155 - 0.09 \log_{10} Q - 0.97 \log_{10} \Gamma_\gamma$.

contained in the outgoing light rather the thermal bath degrees of freedom.

8.4.1 The phase-space Schmidt decomposition theorem

The joint state of the test mass, cavity and environment is in a pure Gaussian state characterized by zero mean and a covariance matrix V_{tot}. The phase-space Schmidt decomposition theorem [3, 1] states that we can substantially simplify the structure of V_{tot} by choosing a different basis than $\boldsymbol{x}$ for the joint test mass and cavity system, and a different basis than $\begin{pmatrix} \boldsymbol{a}^T & \boldsymbol{f}_{th}^T \end{pmatrix}$, where $\boldsymbol{f}_{th}$ denotes the collection of thermal bath operators, for the environment modes. In this new basis, all effective environment modes, except two, are in vacuum, and each of these two modes is in a two-mode squeezed state with an effective system mode.

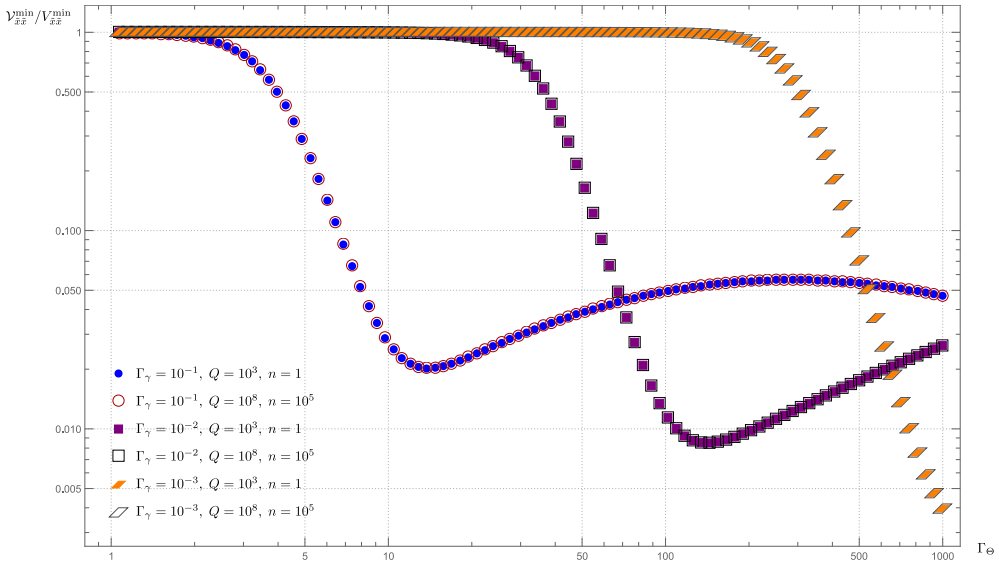

Figure 8.4: Predictions of the optimal squeezing of $\tilde{x}$ at different measurement strengths when the cavity is adiabatically eliminated and when it isn't. $\mathcal{V}^{min}_{\tilde{x}\tilde{x}}$ is the minimum achievable conditional variance of $\tilde{x}$ if the cavity were adiabatically eliminated, and $V^{min}_{\tilde{x}\tilde{x}}$ the minimum achievable conditional variance of $\tilde{x}$ under the full dynamics. We chose the thermal occupation number n to be 1.

Denote the new basis of system and environment modes by

$$\boldsymbol{w}_{sys} \equiv \begin{pmatrix} \hat{s}_{1,1} & \hat{s}_{1,2} & \hat{s}_{2,1} & \hat{s}_{2,2} \end{pmatrix}^T, \quad \boldsymbol{w}_{env} \equiv \begin{pmatrix} \hat{e}_{1,1} & \hat{e}_{1,2} & \hat{e}_{2,1} & \hat{e}_{2,2} & \dots \end{pmatrix}^T, \quad \boldsymbol{w} \equiv \begin{pmatrix} \boldsymbol{w}_{sys} \\ \boldsymbol{w}_{opt} \end{pmatrix}. \tag{8.43}$$

We choose them in such a way that they are linear combinations of the modes in $\boldsymbol{v}^T \equiv \begin{pmatrix} \boldsymbol{x}^T & \boldsymbol{a}^T & \boldsymbol{f}_{th}^T \end{pmatrix}$:

$$\boldsymbol{w} = M\boldsymbol{v}, \quad M \equiv \begin{pmatrix} M_{sys} & 0 \\ 0 & M_{env} \end{pmatrix}. \tag{8.44}$$

For example, $\hat{s}_{1,1}$ is of the form $m_1\tilde{x} + m_2\tilde{p} + m_3\hat{a}_1 + m_4\hat{a}_2$, where m_1, m_2, m_3 and m_4 are real numbers. Moreover, the $\boldsymbol{w}$ satisfy the same commutation relations as $\boldsymbol{v}$:

$$\left[\boldsymbol{w}, \boldsymbol{w}^T\right] = \left[\boldsymbol{v}, \boldsymbol{v}^T\right] = i\Omega, \tag{8.45}$$

where Ω is a block diagonal matrix

$$\Omega \equiv \oplus_{i=1}^{N}\omega, \quad \omega \equiv \begin{pmatrix} 0 & 1 \\ -1 & 0 \end{pmatrix} \tag{8.46}$$

with N the total number of degrees of freedom in the system and environment. Using Eq. (8.44), Eq. (8.45) implies that $M\Omega M^T = \Omega$. Matrices that satisfy such a relation are called symplectic matrices. Similarly, we can also show that M_{sys} and M_{env} are symplectic matrices.

The theorem states that there exists an M such that

$$V_{\boldsymbol{w}} \equiv \left\langle \boldsymbol{w}\boldsymbol{w}^T \right\rangle_s = M V_{tot} M^T \equiv \begin{pmatrix} C & S & 0 \\ S & C & 0 \\ 0 & 0 & I \end{pmatrix}, \tag{8.47}$$

$$C \equiv \begin{pmatrix} C_1 & 0 \\ 0 & C_2 \end{pmatrix}, \quad C_k \equiv \begin{pmatrix} \nu_k & 0 \\ 0 & \nu_k \end{pmatrix}, \tag{8.48}$$

$$S \equiv \begin{pmatrix} S_1 & 0 \\ 0 & S_2 \end{pmatrix}, \quad S_k \equiv \begin{pmatrix} \sqrt{\nu_k^2 - \frac{1}{4}} & 0 \\ 0 & -\sqrt{\nu_k^2 - \frac{1}{4}} \end{pmatrix} \tag{8.49}$$

where $k = 1, 2$ and I is the identity matrix. In addition, notice that M_{sys} is the symplectic diagonalizing matrix for $V_{\boldsymbol{x}\boldsymbol{x}}$:

$$M_{sys} V_{\boldsymbol{x}\boldsymbol{x}} M_{sys}^T = C, \tag{8.50}$$

so ν_1 and ν_2 are the symplectic eigenvalues of $V_{\boldsymbol{x}\boldsymbol{x}}$, and $\nu_1 \geq 1/2$ and $\nu_2 \geq 1/2$. The Williamson theorem guarantees the existence of an M_{sys} that diagonalizes $V_{\boldsymbol{x}\boldsymbol{x}}$ into C.

The structure of $V_{\boldsymbol{w}}$ in Eq. (8.47) indicates that the system is entangled with only two effective environment modes, so studying optimal conditional state preparation is simple when we can measure any environment observable.

8.4.2 Applying the theorem to optimal state preparation

Consider an operator of the system $\hat{O}$, such as the test mass' center of mass position operator $\tilde{x}$, that we are interested in squeezing as much as possible by measuring the environment. We first project $\hat{O}$ onto the system symplectic basis:

$$\hat{O} = \vec{\alpha}.\boldsymbol{w}_{sys} \tag{8.51}$$

$$= \sum_{i=1}^{2} \left(\alpha_{i,1} \hat{s}_{i,1} + \alpha_{i,2} \hat{s}_{i,2} \right). \tag{8.52}$$

Each operator in the sum (8.52) is correlated with only a single environment mode. Therefore, optimally squeezing $\hat{O}$ is equivalent to optimally squeezing 2 operators

with a simple correlation structure. This structure can be made trivial by normalizing each term in Eq. (8.52):

$$\hat{O} = \sum_{i=1}^{n} \sqrt{\alpha_{i,1}^2 + \alpha_{i,2}^2} \frac{\alpha_{i,1}\hat{s}_{i,1} + \alpha_{i,2}\hat{s}_{i,2}}{\sqrt{\alpha_{i,1}^2 + \alpha_{i,2}^2}}. \tag{8.53}$$

Since each $\hat{s}_{i,1}$ and $\hat{s}_{i,2}$ pair, for $i = 1, 2$, are independent and occupy a symmetric thermal state, we can redefine each

$$\frac{\alpha_{i,1}\hat{s}_{i,1} + \alpha_{i,2}\hat{s}_{i,2}}{\sqrt{\alpha_{i,1}^2 + \alpha_{i,2}^2}} \tag{8.54}$$

to be $\hat{s}_{i,1}$. Therefore,

$$\hat{O} = \sum_{i=1}^{2} \sqrt{\alpha_{i,1}^2 + \alpha_{i,2}^2}\hat{s}_{i,1}. \tag{8.55}$$

As can be inferred from Eq. (8.47), each $\hat{s}_{i,1}$ is correlated with a single effective environment mode's quadrature, $\hat{e}_{i,1}$. Therefore, estimating $\hat{s}_{i,1}$ as well as possible entails measuring $\hat{e}_{i,1}$. The error in this estimation can be calculated by noticing that $\hat{s}_{i,1}$'s and $\hat{e}_{i,1}$'s joint Wigner function is Gaussian and has the covariance matrix

$$\begin{pmatrix} \nu_i & \sqrt{\nu_i^2 - 1} \\ \sqrt{\nu_i^2 - 1} & \nu_i \end{pmatrix}. \tag{8.56}$$

The variance of $\hat{s}_{i,1}$ conditioned on measuring $\hat{e}_{i,1}$ is

$$\nu_i - \frac{\left(\sqrt{\nu_i^2 - 1/4}\right)^2}{\nu_i} = \frac{1}{4\nu_i}. \tag{8.57}$$

Using Eq. (8.55), we deduce that$\hat{O}$ can be optimally squeezing to

$$\left\langle \hat{O}^2 \right\rangle\Big|_{min} = \sum_{i=1}^{2} \frac{\alpha_{i,1}^2 + \alpha_{i,2}^2}{4\nu_i}. \tag{8.58}$$

Eq. (8.58) gives us some insights on why approximations that accurately predict unconditional dynamics could horribly fail in predicting the conditional dynamics. When $\nu_1 \gg \nu_2$, the unconditional uncertainty of $\hat{O}$ is dominated by the fluctuations in $\hat{s}_1$ and so it would seem reasonable to ignore $\hat{s}_2$. However, if we measure the

environment in such a way as to optimally estimate $\hat{O}$, then we can only ignore $\hat{s}_2$ if $\left(\alpha_{1,1}^2 + \alpha_{1,2}^2\right)/4\nu_1 \gg \left(\alpha_{2,1}^2 + \alpha_{2,2}^2\right)/4\nu_2$. Interestingly, if $\left(\alpha_{1,1}^2 + \alpha_{1,2}^2\right)$ is of the same order of magnitude $\left(\alpha_{2,1}^2 + \alpha_{2,2}^2\right)$, then we can ignore $\hat{s}_2$ only if $\nu_1 \ll \nu_2$!

8.4.3 When does adiabatic elimination fail?

Using Eq. (8.35), and assuming no detuning and $n = 0$, we can analytically calculate the system's steady state covariance matrix, which we show in Appendix 8.7. We then symplectically diagonalize this covariance matrix. In the parameter regime of small measurement strengths ($\Gamma_\Theta \ll 1$), high Q and small Γ_γ, we obtain that the symplectic eigenvalues are

$$\nu_1 \approx Q\Gamma_\Theta^3\Gamma_\gamma, \quad \nu_2 \approx 1/2, \tag{8.59}$$

$$\alpha_1^2 \approx 1, \quad \alpha_2^2 \approx 2\Gamma_\Theta^3\Gamma_\gamma^4. \tag{8.60}$$

As a result,

$$V_{\tilde{x}\tilde{x}}^{min} \approx \frac{1}{4Q\Gamma_\Theta^3\Gamma_\gamma} + \Gamma_\Theta^3\Gamma_\gamma^4. \tag{8.61}$$

Since we are in the mindset of doubting the validity of approximations, we checked the accuracy of Eq. (8.61) with simulations. We calculated $V_{\tilde{x}\tilde{x}}^{min}$ without making any approximations for 10^5 randomly chosen parameters satisfying

$$10^4 \leq Q \leq 10^{11}; \quad 10^{-5} \leq \Gamma_\gamma \leq 10^{-1}; \quad 10^{-5} \leq \Gamma_\Theta\Gamma_\gamma \leq 10^{-1}, \tag{8.62}$$

and compared them with the approximate expression of $V_{\tilde{x}\tilde{x}}^{min}$ given by Eq. (8.61). As we show in Fig. 8.5, we obtained that the discrepancy between Eq. (8.61) and the exact calculation of $V_{\tilde{x}\tilde{x}}^{min}$ is almost always below 1% and at most 3%.

The second term in Eq. (8.61) represents how much unrecoverable information about $\tilde{x}$ is stored in the cavity. We determined this by looking at the optimal steady state conditional covariance matrix for

$$\check{\boldsymbol{x}} = \begin{pmatrix} \tilde{x} & \tilde{p} \end{pmatrix}^T \tag{8.63}$$

if the cavity is adiabatically eliminated. We call this covariance matrix $\mathcal{V}_{\check{\boldsymbol{x}}\check{\boldsymbol{x}}}^{min}$. Since $\mathcal{V}_{\check{\boldsymbol{x}}\check{\boldsymbol{x}}}$ is diagonal (see Eq. 8.38), it is easy to calculate. We first find the symplectic eigenvalue, ν, of $\mathcal{V}_{\check{\boldsymbol{x}}\check{\boldsymbol{x}}}$ with $n = 0$. Since $\mathcal{V}_{\check{\boldsymbol{x}}\check{\boldsymbol{x}}}$ is already diagonal $\nu = Q\Gamma_q^2/4$. We then use the results of Sec. (8.4.2) which tell us that $\tilde{x}$ and $\tilde{p}$ can be squeezed to

$(4\nu)^{-1}$, thus obtaining

$$\mathcal{V}^{min}_{\check{x}\check{x}} = \begin{pmatrix} \left(4Q\Gamma_\Theta^3\Gamma_\gamma\right)^{-1} & 0 \\ 0 & \left(4Q\Gamma_\Theta^3\Gamma_\gamma\right)^{-1} \end{pmatrix} \tag{8.64}$$

where we've used Eq. (8.24) with the normalized detuning Γ_Δ set to 0. Consequently, Eq. (8.64) combined with Eq. (8.61) tells us that $\Gamma_\Theta^3\Gamma_\gamma^4$ is the amount of information about $\tilde{x}$ that is locked in the cavity and that cannot be recovered by measuring the environment in any which way.

Adiabatic elimination fails when the cavity contains most of the unrecoverable information about the test mass. This occurs when the second term in Eq. (8.61) is larger than the first term, which happens for measurement strengths larger than

$$\Gamma_\Theta > \left(\frac{1}{4Q\Gamma_\gamma^5}\right)^{1/6}. \tag{8.65}$$

Notice that this scaling of $\Gamma_\gamma^{-0.83}Q^{-0.17}$ is similar to the scaling of $\Gamma_\gamma^{-0.97}Q^{-0.09}$ that we obtained numerically when we assumed we can only measure the optical bath (see Eq. (8.42)). Moreover, as we show in Fig. 8.6, Eq. (8.65) is, as is expected, a lower bound of the critical measurement strength, Γ_Θ^c, when adiabatic elimination predicts a minimum conditional variance for $\tilde{x}$ that is half as large as the exact prediction.

8.5 Conclusion

We've shown that although adiabatic elimination accurately describes the dynamics of a cavity-optomechanical system in the bad cavity limit, it fails to accurately describe the conditional dynamics when the measurement rate is large enough.

We've also illustrated how the phase-space Schmidt decomposition theorem can give us a bound when an approximation could break down in conditional calculations. When we approach this bound, we should be very suspicious of our approximation.

The theorem clearly showed us that information about the optomechanical system is stored in three places: the environment, the cavity, and the the test mass. In the bad cavity limit, the test mass couples much more strongly to the environment than the cavity, and so it seems like we can adiabatically eliminate it. However, when the test mass is strongly driven by the environment, it becomes slaved by the environment. It forgets its initial state, and its fluctuations are strongly correlated with different

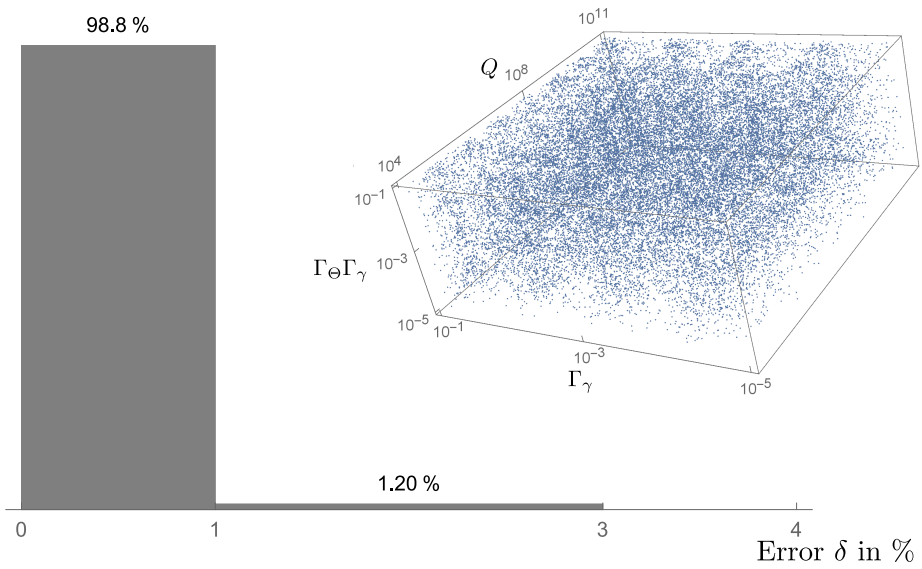

Figure 8.5: Eq. (8.61) is an accurate approximation of $V_{\tilde{x},\tilde{x}}$ in the parameter regime of interest. We generated 10^5 different possible values of the triplet $(Q, \Gamma_\Theta\Gamma_\gamma, \Gamma_\gamma)$, 3×10^4 of which are shown in the inset to demonstrate that they cover most of the regime $10^4 \leq Q \leq 10^{11}$, $10^{-5} \leq \Gamma_\gamma \leq 10^{-1}$, and $10^{-5} \leq \Gamma_\Theta\Gamma_\gamma \leq 10^{-1}$. We evaluated $V_{c,x}$ exactly and Eq. (8.61) over them, and obtained that for 98.8% of the triplets $\delta = \left| V^c_{\tilde{x}}\big|_{exact} - V^c_{\tilde{x}}\big|_{approx} \right| / V^c_{\tilde{x}}\big|_{exact} \leq 1\%$, and for 1.2% of the triplets δ is between 1 and 3%.

modes of the environment, and weakly correlated with the cavity. When we measure the environment, we recover all the information that is lost to the environment. If we drive the optomechanical system strongly enough, the uncertainty of the test mass' state becomes limited by the information that is stored in the cavity.

By having the test mass slaved by the environment, we can substantially squeeze one of its degrees of freedom. The stronger the measurement strength, the stronger the entanglement. Some information is also in the cavity because the test mass is entangled with it (here also the entanglement gets stronger as we measure the cavity). For moderate measurement strengths, we are limited by the information that's stuck in the test mass and not the cavity.

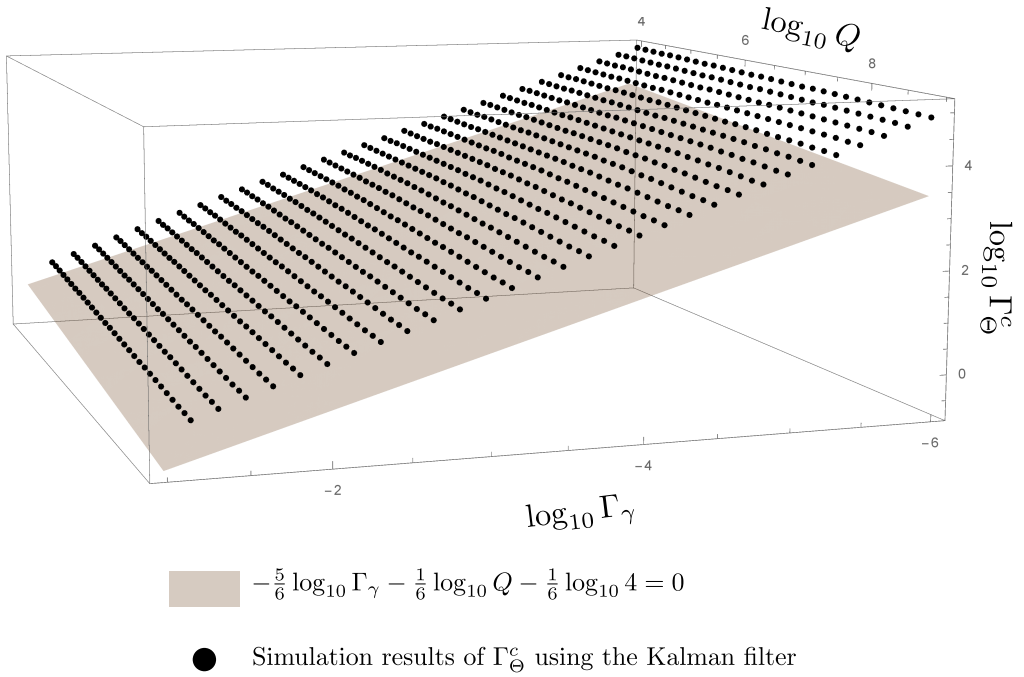

Figure 8.6: Testing the accuracy of Eq. (8.65). The simulation results are the same as those in Fig. 8.3. The plane shows the value of Γ_Θ for which $\tilde{\alpha}_1^2/4\nu_1 = \tilde{\alpha}_2^2/4\nu_2$ for different values of Q and Γ_γ.

8.6 Appendix: Introduction to quantum state preparation in optomechanics

In this section, we provide the background information needed to understand quantum state preparation in optomechanics. We also review how to measure the outgoing light in order to optimally squeeze an operator of interest.

8.6.1 The conditional state of an optomechanical system

If we measure the outgoing light, which is entangled with the system, we modify the dynamics of the system through wavefunction collapse. In general, obtaining the conditional state of a system based on an experimentalist's measurement record is difficult. However, in our case, it is relatively simple because the system is in a Gaussian state. Indeed, the unconditional state is Gaussian (see Eq. (8.33)), and measuring linear combinations of the outgoing light quadratures projects Gaussian states into Gaussian states. Furthermore, the $\hat{a}_{out}(t)$ commute at different times, so are simultaneously measurable and equivalent to a classical Gaussian random process (see appendix D.3 of [4]). Consequently, we can apply Bayes' theorem to determine the Wigner function of a cavity optomechanical system conditioned on a collection of measurement results.

To simplify the presentation of how we obtain the conditional state of the sytem, we

will discretize time into N time steps. The $N \to \infty$ limit can be taken at the end of the calculation. Assume that the following N commuting outgoing light operators are measured:

$$\boldsymbol{y}_\theta \equiv \begin{pmatrix} \cos\theta\left(t_1\right)\tilde{a}_{out,1}\left(t_1\right) + \sin\theta\left(t_1\right)\tilde{a}_{out,2}\left(t_1\right) \\ \cos\theta\left(t_2\right)\tilde{a}_{out,1}\left(t_2\right) + \sin\theta\left(t_2\right)\tilde{a}_{out,2}\left(t_2\right) \\ \vdots \\ \cos\theta\left(t_N\right)\tilde{a}_{out,1}\left(t_N\right) + \sin\theta\left(t_N\right)\tilde{a}_{out,2}\left(t_N\right) \end{pmatrix} \tag{8.66}$$

where $t_i \equiv i \times dt$ for $i = 1 \ldots N$. Moreover, denote the measurement results associated with $\boldsymbol{y}_\theta$ by $\vec{y}_\theta$. If we apply Bayes' rule, we can obtain the Wigner function of the cavity optomechanical system at the end time of the experiment t_N and conditioned on $\vec{y}_\theta$:

$$W^c\left(x, p, a_1, a_2 | \vec{y}_\theta\right) = \frac{W\left(x, p, a_1, a_2, \vec{y}_\theta\right)}{W\left(\vec{y}_\theta\right)} \tag{8.67}$$

$$= \frac{1}{\sqrt{\det\left(2\pi V^c_{\boldsymbol{xx}}\right)}} \exp\left(-\frac{1}{2}\left(\vec{x} - \langle \boldsymbol{x}\rangle_c\right)^T \left(V^c_{\boldsymbol{xx}}\right)^{-1}\left(\vec{x} - \langle \boldsymbol{x}\rangle_c\right)\right) \tag{8.68}$$

where $W\left(\vec{y}_\theta\right)$ is the Wigner function for the measured observables $\boldsymbol{y}_\theta$. It is a zero-mean Gaussian with a variance of

$$V_{\boldsymbol{y}_\theta \boldsymbol{y}_\theta} \equiv \left\langle \boldsymbol{y}_\theta \boldsymbol{y}_\theta^T \right\rangle_s . \tag{8.69}$$

$W\left(x, p, a_1, a_2, \vec{y}_\theta\right)$ is the total Wigner function for the system and $\boldsymbol{y}_\theta$. It is also a zero-mean Gaussian with a variance of

$$\begin{pmatrix} V_{\boldsymbol{xx}} & V_{\boldsymbol{x}\boldsymbol{y}_\theta} \\ V^T_{\boldsymbol{x}\boldsymbol{y}_\theta} & V_{\boldsymbol{y}_\theta \boldsymbol{y}_\theta} \end{pmatrix} \tag{8.70}$$

where $V_{\boldsymbol{xx}}$ is the covariance matrix for $\boldsymbol{x}$ at time t_N (see Eq. (8.34)), and

$$V_{\boldsymbol{x}\boldsymbol{y}_\theta} \equiv \left\langle \boldsymbol{x}.\boldsymbol{y}_\theta^T \right\rangle_s \tag{8.71}$$

is the cross-correlation matrix between $\boldsymbol{x}$ and $\boldsymbol{y}_\theta$. Finally, $\langle \boldsymbol{x}\rangle_c$ and $V^c_{\boldsymbol{xx}}$ and are the conditional mean and variance of the system, respectively, and are given by[1]

$$\langle \boldsymbol{x}\rangle_c = V_{\boldsymbol{x}\boldsymbol{y}_\theta} V^{-1}_{\boldsymbol{y}_\theta \boldsymbol{y}_\theta} \vec{y} \tag{8.72}$$

$$V^c_{\boldsymbol{xx}} = V_{\boldsymbol{xx}} - V_{\boldsymbol{x}\boldsymbol{y}_\theta} V^{-1}_{\boldsymbol{y}_\theta \boldsymbol{y}_\theta} V^T_{\boldsymbol{x}\boldsymbol{y}_\theta}. \tag{8.73}$$

[1] see section 2.3.3 of [2] for how to obtain the first and second moments of conditional Gaussians

For practical calculations of $V^c_{\boldsymbol{xx}}$, we don't use Eq. (8.73) because $V_{\boldsymbol{y}_\theta \boldsymbol{y}_\theta}$ is a very large (in the continuum limit, infinite) matrix and so it is numerically slow, and analytically impossible, to invert it. Instead, we can proceed in two different ways.

To analytically calculate $V^c_{\boldsymbol{xx}}$, we write it as

$$V^c_{\boldsymbol{xx}}(t) = \langle(\boldsymbol{x} - K\boldsymbol{y}_\theta)\rangle_s \tag{8.74}$$

where

$$K \equiv V_{\boldsymbol{x}\boldsymbol{y}_\theta} V^{-1}_{\boldsymbol{y}_\theta \boldsymbol{y}_\theta} \tag{8.75}$$

is a $4 \times N$ matrix (in general $2m \times N$ matrix where m is the system's number of degrees of freedom). In the continuum limit, Eq. (8.75) becomes

$$\int_0^{t_f} dz \, \langle \hat{y}_\theta(t) \, \hat{y}_\theta(z)\rangle_s \, K(z) = \left\langle \boldsymbol{x}\left(t_f\right) \hat{y}_\theta(t)\right\rangle_s \tag{8.76}$$

where t_f is the end time of the experiment. It can be solved with the Wiener-Hopf method [8], which for large systems quickly becomes intractable. For a system with n degrees of freedom, we would need to solve for the roots of a $2n$-th order polynomial. Consequently, exact analytic calculations are impossible for more than 2 modes, and messy for systems with two modes (such as our cavity-optomechanical setup).

In this article, we numerically calculate $V^c_{\boldsymbol{xx}}(t)$ with the Kalman filter, which iteratively solves for $V^c_{\boldsymbol{xx}}(t)$ by applying Bayes rule one measurement record at a time (as opposed to Eq. (8.68), where we used conditioned on all the measurement results in one step). This allows us to obtain a differential equation for $V^c_{\boldsymbol{xx}}(t)$ (see Appendix B of [4]):

$$\partial_t V^c_{\boldsymbol{xx}}(t) = MV^c_{\boldsymbol{xx}}(t) + V^c_{\boldsymbol{xx}}(t) M^T + NV_{\boldsymbol{nn}}N^T - Y(t) BV_{\boldsymbol{nn}}B^T Y(t)^T \tag{8.77}$$

$$Y(t) \equiv \left(V^c_{\boldsymbol{xx}}(t) A^T + NV_{\boldsymbol{nn}}B^T\right)\left(BV_{\boldsymbol{nn}}B^T\right)^{-1}, \tag{8.78}$$

where M and N are defined in Eq. (8.12), A and B in Eq. (8.17), and $V_{\boldsymbol{nn}}$ in Eq. (8.36). At steady state, Eq. (8.77) reduces to a continuous time algebraic Riccati equation.

8.6.2 Introduction to optimal conditional one-mode squeezed state preparation

Since quantum mechanics only allows simultaneously measuring commuting observables, experimentalists have to make the difficult choice of what to measure.

Specifically, in our cavity optomechanical setup shown in Fig. 8.1, experimentalists have to choose the function $\theta(t)$ in Eq. (8.66). The optimal choice of $\theta(t)$ depends on the application. Let's assume that the experimentalists are interested in squeezing a degree of freedom as much as possible. Following Ref. [7], we will summarize how to optimally pick $\theta(t)$ for such an application. We will first derive a lower bound on how much we can squeeze a particular operator, and then show that the bound can be saturated by measuring a particular combination of phase and amplitude quadratures at each instant of time.

We first obtain a lower bound on how well we can squeeze $\boldsymbol{x}$ by assuming that we can measure all quadratures of the optical light. Let V be the total covariance matrix for the system degrees of freedom and for the outgoing light:

$$V \equiv \begin{pmatrix} V_{\boldsymbol{xx}} & V_{\boldsymbol{xa}} \\ V_{\boldsymbol{xa}}^T & V_{\boldsymbol{aa}} \end{pmatrix}, \tag{8.79}$$

where

$$\boldsymbol{a} = \begin{pmatrix} \tilde{a}_{out,1}(t_1) & \dots & \tilde{a}_{out,1}(t_N) & \tilde{a}_{out,2}(t_1) & \dots & \tilde{a}_{out,2}(t_N) \end{pmatrix}^T. \tag{8.80}$$

The optomechanical system's Wigner function conditioned on measuring $\boldsymbol{a}$ is Gaussian and has the following mean and covariance matrix

$$\mu(\vec{a}) = V_{\boldsymbol{xa}} V_{\boldsymbol{aa}}^{-1} \vec{a}, \tag{8.81}$$

$$V_{\boldsymbol{xx}}^{min}(t) = V_{\boldsymbol{xx}}(t) - V_{\boldsymbol{xa}}(t) V_{\boldsymbol{aa}}^{-1}(t) V_{\boldsymbol{xa}}^T. \tag{8.82}$$

where $\vec{a}$ are the measurement results of $\boldsymbol{a}$, and we have used the superscript 'min' to highlight that $V_{\boldsymbol{xx}}^{min}$ contains the minimum achievable conditional variances. Deriving Eq. (8.82) follows the same reasoning as in Sec. 8.66.

If we are interested in squeezing a single operator as much as possible, we can achieve the lower bound given by the corresponding entry in $V_{\boldsymbol{xx}}^{min}$. To be concrete, let's say that we are interested in squeezing the normalized center of mass position operator $\tilde{x}$, which is defined in Eq. (8.7). The argument can be easily generalized to any system operator $\hat{O}$.

Reaching Eq. (8.82) corresponds to estimating $\boldsymbol{x}$ with

$$\boldsymbol{e} \equiv V_{\boldsymbol{xa}} V_{\boldsymbol{aa}}^{-1} \boldsymbol{a} \equiv K \boldsymbol{a}, \tag{8.83}$$

because

$$\left\langle (\boldsymbol{x} - K\boldsymbol{a})(\boldsymbol{x} - K\boldsymbol{a})^T \right\rangle_s = V_{\boldsymbol{xx}}^{min}. \tag{8.84}$$

Consequently, the optimal estimator for $\tilde{x}$ is $\hat{e}_{\tilde{x}} \equiv K_{\tilde{x}}\boldsymbol{a}$ where

$$K_{\tilde{x}} \equiv \begin{pmatrix} 1 & 0 & 0 & 0 \end{pmatrix} K \tag{8.85}$$

and we've used that

$$\tilde{x} = \begin{pmatrix} 1 & 0 & 0 & 0 \end{pmatrix} \boldsymbol{x}. \tag{8.86}$$

In the continuum limit,

$$e_{\tilde{x}}(t) = \int_0^t dz \left(K_{\tilde{x}}^{(1)}(z)\, \tilde{a}_{out,1}(z) + K_{\tilde{x}}^{(2)}(z)\, \tilde{a}_{out,2}(z) \right). \tag{8.87}$$

If we choose $\theta(t)$ in such a way that

$$K_{\tilde{x}}(z) \cos\theta(z) \equiv K_{\tilde{x}}^{(1)}(z) \tag{8.88}$$

$$K_{\tilde{x}}(z) \sin\theta(z) \equiv K_{\tilde{x}}^{(2)}(z) \tag{8.89}$$

for all $z \leq t$, and where $K_{\tilde{x}}(z)$ is a real function, then

$$e_{\tilde{x}}(t) = \int_0^t dz K_{\tilde{x}}(z) \left(\cos\theta(z)\, \tilde{a}_{out,1}(z) + \sin\theta(z)\, \tilde{a}_{out,2}(z) \right). \tag{8.90}$$

Consequently, to achieve the lower bound $V_{\tilde{x}\tilde{x}}^{min}(t)$, we have to measure the quadratures $\left(\cos\theta(z)\, \tilde{a}_{out,1}(z) + \sin\theta(z)\, \tilde{a}_{out,2}(z)\right)$ for all $z \leq t$.

8.7 Appendix: The unconditional covariance matrix for the setup in Sec. 8.2.1

In this appendix, we show the steady state covariance matrix for the setup shown in Fig. 8.1. The optomechanical system's degrees of freedom are

$$\boldsymbol{x} = \begin{pmatrix} \tilde{x} & \tilde{p} & \hat{a}_1 & \hat{a}_2 \end{pmatrix}^T, \tag{8.91}$$

where $\tilde{x}$ and $\tilde{p}$ are the normalized test mass' center of mass position and momentum operators, respectively. The normalization factor is shown in Eq. (8.7). Moreover, $\hat{a}_1$ and $\hat{a}_2$ are the cavity field's amplitude and phase quadratures, respectively.

Using Eq. (8.35), and assuming no detuning and $n = 0$, $\boldsymbol{x}$'s covariance matrix is

$$V_{\boldsymbol{xx}}^{s.s.} = \lambda \begin{pmatrix} Q\Gamma_\Theta^3\Gamma_\gamma\left(Q+\Gamma_\gamma\right) & 0 & -\frac{Q\Gamma_\gamma^2\Gamma_\Theta^{3/2}}{\sqrt{2}} & V_{\tilde{x}\tilde{a}_2}^{s.s.} \\ 0 & Q^2\Gamma_\Theta^3\Gamma_\gamma & -\frac{Q\Gamma_\Theta^{3/2}\Gamma_\gamma}{\sqrt{2}} & \frac{Q^2\Gamma_\Theta^{9/2}\Gamma_\gamma^3\left(2Q+\Gamma_\gamma\right)\lambda}{\sqrt{2}} \\ -\frac{Q\Gamma_\Theta^{3/2}\Gamma_\gamma^2}{\sqrt{2}} & -\frac{Q\Gamma_\Theta^{3/2}\Gamma_\gamma}{\sqrt{2}} & \frac{1}{2\lambda} & \frac{Q\Gamma_\Theta^3\Gamma_\gamma^3}{2} \\ V_{\tilde{x}\tilde{a}_2}^{s.s.} & \frac{Q^2\Gamma_\Theta^{9/2}\Gamma_\gamma^3\left(2Q+\Gamma_\gamma\right)\lambda}{\sqrt{2}} & \frac{Q\Gamma_\Theta^3\Gamma_\gamma^3\Gamma_\gamma^3}{2} & V_{\tilde{a}_2\tilde{a}_2}^{s.s.} \end{pmatrix}, \tag{8.92}$$

where

$$\lambda^{-1} \equiv \Gamma_\gamma + \Gamma_\gamma^2 Q + Q, \tag{8.93}$$

$$V_{\tilde{x}\tilde{a}_2}^{s.s.} = -\frac{Q\Gamma_\Theta^{9/2}\Gamma_\gamma^2\left(2Q^2+\Gamma_\gamma\left(\Gamma_\gamma^2+4\right)Q+2\Gamma_\gamma^2\right)\lambda}{\sqrt{2}} \tag{8.94}$$

$$V_{\tilde{a}_2\tilde{a}_2}^{s.s.} = \frac{4Q^3\Gamma_\Theta^6\Gamma_\gamma^3+\Gamma_\gamma^2+2Q\left(2\Gamma_\gamma^5\Gamma_\Theta^6+\Gamma_\gamma^3+\Gamma_\gamma\right)+Q^2\left(2\Gamma_\gamma^4\left(\Gamma_\gamma^2+4\right)\Gamma_\Theta^6+\left(\Gamma_\gamma^2+1\right)^2\right)}{2} \tag{8.95}$$

Q is the quality factor of the test mass, and the dimensionless parameters Γ_γ and Γ_Θ are defined by Eqs. (8.15-8.16).

Assuming no detuning and $n = 0$, we can solve for $V_{\boldsymbol{xx}}$ at steady state from Eq. (8.35): It seems that Eq. (8.92) can be easily simplified. For instance, we expect that we can neglect the second term in the numerator of $V_{\tilde{x}\tilde{a}_2}^{s.s.}$, which is about Γ_γ/Q smaller than the first term. We obtained for the following parameters: $\Gamma_\gamma = 10^{-2}$, $Q = 10^6$ and $\Gamma_\Theta = 1/2$, that this approximation underestimates the minimum conditional variance of $\tilde{x}$ by three orders of magnitude. This demonstrates how frail the process of calculating conditional variances are.

Bibliography

[1] Gerardo Adesso. *Entanglement of Gaussian states*. PhD thesis, Salerno U., 2007.

[2] Christopher Bishop. *Pattern recognition and machine learning*. Springer, New York, 2006.

[3] Alonso Botero and Benni Reznik. Modewise entanglement of gaussian states. *Phys. Rev. A*, 67:052311, May 2003.

[4] Yanbei Chen. Macroscopic quantum mechanics: theory and experimental concepts of optomechanics. *Journal of Physics B: Atomic, Molecular and Optical Physics*, 46(10):104001, 2013.

[5] H. J. Kimble, Yuri Levin, Andrey B. Matsko, Kip S. Thorne, and Sergey P. Vyatchanin. Conversion of conventional gravitational-wave interferometers into quantum nondemolition interferometers by modifying their input and/or output optics. *Phys. Rev. D*, 65:022002, Dec 2001.

[6] Haixing Miao, Stefan Danilishin, Helge Müller-Ebhardt, Henning Rehbein, Kentaro Somiya, and Yanbei Chen. Probing macroscopic quantum states with a sub-heisenberg accuracy. *Phys. Rev. A*, 81:012114, Jan 2010.

[7] H. Mueller-Ebhardt, H. Miao, S. Danilishin, and Y. Chen. Quantum-state steering in optomechanical devices. *ArXiv e-prints*, November 2012.

[8] Helge Müller-Ebhardt, Henning Rehbein, Chao Li, Yasushi Mino, Kentaro Somiya, Roman Schnabel, Karsten Danzmann, and Yanbei Chen. Quantum-state preparation and macroscopic entanglement in gravitational-wave detectors. *Phys. Rev. A*, 80:043802, Oct 2009.

[9] Witlef Wieczorek, Sebastian G. Hofer, Jason Hoelscher-Obermaier, Ralf Riedinger, Klemens Hammerer, and Markus Aspelmeyer. Optimal state estimation for cavity optomechanical systems. *Phys. Rev. Lett.*, 114:223601, Jun 2015.

[10] Huan Yang, Haixing Miao, and Yanbei Chen. Nonadiabatic elimination of auxiliary modes in continuous quantum measurements. *Phys. Rev. A*, 85:040101, Apr 2012.

Chapter 9

THE CONDITIONAL STATE OF A LINEAR OPTOMECHANICAL SYSTEM THAT IS BEING MONITORED BY A NON-LINEAR, PHOTON-COUNTING, MEASUREMENT

Abstract

We present an analytic method to obtain the conditional state of a linear optomechanical system that is driven by Gaussian states and that is being monitored by a non-linear, photon-counting, measurement. We hope that our work will help researchers explore a range of optomechanics topologies that make use of photon counters. The conditional Wigner function we obtain is a polynomial multiplied by a Gaussian, and its parameters depend on quantities that can be efficiently obtained with the Kalman filter. Normalizing this Wigner function (equivalently, calculating the probability of obtaining a particular measurement record) entails integrating a polynomial multiplied by a Gaussian over a possibly high-dimensional space.

9.1 Introduction

Quantum mechanics has been spectacularly successful at predicting the behavior of microscopic systems, but the macroscopic world around us never seems to behave non-classically. In the past decade, experimentalists have made significant advances in preparing macroscopic objects in non-classical states. In particular, in optomechanics, researchers have cooled test masses to their quantum mechanical ground state cooling [2]. Moreover, the center of mass motion of test masses has been squeezed below the Heisenberg uncertainty level [15, 13, 8].

Preparing a test mass in its ground state or in a squeezed state is an amazing feat, but such states have Wigner functions that are completely positive and so they can be characterized with a classical probability distribution. A test mass is indisputably behaving quantum mechanically when its Wigner function takes on negative values. To prepare such Wigner functions, we need to go beyond linear optomechanical setups that are driven by Gaussian states, and that monitor a linear observable (such as the phase quadrature of the outgoing light). Khalili *et al.* proposed injecting a non-Gaussian optical state (such as a single photon pulse) into an optomechanical system [7]. O'Connell *et al.* prepared a mesoscopic mechanical resonator in a Fock state by coupling it to a superconducting qubit [12]. Galland *et al.* showed that using non-linear photon counting measurements, and an appropriately detuned

driving laser, can prepare a test mass in a non-Gaussian state [5]. Their proposal was realized in Refs. [3, 6] where they measured individual quanta of phonons in mechanical resonators.

The formalism used in [5] can only be applied to simple optomechanical setups, and is only exact in the absence of losses and thermal noise. In this article, we present an analytic filter for calculating the state of a generic linear optomechanical system that is driven by Gaussian light and where the number of outgoing photons is continuously monitored.

The filter we present is genuinely quantum mechanical. A linear Gaussian optomechanical system can be mapped a classical dynamical system [11, 9], and so we can obtain the state of a test mass conditioned on the experiment's measurement results in a tractable way. However, in classical control theory, although analytic non-linear filters exist, they do not exist for discrete measurement equations [4]. Our derivation will make use of the fact that Fock states' Wigner function can be expressed as derivatives of a Gaussian Wigner function.

9.2 Setup

Consider a linear optomechanical system that is continuously probed by light. The number of photons in the outgoing light is then counted with a photodetector. We show an example simple setup in Fig. 9.1, where a movable test mass is probed by a laser. We will denote the outgoing light at time t by $\hat{a}_{out}(t)$. Furthermore, to simplify the analysis, we discretize time into N time steps.

The conditional state of our quantum system, given a measurement record $\boldsymbol{n} = (n_1, ..., n_N)$ where $n_i \geq 0$ are integers and represent the number of photons detected at time $i \times dt$, is

$$\hat{\rho}_c(\boldsymbol{n}) = \hat{\mathcal{P}}_{\boldsymbol{n}} \hat{\rho}_{ini} \hat{\mathcal{P}}_{\boldsymbol{n}} / p(\boldsymbol{n}); \qquad p(\boldsymbol{n}) = \mathrm{Tr}\left(\hat{\mathcal{P}}_{\boldsymbol{n}} \hat{\rho}_{ini} \hat{\mathcal{P}}_{\boldsymbol{n}}\right) \tag{9.1}$$

where $p(\boldsymbol{n})$ is the probability of obtaining the record $\boldsymbol{n}$, and $\hat{\mathcal{P}}_{\boldsymbol{n}}$ projects the output field into a subspace where the outgoing light's number of photons operator, $\hat{n}(t) = \hat{a}^{\dagger}_{out}(t)\,\hat{a}_{out}(t)$, agrees with the measurement record $\boldsymbol{n}$:

$$\hat{\mathcal{P}}_{\boldsymbol{n}} = \hat{P}_{n_N} \hat{U}(t_N) \ldots \hat{P}_{n_1} \hat{U}(t_1). \tag{9.2}$$

We've defined

$$t_i \equiv i \times dt \tag{9.3}$$

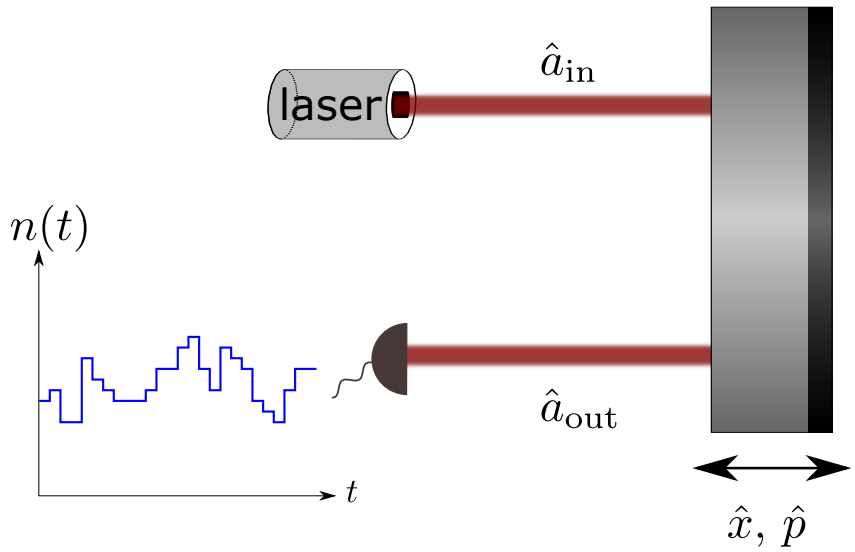

Figure 9.1: A simple example optomechanical setup. A free test mass is driven by an incoming light continuum, labeled by $\hat{a}_{in}$. $\hat{a}_{in}$ then interacts with the test mass' center of mass motion position and momentum operators, $\hat{x}$ and $\hat{p}$. The reflected light forms an outgoing light light continuum, labeled by $\hat{a}_{out}$. $\hat{a}_{out}$ is continuously monitored by a photon counter. We denote the resultant measurement record by $n(t)$.

for $i = 1 \ldots N$. Each $\hat{U}(t_i)$ evolves the system and probe from $t = t_{i-1}$ till $t = t_i$, and each $\hat{P}_{n_i}$, for $i = 1 \ldots N$, projects the outgoing probe light to a Fock state at time t_i

$$\hat{P}_{n_i} = |n_i\rangle \langle n_i| . \tag{9.4}$$

It will be convenient to work in the Heisenberg picture. We rewrite $\hat{\mathcal{P}}_{\boldsymbol{n}}$ in the following way

$$\hat{\mathcal{P}}_{\boldsymbol{n}} = \hat{\mathcal{U}} \hat{\mathcal{P}}^H_{\boldsymbol{n}} \tag{9.5}$$

where $\hat{\mathcal{U}}$ evolves the system and probe from $t = 0$ till the end time of the experiment t_N, and $\hat{\mathcal{P}}^H_{\boldsymbol{n}}$ is the collection of projection operators expressed in the Heisenberg picture:

$$\hat{\mathcal{P}}^H_{\boldsymbol{n}} = \prod_{i=1}^{N} \left(\hat{U}^\dagger (i \times dt, 0) \hat{P}_{n_i} \hat{U} (i \times dt, 0) \right) . \tag{9.6}$$

9.3 Switching to the Wigner function

It will be convenient to express everything in terms of the Wigner function. The conditional Wigner function of our system at time t_N is

$$W(\vec{x};\boldsymbol{n}) = \int \frac{d\vec{\gamma}}{(2\pi)^{2m}} e^{-i\vec{x}^T\vec{\gamma}} \mathcal{J}(\vec{\gamma};\boldsymbol{n}), \tag{9.7}$$

where m is the number of degrees of freedom of our system, and $\vec{x}$ is a vector that runs over the system's degrees of freedom. For example, $\vec{x} = \begin{pmatrix} x & p \end{pmatrix}^T$ for the example setup shown in Fig. 9.1. $\mathcal{J}$ is the generating function:

$$\mathcal{J}(\vec{\gamma};\boldsymbol{n}) = \mathrm{Tr}_{sys}\left[e^{i\vec{\gamma}^T\hat{\boldsymbol{x}}}\hat{\rho}_{sys,c}(\boldsymbol{n})\right] \tag{9.8}$$

where the trace is over the system degrees of freedom, and $\hat{\boldsymbol{x}}$ are the observables associated with the system's degrees of freedom (*e.g.* $\hat{\boldsymbol{x}} = \begin{pmatrix} \hat{x} & \hat{p} \end{pmatrix}^T$ for the setup shown in Fig. 9.1). $\hat{\rho}_{sys,c}(\boldsymbol{n})$ is the conditional density matrix of the system given the measurement record $\boldsymbol{n}$, and is obtained by tracing $\hat{\rho}_c(\boldsymbol{n})$ over the environment degrees of freedom:

$$\hat{\rho}_{sys,c}(\boldsymbol{n}) = \mathrm{Tr}_{env}\left(\hat{\rho}_c(\boldsymbol{n})\right). \tag{9.9}$$

Using Eq. (9.1), we can write that

$$\mathcal{J}(\vec{\gamma};\boldsymbol{n}) = \frac{1}{p(\boldsymbol{n})}\mathrm{Tr}\left[e^{i\vec{\gamma}^T\hat{\boldsymbol{x}}}\hat{\mathcal{P}}_{\boldsymbol{n}}\hat{\rho}_{ini}\hat{\mathcal{P}}_{\boldsymbol{n}}\right]. \tag{9.10}$$

Using Eq. (9.5), that $\hat{\mathcal{P}}_{\boldsymbol{n}}^\dagger\hat{\mathcal{P}}_{\boldsymbol{n}} = \hat{\mathcal{P}}_{\boldsymbol{n}}$, that

$$\hat{\mathcal{U}}^\dagger\hat{\boldsymbol{x}}\hat{\mathcal{U}} = \hat{\boldsymbol{x}}(t_N) \tag{9.11}$$

and that $[\hat{\boldsymbol{x}}(t_N), \hat{n}(t)] = 0$ for $t < t_f$ (the future can't influence the past), we rewrite $\mathcal{J}$ to

$$\mathcal{J}(\vec{\gamma};\boldsymbol{n}) = \frac{1}{p(\boldsymbol{n})}\mathrm{Tr}\left[e^{i\vec{\gamma}^T\hat{\boldsymbol{x}}(t_N)}\hat{\mathcal{P}}_{\boldsymbol{n}}^H\hat{\rho}_{ini}\right]. \tag{9.12}$$

9.4 The Projection operator in terms of the Wigner function

9.4.1 Total projection operator in terms of the Wigner function

How do we represent, for example, $|n\rangle\langle n|(t)$ with ladder operators? Any density operator can be represented with the Wigner function. Consider a bosonic mode whose two quadratures we'll label $\hat{a}_1$ and $\hat{a}_2$. We can write its state in terms of the

Wigner function

$$\hat{\rho} = \pi \int \int W(\alpha_1, \alpha_2) \exp\left[i\left(\beta_2\left(\hat{a}_1 - \alpha_1\right) - \beta_1\left(\hat{a}_2 - \alpha_2\right)\right)\right] d\alpha_1 d\alpha_2 d\beta_1 d\beta_2 \quad (9.13)$$

Reference: [14] section 3.4

For a Fock state (From [1] eq. 1.106) $|n\rangle$

$$W_n(\alpha_1, \alpha_2) = \frac{2}{\pi}(-1)^n e^{-\left(\alpha_1^2+\alpha_2^2\right)} L_n\left(2\left(\alpha_1^2 + \alpha_2^2\right)\right) \quad (9.14)$$

where the L_n is the Laguerre polynomials

$$L_n(x) = \sum_{m=0}^{n} (-1)^m \binom{n}{m} \frac{x^m}{m!}. \quad (9.15)$$

A few example Wigner functions are

$$\begin{aligned} W_0(\alpha_1, \alpha_2) &= \frac{2}{\pi} e^{-\left(\alpha_1^2+\alpha_2^2\right)}, \quad (9.16) \\ W_1(\alpha_1, \alpha_2) &= \frac{2}{\pi} e^{-\left(\alpha_1^2+\alpha_2^2\right)}\left(2\left(\alpha_1^2 + \alpha_2^2\right) - 1\right). \end{aligned}$$

We will express $\hat{\mathcal{P}}_{\boldsymbol{n}}^H$, the total projection operator onto $\boldsymbol{n}$ in the Heisenberg picture, in terms of the Wigner function. Using Eq. (9.13)

$$\begin{aligned} \hat{\mathcal{P}}_{\boldsymbol{n}}^H &= \lim_{N\to\infty} \pi^N \int d\boldsymbol{\alpha}_1 d\boldsymbol{\alpha}_2 d\boldsymbol{\beta}_1 d\boldsymbol{\beta}_2 \left(\prod_{i=1}^{N} W_{n_i}\left(\alpha_1(t_i), \alpha_2(t_i)\right)\right) \times \\ &\quad \exp\left[i \sum_{j=1}^{N} \left(\beta_2(t_j)\left(\hat{a}_1(t_j) - \alpha_1(t_j)\right) - \beta_1(t_j)\left(\hat{a}_2(t_j) - \alpha_2(t_j)\right)\right)\right] \\ &= \lim_{N\to\infty} \pi^N \int d\boldsymbol{\alpha}_1 d\boldsymbol{\alpha}_2 d\boldsymbol{\beta}_1 d\boldsymbol{\beta}_2 \times \\ &\quad \left(\prod_{i=1}^{N} W_{n_i}\left(\alpha_1(t_i), \alpha_2(t_i)\right)\right) \exp\left[i\left(\boldsymbol{\beta}_2^T\left(\hat{\boldsymbol{a}}_1 - \boldsymbol{\alpha}_1\right) - \boldsymbol{\beta}_1^T\left(\hat{\boldsymbol{a}}_2 - \boldsymbol{\alpha}_2\right)\right)\right] \quad (9.17) \end{aligned}$$

where $\hat{a}_1(t)$ and $\hat{a}_1(t)$ are the two quadratures associated with the outgoing light at

time t, and to simplify the notation, we've defined

$$\boldsymbol{\alpha}_{1/2} \equiv \left(\alpha_{1/2}(t_1) \quad \alpha_{1/2}(t_2) \quad \dots \quad \alpha_{1/2}(t_N) \right)^T, \tag{9.18}$$

$$\boldsymbol{\beta}_{1/2} \equiv \left(\beta_{1/2}(t_1) \quad \beta_{1/2}(t_2) \quad \dots \quad \beta_{1/2}(t_N) \right)^T, \tag{9.19}$$

$$\hat{\boldsymbol{a}}_{1/2} \equiv \left(\hat{a}_{1/2}(t_1) \quad \hat{a}_{1/2}(t_2) \quad \dots \quad \hat{a}_{1/2}(t_N) \right)^T. \tag{9.20}$$

9.4.2 Generating projection functional

Since $W_n(\alpha_1, \alpha_2)$ is non-Gaussian for $n > 0$, it seems that we cannot analytically perform out the integrals in Eq. (9.17). However, the W_n have a special structure: they can be written as derivatives of W_0 (which is Gaussian):

$$W_n(\alpha_1, \alpha_2) = (-1)^n L_n\left(2\partial_{f_1}^2 + 2\partial_{f_2}^2\right) e^{\alpha_1 f_1 + \alpha_2 f_2} W_0(\alpha_1, \alpha_2)\Big|_{f_1=f_2=0}. \tag{9.21}$$

For example

$$W_1(\alpha_1, \alpha_2) = \left(2\partial_{f_1}^2 + 2\partial_{f_2}^2 - 1\right) e^{\alpha_1 f_1 + \alpha_2 f_2} W_0(\alpha_1, \alpha_2)\Big|_{f_1=f_2=0}. \tag{9.22}$$

We will use Eq. (9.21) to develop an analytic prescription for obtaining the conditional state of the system based on $\boldsymbol{n}$.

Using Eq. (9.21), we rewrite $\hat{\mathcal{P}}_{\boldsymbol{n}}^H$ to

$$\hat{\mathcal{P}}_{\boldsymbol{n}}^H \equiv \lim_{N\to\infty} \left(\prod_{i=1}^{N} (-1)^{n_i} L_{n_i}\left(2\partial_{f_1(t_i)}^2 + 2\partial_{f_2(t_i)}^2\right) \right) \hat{\mathcal{G}}\Big|_{\boldsymbol{f}=0} \tag{9.23}$$

$$\hat{\mathcal{G}} \equiv \pi^N \int \left(d\boldsymbol{\alpha}_1 d\boldsymbol{\alpha}_2 d\boldsymbol{\beta}_1 d\boldsymbol{\beta}_2 \left(\prod_{j=1}^{N} W_0\left(\alpha_1(t_j), \alpha_2(t_j)\right) \right) \right) \times$$
$$\exp\left[i \left(\boldsymbol{\beta}_2^T (\hat{\boldsymbol{a}}_1 - \boldsymbol{\alpha}_1) - \boldsymbol{\beta}_1^T (\hat{\boldsymbol{a}}_2 - \boldsymbol{\alpha}_2) \right) \right] \exp\left(\boldsymbol{\alpha}_1^T \boldsymbol{f}_1 + \boldsymbol{\alpha}_2^T \boldsymbol{f}_2 \right) \tag{9.24}$$

$$\boldsymbol{f}_1 \equiv \left(f_1(t_1) \quad f_1(t_2) \quad \dots \quad f_1(t_N) \right)^T \tag{9.25}$$

$$\boldsymbol{f}_2 \equiv \left(f_2(t_1) \quad f_2(t_2) \quad \dots \quad f_2(t_N) \right)^T \tag{9.26}$$

$$\boldsymbol{f} \equiv \left(\boldsymbol{f}_1 \quad \boldsymbol{f}_2 \right)^T. \tag{9.27}$$

Substituting Eq. (9.16), we obtain

$$\begin{aligned}\hat{\mathcal{G}} &\equiv 2^N \int d\boldsymbol{\alpha}_1 d\boldsymbol{\alpha}_2 d\boldsymbol{\beta}_1 d\boldsymbol{\beta}_2 \exp\left(-\boldsymbol{\alpha}_1^T\boldsymbol{\alpha}_1 - \boldsymbol{\alpha}_2^T\boldsymbol{\alpha}_2\right) \times \\ &\exp\left[i\left(\boldsymbol{\beta}_2^T\left(\hat{\boldsymbol{a}}_1 - \boldsymbol{\alpha}_1\right) - \boldsymbol{\beta}_1^T\left(\hat{\boldsymbol{a}}_2 - \boldsymbol{\alpha}_2\right)\right)\right] \exp\left(\boldsymbol{\alpha}_1^T\boldsymbol{f}_1 + \boldsymbol{\alpha}_2^T\boldsymbol{f}_2\right). \quad (9.28)\end{aligned}$$

Notice that $\hat{\mathcal{G}}$ is composed of only Gaussian integrals, which we can analytically evaluate.

We can rewrite $\hat{\mathcal{G}}_{\boldsymbol{n}}$ in terms of known operators. Doing so will help us interpret $\hat{\mathcal{G}}$, and evaluate some of the integrals in Eq. (9.28). Specifically, we will express $\hat{\mathcal{G}}_{\boldsymbol{n}}$ in terms of operators that project a time-dependent quadrature into a continuous measurement stream $z(t)$. In the Heisenberg picture, they are of the form

$$\hat{P}^H_{\hat{z}(t)=z(t)} = \int D\xi \, \exp\left(i\int_0^{t_f} dt\, \xi(t)\left(\hat{z}(t) - z(t)\right)\right). \quad (9.29)$$

where $\hat{z}(t)$ is the quadrature we are measuring at time t[7]. If we discretize $\hat{P}_{\hat{z}(t)=z(t)}$, then we obtain

$$\hat{P}^H_{\hat{z}(t)=z(t)} = \int \left(\Pi_j d\xi_j\right) \exp\left[i\sum_j \xi_j\left(\hat{z}\left(t_j\right) - z\left(t_j\right)\right)\right]. \quad (9.30)$$

We rewrite $\hat{\mathcal{G}}_{\boldsymbol{n}}$, given by Eq. (9.28), in terms of such projection operators:

$$\hat{\mathcal{G}} = 2^N \left(\int d\boldsymbol{\alpha}_1 \exp\left(-\boldsymbol{\alpha}_1^T\boldsymbol{\alpha}_1 + \boldsymbol{\alpha}_1^T\boldsymbol{f}_1\right)\hat{\mathcal{P}}^H_{\hat{\boldsymbol{a}}_1=\boldsymbol{\alpha}_1}\right)\left(\int d\boldsymbol{\alpha}_2 \exp\left(-\boldsymbol{\alpha}_2^T\boldsymbol{\alpha}_2 + \boldsymbol{\alpha}_2^T\boldsymbol{f}_2\right)\hat{\mathcal{P}}^H_{\hat{\boldsymbol{a}}_2=\boldsymbol{\alpha}_2}\right) \quad (9.31)$$

where

$$\hat{\mathcal{P}}^H_{\hat{\boldsymbol{a}}_1=\boldsymbol{\alpha}_1} \equiv \int d\boldsymbol{\beta}_2 \, \exp\left[i\boldsymbol{\beta}_2^T\left(\hat{\boldsymbol{a}}_1 - \boldsymbol{\alpha}_1\right)\right], \quad (9.32)$$

$$\hat{\mathcal{P}}^H_{\hat{\boldsymbol{a}}_2=\boldsymbol{\alpha}_2} \equiv \int d\boldsymbol{\beta}_1 \, \exp\left[i\boldsymbol{\beta}_1^T\left(\hat{\boldsymbol{a}}_2 - \boldsymbol{\alpha}_2\right)\right], \quad (9.33)$$

and we've redefined $\boldsymbol{\beta}_1 \to -\boldsymbol{\beta}_1$ so that $\exp\left[-i\boldsymbol{\beta}_1^T\left(\hat{\boldsymbol{a}}_2 - \boldsymbol{\alpha}_2\right)\right] \to \exp\left[i\boldsymbol{\beta}_1^T\left(\hat{\boldsymbol{a}}_2 - \boldsymbol{\alpha}_2\right)\right]$. We can now interpret $\hat{\mathcal{G}}$. It projects a state into a subspace where both quadratures of the outgoing light, $\hat{a}_1(t)$ and $\hat{a}_2(t)$, are simultaneously measured to be $\alpha_1(t)$ and $\alpha_2(t)$. We then average over all possible realizations of $\alpha_1(t)$ and $\alpha_2(t)$ as Gaussian random processes with variance $1/2$ and a mean given by $-f_1(t)$ and $-f_2(t)$ respectively.

9.5 Calculation of the conditional state

Substituting Eq. (9.31) into Eq. (9.23), which we then substitute into Eqs. (9.12) and (9.7), we obtain that the system's conditional Wigner function at the end time of the experiment t_N is

$$\begin{aligned} W\left(\vec{x};\boldsymbol{n}\right) &= \frac{2^N\left(-1\right)^{\sum_i n_i}}{p\left(\boldsymbol{n}\right)}\times \\ &\left(\prod_{i=1}^{N} L_{n_i}\left(2\partial^2_{f_1(t_i)}+2\partial^2_{f_2(t_i)}\right)\right)\int d\boldsymbol{\alpha}\exp\left(-\boldsymbol{\alpha}^T\boldsymbol{\alpha}+\boldsymbol{f}^T\boldsymbol{\alpha}\right)W_c\left(\vec{x};\boldsymbol{\alpha}\right)\Big|_{\boldsymbol{f}=0} \end{aligned} \tag{9.34}$$

$$W_c\left(\vec{x};\boldsymbol{\alpha}\right) \equiv \int \frac{d\vec{\gamma}}{\left(2\pi\right)^{2m}} e^{-i\vec{x}^T\vec{\gamma}}\mathrm{Tr}\left[e^{i\vec{\gamma}^T\hat{\boldsymbol{x}}(t_N)}\hat{\Pi}^H_{\hat{\boldsymbol{a}}_1=\boldsymbol{\alpha}_1}\hat{\Pi}^H_{\hat{\boldsymbol{a}}_2=\boldsymbol{\alpha}_2}\hat{\rho}_{ini}\right], \tag{9.35}$$

where m is the number of system degrees of freedom, and

$$\boldsymbol{\alpha} \equiv \begin{pmatrix} \boldsymbol{\alpha}_1 & \boldsymbol{\alpha}_2 \end{pmatrix}^T.$$

To evaluate $W_c\left(\vec{x};\boldsymbol{\alpha}\right)$, we follow the procedure described in Ref. [10]. We first apply Bayes' rule:

$$W_c\left(\vec{x};\boldsymbol{\alpha}\right) = \frac{\tilde{W}\left(\vec{x},\boldsymbol{\alpha}\right)}{\tilde{W}\left(\boldsymbol{\alpha}\right)} \tag{9.36}$$

where $\tilde{W}\left(\vec{x},\boldsymbol{\alpha}\right)$ is the unconditional Wigner function of the system and outgoing light, and $\tilde{W}\left(\boldsymbol{\alpha}\right)$ is the unconditional Wigner function of the outgoing light. Assuming the incoming light is in a coherent state, and that t_N is large enough so that the optomechanical system's initial (possibly non-Gaussian) state is forgotten, they are both zero-mean Gaussians. $\tilde{W}\left(\boldsymbol{\alpha}\right)$'s covariance matrix is

$$V_{\boldsymbol{aa}} \equiv \left\langle \hat{\boldsymbol{a}}\left(t_N\right)\hat{\boldsymbol{a}}\left(t_N\right)\right\rangle_s, \tag{9.37}$$

where

$$\hat{\boldsymbol{a}} \equiv \begin{pmatrix} \hat{\boldsymbol{a}}_1 & \hat{\boldsymbol{a}}_2 \end{pmatrix}^T, \tag{9.38}$$

$\hat{\boldsymbol{a}}\left(t_N\right)$ is the unitary evolution of $\hat{\boldsymbol{a}}$ from time 0 till time t_N in the Heisenberg picture under the system-environment Hamiltonian. For any operators $\hat{o}_1\left(t\right)$ and $\hat{o}_2\left(t'\right)$, $\left\langle \hat{o}_1\left(t\right)\hat{o}_2\left(t'\right)\right\rangle_s$ is the symmetric expectation value over the system-environment's initial state:

$$\left\langle \hat{o}_1\left(t\right)\hat{o}_2\left(t'\right)\right\rangle_s \equiv \mathrm{Tr}\left[\frac{1}{2}\left(\hat{o}_1\left(t\right)\hat{o}_2\left(t'\right)+\hat{o}_2\left(t'\right)\hat{o}_1\left(t\right)\right)\hat{\rho}_{ini}\right]. \tag{9.39}$$

$\tilde{W}(\vec{x}, \boldsymbol{\alpha})$'s covariance matrix is

$$\begin{pmatrix} V_{\boldsymbol{xx}} & V_{\boldsymbol{xa}} \\ V_{\boldsymbol{xa}}^T & V_{\boldsymbol{aa}} \end{pmatrix} \tag{9.40}$$

where

$$\begin{aligned} V_{\boldsymbol{xa}} &\equiv \langle \hat{\boldsymbol{x}}(t_N)\, \hat{\boldsymbol{a}}(t_N) \rangle_s, \\ V_{\boldsymbol{xx}} &\equiv \langle \hat{\boldsymbol{x}}(t_N)\, \hat{\boldsymbol{x}}(t_N) \rangle_s. \end{aligned}$$

Since $\tilde{W}(\boldsymbol{\alpha})$ and $\tilde{W}(\vec{x}, \boldsymbol{\alpha})$ are Gaussian, $W_c(\vec{x}; \boldsymbol{\alpha})$ is also a Gaussian:

$$W_c(\vec{x}; \boldsymbol{\alpha}) = \frac{1}{\sqrt{(2\pi)^{2m} \det V_c}} \exp\left(-\frac{1}{2}(\boldsymbol{x} - \boldsymbol{x}_c)^T V_c^{-1} (\boldsymbol{x} - \boldsymbol{x}_c)\right) \tag{9.41}$$

where

$$V_c = V_{\boldsymbol{xx}} - V_{\boldsymbol{xa}}^T V_{\boldsymbol{aa}}^{-1} V_{\boldsymbol{xa}}, \tag{9.42}$$

$$\boldsymbol{x}_c = K\boldsymbol{\alpha}, \tag{9.43}$$

$$K \equiv V_{\boldsymbol{xa}}^T V_{\boldsymbol{aa}}^{-1}. \tag{9.44}$$

With $W_c(\vec{x}; \boldsymbol{\alpha})$ at hand, we evaluate the integral over $\boldsymbol{\alpha}$ in $W(\vec{x}; \boldsymbol{n})$, which is given by Eq. (9.34). The integral is

$$\int d\boldsymbol{\alpha} \exp\left(-\boldsymbol{\alpha}^T \boldsymbol{\alpha} + \boldsymbol{f}^T \boldsymbol{\alpha}\right) W_c(\vec{x}; \boldsymbol{\alpha}) = \frac{\exp\left(-\frac{1}{2}\boldsymbol{x}^T V_c^{-1} \boldsymbol{x}\right)}{\sqrt{(2\pi)^{2m} \det V_c}} \int d\boldsymbol{\alpha} \exp\left(-\frac{\boldsymbol{\alpha}^T L \boldsymbol{\alpha}}{2} + \left(\boldsymbol{f}^T + \boldsymbol{x}^T V_c^{-1} K\right) \boldsymbol{\alpha}\right) \tag{9.45}$$

where

$$L \equiv 2 + K^T V_c^{-1} K. \tag{9.46}$$

Eq. (9.45) is a standard Gaussian integral. We evaluate to be

$$\int d\boldsymbol{\alpha} \exp\left(-\frac{\boldsymbol{\alpha}^T L \boldsymbol{\alpha}}{2} + \left(\boldsymbol{f}^T + \boldsymbol{x}^T V_c^{-1} K\right) \boldsymbol{\alpha}\right) = \frac{(2\pi)^N}{\sqrt{\det L}} \exp\left(\frac{1}{2}\left(\boldsymbol{f}^T + \boldsymbol{x}^T V_c^{-1} K\right) L^{-1} \left(\boldsymbol{f} + K^T V_c^{-1} \boldsymbol{x}\right)\right). \tag{9.47}$$

L seems intimidating to invert, but the Woodbury identity can simplify L^{-1}. The

identity tells us that for any 3 matrices A, B, C

$$\left(A + CBC^T\right)^{-1} = A^{-1} - A^{-1}C\left(B^{-1} + C^T A^{-1} C\right) C^T A^{-1}. \tag{9.48}$$

Applying the identity to L^{-1}, we obtain that

$$L^{-1} = \frac{1}{8}\left(8 - 2L - \left(K^T K\right)^2\right). \tag{9.49}$$

Furthermore, in

$$\left(\boldsymbol{f}^T + \boldsymbol{x}^T V_c^{-1} K\right) L^{-1} \left(\boldsymbol{f} + K^T V_c^{-1} \boldsymbol{x}\right) = \boldsymbol{f}^T L^{-1} \boldsymbol{f} + \boldsymbol{x}^T V_c^{-1} K L^{-1} K^T V_c^{-1} \boldsymbol{x} + 2\boldsymbol{x}^T V_c^{-1} K L^{-1} \boldsymbol{f} \tag{9.50}$$

we ignore the $\boldsymbol{f}^T L^{-1} \boldsymbol{f}$ term because $\boldsymbol{f}$ will be set to 0 (see Eq. (9.34)).

9.5.1 Final result

Combining everything, we have that

$$\begin{aligned}
W_{\boldsymbol{n}}(\boldsymbol{x}) &= \frac{1}{p(\boldsymbol{n})} \mathcal{W}_{\boldsymbol{n}}(\boldsymbol{x}) && (9.51)\\
p(\boldsymbol{n}) &= \int d\boldsymbol{x} \mathcal{W}_{\boldsymbol{n}}(\boldsymbol{x}) && (9.52)\\
\mathcal{W}_{\boldsymbol{n}}(\boldsymbol{x}) &= (-1)^{\sum_i n_i} \left(\prod_{i=1}^{N} L_{n_i}\left(2\partial^2_{f_1(t_i)} + 2\partial^2_{f_2(t_i)}\right)\right) \tilde{\mathcal{W}}_{\boldsymbol{n}}(\boldsymbol{x}, \boldsymbol{f})\Big|_{\boldsymbol{f}=0} && (9.53)\\
\tilde{\mathcal{W}}(\boldsymbol{x}, \boldsymbol{f}) &= \frac{(2\pi)^N 2^N}{\sqrt{(2\pi)^m \det V_c \det L}} \exp\left(-\frac{1}{2}\boldsymbol{x}^T V_0 \boldsymbol{x}\right) \exp\left(\boldsymbol{x}^T V_c^{-1} K L^{-1} \boldsymbol{f}\right) && (9.54)
\end{aligned}$$

where

$$\begin{aligned}
L &= 2 + K^T V_c^{-1} K && (9.55)\\
L^{-1} &= \frac{1}{8}\left(8 - 2L - \left(K^T K\right)^2\right) && (9.56)\\
V_0 &= V_c^{-1} - V_c^{-1} K L^{-1} K^T V_c^{-1}. && (9.57)
\end{aligned}$$

Notice that $W_{\boldsymbol{n}}(\boldsymbol{x})$ is a polynomial times a gaussian.

V_c, K and so L can be efficiently obtained with the Kalman filter. Our concern is that the integral in Eq. (9.52) could be difficult to estimate numerically.

Bibliography

[1] Girish S. Agarwal. *Quantum Optics*. Cambridge University Press, 2012.

[2] J. Chan, T. P. M. Alegre, A. H. Safavi-Naeini, J. T. Hill, A. Krause, S. Gröblacher, M. Aspelmeyer, and O. Painter. Laser cooling of a nanomechanical oscillator into its quantum ground state. *Nature*, 478:89–92, October 2011.

[3] Justin D. Cohen, Sean M. Meenehan, Gregory S. MacCabe, Simon Groblacher, Amir H. Safavi-Naeini, Francesco Marsili, Matthew D. Shaw, and Oskar Painter. Phonon counting and intensity interferometry of a nanomechanical resonator. *Nature*, 520(7548):522–525, Apr 2015. Letter.

[4] F. Daum. Nonlinear filters: beyond the kalman filter. *IEEE Aerospace and Electronic Systems Magazine*, 20(8):57–69, Aug 2005.

[5] Christophe Galland, Nicolas Sangouard, Nicolas Piro, Nicolas Gisin, and Tobias J. Kippenberg. Heralded single-phonon preparation, storage, and readout in cavity optomechanics. *Phys. Rev. Lett.*, 112:143602, Apr 2014.

[6] Sungkun Hong, Ralf Riedinger, Igor Marinković, Andreas Wallucks, Sebastian G. Hofer, Richard A. Norte, Markus Aspelmeyer, and Simon Gröblacher. Hanbury brown and twiss interferometry of single phonons from an optomechanical resonator. *Science*, 2017.

[7] Farid Khalili, Stefan Danilishin, Haixing Miao, Helge Müller-Ebhardt, Huan Yang, and Yanbei Chen. Preparing a mechanical oscillator in non-gaussian quantum states. *Phys. Rev. Lett.*, 105:070403, Aug 2010.

[8] F. Lecocq, J. B. Clark, R. W. Simmonds, J. Aumentado, and J. D. Teufel. Quantum nondemolition measurement of a nonclassical state of a massive object. *Phys. Rev. X*, 5:041037, Dec 2015.

[9] Haixing Miao, Stefan Danilishin, Helge Müller-Ebhardt, Henning Rehbein, Kentaro Somiya, and Yanbei Chen. Probing macroscopic quantum states with a sub-heisenberg accuracy. *Phys. Rev. A*, 81:012114, Jan 2010.

[10] H. Mueller-Ebhardt, H. Miao, S. Danilishin, and Y. Chen. Quantum-state steering in optomechanical devices. *ArXiv e-prints*, November 2012.

[11] Helge Müller-Ebhardt, Henning Rehbein, Chao Li, Yasushi Mino, Kentaro Somiya, Roman Schnabel, Karsten Danzmann, and Yanbei Chen. Quantum-state preparation and macroscopic entanglement in gravitational-wave detectors. *Phys. Rev. A*, 80:043802, Oct 2009.

[12] A. D. O'Connell, M. Hofheinz, M. Ansmann, Radoslaw C. Bialczak, M. Lenander, Erik Lucero, M. Neeley, D. Sank, H. Wang, M. Weides, J. Wenner, John M. Martinis, and A. N. Cleland. Quantum ground state and single-

phonon control of a mechanical resonator. *Nature*, 464:697 EP –, Mar 2010. Article.

[13] J.-M. Pirkkalainen, E. Damskägg, M. Brandt, F. Massel, and M. A. Sillanpää. Squeezing of quantum noise of motion in a micromechanical resonator. *Phys. Rev. Lett.*, 115:243601, Dec 2015.

[14] Marlan O. Scully and M. Suhail Zubairy. *Quantum Optics*. Cambridge University Press, 1997.

[15] E. E. Wollman, C. U. Lei, A. J. Weinstein, J. Suh, A. Kronwald, F. Marquardt, A. A. Clerk, and K. C. Schwab. Quantum squeezing of motion in a mechanical resonator. *Science*, 349(6251):952–955, 2015.

Chapter 10

CONCLUSIONS

Optomechanics has undisputably entered the quantum regime. Setups, such as LIGO, have become limited by quantum noise over a certain frequency bandwidth. Moreover, experimentalists have prepared test masses in squeezed states, and have measured individual quanta of phonons. These breakthroughs build upon a rich literature of theoretical optomechanics results. We've made advances to the theory of optomechanics that will hopefully help fuel the next generation of quantum optomechanics technology. In particular, we've proposed two bases to view the environment with. The first simplifies the interaction of a linear Gaussian optomechanical system with its environment. We showed that the interaction can be reduced to one with finite degrees of freedom. The second basis reduces the entanglement structure of a linear Gaussian optomechanical system and its environment at a particular time to a finite collection of two-mode squeezed states.

We were motivated to develop the first basis because researchers had used it for one particular setup to prove that a certain protocol, that makes use of photon counters, can prepare a test mass in a Fock state. We were hoping that we can use the first basis to develop protocols for more complicated optomechanical setups, but this wasn't in general possible because the effective environment modes can be squeezed and so could contain excitations and could be correlated with an infinite number of bath modes, even when the initial state of the environment is at vacuum. Nonetheless, we developed an analytic filter for obtaining the state of a system conditioned on the clicks of a photon counter. We used the second basis to derive the one-shot quantum Cramer-Rao bound in a simple way, and to understand why adiabatic eliminating a lossy cavity could fail to accurately describe the conditional dynamics of a linear Gaussian otpomechanical setup.

Outside of LIGO, some researchers have wondered what quantum optomechanics can be used for. We showed that it can be used to test alternative theories of quantum mechanics. In particular, it can test objective collapse models, which if found true would resolve the measurement problem. We showed that LISA pathfinder places aggressive bounds on the parameters of two of the most popular collapse models: the CSL and DP models. In addition, optomechanics can test whether gravity is fundamentally classical. We showed that such a theory can be made to be

compatible with causality, and that state-of-the-art torsion pendulum experiments could test it. Such experiments would also have merit even if they do not detect any new physics. They would be indirect evidence for quantum gravity, and a stepping stone for developing experiments that test quantum gravity theories, and theories where spacetime resists being in a superposition.